NMR AND EPR SPECTROSCOPY

Papers presented at Varian's Third Annual Workshop on Nuclear Magnetic Resonance and Electron Paramagnetic Resonance, held at Palo Alto, California

by

THE NMR-EPR STAFF
OF VARIAN ASSOCIATES

A Pergamon Press Book

THE MACMILLAN COMPANY
NEW YORK

PERGAMON PRESS INC.
122 East 55th Street, New York 22, N.Y.
P.O. Box 47715, Los Angeles, California

PERGAMON PRESS LTD.
Headington Hill Hall, Oxford
4 & 5 Fitzroy Square, London, W.1

PERGAMON PRESS S.A.R.L.
24 Rue des Écoles, Paris Ve

PERGAMON PRESS G.m.b.H.
Kaiserstrasse 75, Frankfurt am Main

Copyright © 1960
Pergamon Press Inc.

Library of Congress Card No. 60–14575

PRINTED IN GREAT BRITAIN BY J. W. ARROWSMITH LTD.

INTRODUCTION

It is the annual practice of Varian Associates to hold in October an international gathering of scientists who share a common interest in acquiring, expanding or exchanging their knowledge of Nuclear Magnetic Resonance and Electron Paramagnetic Resonance Spectroscopy. The fundamental purposes of this "NMR-EPR Workshop" are twofold: first, to provide new workers with an opportunity to attend introductory, intermediate, and advanced lectures and laboratory sessions in these fields of spectroscopy; and second, to offer experienced workers a meeting ground for keeping abreast of recent developments.

As has been the case with so many other facets of the brief history of Varian Associates (less than twelve years), much of the spirit of the NMR-EPR Workshop can be traced to the inspiration and atmosphere established from the beginning by the late Russell H. Varian. This unusual man proved beyond all doubt that basic and applied science can mix compatibly and beneficially with the necessities and objectives of private enterprise. We join the world-wide scientific community in mourning the passing, in Alaska on July 28, 1959, of this extraordinary scientist and humanitarian.

This book covers in large part the material presented by the NMR-EPR staff of the Instrument Division of Varian Associates at the Third Annual Workshop, held October 19–23, 1959.

The 1959 Workshop was divided consecutively into three parts. The first day was devoted to an introduction to NMR and EPR. The content of this session was tailored specifically to persons approaching these subjects for the first time. The second and third days were devoted exclusively to intermediate and advanced topics in the High Resolution form of NMR Spectroscopy; the content of this part included a number of laboratory sessions designed to supplement and complement the lectures. Finally, the fourth and fifth days were devoted to lecture and laboratory sessions in EPR Spectroscopy. All of the lectures presented during the Workshop week have been included herein in necessarily more formal fashion than originally delivered; on the other hand, several laboratory sessions have been omitted completely in the compilation because they did not lend themselves readily to a written presentation.

The 1959 registration figures show that 160 scientists from a wide variety of disciplines in chemistry, physics, biology, and medicine converged on Palo Alto for the Third Annual Workshop. Of this number, eighteen came from thirteen foreign countries.

Several acknowledgments should be made. First, we are grateful to Gerard Piel, publisher of *Scientific American*, who provided a thought-provoking after-dinner speech—"The Economics of Disarmament"—at the Workshop banquet. We must also pay our tardy respects in print to Professor Bryce Crawford, Chairman of the University of Minnesota Chemistry Department, for having, in the summer of 1957, reminded us of just the precise word—"Workshop"—for describing our proposed gathering of scientists. John Marling, James Shoolery, and Robert Rempel served tirelessly and enthusiastically as the chairmen of the three Parts of the 1959 Workshop. Mr. Marling also merits thanks for having helped compile and check all of the papers which have been reproduced herein. The 1959 Workshop Registrar, Miss Frances Demma, deserves special commendation for her efforts, as does also Edward Vopat, who was in charge of many advance arrangements and the extracurricular programs associated with the Workshop. The wives of Varian participants were hostesses for several of these events; it was their considerable pleasure to meet and entertain the wives of visitors. Finally, we can only express gratitude anonymously and profusely to all of the other persons whose names cannot appear here for space reasons, but whose efforts contributed vitally to the success of the Workshop.

MARTIN E. PACKARD, Director
Instrument Division Research

EMERY H. ROGERS, Chairman
NMR-EPR Workshop

1

BACKGROUND AND FUNDAMENTALS OF NMR-EPR SPECTROSCOPY AND SPECTROMETERS

EMERY H. ROGERS
Varian Associates, Palo Alto, California

NUCLEAR Magnetic Resonance (NMR for short) depends for its existence upon the fortunate and useful fact that most isotopes of the elements possess *gyromagnetic* properties. By this it is meant that they behave like tiny spinning bar magnets.

When a sample containing nuclei exhibiting this immutable gyromagnetism is placed in an appropriate d.c. magnetic field and is simultaneously irradiated by just the right kind of a much weaker rotating radio-frequency magnetic field, the nuclei can be compelled (*a*) to reveal their presence, (*b*) to identify themselves, and (*c*) to describe the nature of their surroundings —all by means of minute radio signals which they transmit to a receiver coil coupled closely to the sample. It can well be imagined that these significant revelations, which can be elicited painlessly and nondestructively from nuclei, can be of immense importance to, among others, the organic chemist, the physical chemist, the analytical chemist, the spectroscopist, the nuclear physicist, the solid-state physicist, the nuclear isotope spectroscopist, the polymer physicist, the biochemist, the biophysicist, and the medical research worker. By a fortunate inverse mechanism which will be explained later, it turns out that any worker interested in making a precise measurement of a d.c. magnetic field is also indebted to NMR for simplifying his endeavors and expanding their precision.

Electron Paramagnetic Resonance (EPR for short) is basically similar to NMR in that it depends upon gyromagnetic properties of sub-atomic particles for its existence. However, in the case of EPR, it is the population of unpaired electrons in the samples which is subjected to the above-described d.c. magnetic field and simultaneously-applied radio-frequency field, and which then responds with transmitted revelations of its own. Because the gyromagnetic constant associated with the spinning electron is some hundreds of times greater than that associated with nuclei, the experimental apparatus

necessary for detecting EPR signals is usually comprised of microwave components, such as wave-guide, cavities and klystron tubes; while on the other hand in NMR the detecting apparatus is replete with lumped inductances and capacitors, wires for conducting the conventional frequency r.f. energy from one place to another, and the standard sort of vacuum tubes which you would encounter in your TV set. But, stripped of the differences in outward experimental trappings, NMR and EPR have many similarities, and the one may be much more readily understood once the other is mastered. In fact, many workers in the wide range of scientific disciplines enumerated above move back and forth between NMR and EPR studies, depending upon which tool offers the most effective means of getting a given job done. Thus, for convenience, I will develop the subject of NMR first and then conclude with EPR, utilizing much of the groundwork built up for the former to explain the latter.

The first successful NMR experiments were performed essentially simultaneously and independently at two American universities, Stanford and Harvard, in the winter immediately following the end of World War II. The co-discoverers—Felix Bloch at Stanford and E. M. Purcell at Harvard—were rewarded for their achievements with the 1952 Nobel Prize in Physics. Significant though these historic experiments were, it is surely true that the co-discoverers would have been pleasantly surprised if they could have envisioned then the vast range of subsequent usefulness to which the original ideas were nurtured and expanded by themselves and thousands of other workers. For an indication of the accomplishments and developments in just the first decade after the initial discovery, the reader is referred to two excellent review articles.* Improvements and discoveries came so rapidly during the years after the first experiments that it is only recently that comprehensive textbooks on the various aspects of magnetic resonance are beginning to appear.† Workers in the field were simply too well aware of the fact that any book which appeared today would inevitably be disastrously obsolete tomorrow.

In order for us to understand the basic principles and instrumentation of NMR, we must first realize that man's quest for this mechanism was bolstered considerably by earlier knowledge. Long before the first NMR experiments were performed, it was well known that nuclear isotopes with non-zero spin also possessed a coupled magnetic moment. Through secondary effects, such as observation of hyperfine structure in the Zeeman Effect, and through atomic and neutron beam experiments, the proof was conclusive even though

* H. S. Gutowsky, *Ann. Rev. Phys. Chem.*, **5**, 1954; and J. N. Shoolery and H. E. Weaver, *Ann. Rev. Phys. Chem.*, **6**, 1955.

† Good examples: Roberts, *Nuclear Magnetic Resonance*, McGraw-Hill (1959); Pople, Schneider and Bernstein, *High-Resolution Nuclear Magnetic Resonance*, McGraw-Hill (1959); and for EPR: Ingram, *Free Radicals as Studied by Electron Spin Resonance*, Butterworths (1958).

the measurements of the moments themselves were crude insofar as accuracy was concerned. But the real trick was recognized as the measurement of this property in a direct and precise fashion in bulk material. Once nuclei could be forced to reveal themselves directly, a valuable new tool for, at the very least, identification purposes would have been devised. This thought followed from evidence that each isotopic species of non-zero spin had not only an immutable gyromagnetic constant, but also one which would be expected to differ from the gyromagnetic constants associated with all the other non-zero-spin isotopic species. Thus, just as the mass spectrometer distinguishes on the basis of mass, an NMR device would be expected to distinguish on the basis of gyromagnetism. Now how was this thought brought to reality?

The success of the 1945–46 experiments was first of all dependent upon a classical theorem enunciated at the turn of the century. J. Larmor showed in effect that a spinning bar magnet, free of all frictional forces, would, when placed in a d.c. magnetic field, precess like a top about the direction of the magnetic field. He further showed that the frequency of precession was directly proportional to the strength of the magnetic field, and that the constant of proportionality was the ratio of the magnetic moment of the spinning bar magnet to its angular momentum. This constant of proportionality is now called γ, the "gyromagnetic ratio" for the spinning magnet. (Since the constant γ is the ratio of magnetic moment to angular momentum rather than the reverse, several workers have rightfully proposed that the constant be called the "magnetogyric ratio". Unfortunately, this literally more accurate nomenclature has not been generally adopted.) Thus, the Larmor Precession Theorem can be stated as follows:

$$\omega = \gamma H$$

where $\omega = 2\pi$ times the precession frequency, γ is the gyromagnetic constant appropriate for the spinning bar magnet, and H is the d.c. magnetic field in which the precession is taking place.

Now if we expand the original Larmor concept to include the inevitable existence of frictional forces, it is evident that the spinning bar magnet will sooner or later come into alignment with the d.c. magnetic field, depending upon the strength of those forces. The time associated with re-alignment is generally called the "relaxation time", or more specifically, the "longitudinal relaxation time". When the frictional forces are large, the time is short, and vice versa. At the point of alignment, the precession ceases, but at all times up to this point, regardless of the angle between the precession field and the spinning magnetic moment, the frequency of precession is given by the basic Larmor expression.

Taking the simple model of a hydrogen nucleus as a rotating charged sphere, we can visualize how its spin might give rise to an associated magnetic moment. We must realize that a spinning charge is the equivalent of a small

current loop, and remember that such a loop can be represented by an equivalent magnetic moment. Thus, the hydrogen nucleus fits the model of the spinning bar magnet, having both a magnetic moment and an angular momentum due to its well-known quantized spin. The ratio of these two quantities, γ, is of course the gyromagnetic constant for the proton.

Since we are dealing with particles subject to the rules of quantum mechanics, we should be able to derive the basic Larmor Equation from these principles.

Equating the Planck quantum of energy, $h\nu$, with the energy of reorientation of a magnetic dipole with magnetic moment μ in a magnetic field H, we have

$$2\mu H = h\nu$$

Rearranging, we find that

$$\omega = 2\pi\nu = \frac{2\mu H}{h/2\pi} = \frac{\mu}{\frac{1}{2}(h/2\pi)} \times H$$

Now the angular momentum of the proton is equal to its spin value ($\frac{1}{2}$) multiplied by $h/2\pi$. Thus

$$\omega = \frac{\mu}{\text{ang. mom.}} \times H = \gamma H$$

i.e. the Larmor Equation.

While a single nucleus is treated according to quantum mechanical laws here, a great ensemble of nuclei, such as one would find in, say, $\frac{1}{10}$ cm^3 of some liquid sample containing hydrogen, can be looked upon as obeying the laws of classical dynamics in the aggregate. This time-honored duality of viewpoint—the classical and quantum mechanical—has so far caused few, if any, nervous breakdowns on the part of countless workers in the various fields of physics and chemistry, and for convenience of understanding magnetic resonance, the alternative viewpoints appear frequently in its literature.

For countless eons, hydrogen nuclei (and all the other non-zero-spin isotopes) have been precessing transiently, according to Larmor's equation, in whatever magnetic field they found themselves. Of course, these nuclei are subject to frictional forces provided by coupling to their environment, and the only way that they can experience brief precessional motion is for their axes to be tilted somehow with respect to the magnetic field in which they are immersed.

Let us consider a simple example. The protons in an undisturbed glass of water are aligned along the earth's magnetic field. During a brief period after a small magnet has been momentarily brought near this glass of water, hydrogen nuclei therein are wrenched around and thereby experience a tilt with respect to the earth's magnetic field. Accordingly they will precess at a fre-

quency determined by the earth's field, until they relax back into alignment again. If there had been an ice cube floating in the water, the time for re-alignment of the protons in the ice would have been shorter by many orders of magnitude than that for the protons in water, but in either case the precession frequency would have been the same. To give specific numbers, the constant γ for hydrogen nuclei is such that, in the earth's field of approximately 0.5 gauss, the Larmor precession frequency is something like 2000 c/s. Of course the O^{17} nuclei in the glass of water would also have experienced a transient precession, but their γ is such that, in the earth's magnetic field of 0.5 gauss, their precession frequency would have been more like 300 c/s. All other non-zero-spin nuclei in the glass–water combination would have also obeyed the Larmor Precession Theorem immediately after tilt had been introduced.

Our glass of water subjected to a momentary small additional magnetic impulse over and beyond the steady earth's field would of course have revealed nothing to our human senses, feeble detectors insofar as magnetism is concerned, or to any artificially contrived detecting mechanism which might have been placed in the vicinity of the glass. In addition to the highly transient nature of the phenomenon, two other factors militated against any apparent observable results. The first additional factor is the one of randomness. Looking at the event in a simplified way, we might say that all of the protons making up the ensemble were without phase reference to one another during the transient precession. Thus, not having coherence, there was no way in which they could combine their forces to produce an effect multiplied by their great number. Unfortunately, and here is where the second additional negative factor comes in, even if they had somehow acquired phase coherence, *all* of their population would not have contributed to the resultant effect. This arises from the Boltzmann condition which tells us that, due to the competing process of thermal agitation within the sample, there is almost the same probability that the protons will be pointing along the field direction as in opposition to it; and furthermore that whatever excess population is pointing along the direction of the field must be directly proportional in magnitude to the precession field strength. Because of the cancellation of opposing vectors, it is only the *excess* population pointing along the field direction which can be considered in any dynamical event in which the whole population participates. An analysis of the Boltzmann distribution of gyromagnetic particles in a d.c. magnetic field yields the sad news that at room temperature only one proton out of each ten billion contributes to any effect at the earth's field, whereas 20,000 protons out of each ten billion serve a useful purpose at a strong field of 10,000 gauss. Even if the effect had not been transitory and even if phase coherence had been miraculously introduced and retained, the effective participating population would have been so small as to produce only the feeblest of effects.

Thus, a successful NMR experiment requires (*a*) some mechanism for replenishing the precessing population in opposition to the frictional relaxing forces, (*b*) some means for introducing phase coherence so that a great effective multiplication of the individual precession occurs, and (*c*) a precession field much stronger than that of the earth in order to obtain a useful working population. It is exactly these three ingredients which Bloch applied to the water sample when he and co-workers performed the first successful "nuclear induction" experiment.

In order to understand how the first two ingredients were supplied in the Bloch experiment, we must refer to Fig. 1, a greatly simplified diagram of an

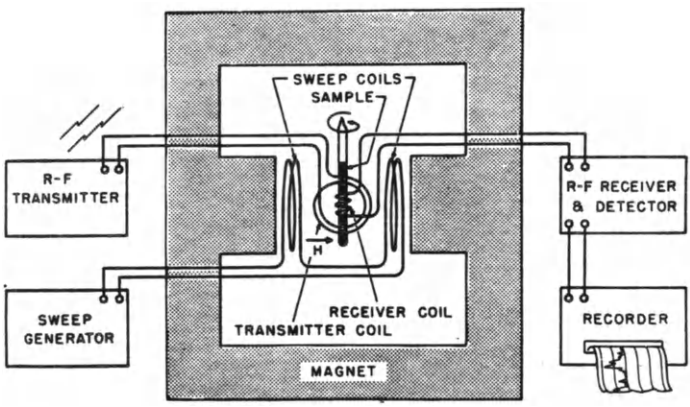

FIG. 1. How an NMR spectrometer works.

NMR detector of the "crossed-coil" type. Our water sample has been placed in a small test tube located at the air gap center of a large magnet with field H of, say, 10,000 gauss. Reality has been blithely ignored in the diagram: the magnet is shown with a very unfavorable pole-diameter-to-air-gap ratio, and, as a consequence, the magnetic field gradient at the sample position would in actual practice seriously impair chances of obtaining a signal successfully.

At right angles to the field direction in the air gap of this mythical magnet has been placed a radio-frequency transmitter coil, which in turn is excited by r.f. energy supplied from the r.f. transmitter. The master oscillator in this r.f. transmitter has been set precisely at 42.577 megacycles to correspond, through the Larmor relation $\omega = \gamma H$, to the assumed 10,000 gauss magnetic field in the air gap. At right angles to both the d.c. magnetic field and the radio-frequency transmitter coil, a receiver coil has been wound tightly around the sample tube. The leads from this receiver coil proceed to a radio-frequency receiver, tuned to the same frequency as the transmitter. An r.f.

detector and a recorder for output display complete the signal chain. Additionally, a sweep generator and sweep coils have been added to produce a slowly changing d.c. or low audio-frequency modulation of the main precession field H. If any recurring phenomenon is to be observed as a signal at the recorder, it will surely be dependent upon the value of the applied magnetic field. Thus the latter is periodically swept in the immediate vicinity of the Larmor precession field determined by the 42.577 Mc radio-frequency so that a dynamically recurring, rather than a static point-by-point, event can be observed.

It will be noted immediately that the key addition to the mere sample of water and the applied precession field has been a small radio-frequency magnetic field, at right angles to H, produced by current flowing in the transmitter coil. Furthermore, this second field has been chosen in such a manner as to oscillate at exactly the frequency of precession which would be experienced according to the Larmor equation by the protons in the water sample. One senses immediately that this simple but dramatically important step should somehow be capable of causing a resonant event; that is, by supplying energy at just the natural frequency of the system, it might be surmised that the nuclear ensemble could be brought into phase coherence and simultaneously provided with enough energy to keep the precessing population replenished in the face of relaxing frictional forces. Furthermore, if the experiment is being carried out in the presence of a strong d.c. magnetic field rather than in a weak one, this factor should increase the useful excess population according to the Boltzmann statistics.

It turns out that we do indeed have a happy set of experimental circumstances. Just as a moving magnet can induce a voltage in a nearby coil, so the nuclear magnets, precessing *en masse*, can now induce a small but detectable voltage in the receiver coil surrounding the sample. Of course, in this "crossed-coil" system, the receiver coil must be located at right angles to the transmitter coil in order to avoid a flooding of the former with r.f. field generated by the latter and thereby an overpowering of the weak NMR signal from the nuclei themselves.

It may be interesting to see here how the oscillating transmitter field can act upon the precessing nuclei to tilt them away from alignment. For a qualitative understanding of the forces at play, we should consider Fig. 2. H_0 in the diagram is the strong precession field, M is the spinning magnetic moment which is precessing about H_0, and H_1 is one of the two equal but oppositely rotating components of the oscillating r.f. field directed along the X axis. (Any oscillating vector can be shown to consist of two equal but oppositely rotating vectors.) We only need consider the one effective rotating component which rotates about H_0 in the same direction as M is precessing; the counter-rotating component can be shown to have essentially no effect on the dynamics of the system. Thus, we use an oscillating field to produce

the desired rotating field only because the latter is effectively present in the former, and the oscillating field is considerably easier to produce. Now, knowing that the rate of change in angular momentum, both in magnitude and in direction, is equal to the torque applied to that angular momentum vector, and realizing that the torque is equal to the vector cross product of magnetic moment and magnetic field, we see that the effect of H is to cause precessional motion. Furthermore, and this is the key additional point, the rotating

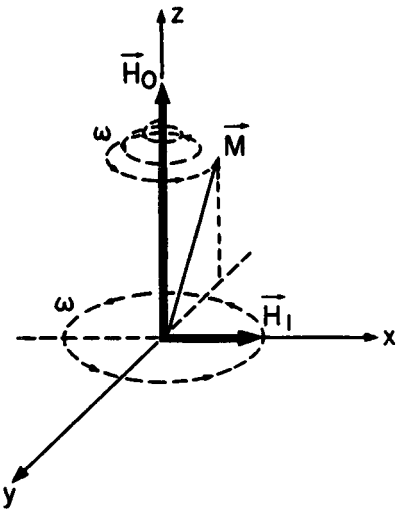

FIG. 2.

radio-frequency field H_1, adjusted by the operator to keep in step with the naturally precessing magnetic moment, causes a secondary, but much lower frequency, precession to take place about H_1. A little thought will convince you that the resultant of these two precessions is such as to retain or even open up the tilt, depending upon the strength of the r.f. field and the opposing relaxing forces.

It has been mentioned earlier that the experiment would be a disastrous failure through circuit overloading if the receiver and transmitter coils were oriented with respect to one another in such a fashion as to couple strongly together. In actual fact, ingenious mechanisms have been devised which permit reduction of this so-called "leakage" voltage to zero, and to keep it at zero. On the other hand, it turns out that it is desirable to permit deliberately a certain amount of controlled r.f. energy to couple directly across from transmitter to receiver. The reasons for this are twofold: first, the detector performs most efficiently when there is a slight bias provided over and above the signal itself; and second, by means of injecting r.f. leakage of controlled phase with respect to the transmitter field, the desired "mode" of the two-component NMR signal can be selected at will. The two types of NMR signal

shapes which may be selected from the complete NMR signal are shown in Fig. 3. At the top right-hand of the Figure is an absorption, or so-called v-mode, signal. (The abscissa is magnetic field deviation about the resonant value, and the ordinate is NMR signal amplitude; for example, the induced voltage in a receiver coil.) At the lower right-hand of the Figure is a dispersion or u-mode signal. Either one may be selected at will by the afore mentioned

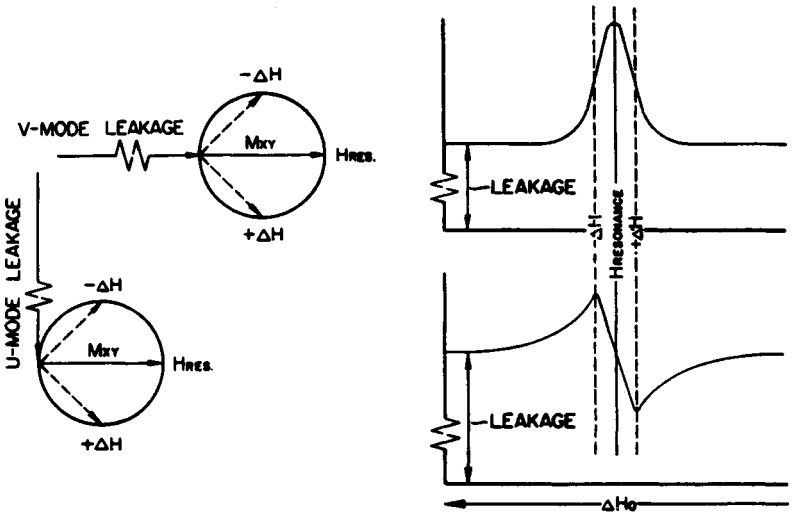

FIG. 3. Addition of the NMR signal to the absorption or dispersion mode leakage.

technique of deliberate injection of controlled phase leakage, also known as "homodyning". In the latest spectrometers the leakage injection is not made at the probe itself through deliberate unbalance from zero; rather it is made at a higher level in the amplification chain for reason of not needlessly multiplying the inevitable minute residual variations in a leakage vector which might be some noticeable percentage of a very weak signal at the limit of sensitivity.

A mathematical investigation of the characteristics of each of the two NMR signal modes shows that they have quite different characteristics. Considering the "slow passage" condition wherein one sweeps through the signal in a time long compared to the relaxation times to avoid ringing effects in the high-Q nuclear circuits, we find that the peak amplitude of the absorption mode increases linearly with r.f. field strength up to an optimum point dependent upon the nature of the sample. Thereafter, increasing the radio-frequency field only depresses the signal amplitude maximum and simultaneously artificially broadens the signal, causing loss of signal strength relative

to the noise. Because of simplicity of interpretation, the absorption mode is by far the most commonly encountered in NMR spectroscopy, but in using it one must make certain that the r.f. field strength is kept near or below its optimum value. Otherwise, the undesirable broadening and amplitude depressing effects of saturation will set in. On the other hand, the dispersion mode of the NMR signal grows symmetrically in left- and right-peak maximum amplitude linearly with the r.f. field strength until, at a particular r.f. field dependent upon the nature of the sample, the side-peak amplitudes become independent of r.f. field strength and merely broaden out each way from the resonance zero crossing. The dispersion mode serves occasional use in certain specialized NMR work where the relaxation times are so unfavorable that the absorption mode would saturate immediately.

Now, let us sum up what we have said so far. If we had placed our sample of water in a test tube in the idealized spectrometer just described, and, if we had adjusted the radio-frequency to 42.577 Mc we would have observed a deflection of the recorder pen when the applied d.c. magnetic field was swept through the resonant value of 10,000 gauss. The shape of this signal would have been dependent upon how we set the leakage controls on the spectrometer. Furthermore, if we had re-tuned the radio-frequency transmitter and receiver to 5.772 Mc we would have found, with somewhat more difficulty and possibly with the need for employing more sophisticated methods of overcoming the signal-to-noise problem, another signal from the naturally occurring O^{17} in the water. Then, again using the more sophisticated detection techniques and readjusting our r.f. equipment to 6.536 Mc, we would have found another signal from the sparse but naturally occurring population of deuterons (H^2) present in the water.

It is immediately evident that such a device is a nuclear isotope spectrometer, capable in principle of detecting the presence (and the amount) of all those isotopes with non-zero spin present in the water, test tube and nearby coils. On the other hand, our NMR spectrometer is totally powerless to deal with the zero-spin isotopes present; in the case at hand, the O^{16} in water. If we had substituted an organic liquid for the water, we would have been unable to observe the large amount of C^{12} present, but our spectrometer would have detected the naturally-occurring or artificially enriched amount of C^{13}.

Two marginal sensitivity signals, obtained by the more sophisticated lock-in detector technique which singles out one harmonic of the NMR signal in a narrow-band detector for reason of rejecting noise background, are shown in Fig. 4. These are typical wide-line NMR signals from gyromagnetically weak isotopes.

Of course, principle and practice not always being perfectly harmonious, real NMR spectrometers bear little resemblance to the simple diagram we have been considering. A drawing of a "probe"—the exceedingly precise

box which positions the sample properly with respect to the various coils and the d.c. magnetic field, which shields the r.f. receiver coil from stray pick-up, and which contains mechanisms for adjusting the leakage—appears in Fig. 5. Figure 6 is a photograph of a probe positioned between the pole pieces of a large magnet producing an exceedingly stable and homogeneous strong field

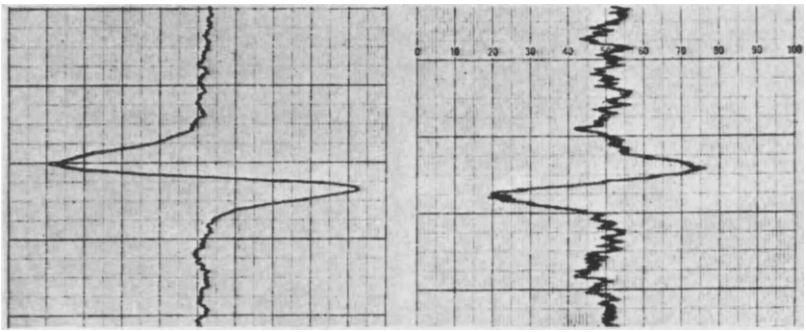

O^{17} at 10 kg field, $f = 5.8$ Mc
Sample: distilled H_2O

H^2 at 10 kg field, $f = 6.5$ Mc
Sample: $H_2O + \frac{1}{2}$ molar $MnSo_4$

FIG. 4. Criteria of spectrometer sensitivity.

in the sample region. A complete spectrometer array, showing the spectrometer console on the left, the magnet at center, and the magnet current generating and stabilizing apparatus at the right, appears in Fig. 7. Later on you will be hearing in great detail about the components of which the various kinds of spectrometers are constituted.

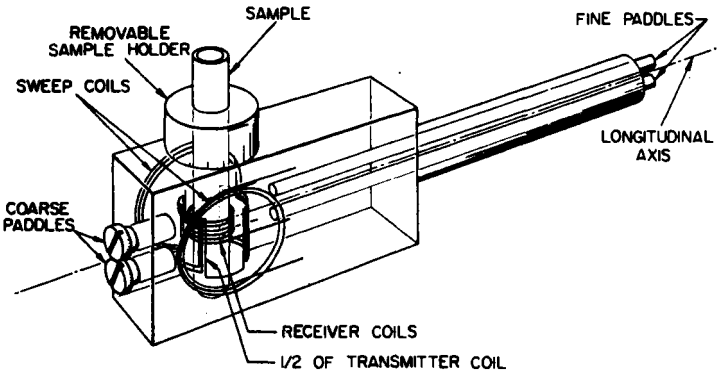

FIG. 5.

So far, we have been discussing the straight detection of isotopes by what has come to be known as Wide Line NMR Spectroscopy. The first spectrometers were all of this variety, and they were put to work in cataloguing the gyromagnetic ratios of a large number of isotopes. Inverse versions of these

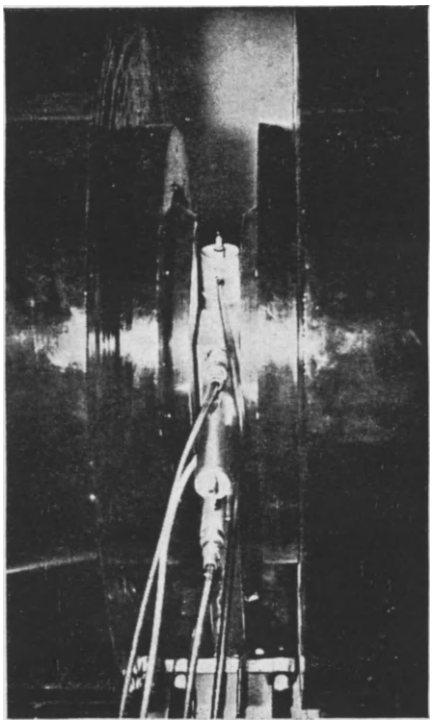

FIG. 6.

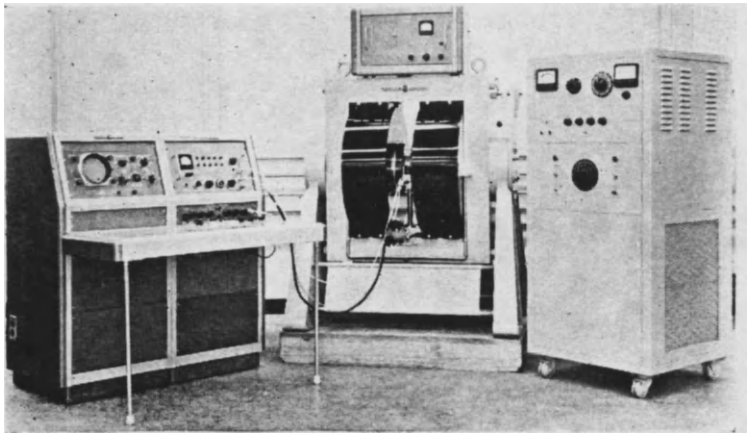

FIG. 7.

spectrometers—ones in which known samples were placed in unknown magnetic fields and subjected to carefully measured radio-frequencies at the condition of resonance—enjoyed immediate and widespread use as fluxmeters. The National Bureau of Standards obliged early in the game by making an independent measurement of gamma for the proton to an absolute accuracy of 1 part in 50,000, thereby permitting precise measurement of magnetic field strengths and variations in field strengths. Field control, utilizing an unchanging nuclear constant as reference, also came into wide usage.

Although a great deal of enthusiasm was generated around the possibility of unlocking nuclear secrets via Wide Line NMR Spectroscopy, an even more fertile field of application lay uncultivated until an historic day in 1950. At that time, Proctor and Yu at Stanford were making a precise measurement of the magnetic moment of N^{14} using ammonium nitrate (NH_4NO_3) dissolved in water as a vehicle for obtaining an abundant supply of nitrogen nuclei. They were greatly surprised one day to find that their spectrometer yielded two distinct nitrogen signals, separated by approximately one gauss out of an applied field of many thousands of gauss. Perplexed by this unexpected result, they spent the next month looking at samples enriched in N^{15}, since they incorrectly suspected that the two peaks were somehow related to nuclear effects. The upshot of the matter was that they discovered that it was the two differing *chemical* environments of the nitrogen nuclei which could be correlated with the two signals. Since the actual fields experienced by the nitrogen nuclei at the two distinct sites differed slightly relative to one another and also relative to the externally applied field, they decided to call this phenomenon the "chemical shift". Simultaneously and independently Dickinson made similar discoveries in fluorine compounds. It was immediately realized that the H in Larmor's Equation would have to be taken as the H at the nuclear site rather than as the H generated external to the sample by the magnet.

The day of the chemist in NMR had dawned. Although the early results only hinted at things to come, it was almost immediately realized that NMR offered a real possibility as a tool for identifying and determining chemical surroundings, using the nucleus itself as an alert "spy" weakly coupled to those surroundings. The nucleus was now less interesting *per se*, but rather took on a new stronger interest for what it could reveal about chemical bonds. The chemist was now poised on the threshold of possessing a technique which could complement and supplement the well-established powerful structural and analytical methods such as infrared, ultraviolet, and mass spectrometry.

But before Arnold, Dharmatti and Packard could take the next historic step of providing the first crude fingerprint of an organic compound, certain instrumental problems had to be solved. Let us try to understand what these were.

Just as the quality of the diffraction grating can determine the performance of the optical spectrograph, so the quality of the magnet system can determine the performance of the NMR spectrometer. If Proctor and Yu had been working with a really bad magnet—say, one which had spread a 10 gauss field inhomogeneity over the sample dimensions—they would never have seen two peaks from nitrogen in ammonium nitrate. They would have seen one broad one, artificially made so by the magnet. Immediately the question came up as to whether there might not be a rich and meaningful spectrum of peaks obtainable from a given sample if the magnet were capable of greater resolution. The over-all resolution of the magnet was clearly made up of two key factors: the homogeneity and the time stability of the magnetic field. A furious program got underway to make a more homogeneous and stable magnet than was used by Proctor and Yu in their wide-line experiments. The result of course was the now historic observation of the three closely spaced but quite distinct hydrogen peaks from ethyl alcohol, published in 1951. The OH, CH_2 and CH_3 protons were found to be chemically shifted apart from one another by some few milligauss. "High Resolution" NMR was born.

The intervening years have brought a relentless quest for ever greater resolving power at higher and higher fields, with occasional spurts provided by such ingenious tricks as spinning the sample to dupe the nuclei (through averaging) into believing that they are in a better field than is actually the case. Dr. Shoolery makes a wonderful analogy when he describes presently attainable resolution as equivalent to a telescope resolving two cats seated one foot apart on the moon.

It may be well at this point to present, in greatly simplified terms, two of the fundamental effects which contribute to a high resolution NMR spectrum. First, let us consider Fig. 8, which illustrates one of these effects, the "chemical shift" mentioned above. You will note that the signals from three different samples are considered: water, benzene and toluene. Looking at the 20 Mc spectra, we see that the proton signal from benzene is shifted some 7 or 8 milligauss down towards lower applied field relative to the signal from the reference compound, water. The benzene ring protons from toluene also appear at -7 milligauss, but here we note a new peak at $+15$ milligauss, arising from the CH_3 protons. Thus, we have found experimentally that the distinctly different chemical bonding situations involved correlate with different magnetic shieldings at the nuclear sites. Furthermore, it turns out that the area under each peak is directly proportional to the number of protons in the chemical environment characteristic of that position on the spectral distribution.

Proceeding to the right-hand signals, we note first that, at 40 Mc, the signal amplitudes are all four times as great as they were at 20 Mc. Furthermore, the chemical shifts relative to the reference compound position have all been enhanced by a factor of two. Thus, we have found that there is urgent reason

for working at the highest possible field strengths compatible with economics and the ability to shim the magnet, since signal amplitude is proportional to the square of the magnetic field, and since the chemical shift is directly proportional to the strength of the field.

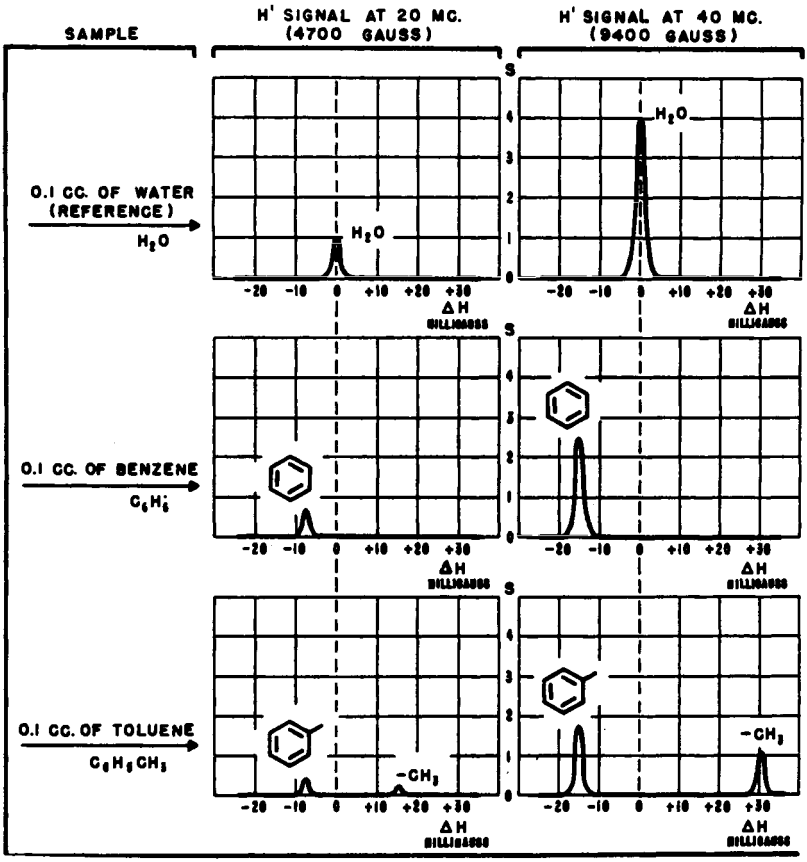

FIG. 8.

Figure 9 illustrates "spin–spin splitting", a second basic contributing factor in High Resolution NMR spectra which was explained originally by Gutowsky, McCall and Slichter, and by Hahn and Maxwell. Here we are looking at the nucleus P^{31}, rather than at our old friend, the proton. We note immediately that the phosphorus nuclei in phosphine are all chemically equivalent, and that, therefore, the observed multiplet structure in the NMR spectrum cannot be traced to chemical shift. What we are observing here is the combined magnetic effect of the three hydrogen nuclei on the phosphorus nucleus they

surround. The key identifying feature of spin–spin splitting is its independence of field strength as shown in the two cases of 8 and 16 Mc. (Of course, in accordance with the field-strength-squared law, the amplitude has been enhanced four times in moving from 4650 gauss to 9300 gauss.)

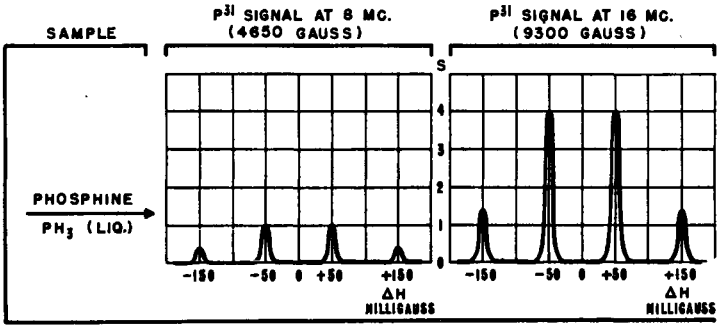

FIG. 9.

These are only simple examples, but subsequent speakers will dwell at great length upon the all-important matter of high resolution NMR spectra interpretation. Just to whet your appetite for what is coming, I am presenting in Fig. 10 segments of the pyridine high resolution NMR spectrum at 40 and 60 Mc. It takes an expert to unravel spectra of this sort, and we trust that

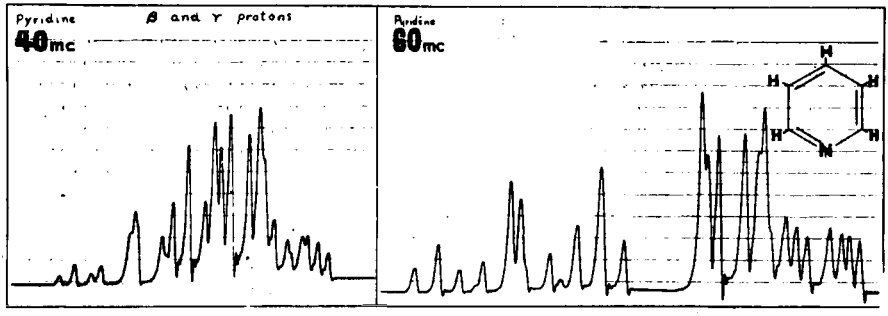

FIG. 10.

all of you will be well on your way to that degree of expertness when the Workshop is over.

In developing the subject of NMR, we have made persistent use of the analogy between spinning bar magnets and nuclei of non-zero spin. But, as stated before, electrons intrinsically satisfy the same analogy. If their individual effectiveness is not cancelled out by an equal and oppositely pointing electron—i.e. when we have an unpaired electron present such as would be the case with, for example, a free radical, a transition element ion, or color

center—we can force these gyromagnetically favorable particles to emit signals in a manner similar to NMR.

I have stated earlier that EPR differs from NMR in that microwave components replace conventional radio-frequency equipment. This arises from the fact of nature that the gyromagnetic ratio for the spinning electron places its resonant frequency at approximately 10,000 Mc for a precession field of 3600 gauss. A simplified block diagram of an EPR spectrometer appears in Fig. 11. Instead of being placed in a probe surrounded by radio-frequency

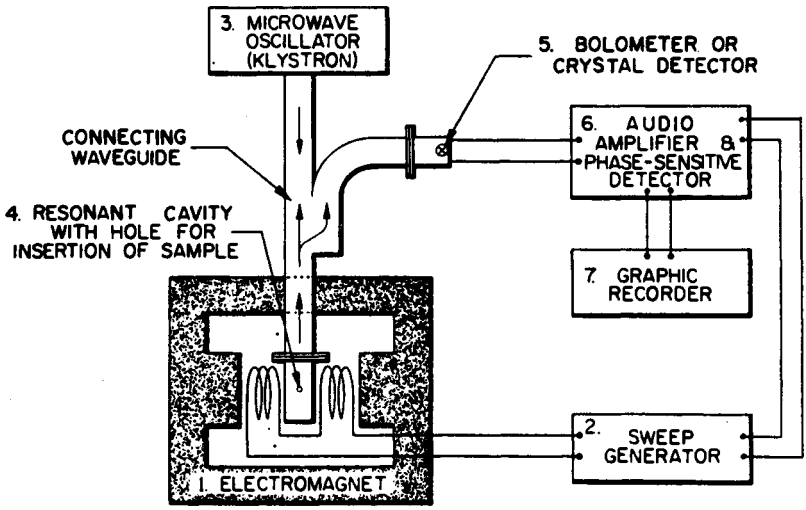

FIG. 11.

coils, the EPR sample is placed in a resonant cavity constructed in such a fashion as to maximize the H field along the sample dimension and minimize the E field to keep dielectric losses down. Then, at resonance, the sample absorbs energy from the microwave field, and this dynamically recurring (i.e. swept) unbalance is detected and amplified for presentation on a recorder. Subsequent speakers will tell you in detail of the clever refinements of this basic scheme which many workers have devised to roll back the signal-to-noise frontier.

It should be noted particularly in Fig. 11 that the magnet associated with an EPR spectrometer must be an electromagnet rather than a permanent type, since the effective gyromagnetic ratios encountered in EPR range widely away from the gyromagnetic ratio for the "free" electron. A 10 kMc EPR spectrometer should be capable of covering at least a field range of 50 to 5500 gauss in order to avoid missing significant peaks. Because the minimum line widths encountered in EPR spectroscopy are not as narrow as those encountered in High Resolution NMR spectroscopy, the requirements on

the resolution of the associated magnet system are not as stringent. Nevertheless, by all other standards, they are severe, with one part in one million stability and homogeneity representing the sort of thing that would be satisfactory for the best work.

Figures 12 and 13 are, respectively, a drawing and a photograph of typical early EPR sample cavities. Figure 14 shows a 6 in. magnet with a microwave

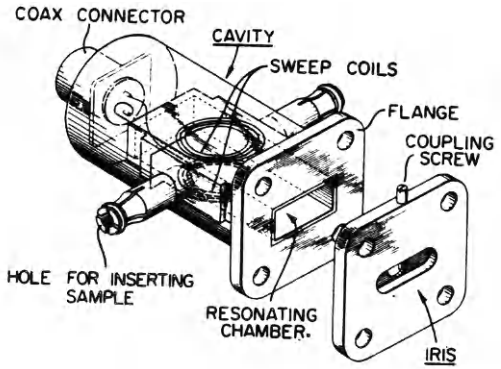

FIG. 12.

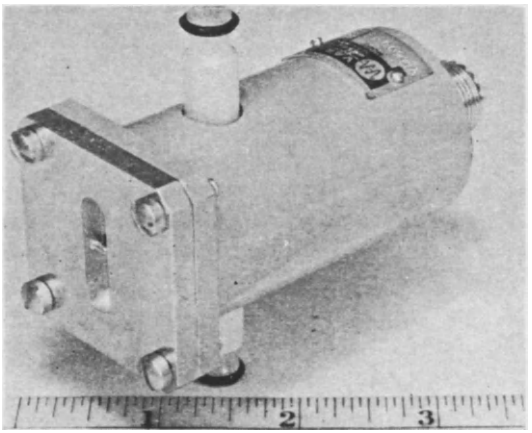

FIG. 13.

bridge mounted thereon along with a liquid helium sample handling system. A typical EPR signal is displayed in Fig. 15. It is the spectrum originating from free radicals formed as a result of the ultraviolet irradiation of polymethylmethacrylate. Again, as in the case of the high sensitivity wide line NMR work, the original EPR signal, replete in all its harmonics, has been

filtered through a synchronous detector to attain optimum signal-to-noise ratio. The result presented here is therefore only the first harmonic of the original signal. Many EPR spectra will be presented and discussed in detail by subsequent speakers.

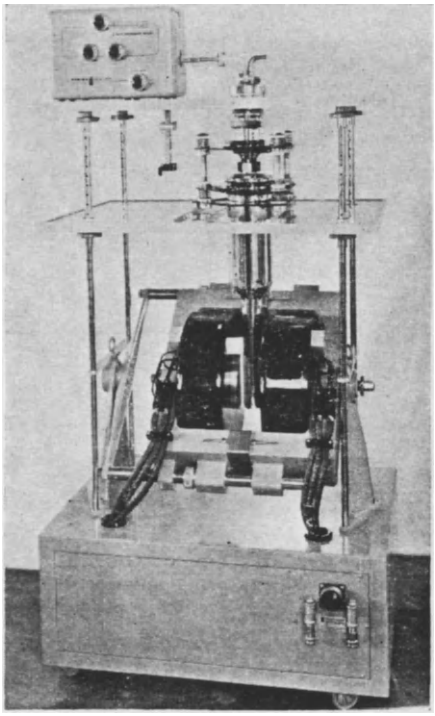

FIG. 14.

I have attempted to demonstrate here that the various forms of NMR and EPR are indeed spectroscopic techniques. The power and the limitations of these techniques will be discussed in detail by subsequent speakers. But before closing, I felt that you might wish to see where NMR and EPR find themselves in the firmament of spectroscopy. You will note particularly from Fig. 16 that NMR and EPR appear well down at the lower end of the frequency scale. Clearly this is a drawback insofar as a simple consideration of energy, $h\nu$, is concerned. On the other hand, the NMR and EPR techniques have the great advantage of utilizing coherent sources of radiation, and of permitting the observer to alter and control the spectrum in a known fashion by readjusting the magnetic field and frequency. This last characteristic is of particular importance in the challenging business of unraveling NMR and EPR spectra.

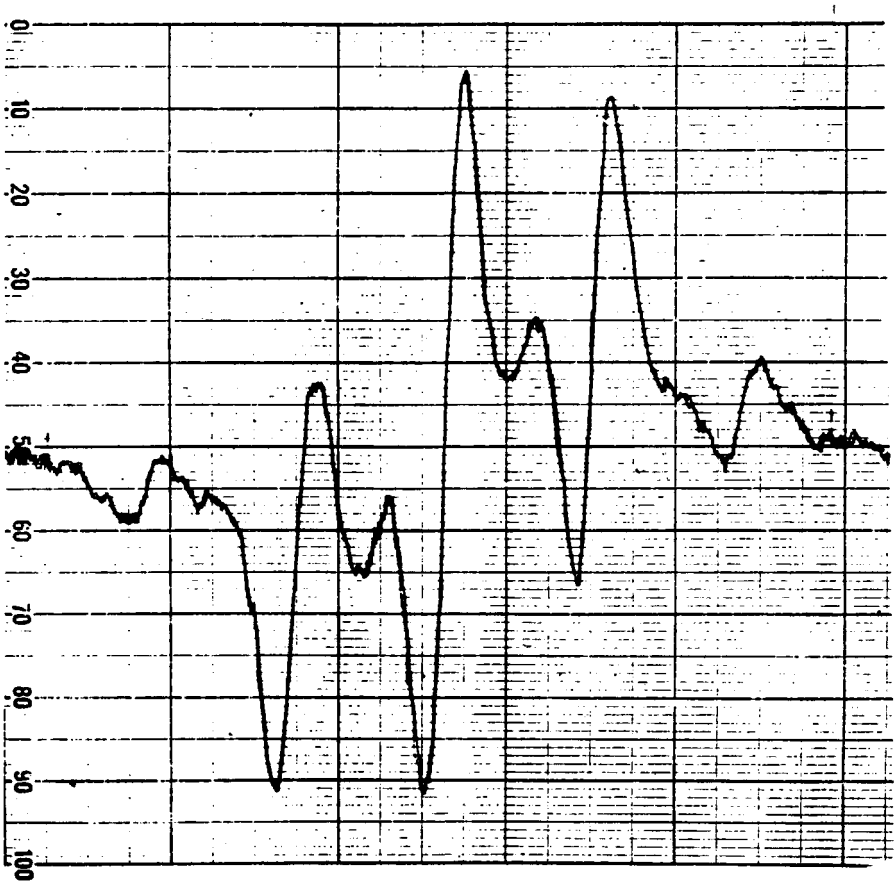

FIG. 15.

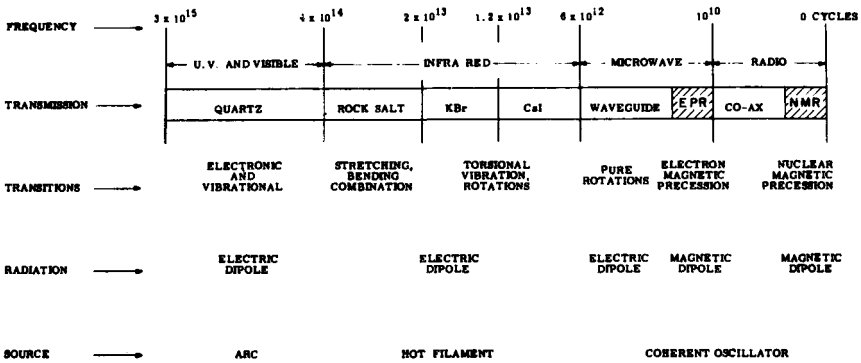

FIG. 16. Electromagnetic spectrum.

2

INTRODUCTION TO HIGH RESOLUTION NMR SPECTROMETRY

JAMES N. SHOOLERY

Varian Associates, Palo Alto, California.

HIGH resolution NMR spectrometry can be defined as the recording of more than one nuclear magnetic resonance signal from a single nuclear species as the field is swept over a small region around the value corresponding to ω/γ, where ω is 2π times the frequency of the spectrometer, and γ is the magnetogyric ratio of the nucleus. Multiple signals arise because the field at the nucleus is altered slightly by the chemical environment and also depends upon the magnetic quantum numbers describing the orientation of the spins of neighboring magnetic nuclei in the molecule. Since these "chemical shifts" and "spin–spin couplings" are seldom more than a few tenths of a per cent, even for nuclei with several shells of electrons, this definition is fairly general, although the term "high resolution" is probably most often thought of in connection with the very small shifts and splittings associated with the proton magnetic resonances in compounds containing hydrogen.

All nuclear species, with spin equal to $\frac{1}{2}$, which have reasonably large magnetic moments, and high natural abundance, yield sufficiently strong narrow lines for high resolution work. Outstanding among these are H^1, F^{19}, and P^{31}. More difficulty is encountered with C^{13}, Si^{29}, and N^{15} due to their low natural abundance and small magnetic moments. Nuclei with spin equal to one or greater usually possess nuclear electric quadrupole moments which interact rather strongly with molecular electric fields, resulting in adverse relaxation times and broad signals. In spite of this, however, B^{11}, N^{14}, and O^{17} have been found to give line widths which are somewhat less than the chemical shifts. However, because of its favorable nuclear properties and widespread occurrence in organic compounds, the hydrogen nucleus, or proton, has received the lion's share of research in high resolution NMR spectrometry.

In addition to the selection of a sample containing nuclei with suitable properties, certain other experimental conditions must be met in order to extract chemical information from the NMR spectrum. It is not sufficient simply to place in a magnet, a test tube filled with the sample, subject it to a radio-frequency magnetic field, and record the voltage induced in a coil of

wire wrapped around the tube. Considerable care is required in the construction of the magnet and placement of the sample within it, the stabilization of magnetic field strength and frequency, the selection of the amplitude of the exciting radio-frequency field, and the selection of the rate at which to sweep through the spectrum. Before considering these in detail, it is appropriate to examine two characteristics of an ensemble of nuclei precessing in a magnetic field; namely, the longitudinal or thermal relaxation time, T_1, and the transverse relaxation time, T_2.

THERMAL RELAXATION

When a sample is first placed in the apparatus, the characteristic time associated with the exponential increase in polarization of the nuclei is a measure of T_1. Any dynamical motions of the nuclear magnetic moments leading to a change in the component M_Z of the total moment, M_0, which is parallel to the applied magnetic field, are influenced by the relaxation time T_1. Since energy is required to align the nuclear moments in the magnetic field, T_1 is a measure of the ease with which energy can be exchanged between the spinning magnetic nuclei and the thermal degrees of freedom of the sample, i.e. the molecular motions. As might be expected, those molecular motions, whose characteristic frequency falls near the natural Larmor precession frequency of the nuclei for the particular field strength being used, are more effective in producing thermal relaxation. If the thermal relaxation time is too short, i.e. the Larmor frequency component of the randomly fluctuating magnetic fields in the sample is too strong, the lifetimes of the nuclear spin states will be shortened and the transitions between them, which we are trying to observe as very sharp lines, will be smeared into broad lines. If T_1 is too long, we may have to wait a very long time before any signals can be observed at all and when a nuclear polarization has finally built up, we find that our efforts to observe it perturb it so badly that we can no longer sweep slowly through the spectrum of lines and observe them under steady-state conditions. Factors contributing to a short T_1 are viscosity, which slows down the tumbling motions of molecules to frequencies nearer the Larmor frequency, high concentrations of strongly magnetic nuclei, which increase the probability that a given nucleus will see a fluctuating magnetic field, and paramagnetic impurities. Long thermal relaxation times are likely to arise in crystalline samples for which the lattice vibrations are much too high compared to the Larmor frequency or in magnetically dilute solutions from which paramagnetic impurities, especially dissolved air, have been removed.

PHASE COHERENCE

The transverse relaxation time, T_2, measures the rate at which the ensemble of precessing nuclei get out of phase with each other. It is thus a measure of the different field strengths found throughout the sample. In order to avoid

a very short T_2 which results in a broad line, it is necessary to have rapid molecular motions such that the dipolar magnetic field surrounding each nucleus averages to zero at its neighbors. High resolution work can, therefore, usually be done only with liquid or glassy samples, the local fields arising from neighbors and next nearest neighbors in crystalline solids being found to smear the resonances into hopelessly broad lines compared to the chemical shifts. Even in a liquid, there are always some molecules which move slowly enough, relative to one another, to make finite contributions to T_2. Typical values for pure organic liquids range from a few tenths to several seconds which corresponds to "natural" line widths between one-tenth and one-hundredth of a milligauss. The inhomogeneity of the magnet will usually be a more serious limiting factor in the attainable resolution than the "natural" line width, although the latter can become dominant in viscous solutions, particularly with molecules of high molecular weight.

MAGNETIC FIELD HOMOGENEITY

The first prerequisite to obtaining a high resolution spectrum is a magnet which produces a very homogeneous field over the volume of the sample. Rotating a cylindrical sample rapidly about its long axis has the effect of averaging out the inhomogeneities in directions perpendicular to this axis in much the same way as random molecular motions average out the magnetic effects of nuclei on their neighbors. If the gradients which are to be averaged out are large, however, compared with the frequency of rotation, the field at the nuclei is modulated at the rotational frequency and a series of "spinning sidebands" will arise which can be very objectionable in the recorded spectrum. Therefore, it is still necessary to begin with a highly homogeneous magnet. Furthermore, the gradient along the spinning axis cannot be averaged out and the resolution attained depends upon the flatness of the field in this direction. Needless to say, it is also important to keep magnetic "dirt" out of the sample cell and the vicinity of the receiver coil. During the past seven or eight years, the resolving power of magnets has steadily improved and it is now possible to operate routinely with resolution corresponding to a small fraction of a milligauss.

SLOW PASSAGE

In accord with a well-known principle, the narrower the resonance we are trying to observe, the more slowly we must sweep through it and the longer the time we must spend observing it. Extremely narrow NMR signals are associated with correspondingly long relaxation times which give rise to an oscillatory exponential decay following the signal unless the sweep rate is slow enough so that the resonance is traversed in a time long compared to the relaxation times. This condition is called "slow passage".

Now, the total length of a typical high resolution proton NMR spectrum

expressed as a fraction of the field strength of the instrument is about ten parts per million or for an instrument operating at 60 Mc (14,092 gauss), a sweep of about 600 c/s. If homogeneity corresponding to one c/s is achieved ($\frac{1}{4}$ milligauss), the "magnet" T_2 is about one-sixth of a second. We must spend several times this length of time going through the resonance, say one second, in order to avoid broadening and ringing. This means a sweep rate of one c/s per second or a total sweep time of ten minutes. The sweep rate required to maintain slow passage conditions and avoid distortion depends upon T_2^2 so that for lines which are much narrower than one c/s, it is not possible to record an entire spectrum free of distortion without the expenditure of an exorbitant amount of time; therefore, in such cases it is common to record only the region of interest with a suitably slow sweep rate.

ABSORPTION AND DISPERSION

The solution of the equations of motion for an ensemble of spinning magnetic nuclei precessing in a strong magnetic field shows that the total precessing magnetic moment consists of two components, an absorption and a dispersion component. These differ in their phase relationship to the driving current in the transmitter coil, the dispersion component being in phase with the transmitter field and the absorption component being out of phase. The form of these two signals is shown below in equations (1) and (2):

$$\text{Dispersion} = \frac{M_0\gamma H_1 T_2^2(\omega_0-\omega)}{1+(\gamma H_1)^2 T_1 T_2+\{(\omega_0-\omega)T_2\}^2} \tag{1}$$

$$\text{Absorption} = \frac{M_0\gamma H_1 T_2}{1+(\gamma H_1)^2 T_1 T_2+\{(\omega_0-\omega)T_2\}^2} \tag{2}$$

where M_0 is the total nuclear magnetic moment along the magnetic field axis in the absence of the radio-frequency driving field, H_1; T_1 and T_2 are the relaxation times; and $\omega_0-\omega$ is the distance in angular frequency units from the center of the resonance. It is clear from inspection of these equations that at large distances from the center of a resonance line where the third term in the denominator dominates, the dispersion component is falling off with the inverse of the distance while the absorption component falls off as the inverse square of the distance. Therefore, the absorption component is much more desirable for avoiding interference between signals which lie close together in the spectrum. It is now common practice to employ a radio-frequency phase-sensitive detector which can be adjusted to select only the absorption component for display on the recorder.

SATURATION

As the radio-frequency driving field, H_1, is increased, the signal is found to pass through a maximum when the second term in the denominator of (2) is equal to unity. At this power level, the signal is twice as broad as it would

be at very low power levels and with further increase of H_1, it broadens still further and decreases in amplitude. This phenomenon is called "saturation". It may be thought of as arising when the nuclei are depolarized by the action of the radio-frequency field more rapidly than they can be repolarized through the relaxation process, T_1. For qualitative applications of NMR, it is often possible to work very close to saturation without any deleterious effects from the slight broadening of the lines, particularly when it is necessary to achieve optimum signal-to-noise ratio. However, if quantitative comparisons are to be made between different samples or between chemically non-equivalent groups of nuclei in the same molecule (which may not necessarily have the same relaxation times), it is necessary to work at power levels about one order of magnitude lower. Although under these conditions the signal-to-noise ratio will suffer, an adequate measurement of the total area under the signal can frequently be made with an electronic integrator.

It will be recalled from the earlier discussion that due to time limitations spectra are seldom recorded under true "slow passage" conditions. The problem of saturation is, therefore, not as serious in practice as it might appear from equation (2). Intuitively, the less time we spend looking at the nuclei the less need there is for the longitudinal relaxation mechanism which repolarizes them; therefore, the saturation term containing T_1 becomes less important with increased sweep speed. In practice, it is found that this is indeed the case and although an oscillatory decay follows the signals, this results in no net area when electronically integrated and the integrals which are obtained are still found to be strictly proportional to the number of nuclei represented by the signal.

APPARATUS

In addition to the requirement of a highly homogeneous magnet, several other requirements must be met by equipment designed for high resolution work. We shall see in the next section that it is important that the field strength of the magnet be as high as possible. Furthermore, it will be of little value to us to achieve extreme resolution with a homogeneous magnet if we cannot record the resulting spectrum of lines in a linear fashion as a function of the magnetic field strength relative to some resonance which we select as a zero of reference. Therefore, the requirements of stability in the field strength and frequency are stringent indeed. Consequently, insulation of the magnet and close control of the room temperature and cooling water temperature can result in an order of magnitude improvement in the performance of the instrument.

The sensing head which contains the transmitter and receiver coils must be very carefully constructed of non-magnetic materials and must include some means of rotating the sample cell, usually a small air turbine. A typical "probe" is shown in Fig. 1. The sample is usually placed in a cylindrical

thin-walled glass cell which can be sealed if necessary and which makes the operation of filling and cleaning very simple.

Since the signals from the small samples used in high resolution NMR spectrometry can be a fraction of a microvolt in amplitude, it is necessary to employ a receiver with a large amount of amplification. A low-noise preamplifier should be used to obtain optimum signal-to-noise ratio. Close control of the transmitter field, H_1, is achieved through the inclusion of a calibrated attenuator. The transmitter and receiver, display oscilloscope, and associated sweep circuits and power supplies are often placed in a console cabinet for convenience. A photograph of the entire instrument is shown in Fig. 2.

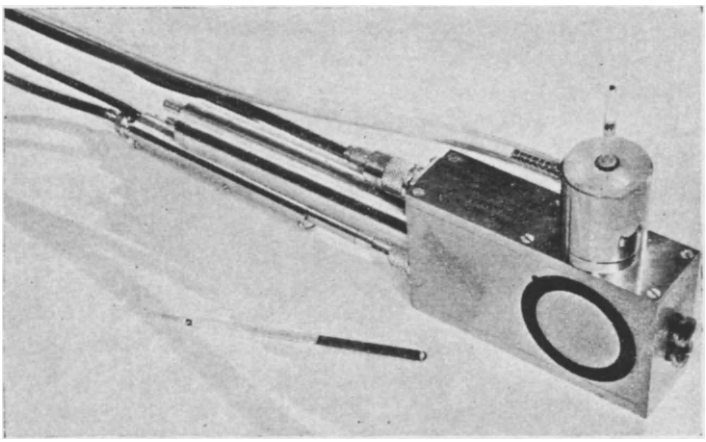

FIG. 1. High resolution probe showing air-driven turbine and typical sample tube.

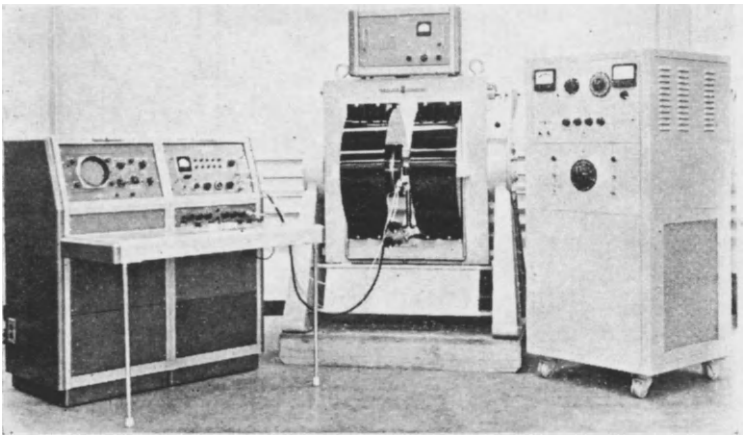

FIG. 2. Typical high resolution NMR spectrometer operating at 60 Mc.

THE CHEMICAL SHIFT

The magnetic field at the nucleus is modified slightly due to the interaction of the surrounding electrons and the applied magnetic field. Those electrons, which are described by spherically symmetric wave functions about the nucleus in question, reduce the field at the nucleus, that is, they produce a dimagnetic shielding of the nucleus. Bonding electrons, which move in more delocalized orbits, can generate magnetic fields which add to the applied field, resulting in a paramagnetic shielding. Variations in the chemical environment can result in changes in the size of both of these terms leading to a dependence of the resonance frequency upon the chemical environment. Sweeping the magnetic field or frequency will then lead to a spectrum of resonance lines whose number and position represent the various chemical bonding situations in the sample and whose intensities represent the number of indistinguishable nuclei in each bonding situation.

Chemical shifts for heavy nuclei, such as F^{19} and P^{31}, seem to depend mainly upon the extent to which an unbalanced orbital magnetic moment due to the sharing of p and d electrons along the bond axes arises. Variations in shielding of tens or hundreds of parts per million are found for these nuclei. On the other hand, the only electrons surrounding the proton are valence electrons and small changes in bonding may affect both types of terms about equally. A knowledge of the excited states of the molecule is necessary to estimate the magnitude of the second-order paramagnetism and this makes the shifts for protons particularly difficult to calculate.

When dealing with proton chemical shifts, it is important to recognize that the field at the nucleus also depends upon several other terms which may be comparable to the chemical shift. The bulk magnetic susceptibility of the solution introduces a correction term $-4\pi\kappa H/3$ for a spherical sample and $-2\pi\kappa H$ for a cylindrical sample of infinite length which must be added to the applied field to find the field inside the cell. Since the nuclei may be presumed to reside in spherical cavities in the liquid, the correction cancels out for spherical samples, but these are rather difficult to construct and use; consequently, a great deal of work is done with cylindrical samples. The net correction for a cylindrical sample is the difference between the two terms above, namely $2\pi\kappa H/3$. One way to avoid having to measure κ is to dissolve both the sample substance and the reference substance in the same solution, in which case both molecules are affected equally and no correction is needed.

A more important reason for working in dilute solution is the need to avoid the problem of intermolecular interactions, i.e. the effect of neighboring molecules on the chemical shift. If we work with pure substances or concentrated solutions, we never deal with the same neighbors from one sample to the next. On the other hand, if we always work with dilute solutions in the same solvent, the characteristic shift for a particular chemical environment will be found to be much more nearly constant from molecule to molecule.

If both sample substance and reference substance are dilute enough, the probability of interaction between them becomes negligible. Working in dilute solution requires, of course, that the sensitivity of the spectrometer be optimum.

Carbon tetrachloride makes a very good standard solvent, except for one shortcoming—it is not polar enough to dissolve a sufficiently wide variety of substances. Deuterated chloroform, $CDCl_3$, is available commercially in high purity and has been found suitable in a high percentage of work. Both of these solvents readily accommodate the inclusion of 1 percent of tetramethylsilane, which gives a strong sharp resonance at the extreme high field end of the spectrum and which does not appear to become readily involved in intermolecular interactions. Figure 3 shows some typical chemical shift

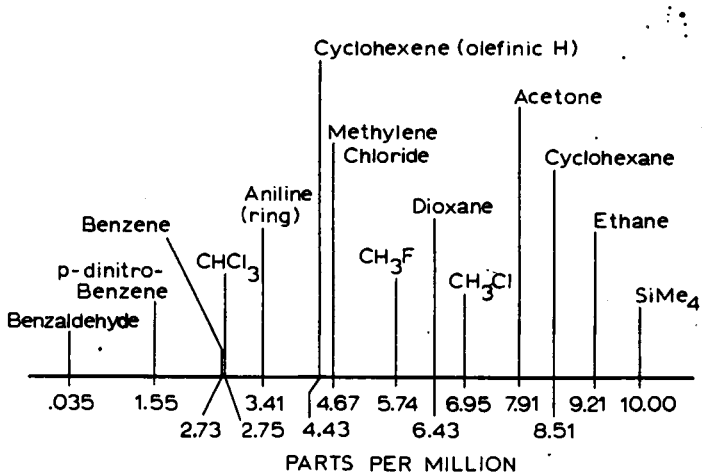

FIG. 3. Some chemical shifts in dilute CCl_4 solution.

values measured in dilute $CDCl_3$ relative to internal tetramethylsilane.

The unique solvent properties of water make it necessary to use D_2O as the solvent in some cases. Unfortunately, tetramethylsilane is insoluble in water and in order to bring the chemical shifts measured in water into line with those measured in chloroform, it is necessary to use a secondary standard which will dissolve in both water and chloroform. For example, the methyl groups in tertiary butyl alcohol could be measured relative to tetramethylsilane in chloroform and then dissolved in water and measured relative to tetramethylsilane contained in an external annular space surrounding the sample. These data would allow the use of tetramethylsilane as an external standard for measuring the chemical shifts in water solution which could then be converted to compare with chemical shifts measured relative to tetramethylsilane in chloroform. Of course, this procedure does not take

into account the different solvent effects of water and chloroform on the chemical shifts.

The same referencing procedure can be used when it is necessary to use deuterated acetone, pyridine, or trifluoroacetic acid in order to dissolve a particularly stubborn compound. Some caution must again be used in interpreting the results, however, since some of these solvents affect different molecular species to different degrees.

It is important to note that since the chemical shift arises from an interaction of the electrons with the applied field, the magnitude of the shift is linearly proportional to the strength of the field. If the resonance lines from all groups were single sharp lines, it would be necessary only to apply sufficient magnetic field to give chemical shifts which would be distinguished with the available resolution of the instrument. However, we shall see that interactions exist between the nuclei, splitting the resonances into overlapping groups of lines and posing an interpretational problem which can be very formidable unless the groups are separated as much as possible. Therefore, it is of paramount importance that the magnetic field be made as high as practical considerations permit.

The field dependence of the chemical shift has led to considerable confusion in the literature when the shifts have been given in units which were not dimensionless. For example, chemical shifts in milligauss or in c/s vary from one instrument to the next depending upon the field strength employed. In 1953, Gutowsky defined a chemical shift parameter, δ, as the field shift between the reference and the sample compound divided by the total applied magnetic field and expressed in parts in 10^5. Water was usually chosen as the reference substance. More recently, some workers have preferred to express the shifts in parts per million on a scale for which the resonance of the internal reference compound tetramethylsilane is defined as 10.00. This leads to the following definition:

$$\delta^{\text{int}}_{\text{SiMe}_4}(f) = 10.00 - (\nu_f - \nu_{\text{SiMe}_4})/\nu_0 \tag{3}$$

where f is the functional group being defined, $(\nu_f - \nu_{\text{SiMe}_4})$ is the frequency separation of the two resonances, and ν_0 is the operating frequency of the instrument. The frequency separation of the signals is best measured using the audio sideband calibration technique of Arnold and Packard.* A small oscillating magnetic field component is applied by means of an audio-frequency oscillator to the sweep coils, resulting in small sideband signals spaced ν cycles away from each line in the spectrum. Super-position of these signals can be accomplished either by observing the oscilloscope presentation or recording the spectra for various values of ν. If the lines are sharp and the resolution of the instrument is good, chemical shifts can be measured in this

* J. T. Arnold and M. E. Packard, *J. Chem. Phys.* **19**, 1608 (1951).

way to within a few hundredths of a cycle per second. If accuracy of this degree is desired, it is also necessary to measure the period of the modulating sine wave to the required number of decimal places using precision electronic frequency counters. For many applications, however, an accuracy of about one c/s is adequate.

SPIN-COUPLING BETWEEN NUCLEI

Although direct magnetic dipole–dipole coupling between nuclei averages to zero for rotation of the molecules, an indirect coupling exists which does not average out with rotation and is found to have the form $J_{12}(I_1 . I_2)$. The coefficient J_{12} measures the strength of the coupling and is expressed in cycles per second while I_1 and I_2 represent the spin angular momenta of the nuclei in units of $h/2\pi$. Therefore, the whole term has the dimensions of energy. This coupling is presumed to arise because of the interaction of the nuclei with the electrons in the intervening bonds. The instantaneous orientation in space of the nucleus is "telegraphed" to the neighboring nuclei in the form of a small component of magnetic field which is superimposed upon the strong field due to the magnet. To a very high order of approximation, the spin-coupling is independent of the strength of the applied field. The effect is found to be transmitted through several bonds, usually but not always with diminishing intensity, and to show a strong dependence upon the bond type and bond angles.

If the resonance frequencies of the coupled nuclei are far apart (large chemical shift or different nuclear species) compared to the coupling, then the precessing components of magnetic field transmitted via the electrons average out, leaving only a term due to the z-components. But there are just $2I+1$ possible values of m, the quantum number describing the z-component of angular momentum, and, therefore, each nucleus splits the resonance of its neighbor into $2I+1$ components. The energy differences between the various spin states are so small that at thermal equilibrium the Boltzmann distribution makes them all equally probable; therefore, all the lines in a multiplet resulting from coupling to a single nucleus are equally intense. If, however, several indistinguishable nuclei couple their spins to a neighbor, the neighbor is split into $2I+1$ lines where I is the total spin corresponding to the sum of the spins of all of the nuclei in the group. In this case, the same value of m can result from several different ways of aligning the indistinguishable nuclei. For nuclei of spin $\frac{1}{2}$, e.g. protons, the intensities of the lines in the multiplet follow the binomial coefficients. An example of this is given in the spectrum of pure ethyl alcohol shown in Fig. 4. The spin orientations leading to the different statistical weights for the various lines in the spectrum have been indicated on the chart.

Since consecutive values of m differ by one unit of angular momentum, the lines in a spin multiplet are equally spaced. Furthermore, the nucleus or

group of nuclei which splits neighboring nuclei into a multiplet is itself split into a multiplet with the same spacing. This test should always be applied when making spectral assignments. For nuclei with spin $\frac{1}{2}$, the number of lines in each multiplet is just $N+1$ where N is the number of nuclei in the neighboring groups. This simple rule allows high resolution NMR spectrometry to be used for the determination of some molecular structures in a very direct way.

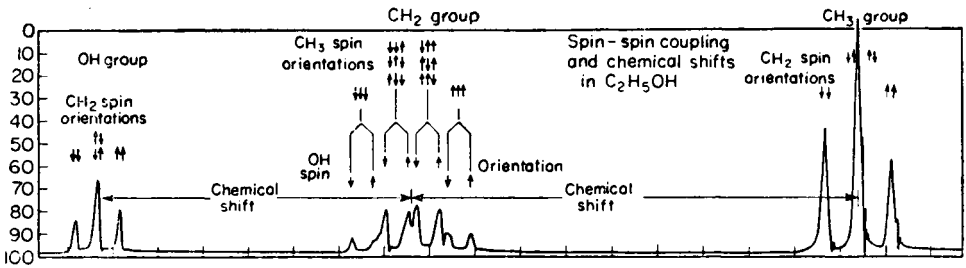

FIG. 4. First order interpretation of spin-coupling in pure ethyl alcohol.

If an isotopic substitution is made in a molecule, for instance the replacement of a proton with deuterium, the number of lines in the spin multiplet due to that proton will change according to the change in I and the spacing will diminish according to the nearly seven-fold decrease in the magnetogyric ratio, γ. This often provides a very unequivocal way to determine where such an isotopic substitution has occurred in a complex molecule, and to measure its extent.

THE CASE WHERE δ/J IS GREATER THAN 5 AND LESS THAN 15

If the spin-couplings are small compared to the chemical shifts but are not negligible, corrections of various orders can be calculated for the line separations and intensities using perturbation theory. In this range of δ/J, many of the lines of the multiplets may be split further (often called second-order splitting) although the additional splittings may not always be resolved. As a general rule, two groups of coupled nuclei give multiplets whose intensities are perturbed in such a way that the inner lines are intensified and the outer lines are weakened. This generally does not interfere with the straightforward interpretation of the spectrum.

EXACT SOLUTIONS

If the resonance frequencies are not far apart compared to J, it becomes necessary to keep track of the effect of the x- and y-components of the nuclear moment. Line positions and intensities can become greatly perturbed and it is necessary to make an exact solution by writing the total energy for the

coupled system and calculating matrix elements of this total energy, using as wave functions linear combinations of the stationary state wave functions of the unperturbed system. If all the particles are of spin $\frac{1}{2}$, a secular equation of order 2^p results for p particles. The extent to which this equation may be factored depends upon the symmetry of the molecule. Some solutions for typical groups of nuclei will be discussed in the lecture on structural applications.

SOME SIMPLE STRUCTURAL APPLICATIONS

Although in general it is necessary to unravel the NMR spectrum of a complex molecule and express it in terms of the chemical shifts and spin-coupling parameters before attempting to draw conclusions concerning the molecular structure of the sample, it is quite frequently possible to solve such problems by simple inspection of the NMR spectra. It is appropriate to examine two such cases at this point in order to obtain a better feeling for the application of the principles discussed in the preceding sections.

The first example is shown in Fig. 5 in which the problem was to determine

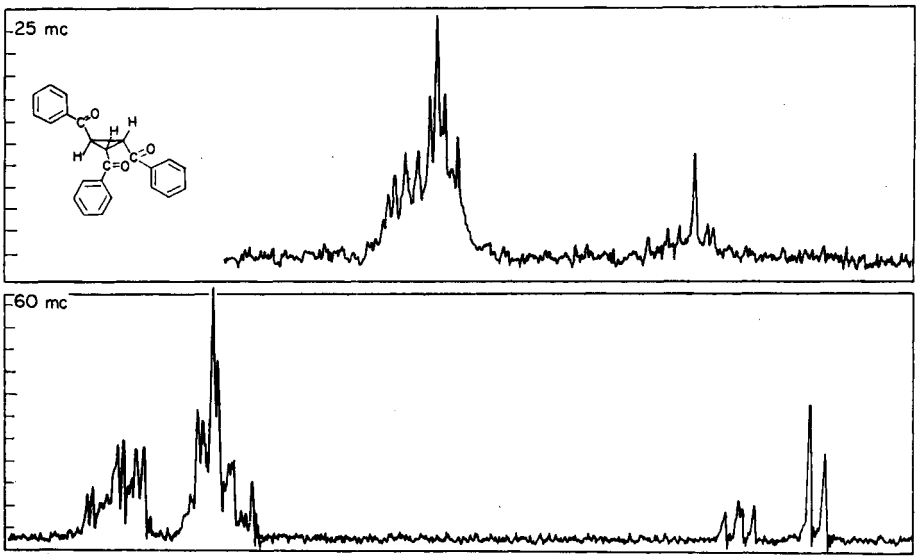

FIG. 5. The NMR spectrum of a tri-substituted cyclopropane.

whether the synthesis of a tri-substituted cyclopropane had resulted in the cis- or trans- configuration of the molecule. The trans- configuration is illustrated and the cis- configuration would differ from it in that the three hydrogen atoms would all be located on the same side of the cyclopropane ring. In the latter case, the complete equivalence of the three protons would lead us to expect no chemical shift or spin–spin coupling between them, and

a single sharp line would be found in the region characteristic of alicyclic hydrocarbons. A glance at Fig. 3 suggests that if cyclopropane protons behave anything like those in cyclohexane, we would expect their signals at the high field or right-hand end of the spectrum, while the benzene ring protons would give a resonance at the low field or left-hand end of the spectrum. The spectrum of the trans-isomer would be expected to show two multiplets in the alicyclic region, a triplet with unit intensity and a doublet with twice that intensity, due to the non-equivalence of the protons on the opposite sides of the 3-membered ring and the spin-coupling between them. This is very evident in the lower trace of Fig. 5 and the structure is thus established as the trans-isomer. This example also illustrates the need for operating at the highest possible magnetic field strength since the collapse of the chemical shift at 6000 gauss (25 Mc) has run the two spin multiplets together and perturbed their intensities so badly that the interpretation becomes very uncertain.

It is a particularly simple matter to determine whether or not a bond exists between two unlike nuclei. Pentaborane, B_5H_9, is an interesting molecule whose structure is described by a tetragonal pyramid of boron atoms each bonded directly to one hydrogen atom, and with four "bridge" hydrogens located symmetrically about the base of the pyramid. The four "basal" boron atoms are thus equivalent and different from the fifth "apex" boron atom. The resonance of each B^{11} atom is split into a doublet by spin-coupling to the directly attached proton, as shown in Fig. 6. A monobromo derivative

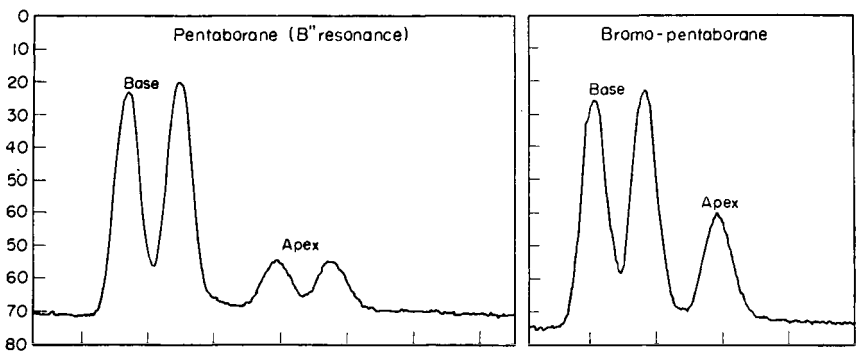

FIG. 6. Determination of the structure of mono-bromo pentaborane from the B^{11}-resonance.

of pentaborane can be prepared whose structure is not readily determined unequivocally by chemical or spectroscopic techniques. The high resolution NMR spectrum of the B^{11} nuclei in this compound shows immediately, however, that the "apex" boron no longer couples its spin to a hydrogen nucleus and it can, therefore, be presumed that the bromine replaces the hydrogen at the *apex* of the pyramid.

CHEMICAL EXCHANGE

If a mechanism exists for the rapid exchange of protons between two species as in the reaction:

$$HA + B \rightleftharpoons HB + A$$

the resulting proton NMR spectrum will be a single concentration-dependent resonance with a chemical shift given by the weighted average of the shifts for each species:

$$\delta = p_1\delta_{HA} + p_2\delta_{HB} \tag{4}$$

where p_1 and p_2 are the fractions of protons in HA and HB respectively.

On the other hand, if HA and HB do not exchange protons, the two resonances at δ_{HA} and δ_{HB} will be observed. Gutowsky and Saika (*J. Chem. Phys.*, **21**, 1688 (1953)) have calculated the behavior of the spectrum for intermediate exchange rates described by an average lifetime, τ, and found that the transition from two sharp lines to a single sharp line occurs as the quantity $2\tau\delta\omega$ is varied from 100 to 10^{-2}. When $2\tau\delta\omega = 10$, the two original lines have broadened and when $2\tau\delta\omega$ reaches 1, these broadened lines have merged to a single broad line at the average frequency. The quantity $\delta\omega$ is the chemical shift expressed in angular frequency units and is 2π times the separation of the lines in cycles per second.

It is perhaps useful to consider the exchange phenomenon in terms of the precessing magnetic moments of the nuclei. In a frame of reference, rotating at the Larmor frequency of the ensemble of protons in the species HA, protons in the species HB will appear to precess at a relative angular frequency $\delta\omega$ radians per second. If the exchange were slow, we would have two discrete ensembles of protons, each made up of a large number of individual protons precessing in phase. If exchange takes place which is rapid compared to $1/\delta\omega$, i.e. if $2\tau\delta\omega \ll 1$, a proton which jumps from the ensemble HA to HB will remain there, on the average, at a time so short that the nuclear moment vector cannot get appreciably out of phase with the remainder of the ensemble. However, since the precession frequency is slightly different during the time spent in the ensemble HB, the *average* frequency of *all* of the protons becomes equal to the weighted average of the two frequencies. Then, although none of the protons precess at exactly that frequency, they spend part of their time going slightly faster, part of their time going slightly slower, and, on the average, never get more than a few degrees out of phase with the total precessing nuclear moment. If $2\tau\delta\omega$ becomes approximately equal to 1, the average time spent in either HA or HB is just long enough to completely lose phase-coherence with the ensemble, and the nuclear moment rapidly becomes randomly distributed in the x–y plane. A low, broad signal results.

In order to study the exchange rate, it may be desirable to vary the magnetic field strength. The τ remains constant and $\delta\omega$ changes linearly with the

applied field. About a ten-fold range of field can be covered. If it is not possible to get into the transition region in this way, it may be possible to adjust τ by changing the concentration. Finally, τ is temperature dependent, and a large range of τ can be covered by varying the temperature 50°C to 100°C above and below room temperature. If temperature can be varied and accurately measured in the transition region, it is possible to determine the activation energy for the exchange.

POTENTIAL BARRIERS

A special case of exchange between non-equivalent groups occurs when the groups can be interconverted by penetrating or going over a potential barrier. An example is dimethyl formamide in which partial double bond character of the CN bond introduces a barrier to free rotation which, at room temperature, forces one methyl group to remain closer to the oxygen than the other for an average time, τ.

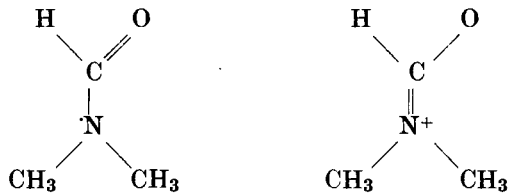

The rate of exchange depends upon a frequency factor and the probability that the particular rotational degree of freedom will have acquired enough thermal energy from the surroundings to go over the barrier. Thus, the rate, which is proportional to $1/\tau$, is given by:

$$1/\tau = \nu_r \exp(-\Delta E/kT) \tag{5}$$

where ν_r is the number of times per second the molecule tries to overcome the barrier, and the Boltzmann factor determines the probability of success per attempt.

In principle, τ can be determined by the shape of the resonances in the transition region, and two measurements would allow elimination of ν_r or ΔE and the solution for both unknown quantities. Figure 7 shows the proton NMR spectrum of dimethyl formamide at 40 Mc. Chart B in Fig. 7 shows the collapse of the two methyl resonances into a single line as the temperature is raised from 25°C to 117°C. Gutowsky and Holm have analyzed this problem in detail and developed a method for determining τ from the measured separations of the peaks. A barrier height of several kilocalories is obtained.

COMPLEX FORMATION

When proton exchange occurs between two species which are involved in an equilibrium, the position of the proton resonance involving the exchanging

protons will be dependent upon the equilibrium constant and the concentrations. For example, consider the formation of the complex: $A+B = AB$

$$K = \frac{(X)(A+B-X)}{(A-X)(B-X)} \tag{6}$$

where K is expressed on a mole fraction basis and

X = moles AB present
A = moles A originally present
B = moles B originally present

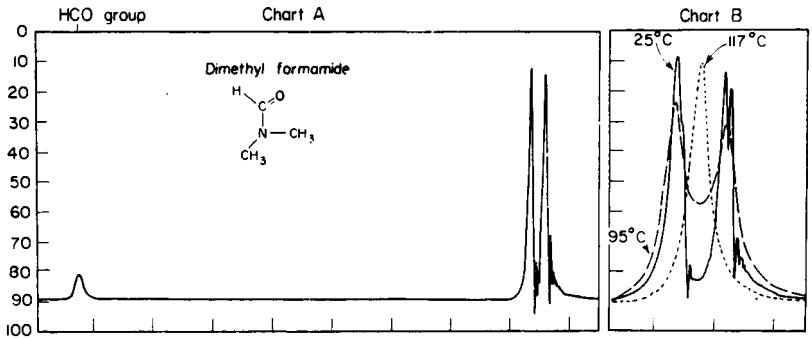

FIG. 7. NMR spectrum of dimethylformamide showing effect of temperature on methyl resonances due to hindered rotation about C–N bond.

To relate the NMR measurements to K, we employ equation (4) and write:

$$\omega_{\text{obs}} = \frac{X}{A}\omega_A + \frac{A-X}{A}\omega_{AB} \tag{7}$$

which is the weighted average of the resonance frequencies for the rapidly exchanged proton in the complexed and uncomplexed species.

There are four unknown quantities in (6) and (7). The two equations can be used to eliminate one of these quantities, say X. Another of these, ω_A, can be measured in pure A. At infinite dilution of A in B, $A \to 0$ and $X \to 0$; however, from (6):

$$\frac{X}{A-X} \to K$$

then

$$(\omega_{\text{obs}})_{A\to 0} = \frac{1}{1+K}K\omega_{AB} + \omega_A \tag{8}$$

Solving for ω_{AB} in terms of K: (writing $(\omega_{\text{obs}})_{A\to 0}$ as $\omega_{A\to 0}$)

$$\omega_{AB} = \omega_{A\to 0} + \frac{1}{K}[\omega_{A\to 0} - \omega_A] \tag{9}$$

The quantity in brackets is just the total shift over the concentration range from pure A to pure B, extrapolated to $A \to 0$.

From K and ω_{AB} the entire curve of ω_{obs} vs. the composition of the solution is determined. Although one measurement in the middle range of concentration is all that is required, it is better to plot the entire curve using several assumed values of K and compare with experiment to see which value gives the best fit over the entire range of concentration. Since:

$$\frac{d \log K}{dT} = -\frac{\Delta H}{RT^2}$$

we can determine the heat of formation of the complex by NMR shift measurements at several temperatures. The slope of the log K vs. $1/T$ plot gives $\Delta H/R$.

HYDROGEN BONDING

The interaction between a proton attached to a strongly electronegative element and the negative end of another dipole (such as a C–O bond) is called a hydrogen bond. A reasonable picture of this interaction is an electric dipole–dipole attraction which places the proton against the negative end of the attracting dipole, partially extracting the proton from its bonding electron cloud and distorting the electron wave functions in the strong electric field. A shift to lower applied fields results. The magnitude of this shift depends upon the strength of the hydrogen bond.

Although a proton may or may not remain bonded to its parent molecule, the breaking and reforming of hydrogen bonds places it in alternate situations of higher and lower magnetic field strength. If the process occurs rapidly compared to the frequency shift, a situation similar to proton exchange exists and the analysis is quite similar. Figure 8 shows the observed shifts of the proton resonance in chloroform as a function of the concentration. The best

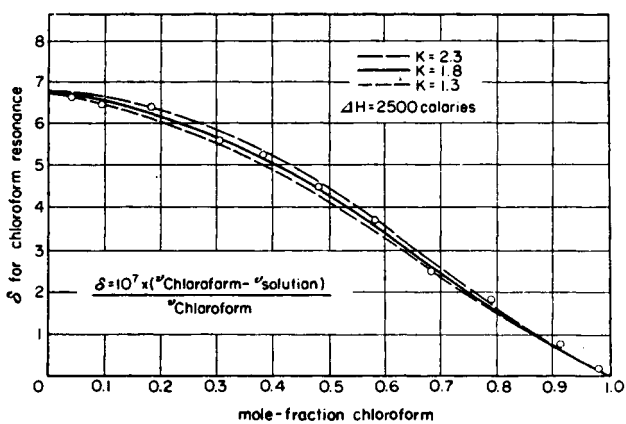

FIG. 8. Equilibrium constant for the system chloroform + acetone.

fit is the solid line calculated for an association constant, $k = 1.8$. Observation at two temperatures allowed an estimate of the heat of formation, $\Delta H = 2.5$ kcal.

Further complications arise beyond those met in a simple complex formation due to the tendency of intermolecular hydrogen bonding to be carried beyond the dimer state with resulting formation of trimers and polymers. The equilibrium constants for trimer and polymer formation are different than K_{dimer}. Therefore, it becomes difficult to relate K_{dimer} to the entire curve of δ vs. concentration, but it has been found that an estimate of K_{dimer} can be obtained by considering the limiting slope at infinite dilution in an inert solvent.

From a qualitative standpoint, it is quite easy to determine which resonances in the spectrum represent protons involved in hydrogen bonding (or other complex formation) and to determine whether the complex is intermolecular or intramolecular. First, the resonances will show a temperature dependence due to a shift of the equilibrium between the bonded and nonbonded species. Intermolecular complexes will show a concentration dependence, while intramolecular complexes will not.

An indirect observation of hydrogen bonding is sometimes possible in large molecules in which the presence of such an interaction results in aggregates of high molecular weight being formed. The molecular-tumbling frequencies are reduced to the critical region where they do not completely average out direct dipole–dipole broadening between neighboring protons in the molecule. A sharpening of all resonance lines then occurs when the hydrogen bond-forming proton is replaced by an inactive group, such as occurs when the acetate derivative is made from a hydroxyl group. Only monomeric molecules can exist in the acetate derivatives and their higher tumbling frequencies result in the observed line narrowing.

It is not uncommon to find that in obtaining the spectrum of a complex molecule a hydroxyl group may not be detected. This is probably due to the breaking and reforming of hydrogen bonds at a critical frequency near the frequency shift resulting from the formation of the hydrogen bond. Under these circumstances the resonance can be smeared out into a line too broad to detect. Another possible explanation is exchange between the hydroxyl proton and small traces of water which may be present either in the sample or the solvent, or adsorbed on the walls of the cell. It is probably a good practice to dry the NMR sample cells in an oven and to take suitable precautions to maintain the solvents as anhydrous as possible.

SENSITIVITY

The need to study extremely weak signals frequently arises in high resolution NMR spectrometry. Studies of complex formation require measurements at high dilution which can be extrapolated to infinite dilution; avoidance

of intermolecular interaction effects and viscosity broadening often dictate the use of very dilute solutions; studies of higher and higher molecular weight compounds lead to ever decreasing molar concentrations and increased probability that the proton being studied will be spin-coupled to neighboring protons, thus splitting the intensity among a number of lines; and finally, many of the more interesting compounds are only slightly soluble in suitable NMR solvents.

We could achieve higher sensitivity simply by increasing the amount of radio-frequency amplification of the signal if it were not for the presence of random noise in the electrical circuits. Most sources of noise can be eliminated by good instrument design, but the Johnson noise due to the thermal agitation of the electrons in the receiver coil sets a limit on the sensitivity of the instrument. A certain amount of noise contributed by the first stage of amplification is unavoidable, the difficulty of maintaining a good "noise figure" increasing with the frequency. A typical noise figure of around 3 dB means that twice the noise power or 1.4 times the noise voltage is amplified when the receiver coil is connected to the amplifier compared to a short-circuited coil. Further improvement in the noise figure, which could be obtained only with great difficulty, would improve performance by less than 40 per cent so that it is apparent that exhaustive effort in this area will lead to diminishing returns.

A more dramatic effect is observed with variations in the "filling factor" which for a cylindrical sample is given by the ratio of the cross-sectional area of the sample to that of the coil. Factors of two or three in performance can be achieved by using thin-walled sample tubes so that the sensitive volume of the receiver coil is filled with the sample rather than with glass or other inert material.

The strength of the signals induced in the receiver coil depends upon the square of the magnetic field strength, everything else being equal. The difficulties of maintaining the same circuit performance at higher frequencies partially offsets this gain but the combined improvement in sensitivity *and increased chemical shifts* can be the deciding factor in determining whether or not a particular problem can be solved by NMR spectrometry.

Two other factors are of importance in regard to sensitivity. The first is the Q of the receiver coil. The signal-to-noise ratio is proportional to the $\sqrt{Q}$ so that elaborate means to increase Q by a slight amount are not justified. However, the high-Q coils used in high resolution work tune very sharply and can accidentally become detuned rather easily. This has the same effect as a drastic reduction in Q and can affect the performance adversely unless the tuning is checked from time to time. The second factor which influences signal-to-noise is the "band width" of the receiver system. This is determined by the time constant of the filter circuit at the output of the phase-sensitive detector. Since the noise is proportional to the square root of the band width,

it is necessary to narrow the band width by a factor of 100 in order to decrease the noise by a factor of 10. In order not to filter out the desired signals, the time of observation must be increased by 100. This may or may not be possible depending upon the stability of the instrument and the importance of the data being obtained. There is usually some compromise between these factors which determines the optimum band width.

It is instructive to examine the spectrum shown in Fig. 9 which illustrates the signal-to-noise problem and the results obtained in a typical case. This

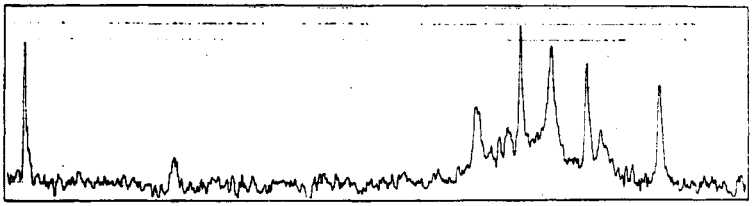

FIG. 9. NMR spectrum of a dilute solution of a steroid.

spectrum was made with 1.3 mg of a steroid with a molecular weight of about 350. The solvent used was deuterated chloroform, the strong peak at the left resulting from the 0.3 per cent $CHCl_3$ remaining in the $CDCl_3$. A thin-walled glass sample tube was used and the sample was dissolved in 0.2 cm^3 of solvent trapped between two precision nylon plugs to permit spinning the sample without formation of a vortex. The molar concentration was, therefore, 0.02 M. One proton in the molecule is attached to a doubly bonded carbon atom and, although broadened somewhat by spin-coupling, is clearly visible as the second peak from the left. The strong peaks at the right-hand end of the spectrum result from methyl groups, each containing three equivalent protons. Comparable results can be obtained with similar amounts or concentrations of other complex organic substances.

OTHER APPLICATIONS

The adduct of dimethylaminopropylamine and formaldehyde is believed to have the structure (I):

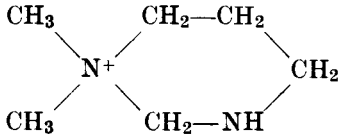

(I)

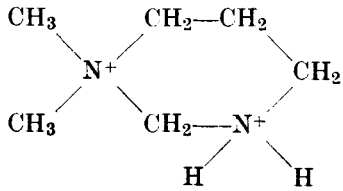

(II)

In acid solution, the compound has structure (II) and slowly hydrolyzes back to dimethylaminopropylamine and formaldehyde. The spectrum of the unhydrolyzed compound in H_2O is shown in the upper left-hand corner of Fig. 10. The strong sharp peak located approximately 2.3 p.p.m. from the H_2O resonance arises from the two methyl groups attached to the nitrogen. Dilution with an equal quantity of 12 NHCl results in the spectrum at the lower left of Fig. 10. The absence of any spin-coupling which would result in a doubling of the peak at 2.3 p.p.m. shows that the nitrogen is forming four bonds to a carbon and therefore cannot accept a proton in acid solution. The small doublet at 2.0 p.p.m. arises from the hydrolysis product, dimethylaminopropylamine hydrochloride, in which a proton has become attached to the nitrogen atom bearing the two methyl groups and couples its spin to them. Looking again at the upper left-hand corner of Fig. 10, we see a small

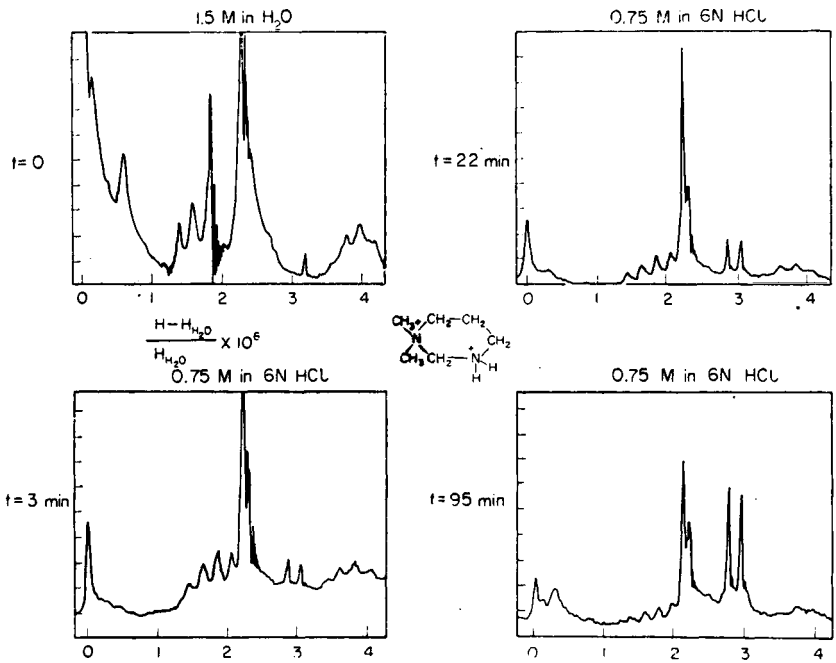

FIG. 10. Rate of hydrolysis studied by NMR.

peak near 3 p.p.m. which represents a small amount of the hydrolysis product initially present at $t = 0$. This peak does not show spin-coupling in neutral solution because the proton does not remain attached to the nitrogen long enough. In the upper right-hand corner of Fig. 10, we see that after 22 min the hydrolysis has proceeded significantly further and in the lower right-hand corner at $t = 99$ minutes, the hydrolysis is about two-thirds complete. It would be a relatively simple matter to study the rate of this reaction by

the use of the high resolution NMR method without disturbing in any way the course of the reaction.

A MORE DIFFICULT STRUCTURAL PROBLEM

The irradiation products of santonin have been the subject of considerable interest, photosantonic acid representing a particularly perplexing case. The absence of a peak at 210 mμ in the ultraviolet, characteristic of conjugated dienes, had discouraged widespread acceptance of the formula given below:

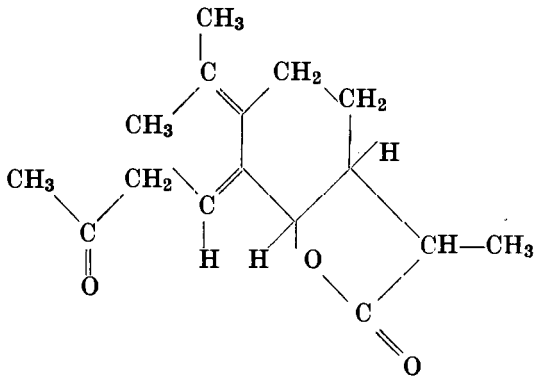

This compound, the methyl ester of photosantonic acid, gives a triplet resonance at 55 c/s* relative to benzene in an external annular space surrounding the sample. This indicates an olefinic proton adjacent to a CH_2 group. We find a doublet with the same spacing at 216 c/s which represents the CH_2 group between the doubly bonded carbon atom and the carbomethoxy group. The assignments for the four methyl groups in the compound are written alongside of the structural formula in Fig. 11. The most important feature of the spectrum, which is compatible with this proposed formulation but with none of the other structures which have been proposed, is the appearance of further small doubling of each of the peaks in the multiplet at 55 c/s and also, with a slightly differing spacing, in each of the peaks near 216 c/s. There is, therefore, another proton in the vicinity of these two groups. The observed couplings are long range, going through four bonds in the case of the olefinic proton and five bonds in the case of the CH_2 group.† The proton

* Since the compound was studied in dilute CCl_4 solution, we can readily convert chemical shifts measured in cycles per second at 60 Mc relative to external benzene to a scale relative to internal tetramethylsilane by subtracting from 385. At 60 Mc this is 5.50 p.p.m., or 4.50 on the scale with tetramethylsilane equal 10.00. This can be compared with the value of 4.43 for the olefinic proton in cyclohexene shown in Fig. 3.

† It has frequently been observed that although the coupling diminishes with each additional intervening chemical bond, the transmission of spin-coupling effects is much better across a trans-double bond than across a cis-double bond. Therefore, the four and five bond couplings observed in this molecule might be expected to be about the same order of magnitude if the structure is written as shown.

which is responsible for the additional coupling is located on the carbon atom adjacent to the oxygen of the lactone ring. The resonance of this proton appears at 148 c/s due to the electron withdrawing effect of the oxygen. It is split into a doublet due to spin-coupling with the proton on the adjacent carbon atom and each component of the doublet shows a broadening due to

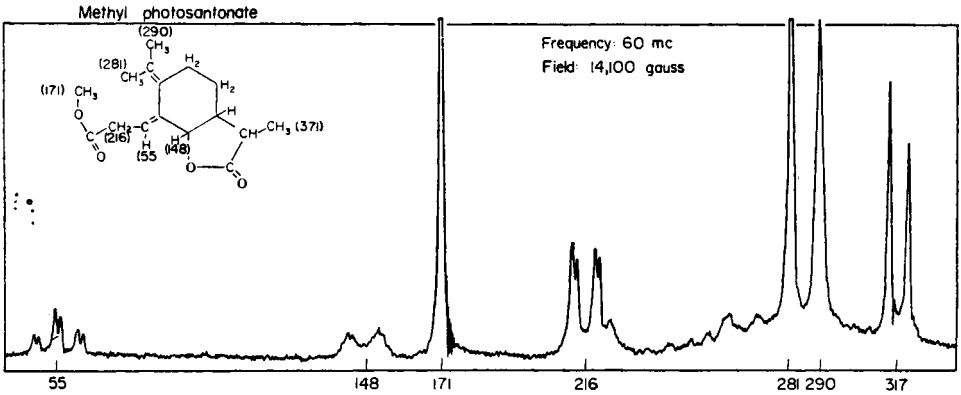

FIG. 11. Structure of photosantonic acid.

the unresolved long-range couplings. Steric interactions between the bulky substituents which result in out-of-plane distortions and decreased π-electron overlap have been proposed to account for the lack of the 210 mμ ultraviolet peak, and probably also account for the distinctly different environment of the methyl groups at 281 and 290 c/s.

CONCLUSION

In addition to the few examples given here, high resolution NMR spectrometry has proven of immense value in a great many problems of chemical structure determination. This is properly the topic of a separate lecture in which the relationship between molecular structure and chemical shift and spin-coupling parameters will be more fully explored along with methods of interpreting actual spectra in terms of these parameters.

3

EPR SPECTROSCOPY

R. H. SANDS

Department of Physics, The University of Michigan, Ann Arbor, Michigan

What is it? What can it do? and How sensitive is it?—these three questions are answered and several examples are shown in regard to applications.

INTRODUCTION

THE phenomenon of EPR (Electron Paramagnetic Resonance*) depends upon the fact that electrons have charge, mass, angular momenta and magnetic moments and therewith interact with their surroundings. EPR makes use of these properties to reveal chemical structure and bonding characteristics with high sensitivity and resolution.

It is necessary for the substance under study to have a resultant electronic magnetic moment: furthermore, this magnetic moment must be such that the material is paramagnetic—the individual magnetic molecules must be independent in first order. Nevertheless, the fields of application are many and varied; for example, one may detect transition element ions, impurities in semi-conductors, electrons in unfilled conduction bands, electrons trapped in radiation damage sites, odd molecules and free radicals, bi-radicals and triplet electronic states. Such observations may lead to identification, one of the fundamental roles of any form of spectroscopy, and to the determination of a variety of information, such as the chemical kinetics of one electron transfer under oxidation-reduction, odd electron wave functions and hence possible chemical activities at various positions around polyaromatic free radicals, electron exchange rates, crystalline and molecular structures, and the extensions and characteristics of conduction band and trapped electrons in metals and semiconductors. Not only is EPR a basic research tool, it also has applications for solid state amplifiers, radiation dosimetry and process control. In summary, one may say that electron paramagnetic resonance

* For an introduction to the fundamentals of EPR the author recommends two review articles: (*a*) G. E. PAKE, "Nuclear Magnetic Resonance", *Adv. Solid State Phys.*, Vol. II., Chapter I, ed. F. Seitz, Academic Press, 1956, and (*b*) J. E. WERTZ, "Nuclear and Electron Spin Magnetic Resonance", *Chem. Rev.* **55**, 829 (1955). There is a book on NMR, E. R. ANDREW, *Nuclear Magnetic Resonance*, Cambridge University Press, 1955, and two books on EPR, D. J. E. INGRAM, *Spectroscopy at Radio and Microwave Frequencies*, Butterworths, 1955, and D. J. E. INGRAM, *Free Radicals as Studied by Electron Spin Resonance*. Academic Press, 1958.

spectrometry has become not only a basic tool in physics, chemistry and biology, but has also acquired importance in the field of electrical engineering. It becomes important, then, that EPR be evaluated for all concerned; this is the purpose of the next few pages.

DETECTION

As an aid toward understanding the phenomenon of Electron Paramagnetic Resonance it is convenient to visualize a typical experiment. One may rigorously describe an electron as a tiny gyroscope having a magnetic moment along the axis of angular momentum.[1] This affords a convenient method for describing the phenomenon of Electron Paramagnetic Resonance. Most of us have played with toy gyroscopes and have been intrigued with the precession of these gyroscopes caused by the torque exerted by the gravitational field of the earth. Were we to adjust the strength of this gravitational field by moving farther and farther away from the earth, we would find that the precession frequency is proportional to the magnitude of the applied torque. In the case of the free electron, however, it is not possible for us to reach out and grab hold of its axis in order to exert this torque. Nevertheless, there is a handle by which we may effect the required torque. This handle is its intrinsic magnetic moment tied rigidly to its axis of angular momentum such that when a strong magnetic field, H_0, is applied to the electron as shown in Fig. 1, there is a torque acting in such a way as to make the electron

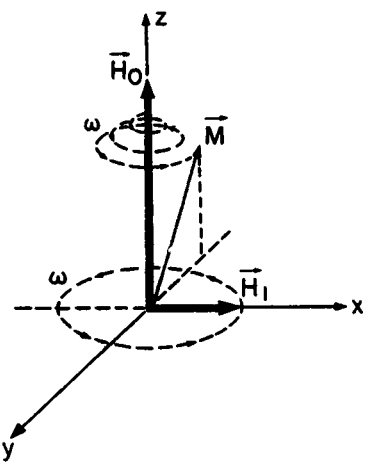

FIG. 1. Precessing electron moment.

precess with a frequency which is both proportional to the applied magnetic field, H_0, and to the electronic magnetic moment. This frequency is called the Larmor precession frequency and its value is given by the relation $\omega = \gamma H_0$, where γ is the "gyromagnetic ratio". $\omega = 2\pi$ 2.8026 Mc/gauss for a free electron.

It is interesting at this juncture to note that if a sample containing many such free electrons were placed in a strong magnetic field, there would be no physically measurable property of the system which changes at the Larmor precession frequency. The reason for this is that each electron precesses with its characteristic frequency but with a completely random phase with respect to its neighbor in such a manner that there is no bulk precessing magnetic moment associated with the sample. However, if in addition to the strong magnetic field H_0 one applies a rotating magnetic field H_1, perpendicular to H_0 and having a rotational frequency equal to the Larmor precession frequency of the electrons, there will be two resulting inter-related effects—(*a*) a phase reference is furnished for all similar electrons in the sample resulting in the phenomenon of induction,[2] and (*b*) a secular torque is exerted on each of the electrons tending to tip its moment relative to the strong field H_0 (see Fig. 1). This latter effect alters the energy of the electrons in the strong applied field and this energy is absorbed from that stored in the rotating field H_1. In this way the Larmor precession becomes observable.

One may discuss this same effect phenomenologically. The sample has resultant microscopic electronic magnetic moments which when placed in an applied static magnetic field H_0 yield a bulk magnetic moment per unit volume proportional to this applied field, $M_0 = \chi_0 H_0$, where χ_0 is the static paramagnetic susceptibility of the sample, $N\mu^2 S(S+1)/3kT$. N represents the number of unpaired electron spins in the sample, μ is the individual magnetic moment, S is the intrinsic spin, k is the Boltzmann constant, and T is the absolute temperature of the sample. It is of interest to note that this bulk magnetic moment is a measure of the ability of the applied field to align the individual unpaired electron moments against the disordering and disalignment tendencies of the thermal processes in the sample; in brief, the sample is paramagnetic.

This paramagnetism and the time rate at which it is established may be inferred from the following model: let us consider a system of spin $\frac{1}{2}$ sites. There are N such spins in the sample, n_+ having their spins aligned with the applied magnetic field and n_- with their spins opposed to the applied magnetic field, such that $n_+ + n_- = N$. If the applied field is H_0, these two levels are separated by an amount $g\beta H_0$:

$$n_+ \text{———————} +\tfrac{1}{2}$$
$$\uparrow$$
$$g\beta H_0$$
$$\downarrow$$
$$n_- \text{———————} -\tfrac{1}{2}$$

Since the electron magnetic moment points opposite to its spin, the $-\frac{1}{2}$ level lies lowest in energy. The time rates of change of the numbers of spins in the two states are given by

$$\begin{array}{c}\text{time rate}\\ \text{of change}\end{array} = \begin{array}{c}\text{number/sec}\\ \text{into the state}\end{array} - \begin{array}{c}\text{number/sec}\\ \text{out of the state}\end{array}$$

i.e.

$$\frac{dn_+}{dt} = n_- W_{-\to+} - n_+ W_{+\to-}$$

$$\frac{dn_-}{dt} = n_+ W_{+\to-} - n_- W_{-\to+}$$

where $W_{-\to+}$ is the probability per second that a spin in the $(-)$-state will make a transition to the $(+)$-state and $W_{+\to-}$ is the probability per second that the opposite transition occurs. One may determine these probabilities from Quantum Mechanics; however, this is not necessary. At thermal equilibrium, one knows that the spin populations are given by the Boltzmann factor and that "detailed balance" holds; i.e. the number going up is equal to the number coming down:

$$n_+^0 W_{+\to-} = n_-^0 W_{-\to+}$$

and

$$\frac{W_{-\to+}}{W_{+\to-}} = \frac{n_+^0}{n_-^0} = \exp\left(\frac{-g\beta H_0}{kT}\right)$$

Therefore,

$$\begin{aligned} W_{-\to+} &= W_{+\to-} \exp(-g\beta H_0/kT) \\ &= W \exp(-g\beta H_0/kT) \end{aligned}$$

if one lets $W_{+\to-} = W$.

Then,

$$\frac{dn_+}{dt} = n_- W \exp\left(\frac{-g\beta H_0}{kT}\right) - n_+ W$$

$$\frac{dn_-}{dt} = n_+ W - n_- W \exp\left(\frac{-g\beta H_0}{kT}\right)$$

The physically measurable variable of interest is the net magnetic moment of the sample. This is given by

$$\begin{aligned} M_z &= \sum_{m=-\frac{1}{2}}^{+\frac{1}{2}} n_m g\beta m; \qquad m = \langle S_z \rangle \\ &= g\beta(n_{+\frac{1}{2}} - n_{-\frac{1}{2}}) \\ &= \tfrac{1}{2} g\beta(n_+ - n_-) \end{aligned}$$

The quantity of interest is thus $n_+ - n_-$ which one may call n.

$$\begin{aligned} n &= n_+ - n_- \\ \frac{dn}{dt} &= \frac{dn_+}{dt} - \frac{dn_-}{dt} \\ &= 2W[n_- \exp(-g\beta H_0/kT) - n_+] \end{aligned}$$

If $g\beta H_0 \ll kT$ as is the case for temperatures above liquid helium, then one may expand the exponential and keep only the first term:

$$\frac{dn}{dt} = 2W\{n_-[1-g\beta H_0/kT]-n_+\}$$
$$= 2W[(n_- - n_+) - n_-(g\beta H_0/kT)]$$

Now

$$n_0 = \frac{N}{2}\left[\exp\left(\frac{-g\beta H_0}{kT}\right)-1\right]$$
$$\simeq -\frac{N}{2}\frac{g\beta H_0}{kT}$$
$$\simeq -n_-\frac{g\beta H_0}{kT}$$

Therefore, to first power in $g\beta H_0/kT$

$$\frac{dn}{dt} = 2W[n_0 - n]$$

which has a solution

$$n = n_0[1-\exp(-2Wt)]$$

and the magnetic moment in the z direction is

$$M_z = M_0[1-\exp(-2Wt)]$$

If $T_1 = 1/2W$, then

$$n = n_0[1-\exp(-t/T_1)]$$

and

$$M_z = M_0[1-\exp(-t/T_1)]$$

Thus $T_1 = 1/2W$ is the "thermal relaxation time", the rate at which the spin population seeks its equilibrium value after being disturbed. Notice that for nuclear systems this T_1 in a liquid sample is of the order of seconds. Thus there are some 10^{12} collisions which a given spin suffers in one second, and yet on the average only one of these is of the proper nature to cause a spin flip. If one evaluates M_0 from the equation for M_z at thermal equilibrium one finds

$$M_0 = \frac{N}{2}g\beta S_z\left[1-\exp\left(\frac{-2g\beta H_0 S_z}{kT}\right)\right]$$
$$\simeq Ng\beta S_z g\beta H_0 S_z/kT$$
$$= N\mu^2 H_0\langle S_z^2\rangle/kT$$

where $\mu = g\beta$. Since the average value of S_z^2 from Quantum Mechanics is $\frac{1}{3}S(S+1)$ one obtains

$$M_0 = \frac{N\mu^2 S(S+1)}{3kT} H_0$$

$$= \chi_0 H_0$$

as previously stated.

In similar fashion one may describe any precessing magnetic moment induced by the rotating magnetic field in terms of a frequency sensitive susceptibility. This susceptibility has a resonant or maximum value at one or more frequencies of the applied rotating magnetic field as discussed earlier in the microscopic approach. In this resonant case, the Kronig–Kramers relations[3] insure that this r.f. susceptibility is complex and there will be both energy absorption from these rotating fields and dispersion.

It is easy to evaluate the hypothetical EPR experiment from this phenomenological point of view. The sample is inserted in the cavity in the region of maximum oscillating r.f. magnetic field as shown in Fig. 2. The oscillating

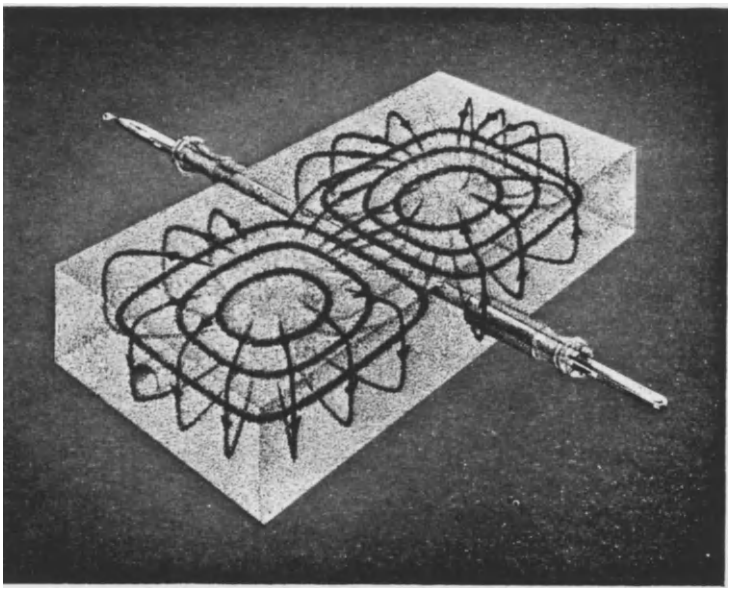

FIG. 2. Microwave magnetic fields in TE_{012} mode.

field may be thought of in terms of two counter rotating magnetic fields, one of which will precess in the same sense as the spin systems and provide the required perturbation.

One may calculate the effect on the losses and resonant frequency shifts

in the microwave cavity and show that they obey the general equation for electrically resonant systems[4]:

$$\Delta\left(\frac{1}{Q}\right)+j\frac{\Delta\omega}{\omega}=j(\chi'-j\chi'')\int_{\text{sample}} H_1^2\mathrm{d}V\Big/\int_{\text{cavity}} H_1^2\mathrm{d}V$$

The detection of these changes is not a difficult task and there are many ways of doing it. Some of these have been discussed in the previous two papers. A convenient method is to employ an impedance bridge system where the oscillator is isolated from the load. Figure 3 shows a block diagram of a reflec-

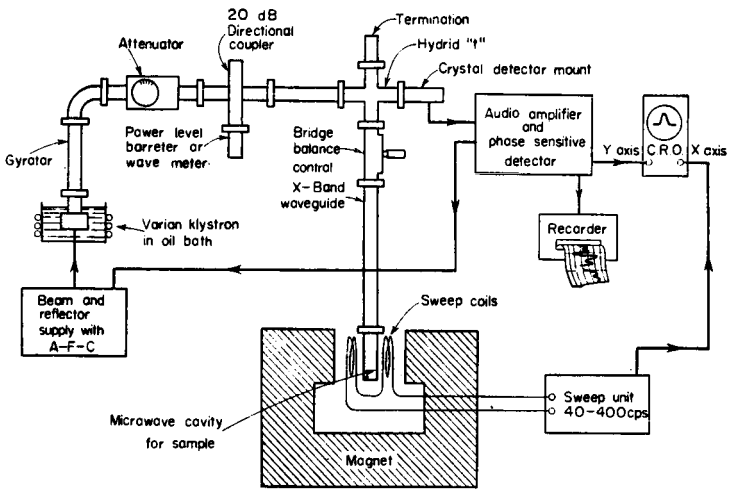

FIG. 3. Block diagram of X-band EPR spectrometer.

tion microwave impedance bridge system employing a crystal detector. Because the precession frequency for a free electron is 2.8026 Mc/gauss of applied static magnetic field, it is convenient to use X-band microwave equipment which operates between 8000 and 12,000 Mc/s and to use applied magnetic fields in the neighborhood of 3000 gauss. With a source of 300 mW of microwave power and using low audio-frequency magnetic field modulation one obtains in practice the theoretical signal-to-noise ratio and may detect $5\times10^{-12}\Delta H$ moles of electron spins where ΔH is the full width of the absorption line in gauss. This is equivalent to 10^{-11} moles of α,α-diphenyl β-picryl hydrazyl, a stable free radical often used as a standard. If instead of a low audio-frequency one employs 100 kc/s magnetic field modulation, the source and detector noise reduce to the point that the sensitivity is improved by approximately a factor of 20.

Other detection systems are in use. The bolometer is quite satisfactory for transmission systems, the balanced bolometer bridge works quite well with

both transmission and reflection systems, and the superheterodyne receiver has been employed with excellent success with a reflection bridge.[5, 6] It is of interest to note here that for room temperature studies the source noise is the limiting factor[6]—the theoretical limit has been reached only for brief periods of quiet operation and this was achieved by employing multiple cavity klystrons.[7]

EPR SPECTRA INTERPRETATION

If the magnetic states of the electron under study were completely independent of its surroundings, then EPR would be of purely academic interest and would certainly not be considered as a spectroscopic tool. On the contrary, one finds that the interactions between the electron and its surroundings are sufficient to perturb the magnetic states of the system and allow interpretation. This interpretation, of course, hinges upon an understanding of the nature of these interactions which affect the unpaired electrons.

The modern picture of an atom consisting of a nucleus and extra nuclear electrons having orbital angular momentum as well as spin angular momentum is familiar to us all. If one imagines this atom placed in the solid state where the electrons are far from free since they have electrical charge and are subjected to large electrostatic fields from the surrounding atoms, one is not surprised to find that the picture must be altered somewhat. For iron group ions, where the electrons of interest are exposed, this interaction is so great that the orbital angular momentum of the electron is almost completely quenched, that is, the orbits are tied to the crystalline electric field and are uninfluenced by any magnetic field which one may apply. The spin of the electron remains unaffected except through the spin orbit coupling which causes some of the orbital angular momentum to be admixed in an amount which is dependent upon the relative orientation of the crystal axes with respect to the applied magnetic field. The spectroscopic splitting factor g, referring to the spin states, is given approximately by $g \simeq 2(1+a\lambda/\Delta)$, where a is a numerical constant, λ is the magnitude of the spin orbit coupling ($\lambda \simeq 100\ \mathrm{cm}^{-1}$ for the iron group ions) and $\Delta(\simeq 1000\text{–}10{,}000\ \mathrm{cm}^{-1})$ is the energy level separation to the first orbital level caused by the crystalline electric field. This results from a perturbation calculation where the spin-orbit coupling admixes orbital angular momentum into the ground state from the higher Stark levels; for clarification the reader is referred to the literature.[8] This interaction makes EPR of use to the crystallographer. An example of this is the work on the structure of crystalline hemoglobin.[9] From the dependence of the spectroscopic splitting factor upon orientation it has been possible to determine the orientations of the four heme rings with respect to the crystal axes and the orientation of the protein molecule as it is attached to these porphyrin rings. This information previously was not available because of the complexity of the X-ray data.

This interaction is of use in solid state physics in that it may be used to measure magnitudes and symmetries of microscopic electrostatic fields. An example is the spectrum from ferric ions located in titanium positions of a single crystal of barium titanate, a ferroelectric. Figure 4 displays the spectrum of a cupric ion in the amorphous phase—a silicate glass. Here the spectrum is a picture of the total anisotropy, but one may still determine the local symmetry and bonding characteristics. One first assumes a symmetry and

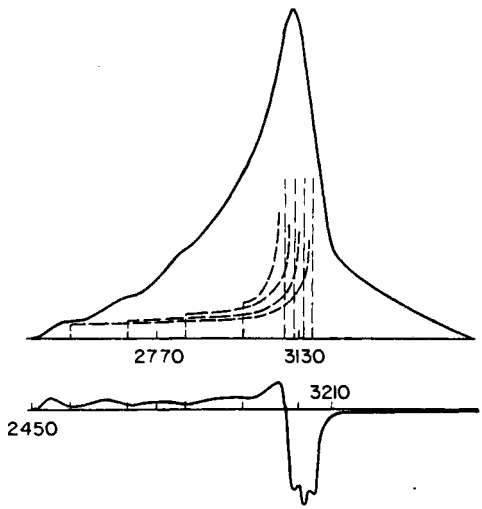

FIG. 4. Spectrum for Cu^{++} in a lattice modifying position in a silicate glass.

calculates the angular dependence of the resonance lines; then one averages over all solid angles and compares the weighted spectrum with the observed one.[10]

It is of interest to note that this spin-orbit interaction is also of use in the solid state MASER (Microwave Amplification by the Stimulated Emission of Radiation) program. These devices use the energy level splitting provided by the spin-orbit coupling and the generalized Overhauser effect[11] to build up sufficient population differences to allow the stimulated emission of radiation with its attendant gain and low noise figure. Two such devices have been used with some success—one employing the chromium ions in the cobalt positions of a crystal of potassium cobalticyanide,[12] and the other using the chromium ions in ruby.[13]

A second interaction of fundamental interest in EPR Spectrometry is that between the electron and nuclear magnetic dipole moments. This dipole–dipole interaction consists of the classical interaction between two bar magnets, $[3(\boldsymbol{\mu}_e \cdot \hat{r})(\boldsymbol{\mu}_r \cdot \hat{r}) - \boldsymbol{\mu}_e \cdot \boldsymbol{\mu}_n]/r^3$, and a quantum mechanical part,

$$(8\pi/3)\mu_e \cdot \mu_n |\psi(0)|^2$$

where $|\psi(0)|^2$ represents the probability of finding the electron in the same place as the nucleus—a phenomenon that is forbidden in classical physics. This last term may be rewritten as

$$(8\pi/3)g_e g_n \beta^2 |\psi(0)|^2 I \cdot S = AI \cdot S$$

and is called the "$I \cdot S$ interaction" or "contact hyperfine interaction". Because this interaction requires the electron to be at the nucleus the electron must be in an "S-state". The magnitude of this interaction is thus a direct measure of the S-state character of the electron at the particular nuclear site in question and herewith furnishes the quantum chemist with an early check on his wavefunctions. This interaction uniquely fingerprints oxidation states of paramagnetic ions and many of those odd molecules and free radicals having molecular weights below 200. One may study the π-electron σ-proton overlap in the π-electron radicals with considerable success[14] by monitoring this hyperfine interaction. Some recent evidence[15] supports the concept of negative spin densities at carbon positions where positive π-electron densities are known. Figure 5 shows how this $I \cdot S$ coupl-

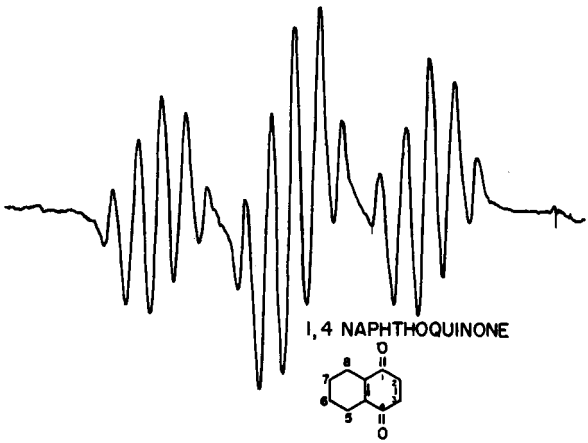

FIG. 5. EPR spectrum of 1,4-Naphthosemiquinone.

ing to the proton nuclear moments in the polyaromatic odd molecules is revealed by the spectrum. This is a spectrum of 1,4-naphthosemiquinone where the basic triplet results from the equivalent 2,3 protons and the quintuplet from the nearly equivalent 5, 6, 7, 8 protons.

Much of the remainder of this Workshop will be devoted to applications of NMR and EPR Spectroscopy. It is, however, appropriate to mention a few such applications.

Considerable work is being done on trapped free radicals at low temperatures.[16] In this work the EPR spectroscopist finds himself confronted with long relaxation times and rapid passage conditions which distort the lines

and lead to erroneous results. A superheterodyne spectrometer or a Model V-4500-41 Low Temperature bridge is a necessity. This point has not been appreciated by many researchers in the field and is emphasized here because of that fact.

Free radical kinetic studies are getting a big boost from EPR. Stop-flow systems can be constructed using standard techniques which will allow millisecond resolution.[17] The theoretical limit to EPR as a kinetic tool is a few millimicroseconds.

The application of this tool to study the kinetics of polymerization and cross-linking in polymer chemistry is a large field. Biochemistry is also reaping a large harvest of new data from EPR. Figure 6 shows the first free radical

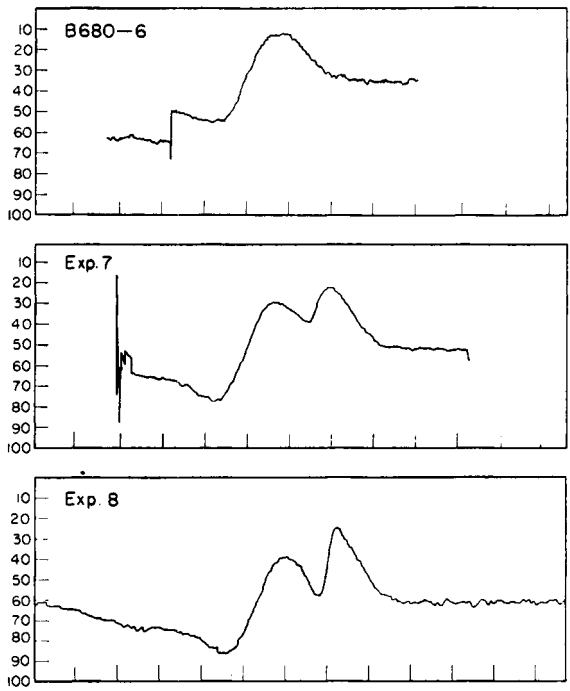

FIG. 6. Free radical signal in fatty acyl (CoA) dehydrogenase-substrate reaction under aerobic conditions. Top spectrum is cavity blank, middle is cavity plus enzyme and bottom is with substrate added.

signal to be observed in an enzyme-substate reaction. This is a free radical which results on the oxidation of the enzyme-substrate complex of fatty acyl (CoA) dehydrogenase by molecular oxygen and is not an intermediate in the dehydrogenation of the enzyme itself as shown by kinetic studies.[18]

Radiation damage studies have been reported on innumerable systems.[19]

Figure 7 displays the spectrum from electron irradiated lucite which has been interpreted by thermal studies to be due to two free radical species.

It is not possible to list all of the fields of application in these few pages. Suffice it to say that EPR has earned its recognition as one of the powerful spectroscopic tools in science.

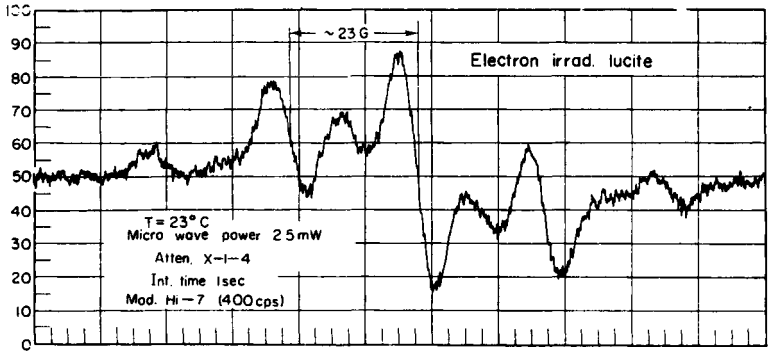

FIG. 7. EPR spectrum of electron irradiated lucite.

REFERENCES

1. I. I. RABI, N. F. RAMSEY and J. SCHWINGER, *Rev. Mod. Phys.* **26**, 167 (1954).
2. F. BLOCH, *Phys. Rev.* **70**, 460 (1946).
3. R. DEKRONIG, *J. Opt. Soc. Amer.* **12**, 547 (1926); H. A. KRAMERS, *Atti Congr. intern. fis Como* **2**, 545 (1927).
4. J. C. SLATER, *Microwave Electronics*, D. van Nostrand, 1950.
5. G. FEHER, *Bell System Tech. J.* **36**, 449 (1957).
6. R. H. SANDS, Invited paper ASTM meeting, San Francisco, Calif., Oct. 12–16, 1959.
7. H. MISRA, *Rev. Sci. Instr.* **29**, 590 (1958).
8. A. ABRAGAM and M. H. L. PRYCE, *Proc. Roy. Soc.* **A205**, 135 (1951); B. BLEANEY and K. W. H. STEVENS, *Rep. Progr. Phys.* **16**, 108 (1953); K. D. BOWERS and J. OWEN, *Rep. Progr. Phys.*, **18**, 304 (1955).
9. J. E. BENNETT *et al.*, *Proc. Roy. Soc.* **A240**, 67 (1957).
10. R. H. SANDS, *Phys. Rev.* **99**, 1222 (1955).
11. A. W. OVERHAUSER, *Phys. Rev.* **91**, 476 (1953); *Phys. Rev.* **92**, 411 (1953).
12. A. L. MCWHORTER and J. W. MEYER, *Phys. Rev.* **109**, 312 (1958).
13. G. MAKHOV *et al.*, *Phys. Rev.* **109**, 1399 (1958).
14. H. M. MCCONNELL, *J. Chem. Phys.*, **28**, 1188 (1958).
15. T. COLE *et al.*, *Proc. Natl. Acad. Sci., U.S.* **45**, 525 (1959).
16. See for example *Proceedings of the Fourth International Symposium on Free Radical Stabilization*, National Bureau of Standards, Washington, D.C., Aug. 31–Sept. 2, 1959.
17. I. YAMAZAKI, H. S. MASON and L. PIETTE, *J. Biol. Chem.*, *to be published*.
18. H. BEINERT, to be published.
19. Two representative references are W. GORDY *et al.*, *Proc. Natl. Acad. Sci., U.S.* **41**, 983 (1945) and B. SMALLER and M. S. MATHESON, *J. Chem. Phys.* **28**, 1169 (1958).

4

HIGH RESOLUTION NMR OPERATING FUNDAMENTALS

LeRoy F. Johnson, Wayne C. Lockhart, and Robert C. Jones
Varian Associates, Palo Alto, California

In discussing the operating fundamentals of an NMR spectrometer, we will first briefly investigate the functions and uses of the various components. Figure 1 is a basic block diagram of a high resolution NMR spectrometer system.

The various components and their functions are:

(1) The electromagnet providing a homogeneous d.c. magnetic field that can be varied from near zero to 15,000 gauss.

(2) The transmitter supplying r.f. energy to the sample under investigation. The frequency of this r.f. energy must remain constant to approximately one part in 10^9.

(3) The probe houses the sample and the electronic circuits required to initiate and detect nuclear resonance signals. The spinner, a part of the probe, provides a means of rotating the cylindrical sample about its vertical axis.

(4) The preamplifier amplifies the resonance signal.

(5) The receiver contains amplifiers and a phase detector circuit. The total amplification of the preamplifier and amplifiers in the receiver must be approximately one million in order to observe signals from weak samples.

(6) The oscilloscope visually displays the signal, and is used to adjust and optimize the spectrometer. The graphic recorder provides a permanent record of the NMR spectrum.

(7) The linear sweep provides a linear sawtooth modulation of the magnetic field while simultaneously driving the X-axis of the oscilloscope. This modulation produces a small change in the static magnetic field (H_0) at the sample position, thus sweeping the field through the resonance value.

(8) The regulated current power supply provides a stable, controlled d.c. current to the coils of the electromagnet.

(9) The flux stabilizer and associated coils are a control system which provides short-time field stability of one part in 10^9.

(10) The slow sweep is a control unit for the flux stabilizer. Selected control voltages fed to the flux stabilizer result in linear sweeps much slower than those provided by the previously discussed sweep unit. Normally the sawtooth unit is used when oscilloscope displays are desired, while the slow sweep unit is used in conjunction with the graphic recorder.

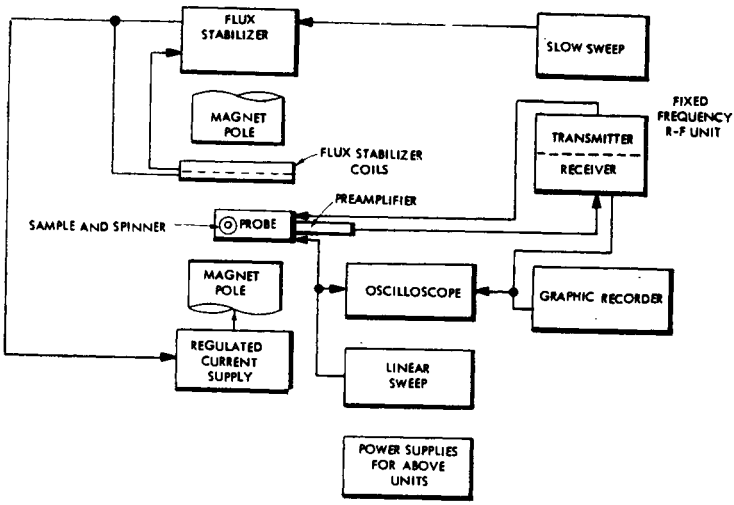

FIG. 1.

A high resolution NMR spectrometer system is shown in Fig. 2.

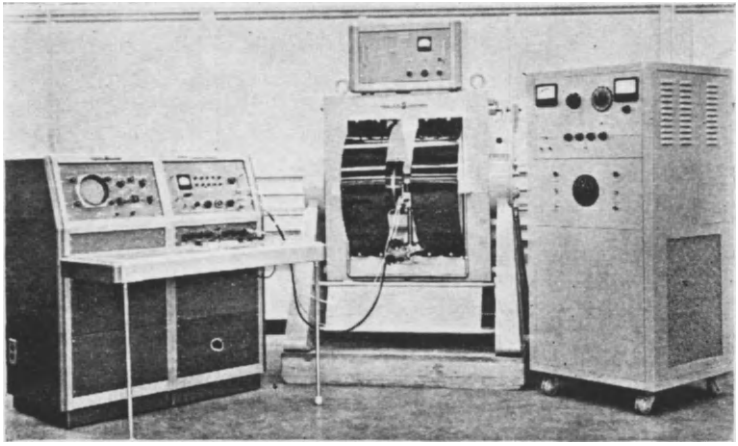

FIG. 2.

The operating fundamentals of an NMR spectrometer are perhaps best described by covering step by step the procedures involved in optimizing the operation of the various components in the system. The first of these steps is tuning and balancing the probe. Figure 3 is a diagram of the probe showing locations of the receiver, transmitter and sweep coils and the coarse and fine balance paddles. Tuning the probe consists of adjusting a trimmer capacitor to tune the receiver coil to the operating frequency. This is done before the probe is balanced by obtaining a maximum reading on the detector level meter on the r.f. unit using a suitable receiver gain position.

Balancing the probe consists of "decoupling" the receiver coil from the transmitter coil. Since both of these coils are physically located in close proximity and are tuned to the same frequency, the mutual coupling between them is ordinarily excessive. As a result, the receiver is literally "swamped" by the transmitter, prohibiting detection of NMR signals. To reduce this coupling the probe is constructed with the receiver coil oriented at right angles to the transmitter coil.

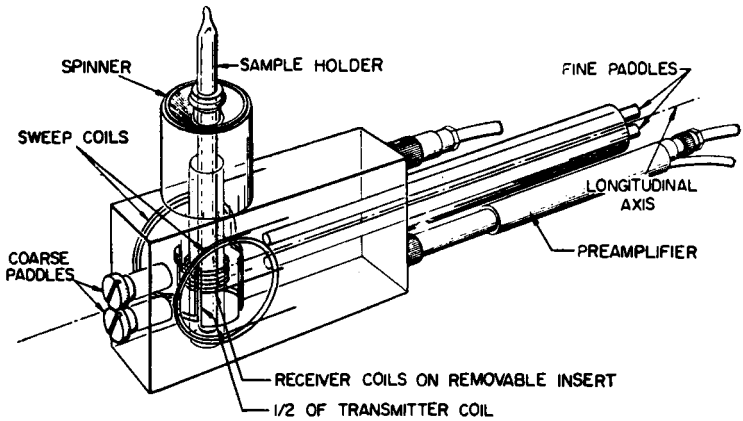

Fig. 3.

Even with the coils so positioned a small amount of mutual coupling between the transmitter and receiver still exists. This coupling is known as "leakage". This leakage can effectively be cancelled by coupling devices called "paddles". These paddles are equivalent to inductors which are mutually coupled to both the transmitter and receiver. The position of the paddles relative to the transmitter and receiver coils determines their effect on the mutual coupling. Thus, by utilizing a bit of energy from the transmitter, shifting its phase by 180 degrees and coupling it into the receiver coil, the leakage can be cancelled. Different materials used in the construction of the paddles allow the phase of the coupled energy from the transmitter to be controlled. Figure 4 is an electrical schematic representing the coils and paddles.

The receiver coil is mounted on a glass tube with an electrical fitting at the bottom. This assembly, called an insert, fits into the probe and is rotated to produce the least coupling between transmitter and receiver as observed with the detector level meter in the receiver. The paddles are used to cancel the residual coupling to a level that is satisfactory for the observation of NMR signals. This decoupling procedure is called "balancing the probe".

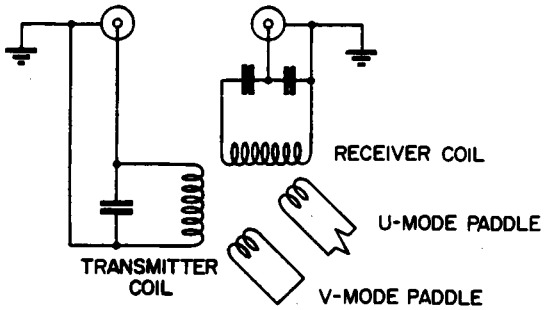

FIG. 4.

Adjustment of the "fine" paddles should be done with the sample in place, since the sample itself can actually enter into the coupling between the transmitter and the receiver.

After inserting a water sample in the probe, it is placed in the center of the magnet air gap. With the magnet operating at approximately the correct field value and with the linear sweep unit producing a maximum sweep field (approximately 5 gauss), the current to the magnet is varied slowly until the resonance falls within the range of the sweep variation. Once this occurs, a signal will appear on the oscilloscope.

With a sweep field of approximately 0.1 gauss, the magnet current is carefully adjusted to center the signal on the oscilloscope. At this point, the flux stabilizer is switched on to stabilize the magnetic field.

A field plot may be made by moving the probe up and down two inches from the center of the field while observing the position of the three lines from ethyl alcohol. Knowing that the outside lines are 60 milligauss apart, the shift to higher or lower field per inch of probe travel can be determined and used to plot the field. A mental plot of the field will often serve the purpose.

When the magnetic field is increased from zero to the resonance value, the plot of the field will be as shown in Fig. 5*a*. Such a field shape is not homogeneous enough over the sample area seen by the receiver coil. The resulting NMR signal shape is distorted and appears as shown in Fig. 5*b*.

The field plot can be changed by increasing the magnet current to several per cent above that required for resonance and allowing it to remain there for a few minutes. When the field is reduced to the resonance value, two things

are observed. The first is the fact that slightly less current is required to obtain the same value of magnetic field. This results from the hysteresis effect in the iron of the magnet. Secondly, the shape of the field with corresponding NMR signal shape now resembles that shown in Fig. 6*a* and *b*.

Such a field shape is termed "overcycled" or "dished", while the previous field is "undercycled" or "domed". The cycling effect can be reversed by

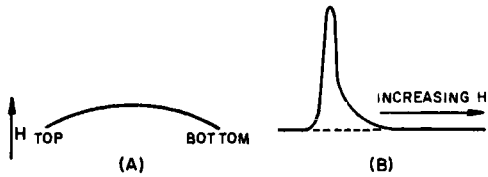

Fig. 5.

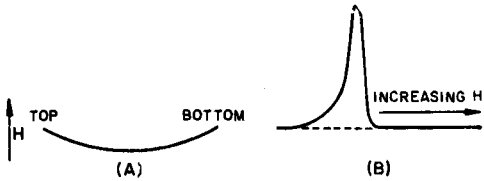

Fig. 6.

reducing the field to slightly less than that required for resonance for a few minutes. Proper cycling can produce an essentially flat field plot. However, due to the diamagnetic aluminum probe the field shape which produces best signal line shape is slightly dished. The proper cycling procedure varies slightly from magnet to magnet, and has to be determined experimentally. Correct cycling is very important, since interference due to "tails" in the NMR signal is minimized, while resolution and signal-to-noise attainable are optimized.

In determining correct cycling by observing signal line shape, it is important to have the r.f. phasing set for pure v-mode (absorption). A slight amount of u-mode (dispersion) component causes distortion in the signal which can be confused with that produced by improper cycling. On close examination, however, the signal shape produced by improper r.f. phasing is seen to have a tail on each side of the resonance signal, one adding to and one subtracting from it. Figure 7*a* shows a signal with proper r.f. phasing, and Fig. 7*b* one with a setting 10 degrees from pure v-mode (absorption).

Although the correct amount of curvature in the Y-axis plot can be obtained through proper cycling, it may be found that the absolute field value is higher above the field center than below, or vice versa. In effect, the field plot is tilted. To correct this, the field trimmer is used. This device alters the

vertical parallelism of the pole pieces by applying stress on one of the vertical members of the magnet yoke.

Adjustment of the field trimmer produces greater signal resolution by creating a more homogeneous field over the sample area. Figure 8 is a picture of a field trimmer.

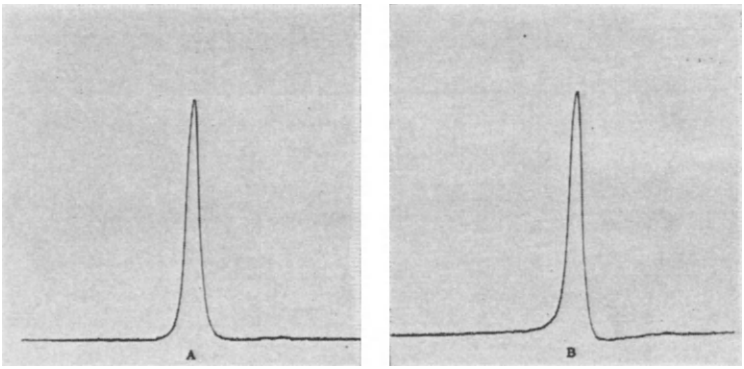

FIG. 7.

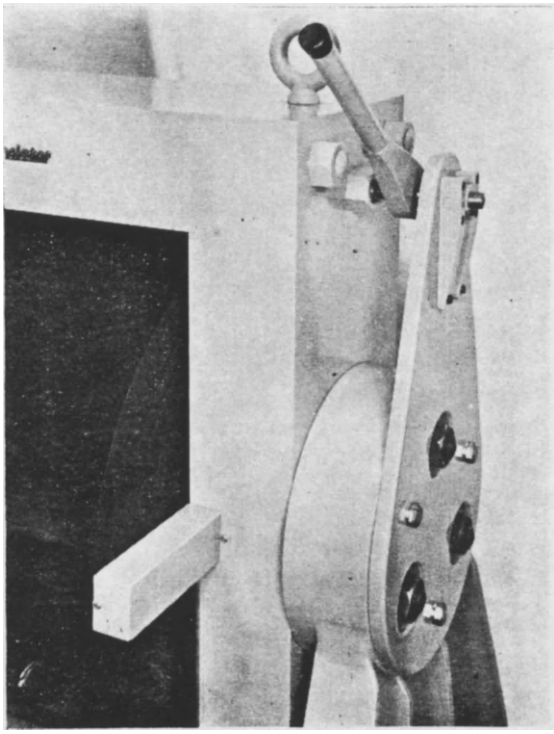

FIG. 8.

To eliminate the need for *exact* control of the X-axis (parallel to the pole faces and horizontal) and Z-axis (from N pole to S pole), the sample is spun at a rate of several hundred r.p.m. This action averages the field seen by the sample perpendicular to the spinning axis. It should be noted that too slow a spinning rate can produce insufficient averaging, while spinning too rapidly can create a vortex in the liquid sample which can have a detrimental effect on resolution. Figure 9 shows the resolution obtained with and without spinning, using identical instrumental settings. The "ringing down" following the sweep through the signal (left-to-right) in Fig. 9*b* is an indication of good resolution.

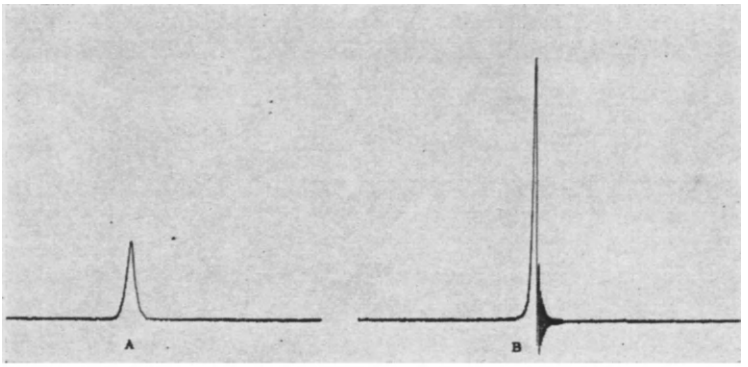

Fig. 9.

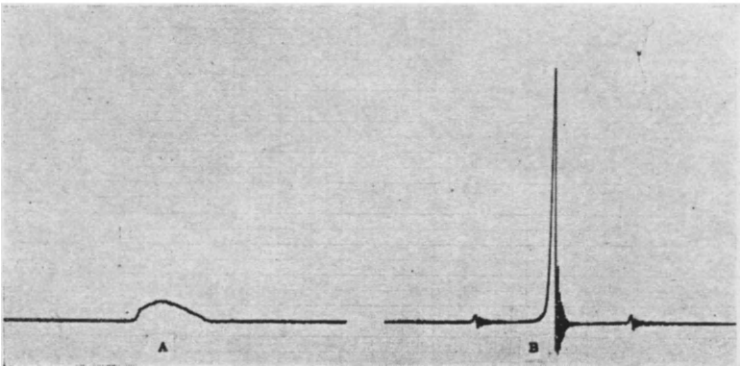

Fig. 10.

Spinning, however, does not eliminate the need for fairly good non-spinning resolution. Although a rather broad non-spin signal (Fig. 10*a*) can be greatly improved by spinning, such a condition can produce interference by the creation of satellite signals, called spinning sidebands, displaced from the center of the non-spin signal by the spinning frequency as shown in Fig. 10*b*.

Following adjustment of the field trimmer, the physical position of the probe within the magnet air gap may be adjusted slightly in order to optimize the resolution. By cycling the magnet, spinning the sample, varying the physical position of the probe, and using the field trimmer, provision is made for either correcting the gradients, averaging the gradients, or for placing the sample in the magnetic field where the gradients are a minimum.

Since optimizing the signal with respect to signal amplitude and resolution are such an important part of the operation of the spectrometer, a few remarks indicating how to identify poor, good and excellent resolution are in order.

Resolution is defined by the ratio of the line width at half amplitude to the total magnetic field. Thus, the narrower the measured line width, the better the resolution. Unfortunately, a minute change in the line width is extremely difficult to detect when comparing traces on an oscilloscope. What can easily be observed, however, is the amount of ringing that follows the signal.

When the signal trace on the oscilloscope indicates that good resolution has been obtained, the next step is to record the signal on the graphic recorder. To do this, the sawtooth sweep unit is turned off and the slow sweep unit, in conjunction with the flux stabilizer, is used to sweep the magnetic field through the resonance value. If additional optimizing of resolution is desired at this time, this can be accomplished by adjusting the spinning rate, or the field trimmer, while observing the recorded signal in order to maximize its amplitude.

Assuming that the homogeneity of the magnet is optimized, the second factor that maximizes signal amplitude is the amount of r.f. power supplied to the sample. The amount of r.f. power that can be supplied to the sample without saturating the signal is dependent on two things. The first is the nuclear relaxation time and the second is the rate of sweep.

A long relaxation time and/or a slow rate of sweep requires a low r.f. power level to avoid saturation. Radio-frequency saturation can be detected by a "rounding" or broadening of the top of the resonance line, and by a loss in amplitude. When sweeping at increasingly slower sweep rates, the first signs of r.f. saturation are easily mistaken for a slight decay in resolution, since the lines are not quite as sharp as those observed previously at slightly faster sweep rates.

To obtain the best signal-to-noise ratio, the r.f. power level should be run as high as possible provided the signal is not being saturated. (The nuclear signal increases in amplitude until saturation is reached.)

Once a recorded spectrum is obtained, calibration of the signal positions relative to a reference compound can be accomplished with an audio-frequency oscillator. Applying the oscillator output to the sweep coils in the probe, a modulation of the magnetic field is produced which results in side-

bands appearing on both sides of the signals. Each sideband will be spaced from the signal resonance line by the frequency of the audio modulation voltage. By adjusting the modulation amplitude and the frequency, sidebands can be made to coincide with sample signals. This can be viewed on the oscilloscope when using the sawtooth sweep unit. Narrow NMR signals can be referenced in this manner to an accuracy of 0.1 c/s (0.02 milligauss). The same technique can be used in conjunction with the graphic recorder and the slow sweep unit.

Since frequencies correspond proportionally to magnetic field values, the frequency used to produce sidebands can be converted to units of magnetic field strength if desired.

In closing this lecture on high resolution NMR operating fundamentals, it might be well to note that a great deal of time has been spent in discussing adjustment of various parameters in the system. It should be remembered that the greatest advantage in being able to optimize a fundamental research tool is the fact that the operator will be able to utilize the instrument to its fullest capacity in his attempt to solve difficult problems.

5

EPR SPECTROMETERS: OPERATING FUNDAMENTALS

WAYNE C. LOCKHART and ROBERT C. JONES
Varian Associates, Palo Alto, California

THE following discussion of EPR operating fundamentals is centered about the operation of a Varian spectrometer. However, it should be pointed out that the fundamentals described herein could be applied to any EPR spectrometer that utilizes similar electronic circuits.

Certain portions of the system are described in detail; for example, the automatic frequency control system. This has been done only to facilitate an understanding of the system operation, and should not be construed to mean that this is the only type of automatic frequency control that can be used. Actually there are other types being used which are quite successful. Another example is that of the sample cavity. The one herein described is a reflection type, although transmission cavities are often used.

Although the fundamental operating techniques used in electron paramagnetic resonance studies are quite similar in theory to those used in nuclear resonance, the instrumentation required is quite dissimilar. In particular, the use of microwave frequencies for EPR dictates the use of klystrons, waveguide, etc., as opposed to the radio-frequency electronic circuits employed in NMR. The block diagram of Fig. 1 identifies the principal components of an EPR spectrometer.

The various components and their functions are:

(1) The electromagnet provides a homogeneous magnetic field (H_0) which can be varied from near zero to at least 5000 gauss.

(2) The magnet power supply provides a stable, controlled current to the energizing coils of the electromagnet.

(3) The scanning unit supplies a control voltage to the input of the current regulated magnet power supply. This control voltage can be varied linearly with respect to time, thus resulting in a linear sweep of the magnetic field (H_0).

(4) The 100 kc sweep generator provides a small modulation of the static magnetic field (H_0) at the sample location within the resonant cavity. It also supplies a phase reference voltage to the signal phase detector.

The audio sweep generator supplies an additional magnetic field modulation to the cavity as well as a sweep for the oscilloscope X-axis.

(5) The klystron oscillator produces r.f. energy which is used to irradiate the sample. Although not included in the diagram, a variable attenuator is required between the klystron and the hybrid tee in order to control the amount of r.f. power applied to the sample.

(6) The hybrid tee is a device which will not allow microwave power to pass in a straight line from one arm to the arm opposite. Thus, power emitting from arm 1 is equally divided between arms 2 and 3. If all of the power is absorbed and none reflected, then no power enters arm 4; thus the crystal detector receives no energy. The hybrid tee can now be considered similar to a balanced bridge, since any change in the terminating impedance of arms 2 or 3 will unbalance it and result in energy reaching the crystal detector.

(7) The resonant sample cavity acts like a tuned circuit which has a very high Q [where Q is defined as ω(energy stored/power lost) and $\omega = 2\pi \times$ frequency]. When a resonance is obtained from the sample, the impedance of the cavity is changed and a signal is reflected to the crystal detector in the hybrid tee.

(8) The crystal detector demodulates the microwave energy. The resulting 100 kc signal voltage contains the EPR information. The frequency of this voltage corresponds to that of the sweep voltage used to modulate the magnetic field and to provide a phase reference for the signal phase detector.

(9) The amplifier following the crystal detector simply amplifies the signal information.

(10) The oscilloscope is a means for rapid visual display of EPR signals.

(11) The signal phase detector combined with an integrator and a graphic recorder provides a means of displaying the first harmonic presentation of the EPR signal. Bandwidth limiting circuits at the input to the signal amplifier afford a higher signal-to-noise ratio to be obtained on the recorder than that which is observed on the oscilloscope.

Although not shown in Fig. 1, an automatic frequency control system is usually included in order to provide optimum stability of the microwave oscillator (elimination of frequency modulation noise is the primary consideration here) and to reduce microphonics. Such a system can be used to lock the frequency of the oscillator to that of the sample cavity with an accuracy of one part per million.

Figure 2 is a block diagram of an automatic frequency control (AFC) system. A control frequency of 10 kc is provided by an oscillator to both the AFC phase detector and the power supply for the klystron reflector. In the AFC phase detector the 10 kc voltage is used as a phase reference,

while in the klystron power supply it is used to vary the reflector voltage, thus resulting in a 10 kc modulation of the klystron output frequency.

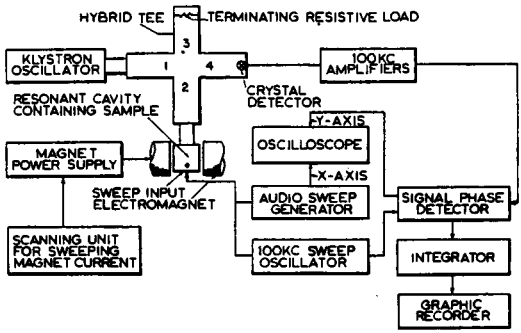

FIG. 1. Block diagram of an EPR spectrometer.

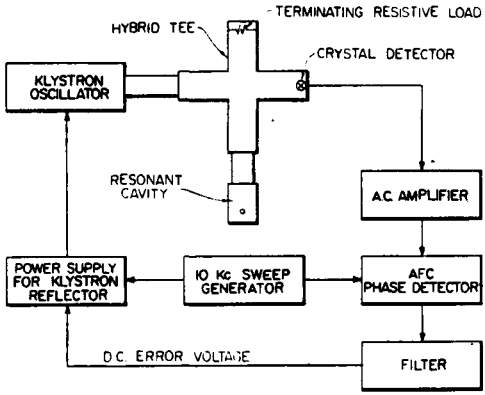

FIG. 2. Block diagram of an AFC system.

This frequency modulation causes the klystron frequency to vary with respect to the resonant frequency of the sample cavity. When the klystron center frequency (f_0) corresponds to the resonant frequency of the sample cavity (f_r), a voltage, the fundamental frequency of which is the second harmonic of 10 kc (20 kc), is reflected from the cavity and appears at the crystal detector. (See Fig. 3*a*.) If the center frequency of the klystron is shifted from that of the resonant cavity, the frequency of the voltage appearing at the crystal detector is 10 kc. Its phase is dependent on whether the klystron center frequency is higher or lower than the resonant cavity frequency. The amplitude of this reflected 10 kc signal will depend on the relative difference between f_0 and f_r. (See Fig. 3*b*, c.)

This error voltage (it can now be considered an error voltage since its phase and amplitude are dependent on the relationship between f_0 and f_r) is amplified by the a.c. amplifier, then phase detected and filtered. The result is a d.c. output voltage which is used to control the klystron reflector voltage

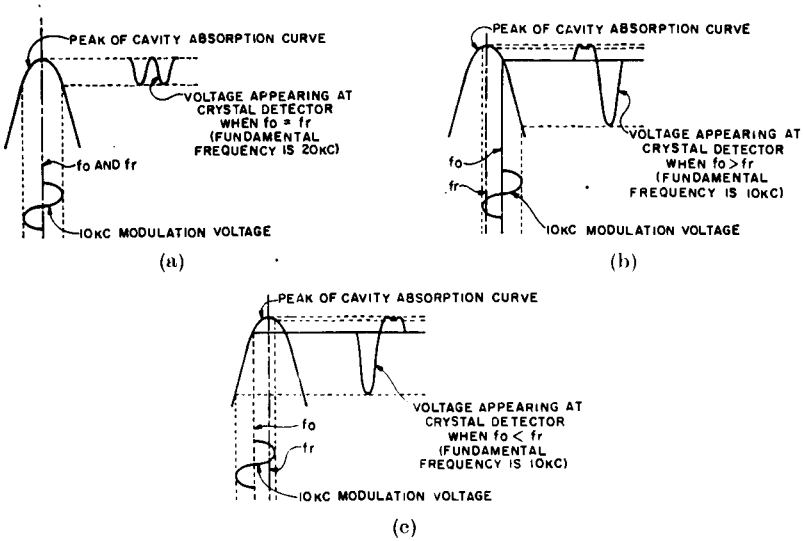

FIG. 3. Output voltages from cavity as result of AFC modulation.

so that the center frequency of the klystron corresponds to the frequency of the resonant cavity.

Figure 4 is a picture of a complete EPR spectrometer including the AFC system, the electromagnet, and its associated power supply.

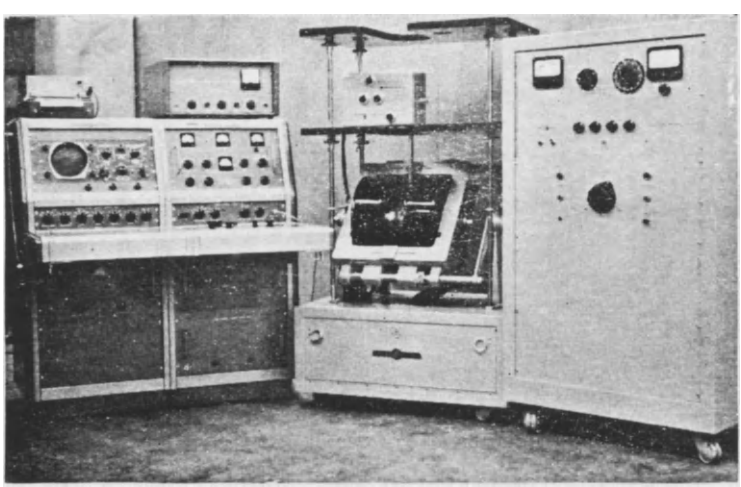

FIG. 4. EPR spectrometer system.

Let us now turn our discussion to the source of microwave energy, the klystron. When a klystron oscillates, it has a power output over a given frequency range. This power output is normally referred to as the "mode of operation" for the klystron. A klystron can have several modes of operation, depending upon the adjustment of the voltages supplied to it and the physical dimensions of its resonant cavity.

When the proper voltages are supplied to the klystron and its mechanical dimensions are correctly adjusted, it will oscillate and provide microwave power to the hybrid tee. In applying voltage to the klystron, one should be careful to determine that the filament voltage is accurately set at its correct value, that the reflector receives a negative voltage before the resonator receives its positive voltage, and finally that the resonator current is not exceeded for the type of klystron being used.

Once this is done, you should be able to observe the power output of the klystron at the crystal detector on one arm of the hybrid tee. The output of this detector can be placed on the vertical axis of the oscilloscope while the horizontal axis of the oscilloscope is driven by a sinusoidal sweep voltage. If the reflector voltage of the klystron is swept by the same sinusoidal sweep as that used to drive the oscilloscope, then several klystron modes can be observed. (See Fig. 5.)

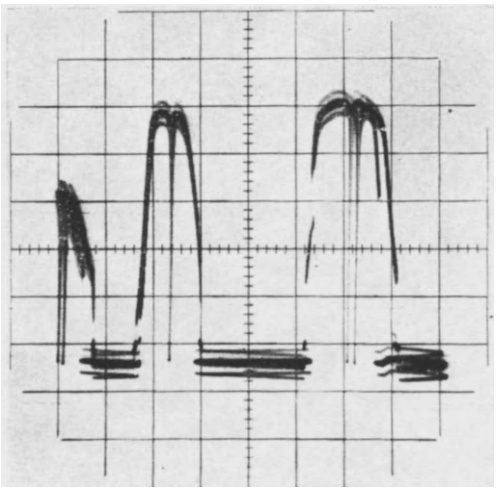

FIG. 5. Klystron modes on oscilloscope.

By adjusting the tuning of the klystron both mechanically and electronically, its mode of operation can be shifted to match the frequency of the resonant sample cavity. This will be indicated by an absorption dip in the klystron power mode at precisely the resonant frequency of the sample cavity. (See Fig. 6.)

At this point in our discussion, it would be well to note that the depth of the absorption dip is an indication of the amount of power being absorbed by the sample cavity. A poor impedance match between the cavity and its arm of the hybrid tee could cause a sharp reduction in the amount of power absorbed. For this reason, we insert an iris with an adjustable coupling screw between the waveguide and the cavity to aid in matching the impedance. (See Fig. 7.)

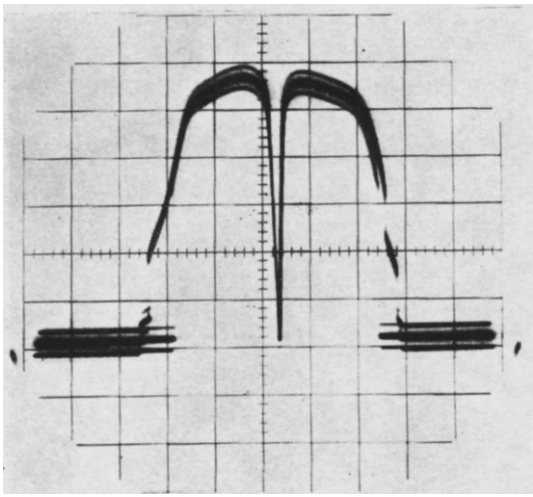

FIG. 6. Klystron mode with cavity absorption superimposed.

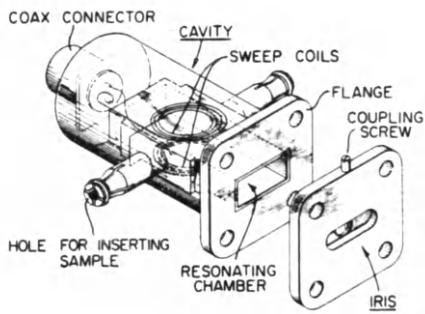

FIG. 7. Sample cavity and iris.

Figure 8*a* indicates the absorption dip with the iris improperly adjusted. The rounded dip only extending a portion of the way to the baseline indicates that not all of the power is being absorbed. The sharp dip in Fig. 8*b* indicates that the cavity is now properly matched to the waveguide as a result of properly adjusting the iris tuning screw.

It should be noted that the impedance match of the cavity will be different when the sample is inserted. Different samples will cause different losses to occur in the cavity. For example, water can cause the losses to be so great that it is impossible to lock the klystron frequency to that of the sample cavity. This occurs as a result of the cavity Q being lowered (due to losses) until the AFC system will not function. Problems such as this can be overcome to some extent by the design of the cavity and the sample cell.

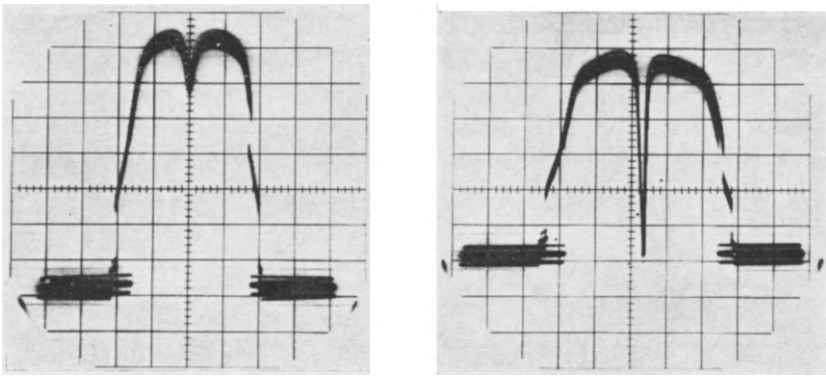

(*a*) (*b*)

FIG. 8. (*a*) Iris improperly adjusted; (*b*) Iris properly adjusted.

After matching the klystron frequency to that of the sample cavity, the AFC unit can then be switched to the operate position; the AFC system can be turned on and the klystron frequency will remain at the frequency of the sample cavity.

It is of interest to consider the sample cavity in a little greater detail. The cavity shown in Fig. 7 is a standard reflection type which can be used only at room temperatures. Many EPR applications require that the sample temperature be lowered to the region of liquid nitrogen temperatures, or perhaps that the temperature of the sample be varied during the experiment. In other experiments it is desirable to irradiate the sample with ultraviolet light or some other form of energy.

If solutions for technical problems such as these are to be developed, a much more sophisticated cavity will be needed. Figure 9 is a picture of a cavity embodying features which aid in solving the above mentioned problems.

Once the frequency of the klystron is locked to that of the cavity to be used, the cavity is then positioned in the center of the magnet and the magnetic field turned on. A sweep voltage should be applied to the modulation coils on the sample cavity.

Now, before searching for an EPR signal, we must consider the crystal diode that is to be used as a detector in one arm of the hybrid tee bridge.

This, like most diodes, requires a bias current to be passing through it if it is to be at all sensitive to the signals which it is expected to detect.

A method of providing the needed bias current is to adjust the iris coupling screw so that a small amount of microwave energy is reflected to the crystal detector. An alternate method is to use a device called a "slide screw tuner".

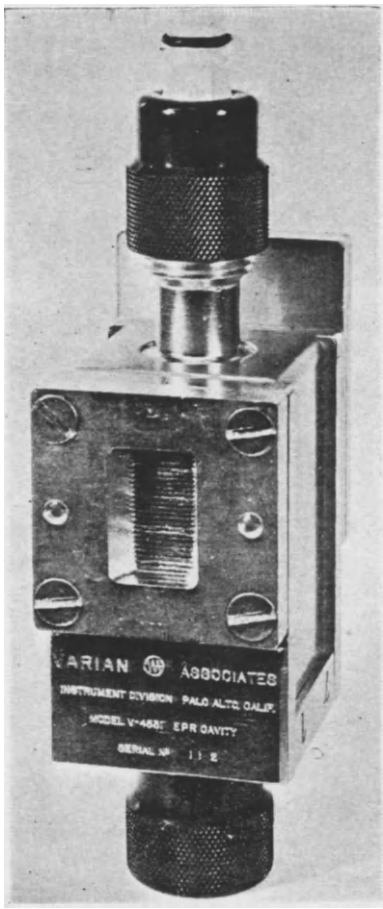

FIG. 9. Sample cavity with provisions for irradiating sample and varying sample temperature

This slide screw tuner is nothing more than a small metal probe which is inserted into a slot in the waveguide arm leading to the sample cavity. When the probe is inserted into the waveguide, the result is that a small portion of the microwave energy going to the cavity is reflected. This reflected energy strikes the detector diode, causing a current to flow, and thus providing the needed bias. The amount of power to be reflected can be controlled

by the distance that the probe is inserted into the waveguide. In addition, the phase of the reflected voltage can be controlled by shifting the position of the probe along the waveguide.

Our instrument is now prepared to receive and detect an EPR signal. By slowly varying the magnetic field until the proper value for resonance is reached, a signal will appear on the oscilloscope. Figure 10 is an oscilloscope picture of the first harmonic presentation of an EPR signal.

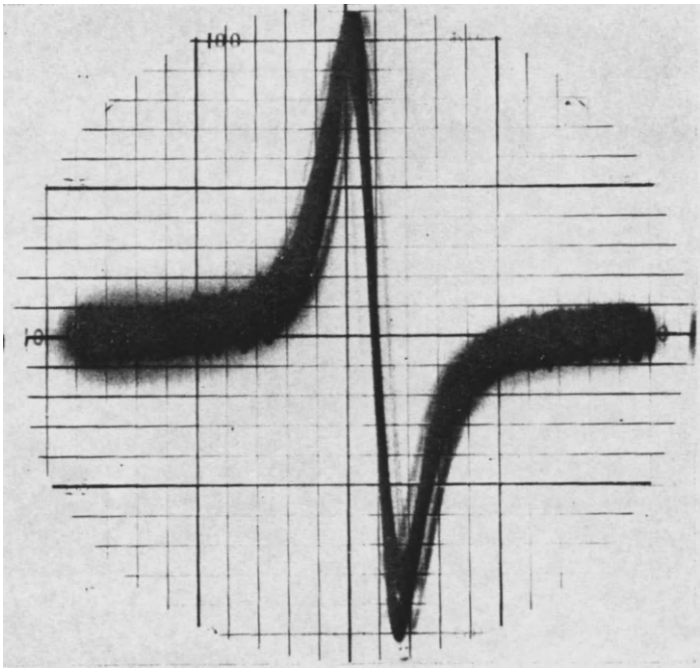

FIG. 10. EPR signal on oscilloscope (first harmonic presentation).

This type of signal presentation is the result of using a modulation and phase detection method of observing the resonance signal. The following discussion will explain how such a presentation is obtained.

As illustrated in Fig. 11, the static magnetic field is positioned on one side of the resonance line. Superimposed on that field is a sine wave modulation at a frequency of 100 kc. (This is effected by applying a 100 kc voltage to a set of coils on the sample cavity walls.) As a result of this 100 kc field sweep and the EPR resonance, the microwave energy in the cavity is modulated. The phase and amplitude of this modulation is dependent on the EPR resonance line and the value of H_0 (with superimposed modulation) relative to the resonance line. (See Fig. 11.)

The microwave energy (modulated by a 100 kc voltage which contains the EPR signal information) strikes the crystal diode in one arm of the hybrid tee. The signal information is then amplified and carried to the input of the phase detector.

Although the mechanical synchroverter is used for a signal phase detector only in the audio-frequency EPR units, nevertheless it provides the best means of explaining the function, use and adjustment of the phase detection system. The moving contacts of the synchroverter are driven by a voltage

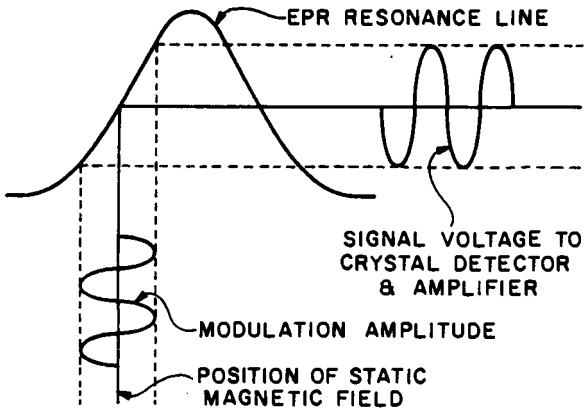

FIG. 11. Signal resulting from field modulation of EPR resonance.

derived from the same oscillator as that used to supply modulation to the EPR cavity. Thus, the switching contacts provide a phase reference for the incoming signal information (see Fig. 12). If a modulation frequency of 100 kc is used, then electronic diodes, switched between a conducting and non-conducting condition, replace the synchroverter.

A phase control has been provided in order to adjust the point in time at which the moveable contacts switch. It is desirable that the contacts break and make just as the input signal voltage is passing through the part of its cycle at which it is zero. These points in time are represented by the dotted lines in Fig. 12.

When signal A (which results from choosing an operation point on one side of the EPR line) is applied to the input of the phase detector, we observe that the output is a pulsating d.c. voltage. In the case of signal B we observe that the output is again a pulsating d.c. voltage, but that the polarity of this voltage is opposite to that observed in A. To summarize, the phase detector develops a d.c. output voltage, the amplitude and polarity of which are dependent on the amplitude and phase of the input voltage. In addition, we observe that it can only develop an intelligible output signal from an input signal whose frequency is the same as that used to switch the contacts. Thus,

we find that a coherent signal results only from our EPR information, since any other signals entering the phase detector have phases which are random.

We should note that if switching does not occur as indicated in Fig. 12 at the dotted lines, the contacts will not receive the full voltage for that half cycle. In fact, if they were to switch at times t_1, t_2, t_3, etc., as indicated in

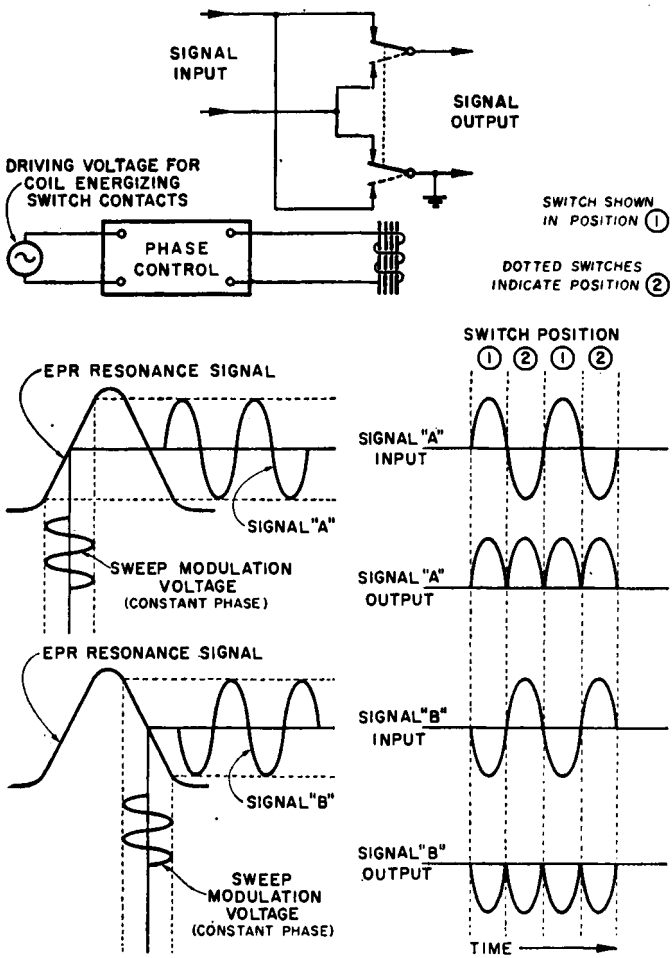

FIG. 12. Input and output signals of phase detector.

Fig. 13 (the phasing of the voltage driving the switching contacts has been adjusted 90° out of phase with the signal input voltage), then no resultant d.c. voltage will exist at the phase detector output because there is as much positive as negative voltage at the output. Thus, the output is zero.

From the preceding discussion it is obvious that in order to phase the synchroverter switching contacts properly, we must introduce an EPR signal

into the phase detector. By adjusting the phasing control to obtain maximum amplitude of the EPR signal on the oscilloscope, we know that we have adjusted the phase detector for the maximum output signal voltage.

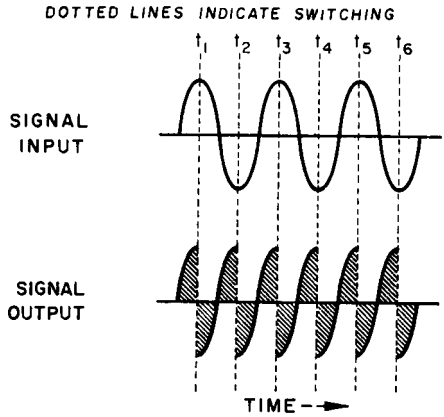

FIG. 13. Improper switching of synchroverter.

By integrating our output voltage over a long time period in comparison with the time periods of the *random* input signals (noise), we are able to average out almost all random signals and thus record only the EPR signal information. The output is a first harmonic presentation of the original EPR line. A typical recorder trace is shown in Fig. 14.

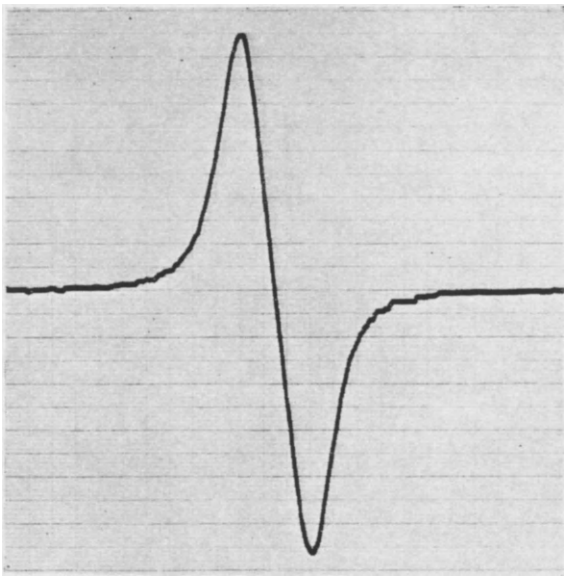

FIG. 14. Recorder trace of EPR signal.

Once a signal is obtained, there are several things that can be done in an effort to optimize the signal-to-noise ratio. One important adjustment is the amount of r.f. power delivered to the sample.

If too much power is delivered to the sample, the signal will be "saturated", with the result that the amplitude will be reduced and the line will be broadened. If too little r.f. power is used, the maximum possible signal obtainable for a particular sample will not be realized. Since optimum adjustment is dependent upon the relaxation time characteristic of the sample being studied, the operator finds that this adjustment must be made on an empirical basis.

In adjusting the instrument, the operator should pass through the resonance line with a given r.f. power; then pass through it once again with a slightly higher r.f. power. If the signal increases in amplitude, this is an indication that the signal is not yet saturated. If the amplitude drops, then this would indicate that saturation has been reached.

It should be noted that when examining samples at room temperatures, most EPR lines are so broad that it is exceedingly difficult, if not impossible, to saturate them. However, if the temperature of the sample is lowered to the region of liquid nitrogen or liquid helium temperatures, then the relaxation times of many EPR samples are increased and r.f. saturation can result.

Figure 15*a* shows a signal with the r.f. power properly adjusted, while Fig. 15*b* shows a line which has been reduced in amplitude and broadened due to r.f. saturation.

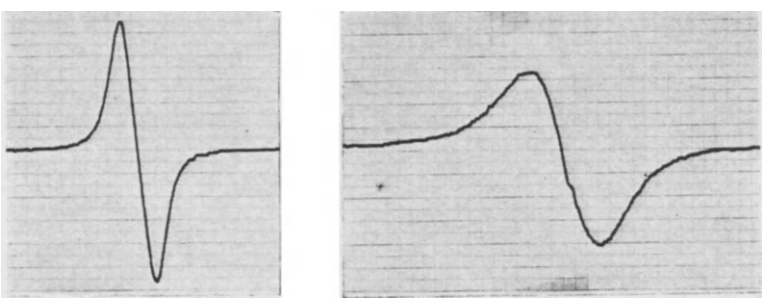

(*a*) (*b*)

FIG. 15. (*a*) EPR signal—r.f. power properly adjusted; (*b*) Saturated EPR signal—r.f. power excessive.

A second adjustment that should be optimized, if maximum signal-to-noise ratio is desired, is the amplitude of modulation voltage to the sample cavity. If this amplitude is infinitely small, a true first derivative curve will result; however, its amplitude will be less than the maximum that can be obtained. (Note: When the amplitude of the modulation is *not* infinitely small, the resulting signal can no longer be called a *true* derivative curve.)

As the amplitude of the modulation voltage is increased, the amplitude of the first harmonic presentation will increase until the sweep magnitude (peak-to-peak) is approximately twice the line width (assuming a Lorentzian line shape). Further increase of the modulation will result in a reduction of the amplitude of the first harmonic presentation. It should be noted that the presentation will also be broadened. This broadening (it is called artificial sweep broadening) begins to occur when the modulation amplitude is approximately equal to the line width. Increasing the modulation voltage leads to the limiting case, which results in an output from the phase detector which is two signals, one positive, one negative, and separated by the peak-to-peak amplitude of the sweep modulation. This effect due to excessive sweep modulation can best be understood by considering the input and output voltages of the phase detector as the magnetic field is swept through resonance.

Even before the static magnetic field is swept onto the resonance line, the peaks of the modulation extend the field until it is the value required for resonance. (See Fig. 16*a*.) A signal voltage is thus produced and then detected

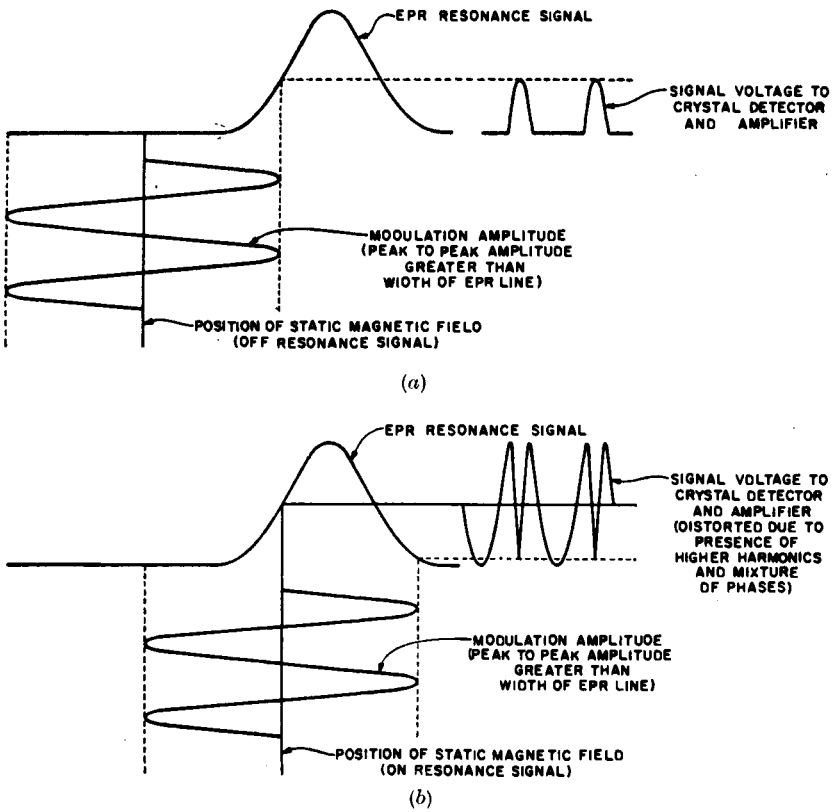

FIG. 16. Signal voltage distortion due to excessive sweep modulation amplitude.

by the phase detector. The result is an output signal voltage to the recorder before the H_0 magnetic field reaches the resonance value.

When the H_0 magnetic field is on one side of the resonance line, the modulation sweeps across and over the top of the resonance. (See Fig. 16*b*.) The signal to the phase detector is now a mixture of phases (one phase resulting from the positive slope of the resonance line, the other resulting from the other side of the resonance line—a negative slope). Therefore, the output signal to the recorder is reduced in amplitude due to this distorted signal information.

As a rough rule of thumb, the operator should use a modulation amplitude equal to one-tenth of the signal line width, if a good representation of the derivative is desired. If a weak signal is to be observed and maximum signal-to-noise ratio is required, then a sweep modulation amplitude approximately equal to twice the width of the line should be used (assuming a Lorentzian line shape). Again, as in the r.f. power case, best results will be obtained by an empirical adjustment. (See Fig. 17*a*, *b*.)

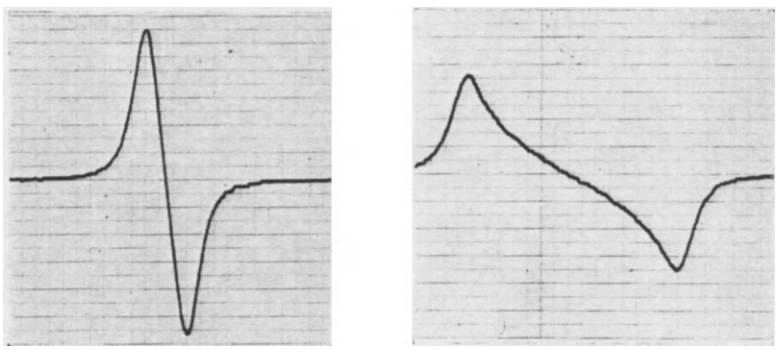

(*a*) (*b*)

FIG. 17. (*a*) EPR signal—modulation amplitude properly adjusted; (*b*) EPR signal—modulation amplitude too large.

A third variable in connection with optimizing the signal is the rate of passage through the signal. The derivative curve may be partially integrated, if the rate of passage is rapid in comparison to the time constant of the noise integrating network. Figure 18*a* and *b* provides a comparison between a signal that was scanned at the correct rate and one which was distorted because it was partially integrated due to the rapid rate of passage through the resonance line.

In closing this discussion, a few comments should be made in regard to calibrating the width of EPR resonance lines. Present day practice makes use of EPR samples which provide a resonance signal composed of several

lines. The separation of these lines having been accurately determined, they can then be used to calibrate other resonance spectra. A sample that is often used for this purpose is peroxylamine disulfonate (Fremy's salt).

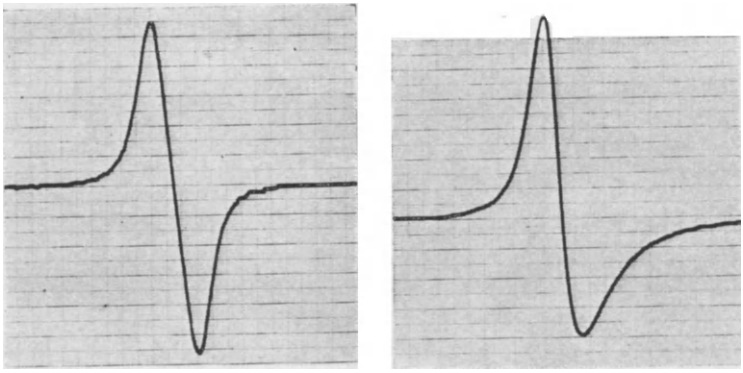

(*a*) (*b*)

FIG. 18. (*a*) EPR signal—scanning rate correct; (*b*) EPR signal—scanning rate too rapid.

A second calibration method is the use of a variable frequency nuclear resonance device and a frequency counter. By measuring the frequency of precession of the nuclei at various magnetic field values, the spectrum can then be calibrated in units of magnetic field.

6

INSTRUMENTATION OF HIGH RESOLUTION NMR

FORREST A. NELSON

HIGH Resolution NMR can be used for the analysis of several types of isotopes, however H^1 is the most common of these and therefore of greatest interest. The gyromagnetic ratio of the proton is 4.257 kc/gauss, so easily obtained magnetic field values will set the frequency in the high radio-frequency range: 40 Mc requires a 9.4 kilogauss magnet field, 60 Mc, a 14.1 kilogauss field. Similarly for the F^{19} isotope, the resonance will be about 6 per cent lower in frequency and will use essentially the same equipment.

An NMR spectrometer can be divided into two general parts, the spectrometer electronics and the magnet system. There is no complete separation, but the radio-frequency unit, the probe (located in the magnet gap and containing the test sample), the sweep system, the signal indicators and the power supplies for these items can be considered as the spectrometer electronics. The magnet, the magnet power supply with current regulator and the magnetic field stabilizer are the magnet system and can operate independently.

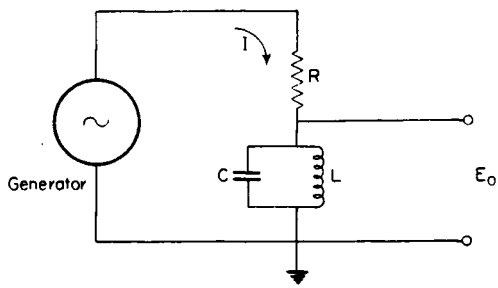

FIG. 1.

There are several circuits which will detect NMR signals. The most simple type is that of a voltage divider circuit shown in Fig. 1. The generator operates at radio frequency ω. The coil, L, which contains the sample, is tuned to resonance by capacitor, C, and, therefore, can be represented as a resistance

of impedance $Z = \omega LQ$. ω is $2\pi f$ where f is the generator frequency and Q is the figure of merit of the coil. The radio-frequency field, H_1, inside the coil is produced by current from the generator. This coil containing the sample is in the magnetic field, H_0. The generator output is a sine voltage of $E_g \sin \omega t$ but for simplicity, the peak voltage, E_g, will be used. If resistor, R, is large compared with Z, a constant current, I, will flow and the voltage output, E_0, will be

$$E_0 = IZ$$

Then at resonance the impedance across the coil is lowered slightly to Z' because of the NMR absorption of the sample, and the output across this tuned coil is proportionally lowered to IZ'. The disadvantage of this system is that the output contains a high level of radio-frequency voltage with a small modulation, and even minute fluctuation or change of generator output will appear as noise at the output.

The divider system can be changed to eliminate the previously defined problem. Figure 2 illustrates the modified circuit which has been connected as a bridge.

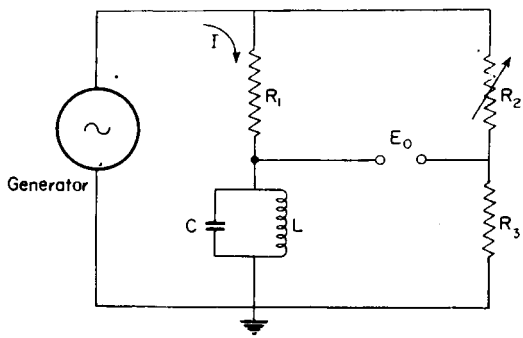

FIG. 2.

When the radio-frequency voltage across R_3 is equal to that across L, the bridge has zero output and, as the impedance, Z, is modified by NMR resonance, the unbalance appears as the output voltage, E_0. There are many bridge circuits such as the bridged T which are more practical than this one, although with most types the degree of balance changes radically with frequency. Systems in which both the generator and the amplifier can be grounded on one side are usually desirable. Two controls are normally required to balance a bridge, control of amplitude and phase, or separate amplitude controls of two phases. These controls are not shown in Fig. 2, but must be included because of stray couplings which always exist.

Another system for NMR detection uses a marginal oscillator. A radio-frequency oscillator is designed so that it can be adjusted to the point at which there is just enough feedback to maintain oscillation. A simplified

diagram is shown in Fig. 3. The sample is placed in the coil, L_1, and the voltage is adjusted so that oscillation is just sustained. When the impedance across L_1 is lowered by NMR resonance in a sample inside L_1, the level of oscillation decreases. Either the change of r.f. voltage across L_1, or the change of grid voltage because of current change through R_1 can be used for output to the amplifiers. Note that in either case the signal is only a small change superimposed on a larger voltage as was the case with the resistor divider method.

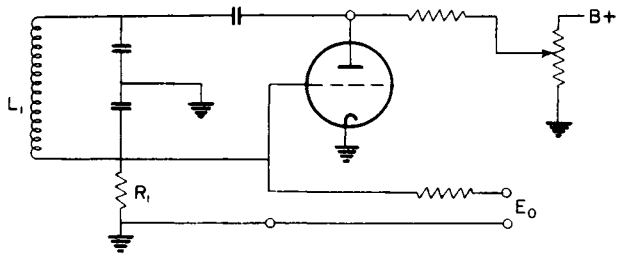

FIG. 3.

Another system of detection of NMR resonance uses crossed coils as illustrated in Fig. 4. The generator or transmitter output is fed to one coil or set of coils and the output is taken from another coil containing the sample. The sample coil is inside the first coil but not coupled directly to it because of orthogonal orientation. The transmitter coil induces magnetic resonance in the sample and the precessing magnetic moment from this sample couples

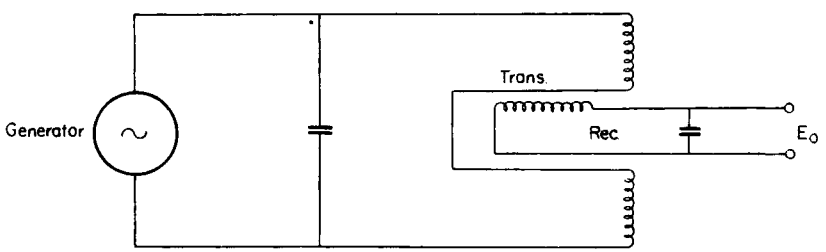

FIG. 4.

a signal into the output receiver coil. There is output only when NMR resonance is present in the sample, providing the coils are completely decoupled.

The crossed coil probe is in general use for high resolution. It is more complicated mechanically but it has the advantage of having an independent output coil which can be optimized for signal pickup and best impedance match to the amplifier which follows. In addition, the balance is less sensitive to frequency change and sample exchange than is that of the single coil

bridge probe. The transmitter coil is large and therefore gives a more uniform field over the sample being measured than is the usual case with a single coil system. The decoupling between coils is done by small mechanically adjusted controls called paddles which add or subtract mutual coupling between the coils.

A Varian Model V-4331 crossed coil high resolution probe can be used to illustrate the previous discussion. This probe has a relatively large volume inside its transmitter coil. This coil is divided into two sections and cemented to a glass form as illustrated in Fig. 5.

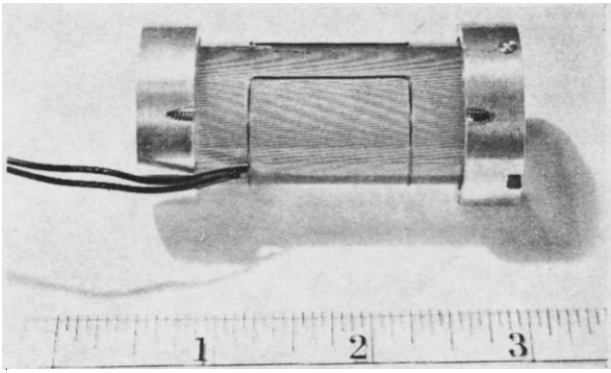

(a)

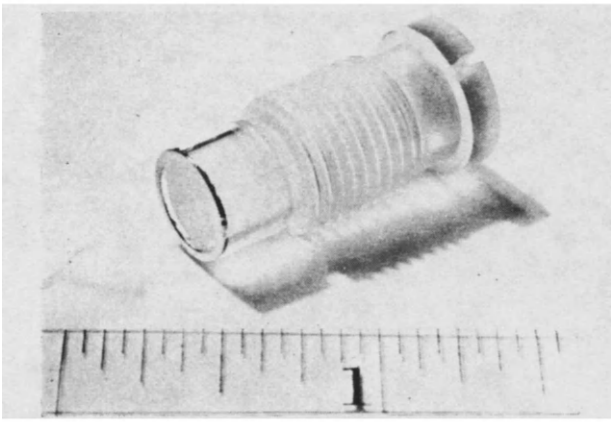

(b)

FIG. 5.

The receiver coils of different diameters plug into a socket inside the transmitter coil form so that the receiver coil and the transmitter coil asssembly have the same geometric center. Thus the receiver coil axis is essentially orthogonal to the other coil axis. The receiver coil is slightly skewed on its

glass form so that an initial balance of the probe is possible by rotation of this receiver coil assembly. A finely divided shield between the transmitter and receiver coils reduces electrostatic coupling without affecting the magnetic field.

After the initial balance, the mechanically adjustable paddles can completely decouple the two coils or can add a coupling of any phase. The operation of these controls is shown by Fig. 6.

If I_T is the current in the transmitter coil, the voltage E_R induced directly into the receiver coil will be:

$$E_R = j\omega M_{TO} I_T$$

where ω is the 2π times the radio-frequency of transmitter, M is a mutual inductance constant, M_{TO} represents the mutual coupling between the coils T and O, and j represents a phase shift of 90° (cosine vs. sine). If another coil is coupled to both the transmitter and the receiver coils, the transmitter will induce a voltage into it and, if the circuit of this coil is closed, current will flow. R is the resistance of coil; ωL is inductive reactance of the coil.

$$E = -j\omega M I_T$$

$$I = \frac{-j\omega M I_T}{Z} = \frac{-j\omega M I_T}{R + j\omega L}$$

The red paddle is a low loss shorted coil (the zero resistance coil 1 of Fig. 6) so its current is approximately

$$I_1 \approx \frac{-j\omega M_{T1} I_T}{j\omega L} = \frac{-M_{T1} I_T}{L}$$

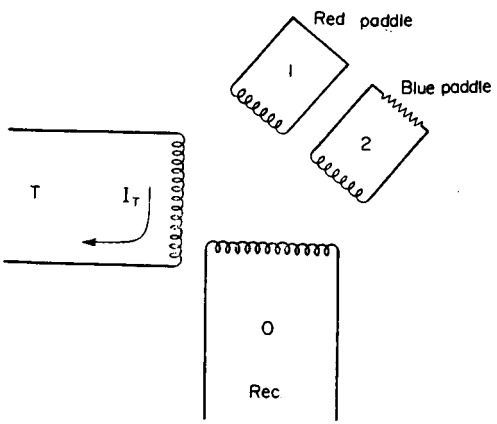

FIG. 6.

Note that the current in the red paddle is now phased 180 degrees from that in the transmitter coil. The voltage induced in the receiver coil from current in the red paddle is therefore

$$E_0 = j\omega M_{1R} I_1 = \frac{+j\omega M_{10} M_{T1} I_T}{L_1}$$

which is 180 degrees different from that induced by the transmitter coil directly. Actually the mutual coupling can be varied mechanically so that it is positive, negative or zero. Therefore, the red paddle can either add or subtract from any direct coupling between T and O.

The blue paddle is made with high resistance so that R_2 is greater than L; therefore, the voltage induced into it is approximately

$$E_2 = -j\omega M_{T2} I_T$$

and the current in it is approximately

$$I_2 = \frac{-j\omega M_{T2} I_T}{R_2}$$

The voltage induced from this coil into the receiver coil will be

$$E_O = -j\omega M_{2O} I_2 = \frac{-\omega^2 M_{2O} M_{T2} I_T}{R_2}$$

with the coupling constants also variable through zero. The variation of this coupling will control an induced voltage which is essentially 90° different in phase from that induced by either the transmitter coil directly or by the red paddle as shown by Fig. 7. This blue paddle is needed in order to balance out couplings due to eddy current losses in probe parts and in the sample.

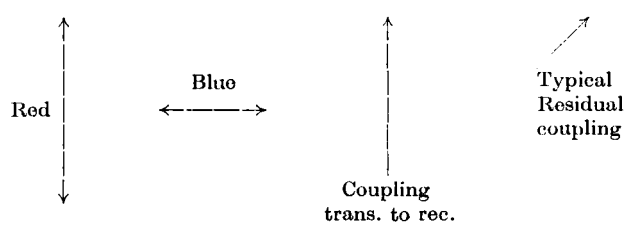

FIG. 7.

If a residual coupling of any phase is to be balanced out, it is done by adjusting for minimum output of the receiver with first a red and then a blue paddle, and repeated until the receiver output is just noise. The blue paddle coupling is not exactly out of phase with respect to that from the red paddle mostly because its resistance is not infinitely larger than the inductance of the blue paddle and so the controls are not completely independent. If the blue paddle

has a resistance several times its reactance, a complete balance is easily obtained.

A small receiver coil is used for a high resolution NMR probe because of the high magnet field homogeneity requirement. A short sample can be used although this makes it difficult to keep the field homogenous inside the sample. Therefore, a long cylindrical sample will be used. The signal pickup along the axis of the sample tube will be approximately

$$E_y = E_{yo}\frac{r^3}{(r^2+y^2)^{3/2}}$$

where r is radius of a short coil, y is distance from coil center along sample axis, and E_y is signal picked up at point y. At $y = 2r$ the pickup per unit volume is about 10 per cent of that at the center, E_{yo}.

If the whole assembly is increased so that the filling factor remains the same, the effective sample is increased by r^3. However, the signal does not increase by such a spectacular amount, as a portion of the signal from the center of the coil is inversely proportional to r. Also to maintain the fixed inductance in the coil, the number of turns must be inversely proportional to the radius. These two factors reduce the signal increase from a third power of the radius to a linear increase. Actually, the larger receiver coil diameter will give more than this indicated signal enhancement because the filling factor can usually be increased in a larger diameter tube.

High resolution NMR resonance lines are very narrow and therefore the transmitter which supplies the radio-frequency power to the probe must have very good frequency stability. If this frequency should vary one part in 10^8 at 60 Mc, this variation would be 0.6 cycles, which is more than the line width in many cases. The transmitter includes a stable crystal oscillator whose frequency is usually multiplied once or twice before it reaches the output amplifier. The output power needs to be constant because, even though the receiver coil is completely decoupled from the transmitter coil, any change in power would alter the signal amplitude. Thus, if the probe is not perfectly balanced, an off-resonance base line would then be modulated by any change in transmitter output. In a simple unbalanced system this effect is extremely annoying and often gives a noise output greater than the signal.

The NMR signal from the tuned receiver coil is coupled into a low noise preamplifier. This preamplifier can be mounted directly on the probe so that maximum signal is amplified; the second half of the r.f. amplifier is then located inside the receiver position of the r.f. unit. A superheterodyne type receiver will give good stability at high gain. In the superheterodyne system, the signal is amplified at the original frequency and mixed with a local oscillator output to produce a lower beat frequency (i.f. frequency of 5 or 10 megacycles) which is also amplified so that the total amplification will be over one million. Figure 8 is a block diagram of a typical superheterodyne and Fig. 9

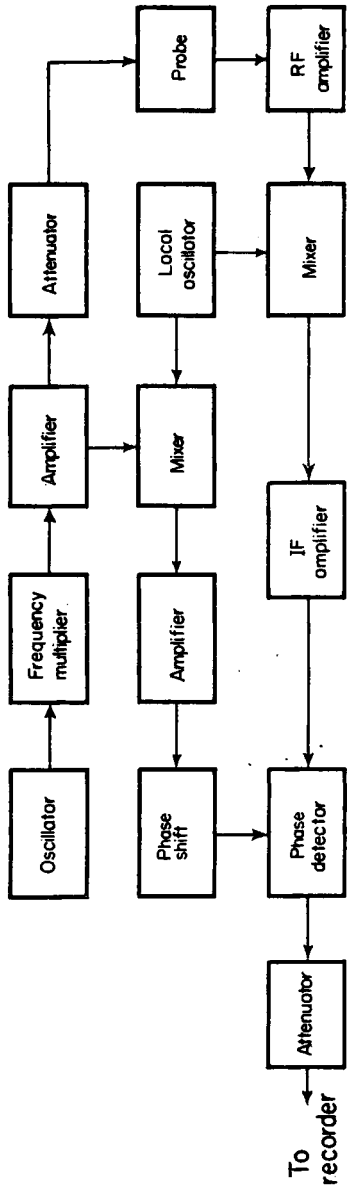
Oscillator
Frequency multiplier
Amplifier
Attenuator
Probe
Phase shift
Amplifier
Mixer
Local oscillator
RF amplifier
Mixer
IF amplifier
Phase detector
Attenuator
To recorder

FIG. 8.

shows such a unit. It is obvious that an extraordinary degree of decoupling is needed to prevent transmitter output from getting into the receiver input.

The signal after amplification is fed into a detector which gives a d.c. output proportional to the radio-frequency input. The detector output is fed into the recorder and oscilloscope. This output is zero or a constant until resonance is reached, then it varies to follow the amplitude of the NMR signal.

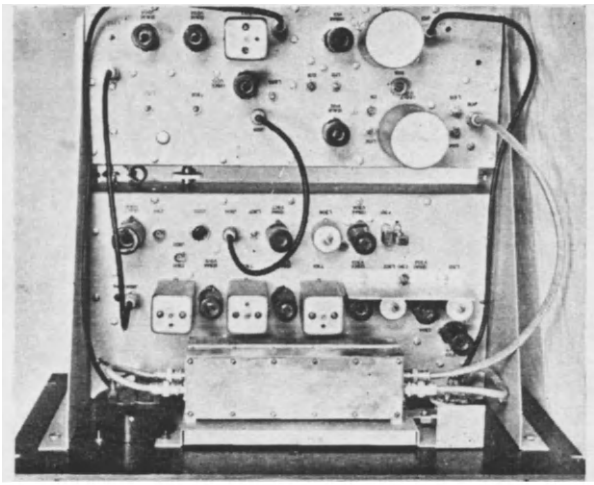

(*a*)

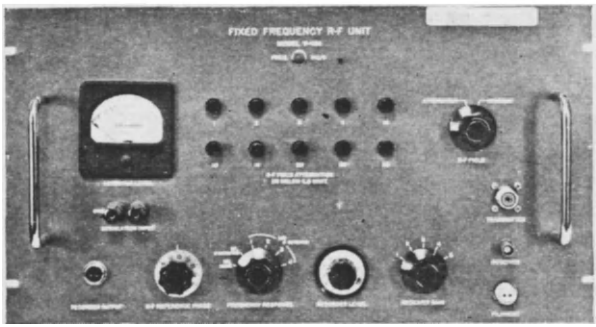

(*b*)

FIG. 9.

Actually for high resolution it is desired to have only the one phase of this signal (the v-mode) so a reference carrier of the same frequency and correct phase must be added to the signal at detection. This can be done simply if the probe is not completely balanced, permitting some of the transmitter power of the proper phase to be amplified with the NMR signal. This simple method has the disadvantage associated with any unbalanced bridge in that

as the transmitter power is changed, the base line moves. For direct coupled output, such as is used in high resolution, this base line shift is not only a nuisance when changing transmitter power but can contribute to noise. A balanced phase detector is much better. In this latter method, the reference carrier is fed to a double detector so that the reference output cancels but the signal output adds. A phase detector can select either the v-mode or the u-mode phase by proper reference phase.

The principle of phase detection is based upon the addition of vectors. If we rotate at the rate of the radio-frequency and select a phase determined by the reference carrier, we see a reference voltage vector of constant amplitude R as shown in Fig. 10a. When we add a signal, S, in phase, it increases the size of the vector as in Fig. 10b; but if the signal is shifted 90° in phase, it

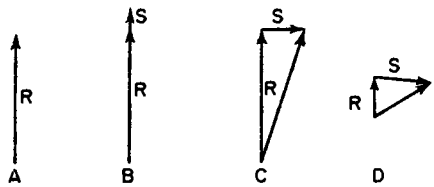

FIG. 10.

adds little to the total magnitude of the reference (Fig. 10c). The detector diodes sense only the magnitude of impressed signal so that whenever the reference is much larger than the signal, the detector output is sensitive only to that portion of the signal which has the same phase as itself. Note also that, as the signal amplitude becomes comparable to that of the reference (Fig. 10d), the quadrature signal is no longer totally rejected. If the u-mode is not rejected, the lines will be broadened and relative areas of strong resonances will be increased. The reference also has another useful purpose. It biases the diode so that the signal output may be both larger and much more linear than would be the case without the reference as illustrated by signal S_1 and S_2 of Fig. 11.

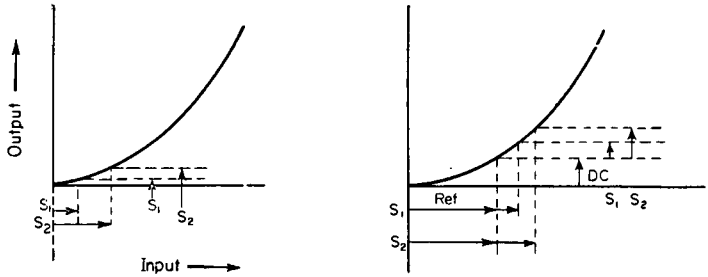

FIG. 11.

The phase reference must be coherent with the NMR signal or the result is a beat between the signal and the reference rather than a slowly changing addition or subtraction. Therefore, an ordinary superheterodyne circuit will not work with a phase detector but instead, as Fig. 8, a system is used in which the reference for the intermediate frequency phase detection is derived by mixing some transmitter output with the same local oscillator that is used for the frequency conversion in the receiver. This means that both the NMR signal and the reference carrier are at the same intermediate frequency. Any system which uses a separate reference to the phase detector is subject to phase drift because each tuned circuit can shift phase slightly during warm-up of the instrument and, whenever the signal and reference are amplified separately, their relative phase can shift. This is minimized by using stable tuned circuits and by cancellation of drift in the NMR signal amplifiers by a similar drift in the reference circuits.

The reference carrier also has one other function. If a signal and noise are fed into a non-linear device such as a detector, the noise not only beats with the signal but also noise beats with noise which produces low frequency outputs that cannot be eliminated after detection. The addition of a large reference (or a large signal input) has the effect of suppressing noise-to-noise beats so that only the signal plus any beating with signal are present in output. A low pass filter after the detector can then eliminate the noise that was not close to the signal frequency by reducing the bandwidth. It is very much simpler to change the bandwidth after detection than before.

In all applications of high resolution NMR the sample inside and near the receiver coil must be in a magnetic field which is extremely homogeneous. One very useful means of getting sharper resonance lines is to spin the cylindrical sample tube. If there is a linear field change across the sample in a direction normal to the axis as shown in Fig. 12*a*, parts of the sample, such as particles *a*, *b* and *c*, will follow paths *a*, *b* and *c* of Fig. 12*b* with rotation of tube. Rotation must be so rapid that the nuclei do not spend enough time in the high or low field to lose phase coherence.

The sample rotation causes the nuclei away from the center first to increase and then decrease in frequency, but all nuclei in the plane shown will have

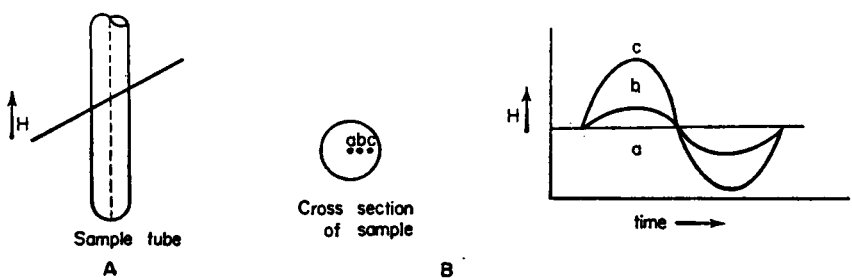

FIG. 12.

an average frequency the same as the nuclei in the center. Therefore, if the field is constant along the axis of rotation, the nuclei will resonate at the average field value and the line will be greatly narrowed. Too much field gradient across the sample tube requires a spinning rate so high that a vortex of the liquid surface will protrude down into the measured volume of this sample and, unless the susceptibility of the liquid is the same as that of air (which is practically impossible with high resolution samples), the magnetic field homogeneity is ruined. Too slow a spin rate is also a cause of trouble in that it will result in a sharpened center line with sideband signals spaced at the spinning frequency as shown by Fig. 13. *A* is non-spinning resolution, *B* is slow spinning, and *C* is a moderate spinning rate.

FIG. 13.

Because objectionable sidebands appear if the spinning rate is not high compared to the field inhomogeneity over the sample, it is always desirable to start with the most homogeneous magnet possible.

The magnetic field strength used for proton high resolution at 60 Mc is approximately 14.1 kilogauss. The axial length of sample sensed by the receiver coil is usually about $\frac{1}{2}$ in. long, and for high resolution the field needs to be constant over this length to 0.1 to 0.2 milligauss, which is a variation of one part in 10^8 of the total field. The homogeneity requirement normal to the sample axis is less because a field change of one or two milligauss across the tube can be easily averaged out by the sample spinning.

A magnet for high resolution NMR can be either an electromagnet or a permanent magnet. The permanent magnet is useful for low fields if the field strength does not need shifting. This type of magnet is often wound with coils which are used to magnetize the Alnico iron to the proper field, then to bias the field to the exact value needed for resonance and lastly to compensate for drift of the field due to temperature or environmental field changes.

The electromagnet used for high resolution has a soft iron yoke and pole pieces with large coils which continuously energize the magnet. The current to these coils must be regulated accurately in order to hold the magnet at the correct field. An electromagnet is both capable of operating at higher field strengths than a permanent magnet and over a wider range of field strengths with good field homogeneity. Operation at high field strengths spreads out and simplifies the NMR spectrum and also improves the signal-to-noise ratio.

The iron yoke of the magnet has to be rigid so that the air gap which contains the probe will not vary and thereby change the field. The field of an

electromagnet at constant current is approximately inversely proportional to the air gap. Field strength at a given gap would be exactly proportional to the ampere turns of the coils, if it were not for the saturation of the iron which reduces its permeability. Figure 14 shows the curve of a magnet with infinite permeability iron and actual iron.

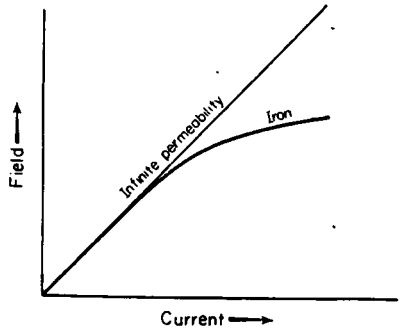

FIG. 14.

It becomes increasingly difficult to make a magnet operate above 10 or 15 kilogauss, not only because of the power required (proportional to second power of current), but also because of the severe degradation of the field uniformity in the gap.

The magnetic field in the gap of a cylindrical magnet is normally maximum at the center of the gap with a rapid drop off near the edge of the pole caps where the field strength is about $\frac{3}{4}$ that of the center. The direction of the entire magnetic field is essentially perpendicular to the pole caps. This direction is designated as the Z direction and a high resolution magnet will have coordinates of X horizontally along the caps, Y vertically along the caps, and Z from cap to cap. Because the NMR resonance frequency is determined by the strength of the magnetic field, the only homogeneity requirement is that this field remain constant over space and time.

Cylindrical pole caps are not always used on the magnet. For high fields, the pole caps can be tapered. By reducing the loss of flux in the fringe field the proper taper can increase the field strength in the useful part of the magnet gap.

The uniformity of a magnetic field over a large gap is sometimes improved by the use of ring shims. With these, the edges of the pole caps are raised so that the normal radical field drop-off is partially compensated by an increase of field strength at the edges due to the smaller gap there. Figure 15 shows the improved field uniformity at the center of the gap. Curve A has normal caps without the compensation and curve B has properly adjusted ring shims. These compensated caps are quite useful at low fields whenever a large volume of homogeneous field is desired, but at high fields the iron of the rings saturates and is less effective and, worse yet, the lower permeability

of all the iron causes a lowering of the magnetic potential just inside the rings with the end result that the central region field can be worse than that of the original cylindrical caps as shown by curve C of Fig. 15.

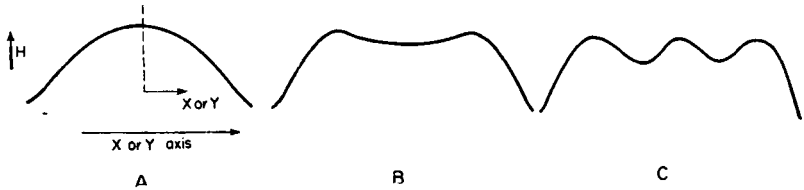

FIG. 15.

Besides pole cap modification, there is a better way to get uniform fields in a magnet designed for high resolution. This is by the method known as "cycling the magnet". If the magnet is turned on from zero field up to the resonance field, both the X and Y field will usually fall off from a point near the center, as in Fig. 16*a*. If the current is increased a few per cent for a minute or two and then returned to NMR resonance, the field may have a shape as shown by Fig. 16*b*. Therefore, at some lower cycling, there will be no change in magnetic field near the center.

FIG. 16.

If the spectra are to be resolved to one part in 10^8 or better, the total sample measured must be within a field whose strength varies less than one part in 10^8 of the total field. If the spinning technique is used, the length of the sample seen by the receiver coil must be in a field with this average homogeneity. A gradient along this axis will produce a broadened line. If the sample is located in a field with a bad linear gradient along the axis of rotation, the signal shape will be determined by the relative coupling from each portion of the sample to the receiver coil. During scanning, the field strength increases and, first, one loosely coupled end of the sample reaches the field required for resonance, then, as resonance progresses along the sample, the signal intensity increases to a maximum when that portion of the sample inside the coil is resonant, and then decreases as the resonant condition progresses toward the other end. Figure 17 shows the approximate shape produced. This assumes high homogeneity of the radio-frequency field H_1. This latter homogeneity is determined by the shape and size of the transmitter coils.

Cycling the magnet is an art that requires some practice to learn. If the magnet is turned on from zero field to the resonance, the only area of good field homogeneity is at the point near the center of the gap. Only the center

of a large coil will be in the good field so the lines of the spectra obtained will appear as in Fig. 18. The reason for this is that the center of the sample (most closely coupled part) will be in resonance first, then the top and bottom of the sample gradually reach resonance and smear out the line.

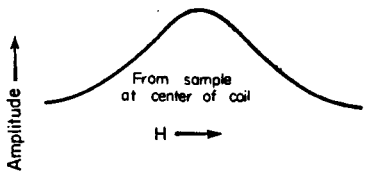

FIG. 17.

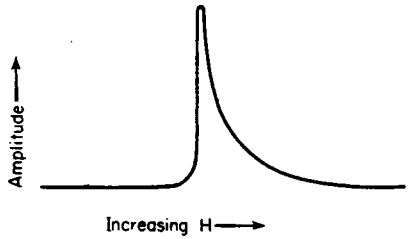

FIG. 18.

By cycling the magnet to a high current and back down to resonance, the "dish" of the field will produce a reversed condition in the Y direction. The result is a line shape shown by Fig. 19.

Note that the loosely coupled nuclei on the top and bottom hit resonance first and the closely coupled central part last, so the signal ends rapidly (usually with a great deal of ringing, which is the beating of the NMR signal with the transmitter reference).

A perfectly flat field, therefore, should produce the ideal line shape as all parts of the sample resonate together, as shown by Fig. 20. Actually this

FIG. 19.

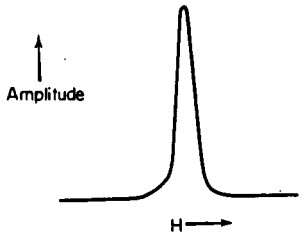

FIG. 20.

is not quite true, as the materials in the probe affect the shape of the field and usually slightly increase the field toward the middle, therefore a slightly overcycled or dished condition is sometimes helpful. The amount of this overcycling is only a few milligauss in inches and may be considered a flat field. The magnet also may develop a linear gradient in either the X or Y direction. The latter is most troublesome in a spinning sample, but the magnet can be deformed very slightly so as to change the pole face parallelism in order to correct this condition. This operation is performed with a mechanical field trimmer. Another means of correction of magnet field gradient is the electric shim. The shim coils can be mounted either on the NMR

probe or on the pole caps and offer the advantages of remote control and extreme ease of operation. Linear field controls in X, Y and Z axes and one curvature control are sufficient if the magnet is built for high resolution work.

The X and Y coils are made so that with a fixed current they will superimpose a field change as shown by Fig. 21. The linear center portions of this

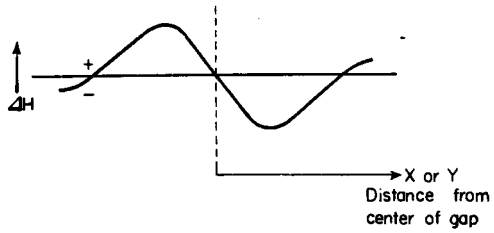

FIG. 21.

curve (with magnitude and direction of the field change controlled either by an X or Y adjustment knob) can cancel any small linear gradient of the magnet in this direction. The Z gradient is corrected by an identical coil on each side of the sample connected so as to have opposing fields as shown by Fig. 22. As with X and Y controls, the magnitude and direction of current will allow a correction of linear gradient.

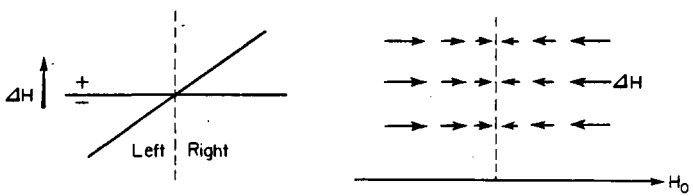

FIG. 22.

The curvature control is composed of sets of coils which increase or decrease the field at the center of the magnet compared to the field a short radial distance from this center. One pair of coils does this by adding a field of the general shape of Fig. 23*a*.

The sample at the center also will experience a change in total field so another set of coils with a small gradient is used to buck-out the total field but leave a net change in effective "cycling" of the magnet as shown by Fig. 23*b*.

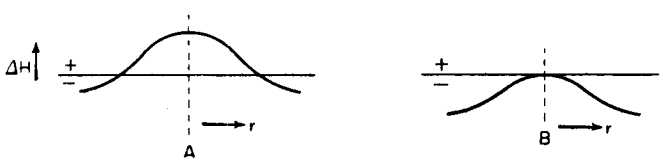

FIG. 23.

All of these shim coils are designed for a sample located at their geometric center. Operation off this optimum location can result in deterioration of results and loss of the ease of adjustment. Although these coils will make a poor magnet better, their best application is on a good magnet so that optimum homogeneity can be maintained with very little effort.

The ability of a magnet to preserve the extremely high homogeneity required is mostly dependent on thermal problems. It has been found that all parts of the iron yoke of a magnet apparently do not have an equal coefficient of thermal expansion, even though they are made out of the same material. It is, therefore, necessary to insulate the yoke to give it a long thermal time constant, i.e. high thermal stability. Also it is helpful to have a temperature controlled room with small heating or cooling cycles of one or two minutes. An electromagnet also has water cooled coils which must be insulated from the magnet core or at least made perfectly symmetrical to the pole pieces and yoke so that heat transfer will not distort the parallelism of the pole caps by expanding the top of the pole piece more than the bottom. If the cooling water is kept at a constant temperature and flow rate, the coil temperature will reach a steady state and produce a constant homogeneity.

The power for an electromagnet can be supplied either by an electronic rectifier power supply, a motor generator or by batteries. For high resolution, the regulation of the current is so important that an electronic current regulated supply is normally used. As can easily be seen, a constant voltage across the magnet is not sufficient because the current and, therefore, the field will decrease as the resistance of the windings increases with warmup. The current regulator should be capable of holding the magnet current constant to better than one part in 10^6 or 10^7. A typical magnet power supply diagram is shown in Fig. 24.

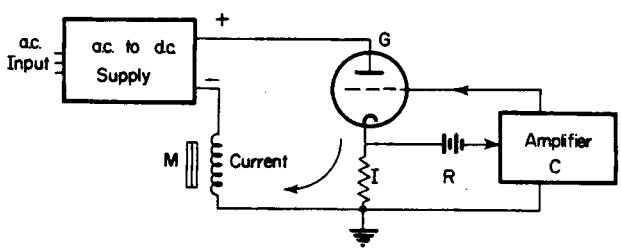

FIG. 24.

The a.c. input voltage is converted to a d.c. voltage somewhat higher than that required for the magnet. The current from this rectifier supply goes through the magnet, M, and the information resistor, I, and the gate tubes, G. The voltage drop produced across the information resistor is compared against a stable reference potential from battery, R, by the chopper amplifier, C, which amplifies any difference between the voltage across I and R and

uses this voltage to control the gate tubes, G. The gate tubes, G, can be considered as a variable resistance; the magnet and information resistor are fixed resistors. The current equals voltage divided by total resistance so, when the chopper amplifier changes the resistance of tubes, G, the current through the system changes.

The current regulator does not in itself have enough stability for best high resolution NMR work, and in addition, it is the magnetic field which must have the maximum stability. The shape of the magnet, the movement of external iron parts, or the change of external magnetic fields can affect the strength of the magnetic field inside the gap to a small extent. A properly designed flux stabilizer can reduce most of these variations about two orders of magnitude.

Figure 25 shows a flux stabilizer. A many-turn pair of pickup coils is wound on the pole caps. These coils feed into a galvanometer whose deflection is

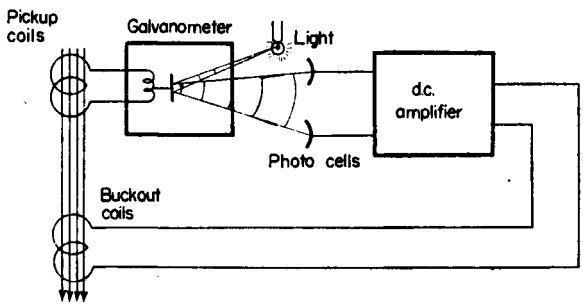

FIG. 25.

proportional to the total change of magnetic flux in this pickup coil. The galvanometer mirror deflects a light beam which initially falls equally on two photo cells, and any subsequent galvanometer deflection increases the light on one cell and decreases that on the other. The difference in photo cell output is amplified and used to degenerate the flux change. This is done by producing a current in a second set of coils wound over the pickup coils. This system does nothing as long as the field is not changing, because there is no pickup as given by:

$$E = N\frac{d\phi}{dt} \times 10^{-8} \text{ volts}$$

E is induced voltage in the input coil of turns N, and ϕ is the total flux (field strength times area). The voltage E is proportional to the rate of change but an integrator (the galvanometer) gives an output proportional to the total flux change.

The amount of field change which can be compensated for is limited by the current which can be put through the buck-out coil. Usually an additional

feedback loop is connected to the magnet power supply so that the buck-out current is kept near zero by a corrective change of magnet current, and the principal use of these output coils is then for reduction of transient field changes.

The flux stabilizer can also be used to sweep the magnetic field. If a small voltage from an external battery is applied to the input circuit of the galvanometer, the system will change the flux so as to keep the galvanometer input at approximately zero voltage. By this means, a steady input voltage will result in a constant flux sweep rate which is proportional to the input voltage. Figure 26 shows such a sweep circuit. A resistor, R_1, with resistance small compared with the galvanometer and coil resistance, is connected

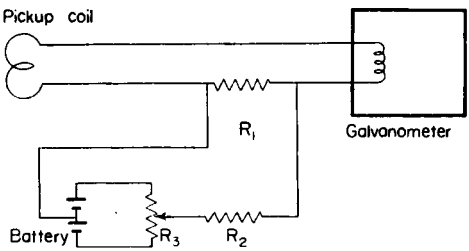

FIG. 26.

as shown. Part of the adjustable voltage appears across R_1. The amplifier will then continually change the buckout coil current and thereby change the flux in the pickup coil so that the voltage from this coil is kept equal to and opposite to the voltage applied across R_1. This feedback therefore results in a constant sweep of the magnetic field as long as a constant external voltage is applied.

This short description of the high resolution NMR instrument has not covered all the parts but has stressed the more important and unique components with the purpose of showing performance and operation. An understanding of the instrumentation will facilitate easier and better operation of the spectrometer.

7

HIGH RESOLUTION NMR AS A STRUCTURE DETERMINING TOOL

JAMES N. SHOOLERY
Varian Associates, Palo Alto, California

As early as 1952, shortly after the first demonstration that separate radio-frequency signals from chemically non-equivalent hydrogen nuclei precessing in a magnetic field could be obtained with an NMR apparatus of sufficient resolving power,[1] it had become evident that the high resolution NMR technique was destined to play a major role in chemical structure determination, particularly for organic compounds. In particular, its ability to locate hydrogen nuclei which often elude other forms of spectroscopy and to provide information about their surroundings appeared to be extremely promising. Today, scarcely seven years later, we find that diligent application of this technique to chemical structure problems during this period has resulted in widespread acceptance of high resolution NMR spectroscopy.

Since the NMR instrument is often applied to the same kind of problems as the infrared spectrometer, the two techniques being complementary to one another, it is instructive to review briefly the similarities and differences in the two instruments. High resolution NMR is similar to infrared in that:

(1) It gives characteristic responses for particular functional groups of atoms.
(2) It provides a "finger print" of the molecule in those cases where complete resolution of all signals is not achieved.
(3) The spectrum is sensitive to intra- and intermolecular interactions.
(4) It is often necessary to resort to empirical correlation in order to interpret the spectra.

On the other hand, high resolution NMR differs from infrared in several important ways:

(1) It is equally sensitive to whatever functional group in which a nucleus is found. The total integrated intensity of a resonant line or group of lines depends only on the number of nuclei represented by those signals.
(2) The spectra are very often considerably simpler than infrared spectra, it being possible to assign every single line in the spectrum in a high percentage of cases.

(3) Due to direct magnetic dipole–dipole interactions in solids which broaden the lines considerably, the high resolution NMR technique requires liquid samples or solutions.

(4) The actual frequency range covered in scanning a typical infrared spectrum is several times the spectral frequencies at the low end of the range, while the region over which high resolution signals from hydrogen nuclei are usually expected can be scanned by varying the frequency only 1/100,000 of the resonance frequencies themselves. Thus, calibration, standardization, and control of drift in the two instruments differ greatly and must be approached in rather different ways.

The extreme narrowness of the proton resonance signals means that if, for any reason, the resonance frequency becomes sensitive to the chemical surroundings, it should be possible to resolve the signal into a spectrum of lines, one for each chemically non-equivalent group of nuclei present. Fortunately, the electrically charged electrons, circulating in various orbits in a molecule generate magnetic fields which average to different strengths at different points in the molecule. It is a very difficult business to calculate rigorously the strength of the field at the nuclear positions due to the electrons in a molecule,[3] owing to our lack of knowledge of the exact wave functions and the complicated mathematics involved. However, these fields can be thought of as the sum of a number of terms, some of which may aid the applied field (paramagnetic) and some of which oppose it (diamagnetic). These terms are:

(1) Simple diamagnetic circulation of immediately surrounding electrons leads to a shielding term which is proportional to the electron density and hence to the electronegativity of nearby atoms.

(2) In forming a bond to another atom the electron cloud departs from spherical symmetry about the nucleus. The large chemical shifts associated with fluorine, phosphorus and many other heavy nuclei can be explained in terms of an actual sharing of an electron possessing orbital angular momentum, leaving a net unbalanced orbital angular momentum for the remaining shell of electrons. This leads to an orbital magnetic moment and interaction of this strong magnetic moment with the applied field gives a paramagnetic shift, i.e. unshields the nucleus. Terms of this type are very dependent in magnitude on the kind of bond formed. In the case of hydrogen, the ground state wave function is mainly $1s$, but some excited state functions ($2p$, $3p$, etc.) must be admixed to describe the departure from spherical symmetry. Differences in the amount of these states, which are admixed to describe a ground state of the bonded proton in various bonding situations, are large enough to represent a very significant contribution to the total proton "chemical shift".

(3) A whole group of electrons can become delocalized; for example, π-electrons of the benzene ring, and circulating currents can arise in portions of a molecule due to the Larmor precession of these electrons in the magnetic field.[4, 5] The magnetic moment associated with such a circulating current is anisotropic, that is, it depends upon the molecular orientation with respect to the magnetic field, Thus, the field produced by the induced moment does not average to zero, upon averaging over all possible molecular orientations, and fairly sizable shifts can be observed at considerable distances from such a group. Other groups of electrons, such as the shell of electrons associated with halogen atoms, are less delocalized but still possess a magnetic anisotropy. Smaller shifts of the same type are observed in molecules containing such substituents.

(4) The near approach of an electrically charged atom or one end of a dipole to the electron cloud surrounding a hydrogen nucleus results in a sufficient polarization of the electrons to produce quite sizable chemical shifts.[6] The shifts observed in connection with the formation of strong hydrogen bonds can be explained in this way.

The sum of the first three terms above, averaged over all molecular tumbling orientations, seems to give an experimentally determinable "shielding constant" for each functional group. Since the shielding effects fall off rapidly with distance, measurements of the shifts have been largely confined to the proton or protons on the immediately adjacent carbon atoms. The "shielding constants" appear to be roughly additive, making it possible to estimate chemical shifts of di- and tri-substituted methanes with fair accuracy.[7] One must expect some departure from additivity in molecules with ring systems which tie down protons and functional groups relative to one another and may lead to a different average value of the anisotropic part of the shielding. Figure 1 shows a table of effective shielding constants for a number of substituent groups in c/s for an operating frequency of 60 megacycles (14,092 gauss) and in parts per million of the applied magnetic field for instruments operating at other field strengths. In order to avoid intermolecular interaction effects, it is assumed that all measurements are made in dilute solutions, using either carbon tetrachloride or chloroform as a solvent, and that a small quantity of the symmetrical reference substance, tetramethylsilane, is added to the solution. The predicted position of a resonance for a particular CH or CH_2 group is obtained by adding the shielding constants of the substituents to the shift for methane itself. The total shielding for the proton, predicted in this way, is a net paramagnetic one; that is, the effect of all of these groups is in the direction corresponding to reducing electron density around the proton, leading to a resonance at lower applied magnetic field than that for the reference substance. The shielding constants have been

found to be a great help in assigning resonances in complex organic molecules for which no closely similar model compounds are available.

If the chemical shift were the only perturbing mechanism operating in molecules, the spectrum of any substance would have the appearance of a number of sharp lines with intensity ratios corresponding to the ratios of integers representing the numbers of protons in each of the chemically non-equivalent groups in the molecule. While this would be useful information,

GROUP	CPS (60 mc)	PPM
Cl	152	2.53
-OR	142	2.36
Br	140	2.33
C_6H_5-	110	1.83
I	109	1.82
>C=O	102	1.70
-S	98	1.64
-N	94	1.57
-C=C<	79	1.32
$-CH_3$	28	0.47
CH_4 RESONANCE (relative to internal $Si(Me)_4$ in CCl_4)	10	0.16

FIG. 1. Effective constants for unshielding of the adjacent proton by various groups in substituted methane.

it is fortunate that the additional spin–spin coupling interaction exists, splitting each of the resonances in a characteristic way and depending upon the number, distance and symmetry of neighboring nuclei in the molecule. The coupling mechanism involves the electrons in the intervening bonds, the size of the coupling being proportional to the importance of the wave function in the molecular orbital description of the molecule which places two electrons with paired spins in an orbital joining the two protons under consideration. As might be expected, the coupling falls off rapidly with an increase in the number of intervening bonds, being quite negligible for four and five bonds unless multiple bonds with more delocalized electrons are involved. A selection rule forbids the observation of coupling between identical protons, all of the intensity appearing at the unperturbed chemical shift position.

In the case of protons, which have electrons only in s-orbitals, the Fermi contact interaction between the protons and the bonding electrons appears to dominate the coupling. In this case, the coupling is proportional to the probability of finding the electrons at the nuclei which are being coupled. It has recently been observed[8, 9] that for protons coupled to C^{13} the coupling is linearly related to the s-character of the bond, as shown in Fig. 2. It also

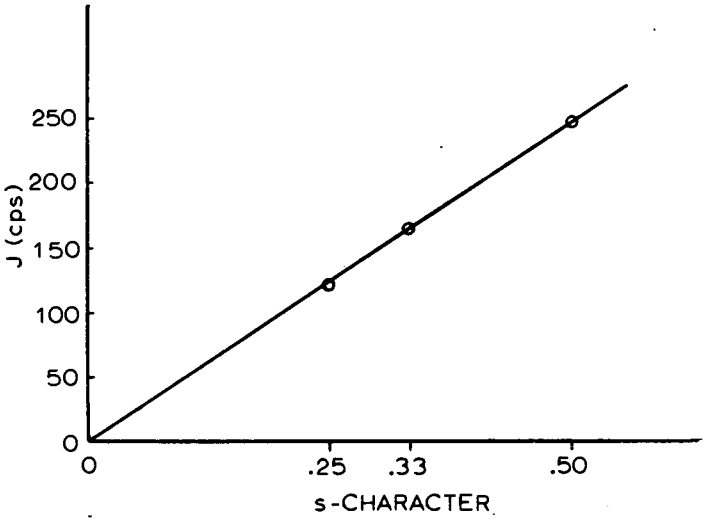

FIG. 2. Dependence of C^{13}–H spin–spin coupling on s-character.

varies as the cube of the effective charge, so that the electronegativity of adjacent groups can affect the electronic screening of the nucleus and hence the coupling. It is even possible[8] to calculate from the observed C^{13}–H coupling in CH_4 the H–H coupling in molecular hydrogen to within about 20 per cent by taking the appropriate factors into account.

As discussed in an earlier lecture, in the case of coupling between nuclei which are separated by a large chemical shift, that is, precessing at quite different frequencies, only the z-components (parallel to the field) of the spins couple, and the number and relative intensities of the lines arising from a particular group of protons depend only upon the number of ways in which the neighboring spins can be arranged parallel and anti-parallel with the magnetic field. This results in the simple rule that, for protons, the number of lines in the multiplet is $N+1$, where N is the number of equivalent neighboring protons. The intensities follow the well-known binomial coefficients. In the more general case, a group of nuclei with total spin I will split the resonance of adjacent nuclei into $2I+1$ components.

As the chemical shift becomes smaller and smaller, eventually becoming comparable to the spin-coupling in magnitude, the nuclei tend to precess

more nearly at the same frequency and remain "in phase" for longer periods of time. Under these conditions, the precessing x- and y-components of the spins become important and a quantum mechanical problem must be solved. Considerable perturbations in the intensities and positions of lines predicted on the basis of the z-components alone are found. Some of the resulting patterns are so distinctive that they provide an immediate "finger print" for certain arrangements of nuclei in a molecule. Correct interpretation of these patterns is of immense value in structure determination work. It is instructive at this point to examine some of the more common coupling schemes in detail.

Following Bernstein, Pople and Schneider,[10] it is convenient to designate non-equivalent nuclei separated by a small chemical shift with the letters A, B, C, etc., and nuclei which are separated from these by a large chemical shift with the letters X, Y and Z. If we overlook for a moment the hydroxyl group in ethyl alcohol, the ethyl group would then be described as an A_2X_3 case. Due to rapid internal rotation about the bond joining the CH_2 and CH_3 groups, the nuclei in each group are completely equivalent and the problem can be solved using the simple theory involving only z-components of the spins. If the molecules were frozen into one of the rotational conformations, resulting in different spin coupling constants between different protons of the groups, the problem would be much more complicated and would require an exact quantum mechanical treatment.

One of the simplest and most frequent multiplet patterns encountered in NMR spectra is that arising from an AB set of two nuclei. This pattern can arise from either two protons on the same carbon atom with hindered rotation relative to some other part of the molecule or, if the CH_2 group is part of a ring, one proton may be axial and the other equatorial. The pattern can also arise from two protons on adjacent carbon atoms when the chemical shift is not large. Figure 3 shows the typical four-line pattern which results from the

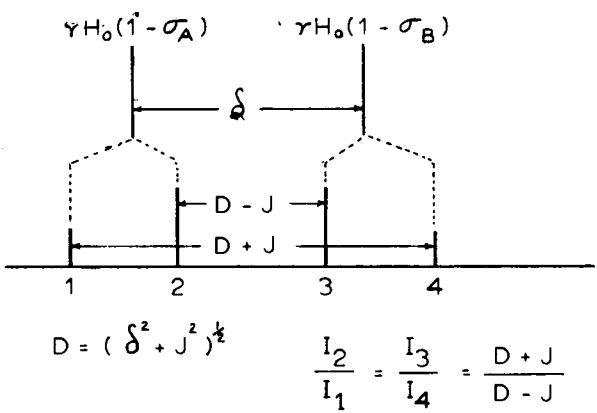

FIG. 3. Two nuclei AB.

spin-coupling of two such protons, the inner pair of lines being more intense than the outer pair.

A much more complex spectrum is obtained if a third proton with a large chemical shift relative to the other two is added, giving an ABX pattern. The coupling scheme for this system is shown in Fig. 4. Twelve fairly strong

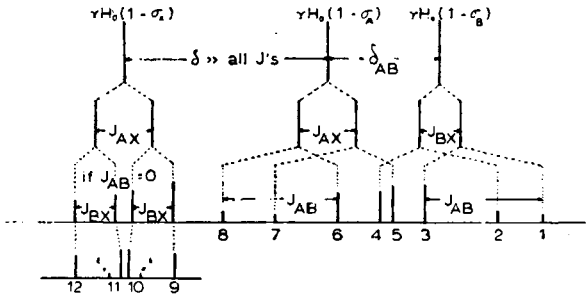

FIG. 4. Three nuclei ABX.

Definitions	Transition	Origin	Energy	Relative Intensity
$J' = \frac{1}{2}(J_{AX}+J_{BX})$	1	B	$C-\frac{1}{2}(J_{AB}+J')-D^-$	$1-(J_{AB}/2D^-)$
$J'' = \frac{1}{2}(J_{AX}-J_{BX})$	2	B	$C-\frac{1}{2}(J_{AB}-J')-D^+$	$1-(J_{AB}/2D^+)$
$D^+ = \frac{1}{2}\{(\delta+J'')^2+J_{AB}^2\}^{\frac{1}{2}}$	3	B	$C+\frac{1}{2}(J_{AB}-J')-D^-$	$1+(J_{AB}/2D^-)$
$D^- = \frac{1}{2}\{(\delta-J'')^2+J_{AB}^2\}^{\frac{1}{2}}$	4	B	$C+\frac{1}{2}(J_{AB}+J')-D^+$	$1+(J_{AB}/2D^+)$
$C = \frac{1}{2}\gamma H_0(2-\sigma_A-\sigma_B)$	5	A	E_1+2D^-	I_3
$F = \gamma H_0(1-\sigma_X)$	6	A	E_2+2D^+	I_4
ϵ denotes weak combination lines which occur at $F-D^+-D^-$ and $F+D^++D^-$.	7	A	E_3+2D^-	I_1
	8	A	E_4+2D^+	I_2
	9	X	$F-J'$	1
	10	X	$F+D^+-D^-$	$1-\epsilon$
	11	X	$F-D^++D^-$	$1-\epsilon$
	12	X	$F+J'$	1

lines occur whose positions and intensities depend in a fairly complex way on the chemical shift and spin-coupling constants. The upper trace in Fig. 5 is a good example of the structural information available from interpreting patterns of the ABX type. This molecule, a naturally occurring alkaloid called lunacrine,[11] was believed to have the structure (I), but it could not be

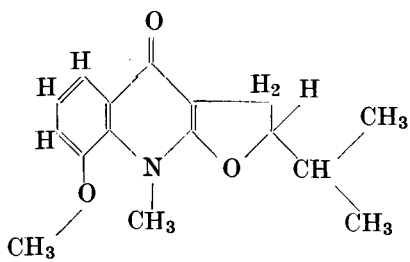

(I)

proved by chemical means. Analysis of the *ABX* pattern at the extreme left (groups of lines *a* and *b*), arising from the three protons on the benzene ring, showed that the *X* proton is coupled strongly to the *A* proton and weakly to the *B* proton. It is well known that a carbonyl group attached to a benzene ring shifts the ortho-proton much more than any of the others, so that the *X* proton (lines *a*) can be assigned as the proton at the top of the ring. A glance at Fig. 11, which gives some typical coupling constants for various

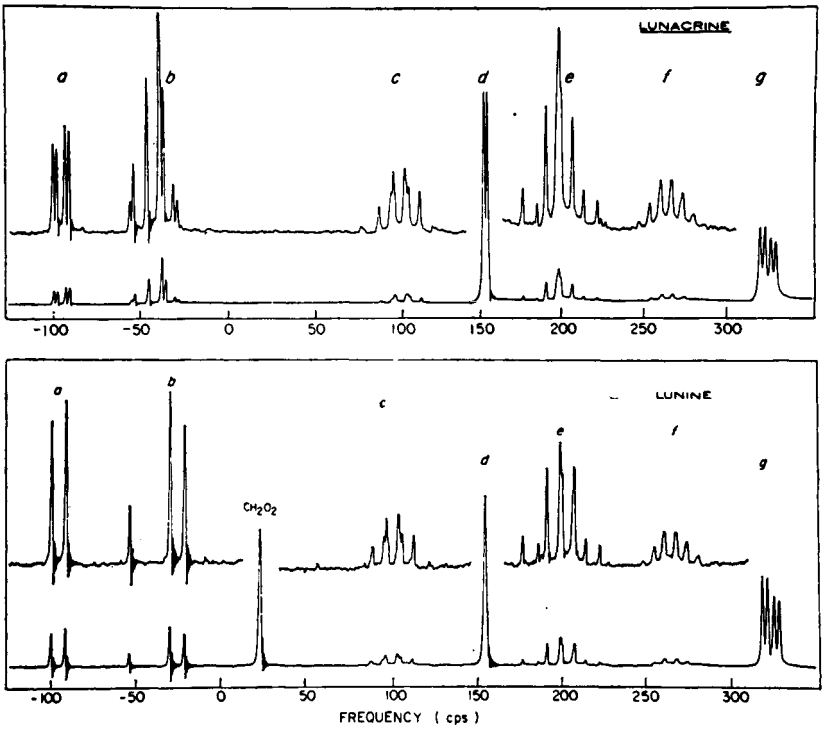

FIG. 5. NMR spectra of lunacrine and lunine in $CDCl_3$ at 60 Mc relative to an external benzene reference taken as zero.

bonding situations, shows that the coupling between protons ortho to one another on a benzene ring is typically several times the coupling between protons meta to one another on the ring. Thus, the observed pattern for the *X* proton confirms the adjacent placement of the three protons on the benzene ring and the position of the methoxy group is required to be as shown. Another region of interest contains two groups of lines (*c* and *e*), surrounding the strong line *d* at +150 c/s which arises from the N-methyl and O-methyl groups. These reveal another *ABX* pattern due to the three protons in the

5-membered ring. This confirms the 5-membered nature of the ring and requires an isopropyl side-chain in order to fit the known formula for the compound. The presence of the isopropyl group is confirmed by the two multiplets at the extreme right of the trace, the number of observable lines and the relative intensities being fully in accord with this kind of group.

It is interesting to consider that the structure of the compound shown in the lower trace of Fig. 5 is determined solely by NMR spectroscopy. This compound, called lunine, displays an NMR spectrum nearly identical with that of lunacrine from about the center on to the right-hand side, showing that it possesses the 5-membered ring, isopropyl side-chain, and N-methyl group. The left-hand half of the spectrum contains an *AB* pattern showing one aromatic ring proton adjacent to the carbonyl group with ortho- coupling to the other proton. A strong line is also observed at about 20 c/s and can be shown to be characteristic of a methylene dioxy group from studies of model compounds. Thus, lunine must be regarded as having the structure (II) which is in accord with its chemical behavior.

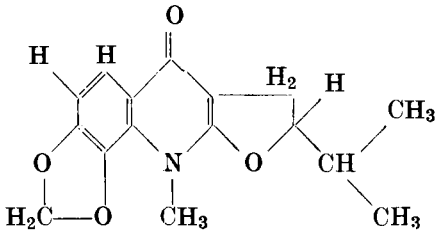

(II)

Another case in which the recognition and analysis of *ABX* patterns was useful in drawing a structural conclusion is illustrated in Fig. 6. This molecule, xanthoperol, shown in the upper trace of Fig. 6, was believed to have either the structure shown, or one in which the angular methyl and angular proton exchanged places. The structure in Fig. 6 is supported by the NMR spectrum since we find a strong sharp line at the left (at approximately 240 c/s) due to the angular proton which has no neighbors to give rise to spin–spin splitting. It was believed that the ring fusion was trans- and one could then argue that the mono-keto reduction product in that case would be identical with 9-keto ferruginol. However, this conclusion could be shown chemically and also by the NMR spectra in Fig. 6 to be incorrect. The mono-keto reduction product shows an *AB* pattern shifted down field due to a CH_2 group adjacent to a carbonyl group, and an *X* pattern due to the angular proton having been shifted up field by the reduction of the adjacent keto group. This would appear to rule out the structure with an angular methyl group adjacent to the carbonyl. The compound 9-keto ferruginol, known to have two protons adjacent to the carbonyl group and an angular proton, also shows an *ABX* pattern which differs from that of the mono-keto reduction

product only in the size of the couplings. These findings can be reconciled by assuming that xanthoperol has a cis-ring fusion rather than the trans-ring fusion known to exist in 9-keto ferruginol.*

Additional complexity is encountered in the A_2B_2 case[12] illustrated in Fig. 6. The diagram in the upper left-hand corner shows that each A proton

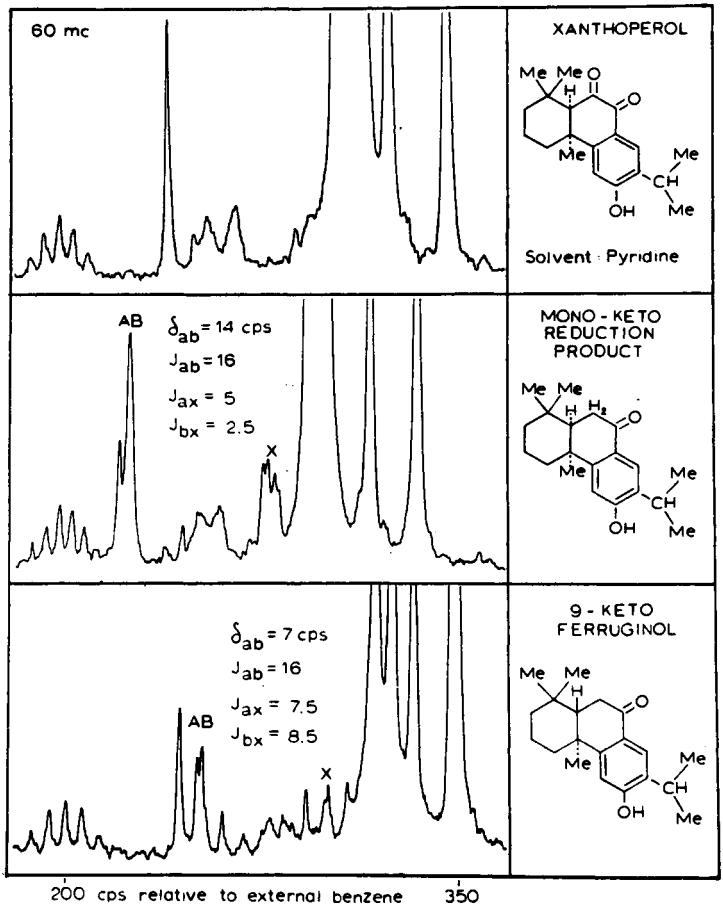

FIG. 6. NMR spectra of some diterpene derivatives.

sees the two B protons with different coupling constants J and J' and vice versa. There is also a coupling J_A between the A protons and J_B between the B protons. Even if one uses wave functions which correspond to the symmetry of the molecule, it is still necessary to solve a 4×4 secular equation in order

* This work was instigated by Dr. J. B-son Bredenberg, Finland Institute of Technology, Helsinki, Finland, to whom appreciation is due for permission to mention these results.

to obtain all of the energies and transition frequencies. Twenty-four transitions are found which occur in two sets of 12 lines that are mirror images of each other. A typical spectrum of 12 lines arising from the A protons is shown at the top of Fig. 7.

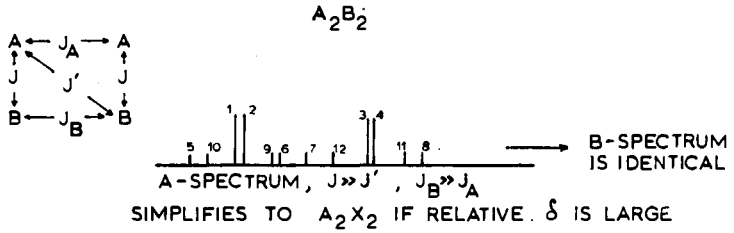

ENERGIES AND INTENSITIES OF A-TRANSITIONS FOR A_2X_2

DEFINITIONS	TRANSITION	SYMMETRY	ENERGY + $\gamma H_0(1-\sigma_A)$	INTENSITY
$K = J_A + J_B$	1, 2	s	$\frac{1}{2}N$	1
$M = J_A - J_B$	3, 4	s	$-\frac{1}{2}N$	1
$L = J - J'$	5	s	$\frac{1}{2}K + \frac{1}{2}K'$	$1 - (\frac{1}{2}K/K')$
$N = J + J'$	6	s	$-\frac{1}{2}K + \frac{1}{2}K'$	$+ (\frac{1}{2}K/K')$
$K' = (K^2 + L^2)^{\frac{1}{2}}$	7	s	$\frac{1}{2}K - \frac{1}{2}K'$	"
$M' = (M^2 + L^2)^{\frac{1}{2}}$	8	s	$-\frac{1}{2}K - \frac{1}{2}K'$	$1 - (\frac{1}{2}K/K')$
	9	a	$\frac{1}{2}M + \frac{1}{2}M'$	$1 - (\frac{1}{2}M/M')$
	10	a	$-\frac{1}{2}M + \frac{1}{2}M'$	$+ (\frac{1}{2}M/M')$
	11	a	$\frac{1}{2}M - \frac{1}{2}M'$	"
	12	a	$-\frac{1}{2}M - \frac{1}{2}M'$	$1 - (\frac{1}{2}M/M')$

FIG. 7. Enorgies and intensities of NMR transitions for two pairs of equivalent nuclei.

If the relative chemical shift between the two pairs of protons is large compared to the spin-couplings, the A_2B_2 case simplifies to the A_2X_2 case and the energies and intensities of the 12 lines can be written explicitly. It will be noted that in the left-hand column of the table in Fig. 7 several terms are defined which are merely sums and differences of the J couplings. The two right-hand columns of the table show that the energies and intensities of the transitions are simple functions of these terms. In interpreting such a spectrum it is necessary first to assign the lines in the spectrum according to some estimate of the probable values of the coupling constants. Then the measured frequency differences between certain lines in the spectrum will allow the elimination of some quantities and permit one to solve for others. This will either lead to a set of corrected coupling constants or will show that the original assignment was incorrect.

A very nice example of the A_2X_2 coupling situation has been discussed by Cohen, Sheppard and Turner.[13] This is the molecule 1,4-dioxane whose

proton spectrum is shown in Fig. 8. In the molecular species with only C^{12} atoms, all of the protons are indistinguishable and a very strong sharp line results. However, a small fraction of the molecules have one C^{13} atom and the two protons attached to the C^{13} have their resonance shifted in frequency due to the spin coupling with the C^{13} nucleus. This shifted resonance is then split into a multiplet due to an A_2X_2 type interaction with the adjacent $C^{12}H_2$ group. One of the resulting 5-line patterns is shown in Fig. 8. There is

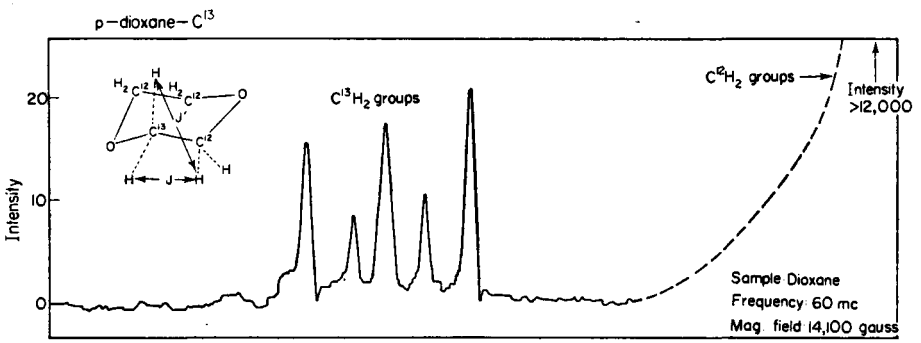

FIG. 8. C^{13} satellites in proton spectra of symmetrical molecules.

an identical pattern (not shown) an equal distance on the other side of the strong central line due to the equal probability that the C^{13} nucleus will point its spin either parallel or anti-parallel to the magnetic field. The splitting of the inner pair of lines gives $J-J'$ and the splitting of the outer pair gives $J+J'$. In the conformation of the molecule shown, $J' = J_{aa}$ and $J = J_{ae}$, where a represents an axial proton and e is equatorial. The other equally probable conformation gives $J' = J_{ee}$ and again $J = J_{ae}$. Therefore, $J'_{avg} = \frac{1}{2}(J_{aa}+J_{ee})$ and $J_{avg} = J_{ae}$. By making the reasonable assumption that both the *gauche* couplings are similar, i.e., J_{ae} is approximately equal to J_{ee}, the interesting result is obtained that $J_{aa} = 9.4$ c/s and $J_{ae} = 2.7$ c/s.

The recognition of A_2B_2 or A_2X_2 patterns aids in the correct assignment of spectra and allows definite structural conclusions to be drawn in many cases. An example of this is shown in Fig. 9. The two structures* illustrated, (I) and (II), represent possible structural formulas for an alcohol. The arrangement of the functional groups in either of the two structures is such that the chemical shifts and spin-couplings would be about the same. Therefore, the spectrum of the compound shown in the lower trace does not permit a choice to be made between (I) and (II). However, it is clear from both the areas under the peaks and the general shape of the patterns that the peak at 77 c/s is due to the CH group attached to both an oxygen atom and the benzene

* Samples furnished by G. D. Searle and Company to whom we are grateful for the permission to publish these results.

ring, while the multiplet at 154 c/s is half of an A_2B_2 pattern corresponding to the CH_2 group adjacent to an oxygen atom. In order to solve the problem, we can take advantage of the fact that converting a hydroxyl group to an acetate group results in a considerable shift of the protons on the attached carbon atom. We note that the upper spectrum in Fig. 9, which represents the acetate derivative of the alcohol, shows no shift of the CH group and a considerable shift of the CH_2 groups. Therefore, the correct structure is (I).

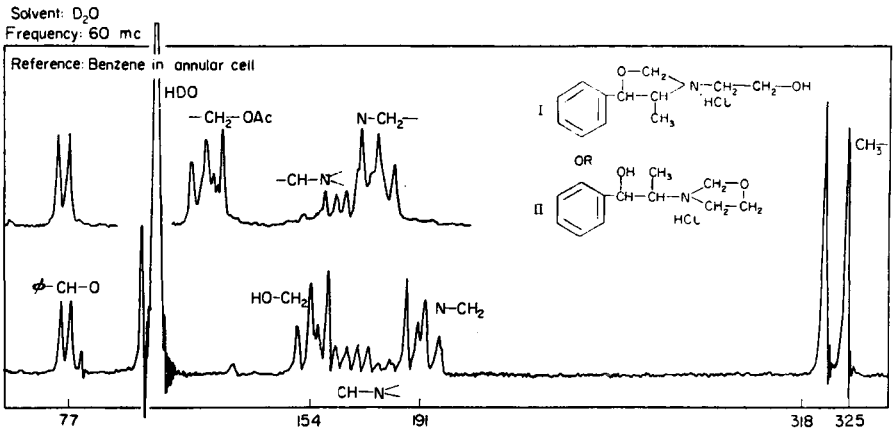

FIG. 9. Distinguishing primary from secondary alcohols.

The A_3B system of nuclei gives rise to a fairly complicated spectrum. The exact solution of the line positions and intensities for a large number of possible values of the ratio J_{HH}/δ has been performed with the aid of an electronic computer in this case. The solutions over the entire possible range of J_{HH}/δ have been plotted as a set of curves, both for positions and intensities. For a given value of J_{HH}/δ one has only to lay a straight-edge across the curves and read the line positions and intensities from the point of intersection. These curves will be published elsewhere as part of a continuing program to compute theoretical NMR spectra.

When J_{HH} becomes larger than δ, the pattern for the A_3B case loses all resemblance to two sets of lines and degenerates to several very strong central lines surrounded by very weak satellites. An example of such a situation is the molecule methyl acetylene whose spectrum is shown in Fig. 10*a*. The chemical shift between the methyl group and the acetylenic proton is 2.1 c/s at 60 Mc, while the spin-coupling is 2.93 c/s. The intensities of the center lines are so great compared to those of the satellites and their spacing is so small (particularly at 40 Mc) that earlier observations of the spectrum of methyl acetylene report it as a single line. It has even been suggested that in the liquid state methyl acetylene is in sufficient rapid equilibrium with its isomer allene to average the precession of all protons to the same frequency,

even though this is contrary to all chemical evidence. However, the fit of the actual spectrum of methyl acetylene to the calculated spectrum shown in Fig. 10*b* proves that the molecule can be represented by an A_3B system of nuclei and, therefore, remains in the acetylenic form. Further confirmation of this can be obtained by examining the weak satellites which appear on either side of the pattern and are due to the presence of molecular species with one C^{13} nucleus. The satellites which arise from the acetylenic proton

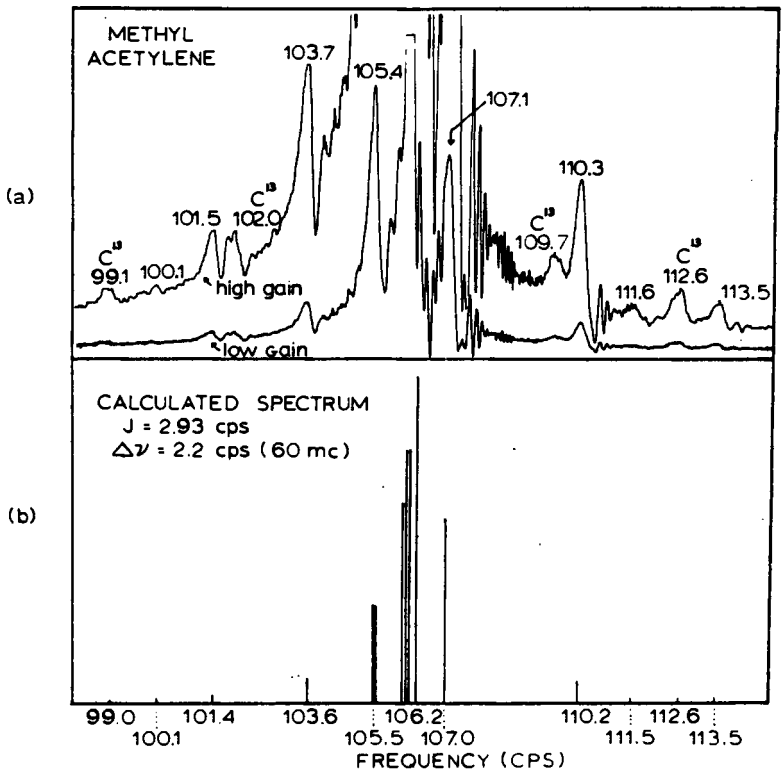

FIG. 10. Calculated and Observed Spectrum for the four nuclei A_3B case, methyl acetylene.

show a 1–3–3–1 quartet pattern while those which correspond to the methyl group show a doublet character. The simple first order spin-coupling is observed in this case because the C^{13} coupling constants are so different for the methyl protons and acetylenic protons that there is a large energy separation between the resonances in the isotopically substituted molecules.

It is perhaps instructive at this point to examine more closely Fig. 11 which gives some typical coupling constants for various proton bonding situations. Most of the situations which arise in actual practice are covered by this table.

Of particular interest is the curve at the right showing the change of proton–proton coupling for two protons on the same carbon atom as a function of the H–C–H angle. This curve was derived theoretically by H. S. Gutowsky, Martin Karplus, and D. M. Grant.[14] Spin-couplings measured in a large number of compounds have been found to fall on, or near the curve. In particular, vinyl compounds for which the H–C–H angle is about 120° usually show coupling constants of only a few c/s. Deviations from the curve can result if

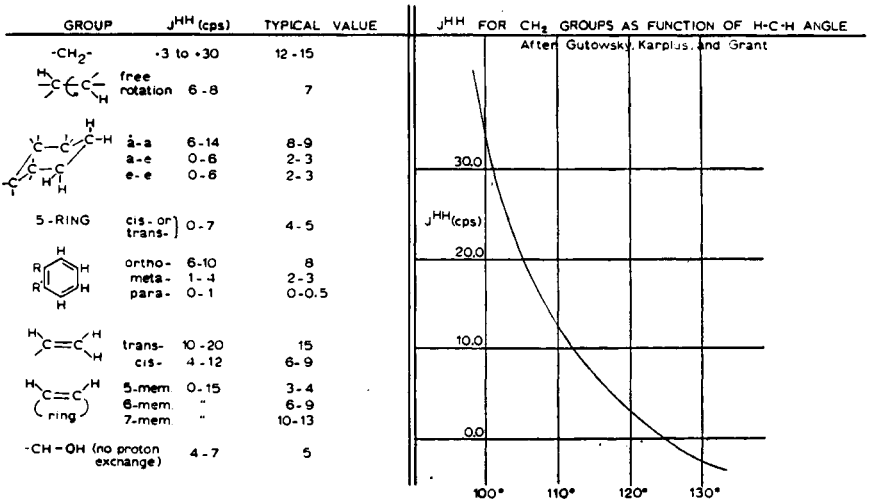

FIG. 11. Typical spin coupling constants for protons.

strongly negative atoms are bonded to the same carbon atom. For example, the CH_2 protons in a methylene dioxy group can be non-equivalent in some molecules and the coupling between these protons has been found to be quite small.

The coupling between two protons on adjacent carbon atoms is quite characteristic for molecules with free rotation about the C–C bond. This is true because we see an average over all possible dihedral angles between the planes containing the protons and the two carbons atoms. For molecules which are rigidly fixed in one orientation, however, we find a wide variation in J_{HH}, depending upon the size of the dihedral angle. Karplus[15] and Conroy[16] have attacked this problem theoretically using the valence bond treatment and a molecular orbital treatment respectively. A curve which is essentially a modified cosine squared function is obtained relating J_{HH} to the dihedral angle. The agreement of theory and experiment is remarkably good for those molecules in which the dihedral angle is known with sufficient accuracy. An approximate reproduction of the curve is given in Fig. 12, from which it can be seen that when the two protons lie in the same plane, the

coupling is maximum, being about 8 c/s for the cis arrangement ($\phi = 0$) and about 10 c/s for the trans arrangement ($\phi = 180°$). The coupling is predicted to decrease to zero when one proton is twisted nearly 90° out of the plane of the other.

One consequence of the good agreement between theory and experiment will be the necessity of constructing accurate models of proposed structural

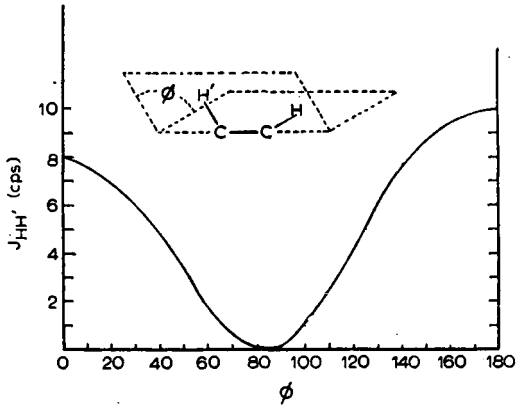

FIG. 12. Dihedral angle vs. $J_{HH'}$.

formulas in order to determine the dihedral angles for adjacent protons and thus predict coupling constants for comparison with the spectra. The additional labor involved will be worthwhile if accurate information about molecular conformations can be obtained.

An example of the use of spin multiplet analysis for making spectral assignments is encountered in the case of the isomeric molecules, ergosterol and i-ergosterol, whose spectra appear in Fig. 13. Only the olefinic regions of the

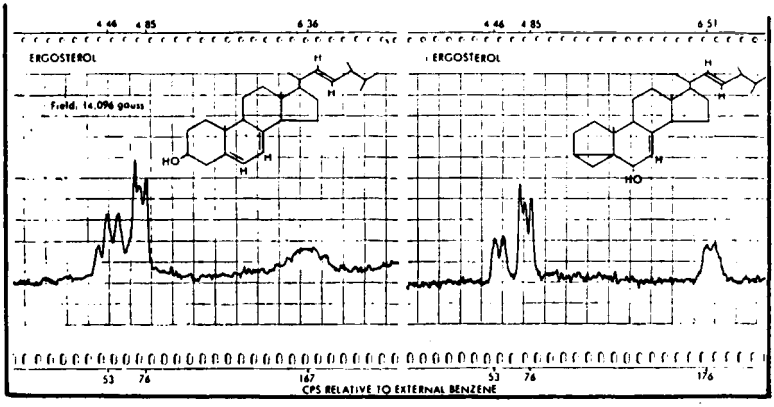

FIG. 13. NMR Spectra of i-steroids.

spectra are shown. The group of peaks centered around 4.46 p.p.m. (relative to internal tetramethylsilane defined as 10.00) has the appearance of the first three peaks of a small–large–large–small AB multiplet and is therefore assigned to the two protons in the B-ring of ergosterol. Confirmation of this assignment is evident in the spectrum of i-ergosterol since the replacement of one of the olefinic protons by a CHOH group has resulted in the remaining olefinic proton at 4.46 p.p.m. displaying the doublet character of half of an AX multiplet. The other half of the multiplet, due to the adjacent CH group, appears at 6.51 p.p.m.

The multiplet at 4.85 p.p.m. in both of the steroids has an integrated intensity corresponding to two protons and, in view of its identical appearance in both spectra, is assigned to the trans-olefinic protons in the C_8H_{17} side chain. A few plausible assumptions concerning the magnitude of the various spin-couplings allow one to calculate that the appearance of the multiplet is in agreement with the assignment. If we assume that the two olefinic protons are chemically nearly identical, we can label them the A_2 protons of an A_2X_2 group. The X_2 protons are then immediately adjacent protons on either side of the double bond. These are also assumed to have nearly the same chemical shift in order to simplify the calculation. We are then dealing with a special A_2X_2 case in which $J_a \cong 15$ c/s, $J_b = 0$, $J \cong 7$ c/s, and $J' \cong 0$. A glance at Fig. 6 then shows that the defined quantities $K = M = 15$ c/s and $L = N = 7$ c/s. Furthermore, K' and M' are only slightly greater than K and M. From the columns which give the energies and intensities of the 12 lines in the A-spectrum we predict strong lines at $+3.5$ c/s and -3.5 c/s, i.e. 7 c/s apart. The lines which appear at positions given by the sums of K and K', M and M', have intensities which are lost in the noise. The lines corresponding to the differences in the Ks and Ms fall near the center of the pattern between the two strong outer lines. Therefore, the observed multiplet corresponds to what would be expected from the two olefinic protons in the side chain.

The NMR spectra of many other steroids have recently been the subject of detailed study,[17] and illustrate the application of this form of spectroscopy to molecules containing a relatively large number of chemically non-equivalent protons. Figure 14 shows the spectrum of Δ^5, ^{16}–pregnadiene–20–one–3β–ol acetate taken at 40 Mc in a field of 9400 gauss. The two small peaks at the left end of the trace show the presence of two protons attached to doubly bonded carbon atoms in this molecule, the conjugated double bond resulting in a much larger shift than the unconjugated one. By measuring the areas of these peaks in an unknown steroid, one can decide how many such protons are present. The very broad peak falling at 73 c/s from the zero of reference arises from the proton attached to the same carbon atom as the acetate group. While this peak does not look very informative, it confirms the fact that the acetate group has the β-orientation. Systematic studies of a number of steroids have shown that this proton must be axial; if it were equatorial,

the resonance would lie about 20 c/s farther to the left. Furthermore, its breadth arises from the spin-coupling to the four neighboring protons and a glance at Fig. 11 shows that only an axial proton would be coupled strongly enough to the neighbors to be smeared out into such a broad peak. Therefore, the acetate group is equatorial and β. The four sharp strong peaks at the right-hand end of the spectrum represent the methyl groups in the molecule and illustrate how effectively NMR spectroscopy can provide information

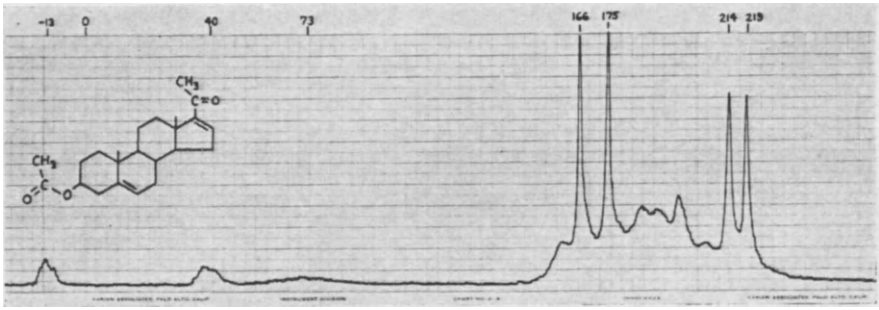

FIG. 14. NMR spectrum of $\Delta^{5,16}$-pregnadiene-20-one-3β-ol acetate at 40 Mc relative to external benzene as a zero of reference.

concerning the number of methyl groups. The observed shifts from left to right are characteristic of the methyl ketone, acetate methyl, and the two angular methyls. The positions of the angular methyl resonances have been found to be particularly sensitive to double bonds, carbonyl groups and hydroxyl groups attached to nearby carbon atoms. From the observation of the resonance position for the two angular methyl groups in an unknown steroid, a great deal can be said concerning the possible location of double bonds and oxygen atoms in the molecule.

The fact that there is a chemical shift associated with changing an axial proton to an equatorial position with respect to a 6-membered ring is illustrated in Fig. 15. The spectra of several steroids were examined at 40 Mc (9400 gauss) and the chemical shifts in cycles per second relative to an external benzene reference sample are written in parentheses alongside the protons in question. A comparison of the numbers for epiandrosterone and androsterone shows that the axial proton lies 22 c/s towards higher field than the equatorial proton. That this is due to the conformation with respect to the 6-membered ring on which the proton is located and not due to the orientation with respect to the entire molecule is demonstrated by the results for 5-isoandrosterone. In this case, inversion of the *A*/*B* ring junction has converted the C_3-proton back to an axial conformation with respect to the *A*-ring although located somewhat equatorially with respect to the entire molecule. We find, however, that the chemical shift is identical with that

found for epiandrosterone in which the proton was axial with respect to the A-ring. Similar results are obtained for the 11-position, a shift of 18 c/s upfield being found for the axial proton relative to the equatorial proton. Unfortunately, the functional group attached to the same carbon atom also influences the chemical shift as can be seen from the chemical shift of the axial proton at the 11-position in 11 α-acetoxyprogesterone. Therefore, before attempting to determine the conformation of an unknown molecule

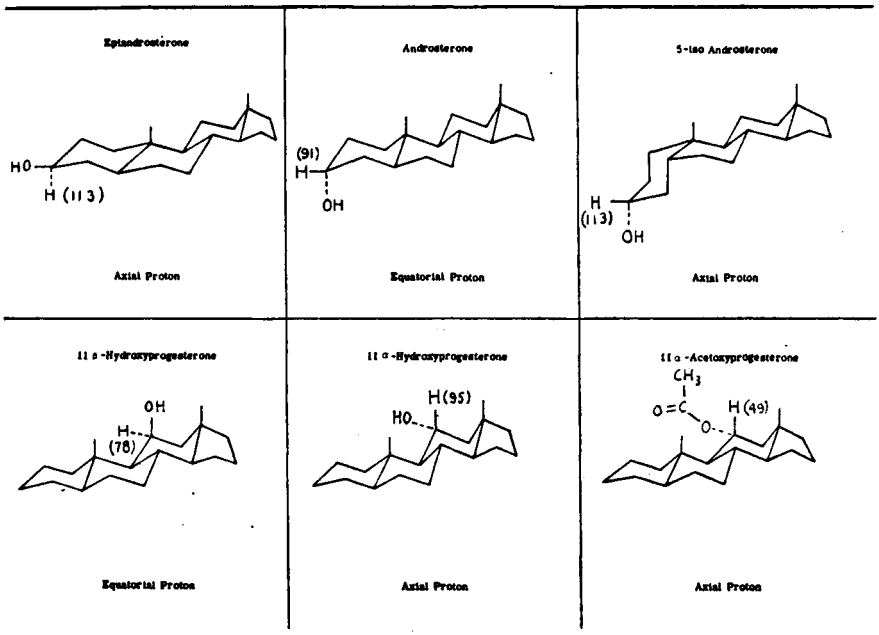

FIG. 15. Chemical shift and conformation in steroids.

it will be necessary to study related model compounds with similar functional groups. It is to be hoped that systematic studies will be carried out and tabulated in the literature.

The recent application of audio-frequency modulation techniques to high resolution NMR spectrometry has permitted highly accurate electronic integration of the spectra and thus added a powerful weapon to the NMR arsenal. Two examples will suffice to indicate the nature of the information to be obtained from integrated spectra and its value in structure determination problems.

Figure 16 shows the NMR absorption spectrum and its integral for a compound* which could have one of the two structures illustrated. Both struc-

* Sample furnished by Task Scientist Sidney Baldwin, Chemistry Research Branch, Aeronautical Research Laboratory, Wright Air Development Center, Dayton, Ohio.

tures have four protons attached to a benzene ring and 10 methylene protons. The left-hand structure has two equivalent amine protons while the right-hand structure possesses one imine proton and a proton attached to the same carbon atom as the CN group. The integral spectrum shows three regions with areas in the ratio 4–2–10 which suggests strongly that the left-hand structure is the correct one. There is a small probability that the imine proton

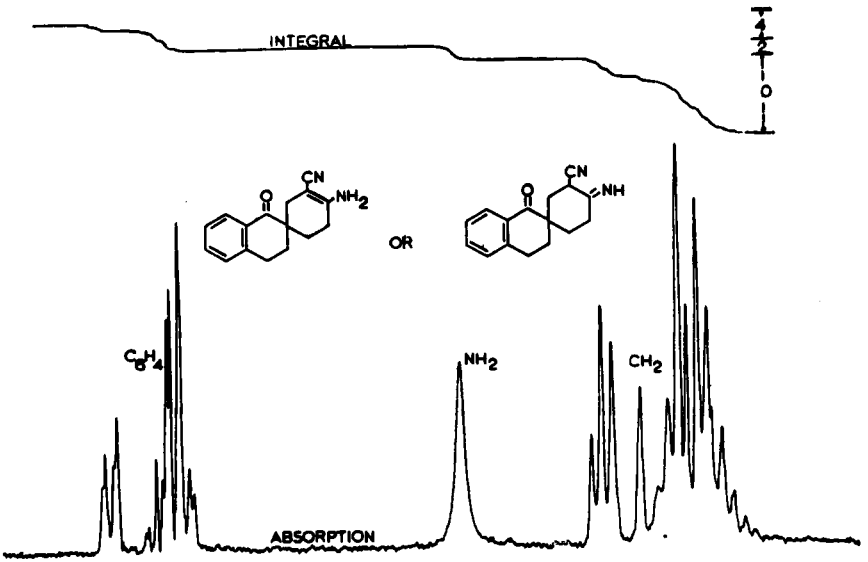

FIG. 16. Illustration of the use of the integral of the absorption curve for structure determination.

and the proton on the carbon atom attached to the CN group might accidentally have the same chemical shift. This can be ruled out by looking at the absorption spectrum which shows no evidence of fine structure due to spin-coupling with the neighboring methylene group.

Recent structure studies on the coenzyme Q group of compounds* relied heavily on high resolution NMR information. The relative areas of the various signals in the spectrum of coenzyme Q_{10} shown in Fig. 17 were very useful in making spectral assignments and in determining the number of isoprene units in the side chain. In analyzing this spectrum the sharp resonance at 235 c/s arising from the methoxy groups is taken as a standard area representing six protons. The broad peak at 304 c/s arises from the olefinic protons, one for each isoprene unit. From the ratio of these two areas it is readily determined that the number of isoprene units is 10.1 ± 0.15. The total integral of all of the absorption lying on the high field side of the methoxy

* WOLF *et al.*, *J. Am. Chem. Soc.* **80**, 4752 (1958). Appreciation is due to the Merck, Sharp and Dohme Laboratories and to Dr. Nelson Tremner for a sample of coenzyme Q_{10}.

group resonance should represent the seventy protons remaining in the ten isoprene chain units plus the three protons in the methyl group attached to the quinone ring and the proton which terminates the side chain. If we subtract the area corresponding to four protons (defined as two-thirds the area of the methoxy groups) from the appropriate integral, we have left the

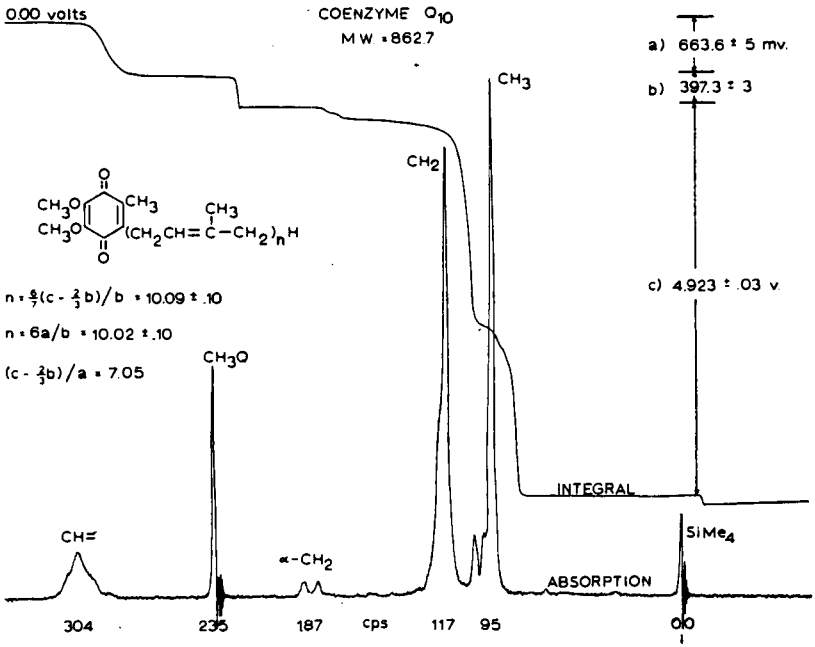

FIG. 17. Determination of the structure of a complex naturally occurring quinone, coenzyme Q_{10}, by high resolution NMR spectrometry.

integral corresponding to seventy protons. The ratio of this to the peak at 304 c/s should be 7.00 and it is experimentally found to be 7.05. The chemical shifts and integrated intensities in this spectrum are completely in accord with the proposed structure for coenzyme Q_{10}.

SUMMARY

In summary, we have seen how the chemical shift separates the resonances from the chemically non-equivalent hydrogen nuclei in a molecule so that they can be observed individually, and that spin–spin interactions between them result in information which can be interpreted to show the structural relationships of the groups to one another in the molecule. Tables of measured chemical shifts, empirically determined shielding constants for various groups, and tables of typical spin-coupling constants can now be employed with relatively little experience to draw valid structural conclusions. Most of the

possible coupling situations which can arise between several protons have been worked out exactly and can be found in the literature. Consequently, it is no longer necessary to solve a complex secular equation in order to obtain from the measured line positions the chemical shift and spin-coupling parameters which can be related to the structure. Finally, integrated intensities allow cross checks on assignments and sometimes even eliminate the need for detailed assignments in solving structural problems. As a result of this progress in the field of high resolution NMR spectrometry, it seems probable that we are seeing now only the beginning of its widespread use by organic chemists as a complementary tool to optical spectroscopy and even as the preferred method for many classes of problems.

REFERENCES

1. Arnold, Dharmatti and Packard, *J. Chem. Phys.* **19**, 507 (1951).
2. F. Bloch, *Phys. Rev.* **70**, 460 (1956).
3. N. F. Ramsey, *Phys. Rev.* **78**, 699 (1950).
4. J. A. Pople, *J. Chem. Phys.* **24**, 1111 (1956).
5. C. E. Johnson, Jr. and F. A. Bovey, *J. Chem. Phys.* **29**, 1012 (1958).
6. T. W. Marshall and J. A. Pople, *Mol. Phys.* **1**, 199 (1958).
7. *Varian Associates Tech. Info. Bull.* Vol. 2, No. 3.
8. J. N. Shoolery, *J. Chem. Phys.* **31**, 1427 (1959).
9. N. Muller and D. E. Pritchard, *J. Chem. Phys.* **31**, 768 (1959).
10. H. J. Bernstein, J. A. Pople and Schneider, *Canad. J. Chem.* **35**, 65 (1957).
11. S. Goodwin, J. N. Shoolery and L. F. Johnson, *J. Amer. Chem. Soc.* **81**, 3065 (1959).
12. J. A. Pople, W. G. Schneider and H. J. Bernstein, *Canad. J. Chem.* **35**, 1060 (1957).
13. A. D. Cohen, N. Sheppard and J. J. Turner, *Proc. Chem. Soc.*
14. H. S. Gutowsky, M. Karplus and D. M. Grant, *J. Chem. Phys.* **31**. 1278 (1959).
15. M. Karplus, *J. Chem. Phys.* **30**, 11 (1959).
16. H. Conroy, private communication.
17. J. N. Shoolery and M. T. Rogers, *J. Amer. Chem. Soc.* **80**, 5121 (1958).

8

HIGH RESOLUTION NMR AS AN ANALYTICAL TOOL

JAMES N. SHOOLERY
Varian Associates, Palo Alto, California

ALTHOUGH the acceptance of high resolution NMR as an important tool in chemical structure determination has become widespread during the past several years, the use of this technique for analytical purposes has undergone much slower development in spite of the obvious potentialities of the method. This stems largely from the much more stringent requirements of resolving power, scanning stability and linearity of amplifiers and detectors, particularly when quantitative information is desired. As a result, many workers have concentrated their efforts on structural-type problems which could be solved with their existing instrumentation with the result that the analytical capabilities of the instrument have been to some extent neglected.

Analytical work falls into two categories—qualitative and quantitative. For a long time, it has been realized that the NMR spectrum of a compound is unique; i.e. the number and relative amplitudes of the resonances, their chemical shifts and multiplicities due to spin-coupling, and even their relaxation times allow so many possibilities that there is little likelihood that two different chemical compounds would have the same NMR spectrum. Even though the total length of the proton NMR spectrum is not great compared to the typical spin–spin multiplet widths and to the variations in the chemical shifts of functional groups, it will often be possible in mixtures of hydrogen-containing compounds to find a line in the clear, i.e. an "analytical peak", for each component of the mixture. If one wishes to know whether or not a certain compound is present, one simply looks for a peak from that compound which would be expected in an otherwise clear region of the spectrum. In case of doubt, one can often run the spectrum and then add some of the compound in question, noting whether or not the appropriate peaks increase in amplitude or whether additional peaks appear in the spectrum. It should be noted that the peak which is selected as representative of a given compound in a mixture may arise from a very small percentage of the hydrogen in that compound; therefore, the sensitivity of the method in this application will not always be large. Also, the solvent effects which cause variations

in the chemical shift will change from mixture to mixture and only by dilution in a standard solvent, e.g. carbon tetrachloride, which further decreases sensitivity, can we be reasonably certain of eliminating this effect. Therefore, the method should not be regarded as suitable for trace analysis in most cases. Nevertheless, in favorable cases extremely high sensitivity can be achieved, as is found in the analysis for the residual hydrogen in a totally deuterated solvent. For example, Fig. 1 shows the signal-to-noise ratio and

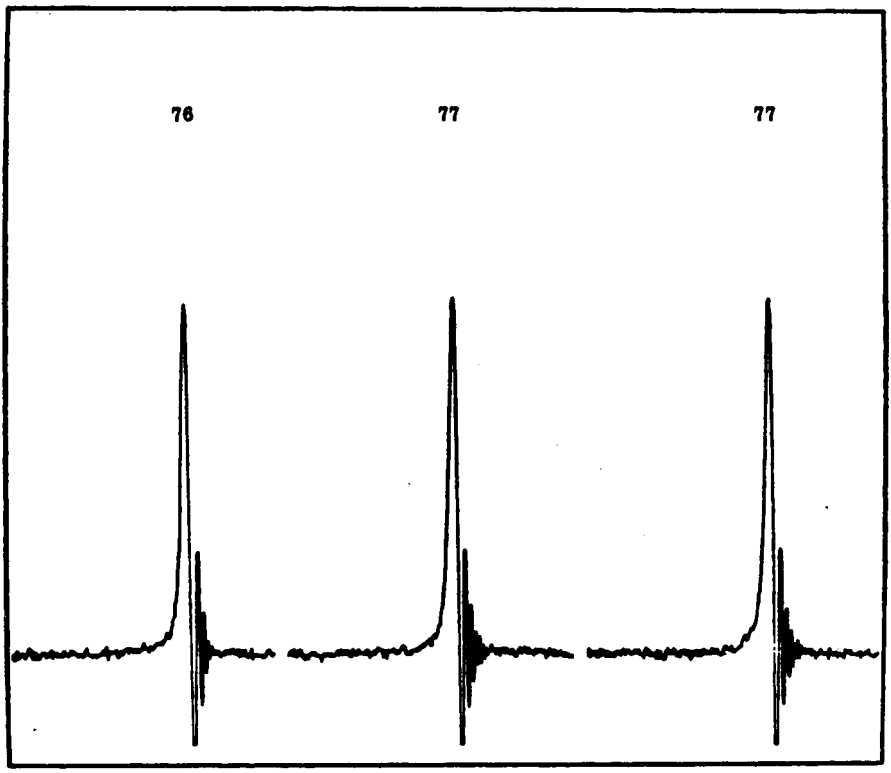

FG. 1. Signal amplitude for three successive recordings of the residual H_2O resonance in high-purity D_2O

reproducibility of the H_2O in high purity D_2O. In this case the relaxation times are sufficiently similar from sample to sample so that the amplitude is a measure of the amount of H_2O present. Figure 2 shows how an analysis can be obtained by adding weighed amounts of H_2O and extrapolating to zero signal.

Although the uniform sensitivity of NMR to the number of hydrogen nuclei present, regardless of the compound in which they are located, can be a detriment in trace analysis, it is definitely an asset in mixtures containing several

substances in high concentration. In such cases, no single substance will swamp the others as would be the case if the sensitivity to different compounds varied widely.

An example of the analysis of a complex mixture is illustrated in Fig. 3. A qualitative analysis of the components of the mixture is obtained immediately by comparison of the spectrum in Fig. 3 with the individual spectra of the seven constituent terpenoid compounds. In fact, by simply estimating

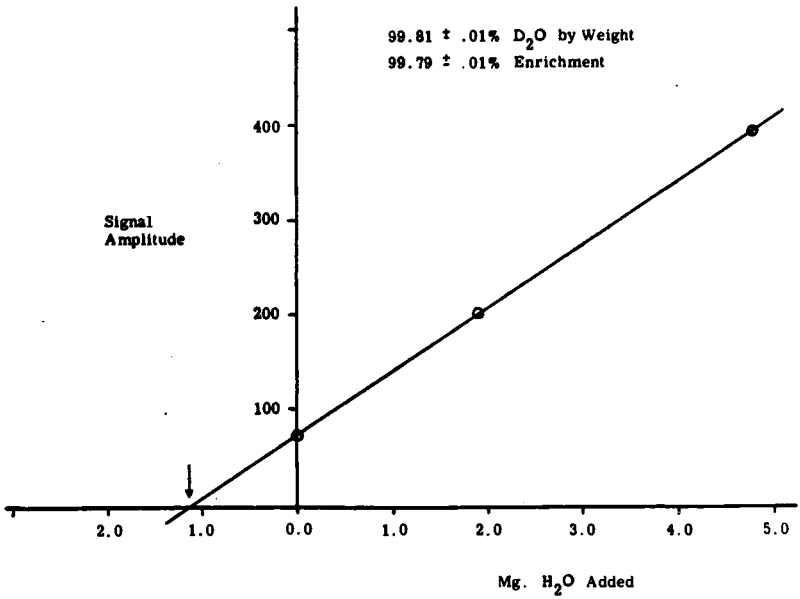

FIG. 2. H_2O remaining in high purity D_2O by the method of adding known amounts of H_2O and extrapolating to zero signal amplitude.

the amounts present from the peak heights a fairly good semi-quantitative analysis can be obtained.

Another example of qualitative analysis is the problem of determining whether or not deuterium has entered an organic compound and furthermore, where it has been substituted for hydrogen. The spectra of cumene and partially deuterated cumene are shown in Fig. 4. Here we see that the problem can be solved in two different ways. Comparison of the two spectra shows that the complex multiplet which represents the CH group α to the benzene ring diminishes in amplitude proportional to the extent of replacement by deuterium. At the same time, the doublet (peaks 1 and 2) collapses to a much more closely spaced triplet (labeled 5) and centered about the same chemical shift position. Either of these observations confirms the fact that partial deuteration has occurred in the position α to the benzene ring.

A similar example is found in Fig. 5, which illustrates at the left the benzene ring resonances from anisole (methoxy benzene) and at the right the spectrum of deuterated anisole. The assignments of the various lines in the spectrum attribute the peaks at 430 c/s to the protons meta to the methoxy group and the peaks at 410 c/s to the ortho and para protons. The spectrum of the deuterated compound shows that nearly all of the deuteration has occurred in

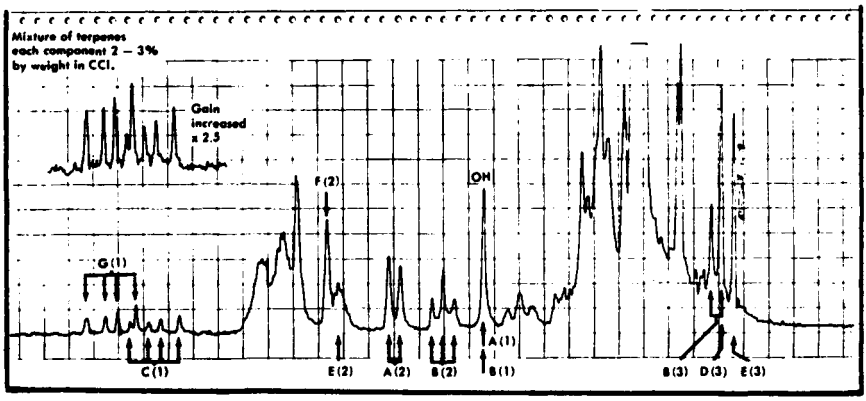

FIG. 3. Analysis of a mixture of terpenes.

Compound	Mol per cent	NMR result
A (Geraniol)	18.3	16.2
B (Citronellol)	15.6	15.3
C (Myrcene)	11.6	11.1
D (α-pinene)	11.5	12.7
E (β-pinene)	12.7	14.5
F (Limonene)	14.5	14.5
G (Terpene)	16.3	15.5

Interpretation: A mixture of seven terpenes listed in the accompanying table yielded an NMR spectrum shown above. From a study of the spectra of the pure compounds it was possible to make the assignments shown for the various groups of lines, giving the compound and number of protons represented. A rapid semi-quantitative analysis can be obtained from *simple* measurements of line amplitudes and areas. If we assume that the amplitude of the OH line represents $A+B$, one third the amplitude of the E (3) line represents E, while the sum of the four C (1) lines represents C, and similarly G, we have left only to determine D and F. The pure spectrum of B shows us how much to subtract from the D (3) line to take account of the interference from compound B. One third of the remainder gives D. Compound F should be determined from an area measurement, but a good result is obtained by comparing the product of amplitude and line width with $A+B$ or E. Finally, the ratio of A to B was obtained from an area measurement under the lines A (2) and B (2). The results, expressed in mol per cent, are presented in the right-hand column of the Table for comparison with the known composition of the mixture.

the ortho and para positions, although the peak at 430 c/s is not quite large enough to represent two protons, suggesting that a small amount of meta-deuteration has taken place.

The ability of NMR to measure without perturbing the system being measured is of value in systems which are in equilibrium. In such cases a chemical analysis for a molecular species would remove it and shift the equilibrium in such a manner as to replace it, resulting in a high value for the analysis. A very difficult system to study chemically is illustrated in Figs. 6, 7 and 8. The

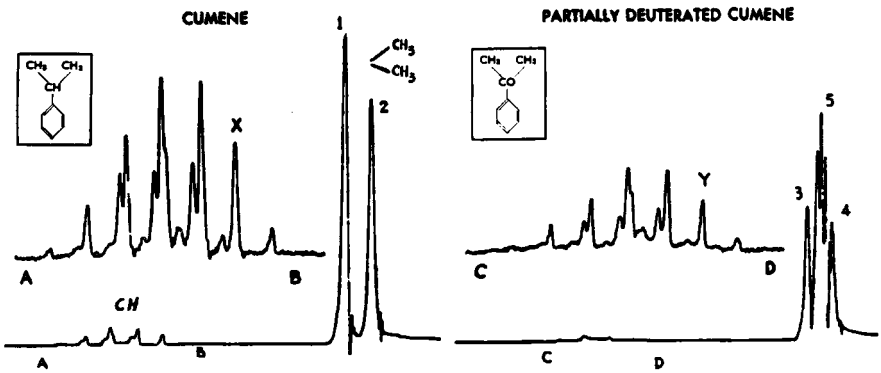

FIG. 4. Measuring degree of deuteration.

Interpretation: Cumene (isopropyl benzene) can be deuterated in the position alpha to the ring by partial exchange. Spin-coupling between the CH group and the two CH_3 groups leads to a strong doublet (peaks 1 and 2 or 3 and 4) and a complex multiplet (region *A–B* or *C–D*). If the CH is replaced by CD, the complex multiplet disappears and the peaks 3 and 4 collapse to the triplet (peak 5) due to the spin of deuterium ($I = 1$). The percentage of deuterated cumene is given by the ratio of any two corresponding peaks. Peaks 1 and 3 yield the result $70 \pm 1\%$ deuteration, while peaks *X* and *Y* provide a check on this result, also yielding $70 \pm 1\%$.

The samples were supplied through the cooperation of D. G. A. Russell, General Electric Research Laboratory, Schenectady, New York.

ortho phosphoric acid, pyrophophoric acid and polyphosphoric acids in an equilibrium mixture of P_2O_5 and H_2O are observed as three peaks in the P^{31} NMR spectra from left to right respectively. As the P_2O_5 excess is increased from 6 per cent to 18 per cent the equilibrium population of the three peaks can be seen to shift from a preponderance of ortho phosphate to polyphosphate.

One type of qualitative analysis which is useful in structure determination work might be called "functional group analysis". Given the high resolution NMR spectrum of an unknown compound or mixture, the spectroscopist, finding a complex multiplet of lines about 7 p.p.m. on the low field side of the internal reference substance, tetramethylsilane, would consider it highly

probable that a substituted aromatic compound is present. On the other hand, a single sharp line lying less than 1 p.p.m. from the same reference would almost certainly represent a methyl group bonded to a saturated carbon atom which, due to the lack of spin-coupling, would be deduced to be tertiary. In between these two regions, however, the spectroscopist would

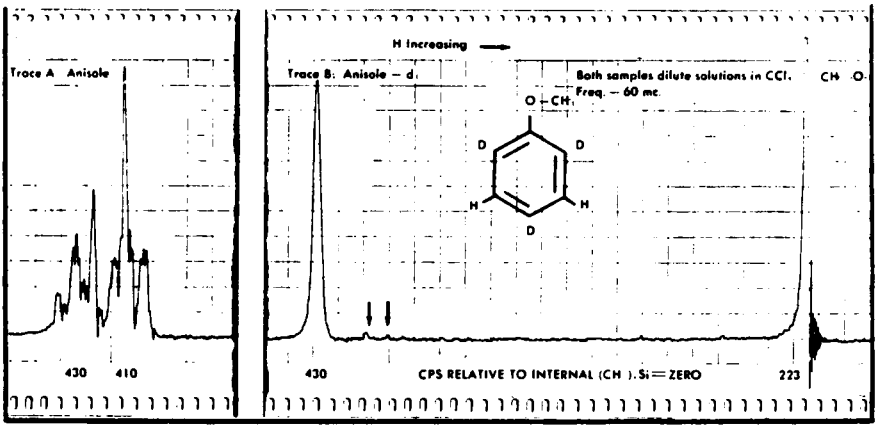

FIG. 5. Location of deuterium in anisole-d_3.

Interpretation: This example demonstrates the ease with which not only the degree of replacement of hydrogen by deuterium can be determined by the NMR method, but also the location within the molecule. Trace *A*, ordinary anisole, shows two regions of NMR response characteristic of hydrogen on a benzene ring, at 410 and 430 c/s. The relative areas are respectively 3 and 2. This pattern is believed to result from a conflict between the inductive withdrawal of electrons from the ring by the oxygen (decreasing in the order *o*, *m*, *p*) and the mesomeric contribution of electrons to the ring (stronger at *o* than *p*, negligible at *m*). The net result is roughly no change of electron density at the meta-hydrogens and about the same increase in electron density and consequently the shielding at the ortho- and para-hydrogens. Removal of the *o*- and *p*-hydrogen collapses the multiplet at 430 to a single line (Trace *B*) due to the much smaller spin-coupling associated with the deuterons. The area of this line is slightly less than $\frac{2}{3}$ the CH_3–O– area, suggesting a small amount of *m*-replacement. The two small signals marked by arrows arise from a few percent of the species with one *o*- and one *p*-deuterium, which gives a doublet due to the spin coupling to the adjacent meta-hydrogen.
We are indebted to Prof. Ernst Berliner of Bryn Mawr College, Pennsylvania, for furnishing the sample.

be more wary of making definite statements unless more information were available. There are many possible functional groups which will produce resonances in this central region; so many, in fact, that the high resolution NMR method is usually more suited for making a choice between several possibilities than for initially defining the possible groups which might be present.

In view of this difficulty, the high resolution NMR technique is sometimes employed to determine the groups which are *not* present. For example, if no absorption is found in the region characteristic of olefinic protons, one can say that the compound is either saturated or that there are only tetra-substituted double bonds present.

Some functional groups have sufficiently unique chemical shifts or spin-couplings that the NMR response can be considered diagnostic for them. The resonance of an aldehyde proton appears to be uniquely located about 10 p.p.m. from the reference tetramethylsilane. As an example of a diagnostic

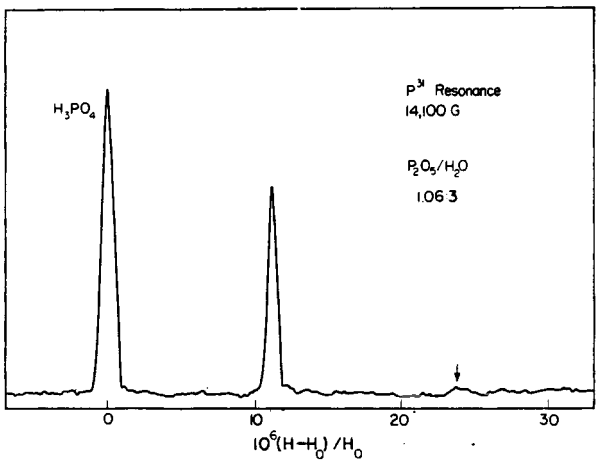

FIG. 6. P^{31} signals from the three types of phosphorus present in a mixture of ortho, pyro, and polyphosphoric acids.

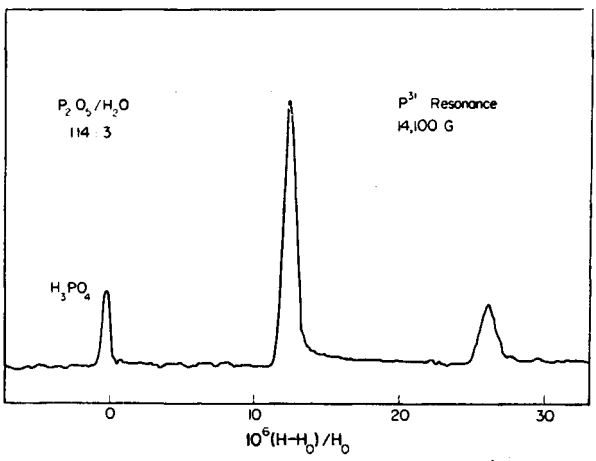

FIG. 7. P^{31} spectrum showing increased polymerization of phosphate groups with increasing excess of P_2O_5.

spin-coupling, we might consider an AB pattern with $J = 12$ to 15 c/s. This is practically certain evidence for the presence of a CH_2 group which, furthermore, must be structurally located in such a manner that the two protons are non-equivalent. One, therefore, looks either for a ring or for an asymmetric carbon atom.

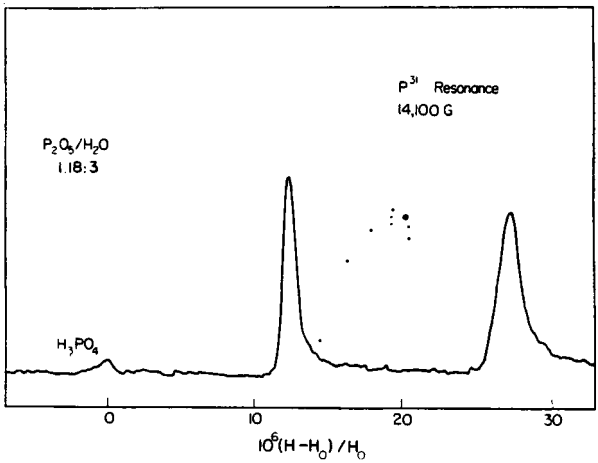

FIG. 8. P^{31} signals from glassy 118 per cent phosphoric acid.

Of course, when the number of possible structures can be narrowed down in advance from other available data, the ability of the NMR method to distinguish unequivocally between them is well recognized and has led to widespread application of the technique to structural problems.

QUANTITATIVE ANALYSIS

When, in addition to asking the question "What is present?", we begin to ask "How much?", we find that it is first necessary to stop and take a look at the theory and instrumentation of nuclear magnetic resonance. We have seen in the introductory lecture on high resolution NMR spectrometry that the NMR signal is a mixture of two modes, the absorption and dispersion, either of which can be selected for study by a radio-frequency phase detector. The form of these two signals is reproduced again below:

$$\text{Dispersion} = \frac{M_0\gamma H_1 T_2^2(\omega_0-\omega)}{1+(\gamma H_1)^2T_1T_2+\{(\omega_0-\omega)T_2\}^2} \tag{1}$$

$$\text{Absorption} = \frac{M_0\gamma H_1 T_2}{1+(\gamma H_1)^2T_1T_2+\{(\omega_0-\omega)T_2\}^2} \tag{2}$$

The amplitudes of these signals are different functions of the distance away from the center of the resonance and both functions depend upon the total

nuclear magnetic moment which is proportional to the number of nuclei in the coil, and also upon H_1, the radio-frequency driving field, and the relaxation times T_1 and T_2. Since the relaxation times differ for different substances and even for different nuclei within the same molecule, the maximum amplitudes of both the absorption and dispersion mode signals are not necessarily a measure of the number of nuclei in the sample. Consequently, only under special conditions can peak amplitudes be used with confidence in quantitative analytical work.

The dispersion mode, sometimes called the u-mode, when integrated over the whole range of magnetic field values gives infinite areas of opposite sign on either side of the center of the resonance. Actually, most of this area is in the wings of the resonance and if one would always start measuring the integral from a definite distance ahead of the true resonance position and terminate the integration when the integral changes sign, the result would be proportional to the number of nuclei in the coil. Under some conditions, the result would even be independent of the relaxation times, which would appear to be an advantage. However, the fact that the dispersion mode falls off only with the inverse of the distance from the resonance, makes these signals much too broad for most work in which the integrals of the various peaks and the peaks themselves must be distinguished from one another. In the case of a complex multiplet of lines there would be no way to determine just where to start and stop the integration.

The integral of the absorption mode or v-mode is more well behaved, being finite and proportional to the number of nuclei in the coil. If we assume a linear sweep of magnetic field at a rate r and integrate against time, we obtain the following expression for the area under the absorption mode:

$$\text{Area} = \frac{C}{T}\frac{H_1}{r}\frac{N}{[1+(\gamma H_1)^2 T_1 T_2]^{\frac{1}{2}}} \tag{3}$$

where C includes the various nuclear and instrumental constants, T is the absolute temperature, H_1 is the r.f. driving field, and the expression in brackets shows the dependence upon relaxation times. Only when the relaxation times are very short, or the r.f. power level very small, such that $(\gamma H_1)^2 T_1 T_2 \ll 1$, does the area become independent of the relaxation times for slow passage conditions.

The line shapes and the integrals of the u- and v-modes are shown in Fig. 9.

Most NMR spectra are actually obtained under conditions of passage intermediate between "slow" and "rapid". The theoretical treatment of the integral to be obtained from the distorted signal with its trailing exponentially decaying oscillatory "wiggles" is quite difficult. As long as the r.f. power level is kept reasonably low during passage through resonance so that the nuclear moments are not greatly perturbed from the equilibrium position, it can be shown experimentally that even though considerable "ringing" is

encountered, it integrates out to zero and the remaining integral is still strictly proportional to the number of nuclei in the group whose resonance is being studied. Figure 10 shows the effect of sweep rate on the ratio of the peak areas for the ring protons and the methyl protons in toluene. No appreciable effect is noted over a range of four in sweep rate even though none of

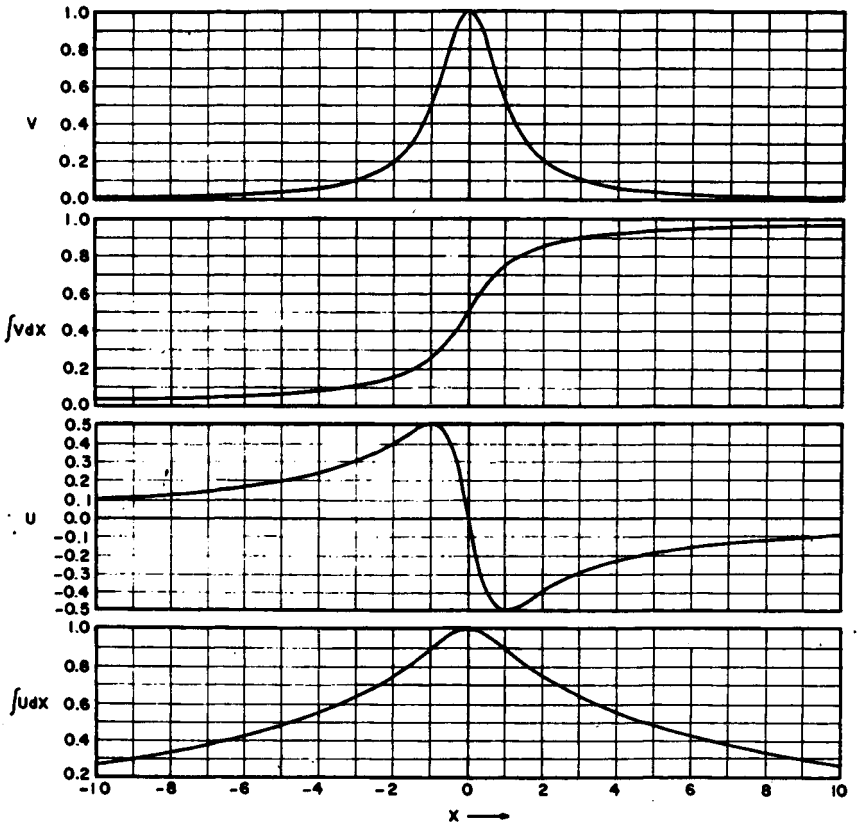

FIG. 9. Line shapes and integrals of u- and v-mode signals as a function of the number of half line-widths from the center.

SWEEP RATE	LINE WIDTH	C_6H_5/CH_3 [a]
0.5 mg/sec.	0.5 mg	1.67
1.0	0.5	1.66
1.0	1.0	1.67
1.0	2.0	1.67
2.0	0.5	1.68

a) Toluene sample

FIG. 10. Effect of sweep rate and field uniformity on NMR intensity ratios.

the data represents true "slow passage" conditions. The value obtained is close to the actual value in toluene which is also found experimentally to be the value obtained when data obtained for various r.f. power levels are plotted and extrapolated to zero r.f. power. Thus, as we might expect, sweeping faster alleviates the saturation problem so that we no longer need to meet strictly the condition $(\gamma H_1)^2 T_1 T_2 \ll 1$ as long as we do not let the power get too high and use an integrator which can follow the rapid oscillations of the "wiggles" without developing a non-linear response which would lead to rectification and unwanted area.

It will also be noted from Fig. 10 that changing the homogeneity of the magnet had no effect on the areas. This, of course, is one of the main reasons for measuring areas rather than amplitudes, since variations in line widths due to magnet homogeneity or relaxation effects are exactly compensated by corresponding variations in the amplitudes such that the area is constant as shown in equation (3).

If H_1 is allowed to become too large, even under intermediate passage conditions, the signals become dependent upon the individual relaxation times of the nuclei in the chemically non-equivalent groups. Figure 11 shows

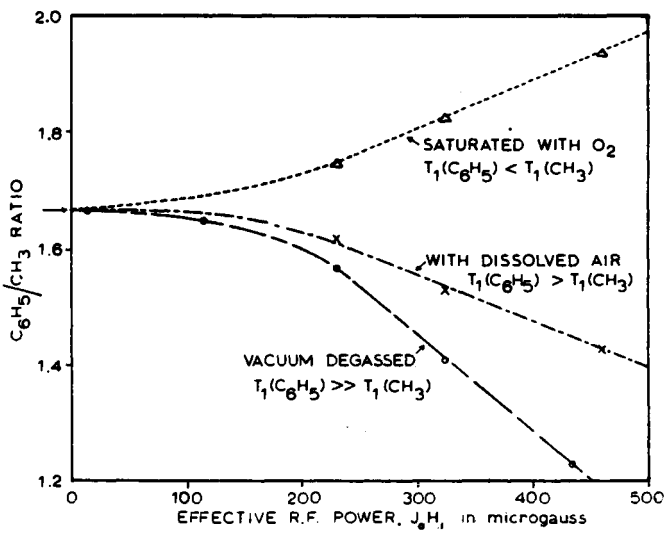

FIG. 11. Effect of relaxation time and r.f. power level on integrated intensity ratios in toluene.

the effect on vacuum-distilled toluene, ordinary toluene and oxygen-saturated toluene as the power is increased to the point at which one group of nuclei saturates before the other. In vacuum-distilled toluene the ring protons have the longer relaxation time and at high power level the area ratio drops below the value 5 to 3. The oxygen-saturated sample shows a reverse behavior, i.e.

the oxygen shortens the relaxation time of the ring protons without particularly affecting the methyl protons. The ordinary sample in equilibrium with air shows intermediate behavior. It is rather interesting that by this method some information can be obtained about the formation of a molecular complex between oxygen and toluene and even something about its structure.

A study of the shape of the curves in Fig. 11 shows that there are two fairly linear regions separated by a region of curvature. Extrapolation of data taken in the high r.f. power region to zero r.f. power would lead to serious errors. The low r.f. power region which is linear has such a small slope that extrapolation is hardly necessary. In case of doubt about the correctness of an area ratio measurement, the measurement should be repeated at several r.f. power levels differing by factors of two. If a constant ratio is obtained, differences in relaxation times can be disregarded and the measurement taken as the true area ratio. Unless the data are measured a large number of times so that the probable error can be estimated, extrapolation to zero power may actually introduce an error. Of course, this method applies only for area ratios since the areas themselves are linear in H_1 at low values of H_1 and extrapolate to zero at vanishing H_1.

It should be noted in equation (3) that the Boltzmann distribution of population between the nuclear energy levels results in a dependence of the integral on the reciprocal of the absolute temperature. This dependence upon temperature would cancel out in an area ratio measurement unless the temperature were changing rapidly during the measurement. In cases where the temperature is purposely varied in order to adjust a reaction rate or shift an equilibrium, it will be necessary to recognize this dependence of the integral upon T.

Equation (3) also shows that the integral is inversely proportional to the rate, r, at which the magnetic field is varied. This means that there will be an optimum rate for each sample, since sweeping too slowly will result in saturation except at extremely low power levels where the integral becomes vanishingly small, while sweeping too rapidly will also have the effect of making the integral too small to measure accurately.

The instrumentation used for quantitative analysis in high resolution NMR is conventional as far as the radio-frequency transmitter, sample head and receiver are concerned. The output of the receiver should be kept small, however, in order to avoid detecting a mixture of u- and v-modes by the r.f. phase sensitive detector and also to avoid non-linear amplification of the signals. A peak r.f. swing of about 1 volt is a conservative limiting value. This may require reducing the r.f. power or receiver gain considerably for strong signals with the result that there will be insufficient sensitivity for recording weaker signals. This presents no problem, however, because additional amplification (following the r.f. unit) is added with the special circuitry to be described in the next section.

AUDIO-FREQUENCY MODULATION

The conventional NMR spectrometer r.f. unit detects the d.c. component of the v-mode superimposed upon a d.c. voltage resulting from the direct coupling (leakage) of transmitter energy into the receiver coil with the same phase relationship as the signal. This d.c. component of leakage can be reduced to zero by careful probe balance, but in order for it to remain equal to zero, a stringent stability requirement is placed upon the probe balance. If the probe becomes slightly unbalanced, the d.c. appearing at the output of the receiver can still be bucked out with a battery, but the difference between the two d.c. voltages now becomes sensitive not only to the stability of the probe balance, but also to the minute changes in the total gain of the radio-frequency receiver.

It has been found[1] that when an audio-frequency magnetic field modulation is applied to the sample at a frequency which is large compared to the line width, signals are found at the usual resonance position and also in pairs of sidebands separated from the central signal by the modulation frequency. Analysis[2, 3] shows that the central signal and each sideband signal contain not only a component whose frequency is equal to the transmitter frequency but also other components, each with a frequency separated from the transmitter frequency by an integral multiple of the modulation frequency. By using an audio phase sensitive detector[4, 5, 6] following the r.f. phase sensitive detector, we can select from the central resonance or from any one of the sideband resonances the component which occurs at the audio frequency. The advantage of this system is that *only* the nuclear signal is modulated at the audio-frequency, the probe balance being independent of the modulation. Therefore, an output different from zero at the audio-frequency phase detector will occur only when passing through an NMR signal. The details of construction and operation of such a system will be discussed in the laboratory session.

Since the output of the radio-frequency r.f. unit is now an audio-frequency signal, one can introduce additional amplification with a simple audio amplifier preceding an audio-frequency phase sensitive detector. In order to select the v-mode for integration, it is also necessary to introduce the correct amount of radio-frequency phase shift and also the correct amount of audio-frequency phase shift. Finally, optimum performance is obtained only for a certain critical value of the modulation index, β, which is defined as the amplitude of modulation expressed in frequency units divided by the frequency of modulation. The modulation frequency itself is not critical but since signals occur in sidebands spaced ν cycles per second apart, it is important to choose ν larger than the largest chemical shift to be expected in the high resolution NMR spectrum. In the case of hydrogen nuclei, the shifts are seldom larger than about 10 p.p.m. or 600 c/s at a frequency of 60 Mc. If we did not make

the modulation frequency larger than 600 c/s, we might find that while integrating the center band signal at one end of the spectrum, we would encounter interference from the first sideband signal from the other end of the spectrum. Most of the work illustrated here has been performed with a modulation frequency of 1200 c/s. Still higher modulation frequencies could be employed, but the power requirements to maintain the proper index of modulation and the losses in the aluminum body of the probe become excessive.

The output from the audio-frequency phase detector can be filtered and displayed on a recorder in the usual fashion. It is no longer sensitive to changes in probe balance or minor receiver gain fluctuations. Therefore, it can be fed into a suitable integrating device whose output will represent a true measure of the number of nuclei corresponding to the NMR peak being integrated.

Many different types of integrating devices exist. The form of the high resolution NMR signals places rather stringent requirements on the integrator. The total integrals of most NMR signals are not large in terms of volt seconds. The rate of change of the voltage can be very rapid and can change sign in an oscillatory way due to the "wiggles" following the peaks. A type of integrator which can cope with these difficulties successfully is known as a Miller integrator. This consists of a series *RC* circuit with the output side of the capacitor fed back to the input side through a stable high-gain amplifier. The effective time constant of the integrator is *RC* times the gain of the amplifier. It is quite feasible to construct a stable device with an effective time constant of many thousands of seconds and with sufficient gain to accumulate integrals amounting to several volts during passage through even the smallest NMR signals. The integral of the spectrum can either be recorded by a strip chart recorder or read off, point by point, with a digital voltmeter or other voltage measuring device.

Equation (3) shows that since the integrals depend upon the reciprocal of the sweep rate, ratios of integrals will be limited in accuracy by the constancy of the sweep rate. There will be an optimum sweep rate for integration determined by the amount of random drift in the instrument. If the amount of drift is small, it will be possible to sweep very slowly and to obtain large integrals which can be measured accurately. If the drift is large, it may be necessary to sweep quite rapidly in order to obtain reproducible results with the consequence that the sensitivity of the entire system will be reduced. Since the sensitivity and the stability both affect the accuracy, it is worth noting that by taking steps to achieve the highest sensitivity possible we can reduce somewhat the stringent requirements on the sweep stability. The use of an insulation jacket on the magnet and a temperature controller on the cooling water appears to give more than adequate stability for obtaining results of the usual analytical accuracy.

Figure 12 illustrates the precision and accuracy which can be expected with a properly adjusted spectrometer equipped with an audio-frequency modulation system and a Miller integrator. A dilute solution of about 5 per cent of ethyl benzene in carbon tetrachloride was recorded and integrated in the region of the CH_2 and CH_3 peaks. Assuming a pure sample, the ratio of the three protons in the methyl group to the two protons in the methylene

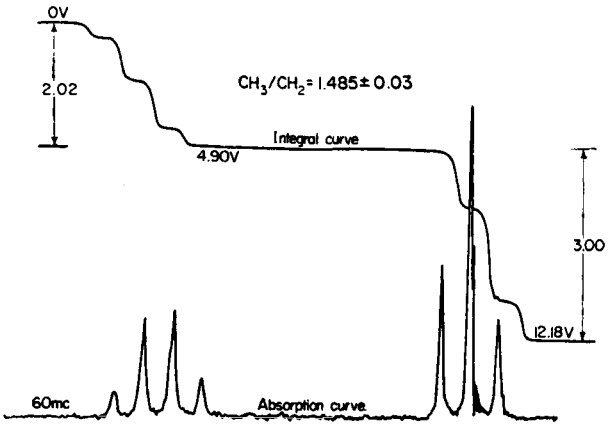

FIG. 12. Absorption curve and integral of a dilute solution of ethyl benzene (aliphatic region) with r.f. power and sweep rate adjusted for operation on the linear part of the saturation curve for both CH_2 and CH_3 groups.

group is observed to be 1.485 ± 0.03 which is within 1 per cent of the true value. The boiling range of the ethyl benzene used in this experiment was 134–136°C, suggesting that impurities may account for part of the difference between the theoretical and observed ratio.

An application of considerable interest in its own right, also illustrating the accuracy and precision attainable with the high resolution technique, is presented in Fig. 13. The total hydrogen content of seven samples was mea-

COMPOUND	% H by wt.	% H (NMR)
ETHYL BENZENE	9.48	9.48[a] ± .04[b]
WATER	11.17	11.08 ± .04
CHLOROFORM	0.843	0.830 ± .01
TOLUENE	8.75	8.76 ± .03
p-DIOXANE	9.16	9.13 ± .09
17α-HYDROXY-PROGESTERONE (17.4 mg)	9.16	9.18 ± .04
3α-ACETOXY PREGNANE-20-ONE (24.5 mg)	9.99	9.99 ± .06

a) Reference compound
b) Standard deviation

FIG. 13. Total hydrogen analyses from NMR integrated intensities.

sured by comparing the total integrated intensities of the entire spectrum of each compound. It will be noted that some of the compounds are sufficiently complex to yield very complicated spectra. Since the samples were studied in different cells, it was necessary to determine that the cross sectional areas of all the cells were identical. This was done by filling all cells with the same liquid and integrating the resulting NMR signal. Inasmuch as all of the cells were precision tubing which had been shrunk on a mandrel, it was expected that they would give identical results, but although five of the cells were within a fraction of a percent of the same area, two were found to differ by several percent. This was traced to the fact that they were from a different production lot and were in fact different in their internal diameters. The NMR results, corrected for the tube diameters, are displayed in the third column of Fig. 13 for comparison with the weight per cent of hydrogen in the second column calculated from the molecular formulas. The agreement between the two columns shows the remarkable dynamic range over which the entire system performed in a linear fashion. For example, the total integral from the liquid water sample would be twenty-eight times larger than the total integral obtained from the 17.4 mg sample of 17 α-hydroxy progesterone. This in itself represents a good dynamic range, but when we consider that the spectrum of the steroid is spread out over hundreds of c/s while the water signal is concentrated in a single sharp line a fraction of one c/s in width, the true dynamic range of linearity can be seen to be much greater.

The accuracy of the total hydrogen measurement from several milligrams of a complex organic compound, such as the two steroids illustrated in Fig. 13, compares favorably with the standard combustion method. It has the advantage of being many times more rapid and, in addition, is non-destructive, the entire sample being available for other physical studies at the conclusion of the determination. These two advantages may well lead to increasing use of high resolution NMR spectrometers in this application.

A final example of the analytical capabilities of the high resolution NMR spectrometer is to be found in the analysis of the tautomeric mixture of keto and enol forms of acetyl acetone. The equilibrium between the two forms of the molecule is established slowly enough for the amount of enol to be measured approximately by bromine titration[7]. However, the equilibrium is disturbed by the chemical measurement and an inaccurate value for the relative amounts of the two forms is obtained. Several earlier NMR measurements[8, 9, 10] have been attempted in an effort to take advantage of the non-perturbing nature of the method with results varying between 15 and 24 per cent keto. None of these earlier studies employed electronic integration of the peaks. The present work was carried out at 60 Mc at a temperature of 26.5°C. The spectrum and its integral are shown in Fig. 14. Each region was integrated four times and the results, which were read with a digital voltmeter, were averaged. If we assume that the total integral of the methyl

peaks (including the C^{13} satellites which account for one per cent of the integral) represents six protons, the percentage of keto and enol forms can be calculated independently from the areas under the CH_2 and =CH peaks. A check on the accuracy is obtained by adding the two percentages which are found to account for 99.9 per cent of the protons. A similar procedure could be used to analyze any mixture of two or more substances regardless of whether or not they are in tautomeric equilibrium.

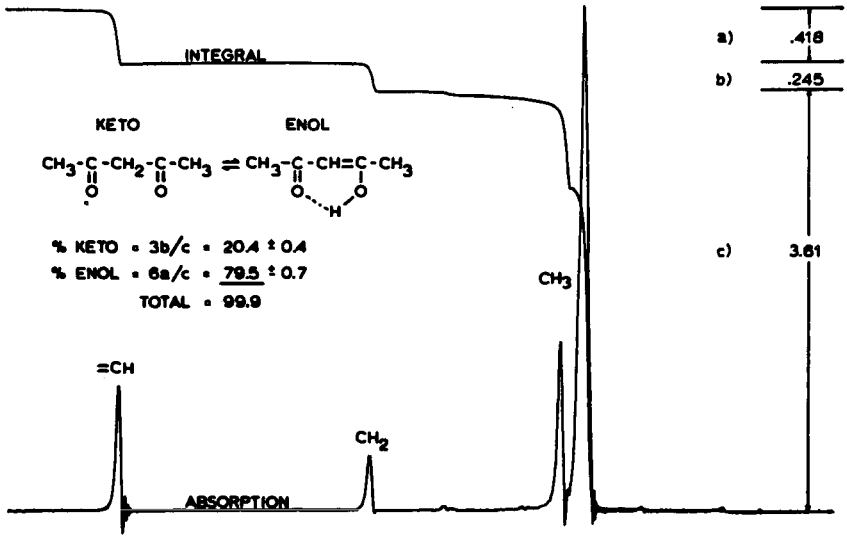

FIG. 14. Analysis of a tautomeric mixture.

SUMMARY

We have seen that by proper attention to experimental technique the NMR method can be an accurate, rapid and non-destructive method of analysis. Quantitative precision and accuracy rivaling accepted techniques such as gravimetric combustion and volumetric titration are being achieved. It is well to keep in mind, however, that this may not generally be true unless every effort is made to meet the following conditions:

(1) Work at as high a field as possible in order to take advantage of increased resolving power and sensitivity.

(2) Stabilize the instrument by environmental and cooling water temperature controls plus insulation of the magnet yoke.

(3) Maintain high sensitivity through use of thin-walled cells with good filling factor and check signal-to-noise performance of the receiver frequently.

(4) Employ auxiliary audio-modulation detection techniques and an electronic Miller integrator with a precision readout.

Of course, it is not always necessary to go to such great lengths to solve many routine chemical problems. Indeed, one of the great advantages of the NMR method of analysis is the simplicity with which samples can be prepared and the rapidity and straightforwardness of many of the analyses. However, when quantitative work of high accuracy is desired. it can now also be regarded as within the scope of the high resolution NMR method. As a result, it seems likely that intensified efforts to make use of these capabilities will rapidly develop and progress in this area may surpass all expectations.

REFERENCES

1. J. T. Arnold and M. E. Packard, *J. Chem. Phys.* **24**, 468 (1951).
2. K. Halbach, *Helv. Phys. Acta.* **27**, 259 (1954).
3. W. A. Anderson, *Phys. Rev.* **102**, 151 (1956).
4. K. Halbach, *Helv. Phys. Acta.* **29**, 37 (1956).
5. R. V. Pound, *Rev. Sci. Instrum.* **28**, 966 (1957).
6. H. Primas, *Helv. Phys. Acta.* **31**, 17 (1958).
7. K. Meyer, *et al.*, *Ber.* **44**, 2718 (1911); **45**, 2843 (1912); **47**, 826 (1914).
8. H. S. Jarrett, M. S. Sadler and J. N. Shoolery, *J. Chem. Phys.* **21**, 2092 (1953).
9. B. N. Bhar, *Arkiv. Kemi.* **10**, 223 (1956).
10. L. W. Reeves, *Can. J. Chem.* **35**, 1351 (1957).

9

NMR FOR THE PHYSICAL CHEMIST

LAWRENCE H. PIETTE
Varian Associates, Palo Alto, California

INTRODUCTION

IT is virtually impossible to assign distinct applications of NMR to physical chemistry as compared to other disciplines. Nevertheless, it is probably safe to say that the application of NMR to the general field of "reaction kinetics" is one of the more important fields of interest for the physical chemist.

The usefulness of NMR as a tool in the study of chemical kinetics has been well established. Its largest single application has been in the general field of proton exchange reactions. Most of the exchange reactions studied have been those in which a hydrogen atom is rapidly exchanging from a nitrogen, oxygen, sulfur or phosphorus atom to another N, O, S or P atom in another molecule. Studies have also been made on fluorine atoms exchanging from sulfur or from nitrogen atoms. In general, these exchange reactions are too fast to study by ordinary isotope-labeling techniques. In typical NMR data, however, one obtains not only the various exchange rate constants, but fundamental information about hydrogen bonding, equilibrium constants, activation energies and in many cases an elucidation of the mechanism for exchange.

NMR exchange techniques also have been extended to general studies of hindered internal rotation in molecules. Potential energy barriers to hindered rotation too large for microwave determinations have been measured quite accurately by NMR. Most of the barrier measurements have been made on molecules that have restricted rotation about the C–N bond, as in the amides, or about the O–N bond, as in the alkyl nitrites, or about the N–N bond, as in the nitrosoamines. Barriers have also been measured for the inversion about the nitrogen nucleus in the imides.

NMR can be used in two ways to study the rates of reactions:

(1) The first method involves the use of the NMR Spectrometer merely as an analytical tool for measuring the change in concentration of the different species with time. Such measurements are straightforward and are only practical for slow reactions and therefore require no further explanation.

(2) The second method is to correlate some change in the spectral features of the NMR resonance lines (i.e. line widths or spacings) with the

lifetimes of the different reacting species. Such a method is applicable to reactions involving lifetimes of 1 sec to 0.001 sec. These reactions can be referred to as relaxation reactions because the reaction itself produces a perturbation on the relaxation mechanism of the nuclei responsible for the resonance absorptions. Exchange reactions and rapid molecular reorientations fall into the latter category.

PHYSICAL MODEL OF THE EXCHANGE REACTION

Consider the system consisting of two molecules, HA and HB, which are capable of mutually exchanging their protons according to the reaction

$$HA + H^*B \underset{k_2}{\overset{k_1}{\rightleftharpoons}} H^*A + HB$$

Assuming that the protons associated with HA are chemically different from those in HB, then, at the extreme of very slow exchange, one observes two sharp proton resonance lines, one corresponding to HA and the other to HB. Such a situation is realized when τ_{HA} and τ_{HB}, the mean lifetimes of protons on HA and HB respectively, are large compared to the inverse of the frequency separation $\delta\omega$ between the resonance lines HA and HB. As the exchange speeds up, one observes lines HA and HB broaden initially, merge together and eventually sharpen up at a position which corresponds to the average of the contribution of the protons from HA and HB.

These changes in the spectral features of the resonance lines are easily explained in terms of the actual lifetime a proton spends on each different molecule. In the region of slow exchange, protons associated with molecules HA are in a different electronic environment than those of HB and therefore see a different effective magnetic field; thus, two resonance lines are observed. As the exchange increases, the protons find themselves midway between the two environments in the time interval between measurements and therefore see only the average of the effective magnetic field and only one resonance line is observed.

Actually the exchange does not have to take place between two different molecules but the exchange can be between different positions on the same molecule, provided there is a chemical shift between these two positions (i.e. different electronic environment). The effect of the kinetic reaction is not always observed in the resonance of the exchanging nuclei but can be observed in nuclei which are spin coupled to the exchanging nuclei.

THEORETICAL EXPLANATION OF KINETIC PHENOMENON ON RESONANCE LINES

There are generally two approaches that one can take to derive relationships between the changes in line shapes or frequency separation of lines and the kinetic phenomenon of exchange or rapid molecular reorientation. The

first of these is the method developed by Gutowsky and Saika[1] which consists of solving the Bloch[2] equations directly for chemical exchange; the second is the method of McConnell[3] which is to show how the Bloch equations can be generalized to include chemical exchange. The two techniques yield the same result and the McConnell treatment is the simpler of the two.

Essentially what McConnell does is to assume that the exchange is a simple reversible molecular process that exchanges nucleus H back and forth between two different molecular environments, HA and HB, with the lifetimes, τ_{HA} and τ_{HB}, while defining that the time for exchange is short compared to the lifetime of the nucleus in any one environment. Using the Bloch notations, McConnell defines u and v as the transverse components of the macroscopic moment in the coordinate frame which are rotating in phase and out of phase with the applied r.f. field H_1. If the rotating field H_1 is small, then the polarization M_z is not appreciably altered from its equilibrium value M_0 and the Bloch equations for u and v become

$$\frac{\mathrm{d}u}{\mathrm{d}t}+\frac{u}{T_2}+(\omega_0-\omega)v = 0 \tag{1}$$

$$\frac{\mathrm{d}v}{\mathrm{d}t}+\frac{v}{T_2}-(\omega_0-\omega)u = -\gamma H_1 M_0 \tag{2}$$

$$\frac{\mathrm{d}M_z}{\mathrm{d}t}+\frac{M_z-M_0}{T_1}-\gamma H_1 v = 0 \tag{3}$$

If the rotating field H_1 is small, then the polarization M_z is not appreciably altered from its equilibrium value, M_0. As a result, only the equations in u and v need be solved and the out of phase component v is then proportional to the absorption intensity.

These equations in their simplest form apply to the macroscopic moment M, when all the nuclei are acted on by the same field H_0. In the region of very slow or no exchange, there are two positions, HA and HB, having different chemical shifts which will be acted upon by two different fields and the corresponding two Larmor frequencies ω_{HA} and ω_{HB}. The chemical shift in cycles per second is given as $\omega_{HA}-\omega_{HB}/2\pi$. Two separate sets of equations similar to (1), (2) and (3) can be written

$$\frac{\mathrm{d}u_{HA}}{\mathrm{d}t}+\frac{u_{HA}}{T_{2HA}}+(\omega_{HA}-\omega)v_{HA} = 0 \tag{4}$$

$$\frac{\mathrm{d}v_{HA}}{\mathrm{d}t}+\frac{v_{HA}}{T_{2HA}}-(\omega_{HA}-\omega)u_{HA} = -\gamma H_1 M_0 \tag{5}$$

and similar expressions in HB.

As was indicated before, McConnell assumes the exchange is completely random and that the time τ_{HA} any one nucleus spends at HA is long compared to the time it takes to make a jump to HB. The fractional populations of HA and HB sites P_{HA} and P_{HB} are related to τ_{HA} and τ_{HB} by

$$P_{HA} = \frac{\tau_{HA}}{\tau_{HA}+\tau_{HB}} \qquad P_{HB} = \frac{\tau_{HB}}{\tau_{HA}+\tau_{HB}} \tag{6}$$

The modified Bloch equations proposed by McConnell are

$$\frac{\mathrm{d}u_{HA}}{\mathrm{d}t}+\frac{u_{HA}}{T_{2HA}}+(\omega_{HA}-\omega)v_{HA} = -\frac{u_{HA}}{\tau_{HA}}+\frac{u_{HB}}{\tau_{HB}} \tag{7}$$

$$\frac{\mathrm{d}v_{HA}}{\mathrm{d}t}+\frac{v_{HA}}{T_{2HA}}-(\omega_{HA}-\omega)u_{HA} = -\gamma H_1 M_0-\frac{v_{HA}}{\tau_{HA}}+\frac{v_{HB}}{\tau_{HB}} \tag{8}$$

and similar equations in HB. T_{2HA} is the transverse relaxation time in absence of exchange.

These modified equations, (7) and (8), differ from the Bloch equations, (4) and (5), by the addition of terms to allow exchange. Thus u_{HB}/τ_{HB} in equation (7) represents the rate of increase of magnetization u_{HA}, due to the transfer of u magnetization into HA from HB, and $-u_{HA}/\tau_{HA}$ measures the corresponding rate of loss of u_{HA}, due to the chemical transfer of u magnetization out of HA into HB.

The steady state solution of the modified Bloch equations in which M_z is constant and the transverse components rotate with the applied r.f. field, H_1, are easily obtained from equations (7), (8) and the corresponding equations in HB by putting all time derivatives equal to zero and applying the conditions of small H_1 and slow passage. One obtains for the total complex moment

$$G = G_{HA}+G_{HB}$$

where

$$G_{HA} = u_{HA}+iv_{HA}$$

$$G = -i\gamma H_1 M_0 \frac{\tau_{HA}+\tau_{HB}+\tau_{HA}\tau_{HB}(\alpha_{HA}P_{HA}+\alpha_{HB}P_{HB})}{(1+\alpha_{HA}\tau_{HA})(1+\alpha_{HB}\tau_{HB})-1} \tag{9}$$

and

$$\alpha_{HA} = \frac{1}{T_{2HA}}-i(\omega_{HA}-\omega)$$

Slow Exchange

If the life times, τ_{HA} and τ_{HB}, are large compared to the inverse of frequency separation, $(\omega_{HA}-\omega_{HB})^{-1}$, the spectrum will consist of two resonance lines in the vicinity of ω_{HA} and ω_{HB}. If the radio-frequency is close to ω_{HA}

and thus far from ω_{HB}, then v_{HB} is effectively zero and the slow exchange solution of the Bloch equations becomes

$$G \approx G_{HA} = -i\gamma H_1 M_0 \frac{P_{HA}T'_{HA}}{1-i(\omega_{HA}-\omega)T'_{HA}} \tag{10}$$

and

$$v \approx v_{HA} = -\gamma H_1 M_0 \frac{P_{HA}T'_{HA}}{1+(T'_{HA})^2(\omega_{HA}-\omega)^2} \tag{11}$$

which yields a broadened signal at ω_{HA} with a line width given by

$$\frac{1}{T'_{HA}} = \frac{1}{T_{2HA}} + \frac{1}{\tau_{HA}} = \pi\Delta\nu \tag{12}$$

$\Delta\nu$ = full line width at one-half maximum in c/s. It can be seen that when τ_{HA} is very large, $1/T'_{HA} = 1/T_{2HA}$ and equation (11) simplifies to the normal slow passage solution of the Bloch equations.

For our simple exchange reaction then we can define a specific rate k as

$$k = \frac{1}{\tau_{HA}} = \frac{1}{(HA)}\frac{\mathrm{d}(HA)}{\mathrm{d}t} \tag{13}$$

It then follows that if we know $1/T_{2HA}$, we can obtain measurements of $1/\tau_{HA}$ and the specific rate of the reaction from a simple line width measurement according to equation (12).

The same expressions can also be used in barrier measurements to hindered rotation where there is a very slow flip from one configuration (cis) to the other (trans) and where there is a definite chemical shift between the two configurations. These reorientations, like the exchange reactions, are assumed to follow a simple rate process and therefore the Arrhenius equation is applicable:

$$k = v_0 \exp(-E_a/RT) \tag{14}$$

A substitution of Eqs. (12) and (13) into (14) yields

$$\log(\pi\Delta\nu - 1/T_{2HA}) = \log v_0 - E_a/2.3RT \tag{15}$$

Now a plot of the line width parameter $\log(\pi\Delta\nu - 1/T_{2HA})$ vs. $1/T$ yields a straight line, the slope of which gives the barrier to rotation E_a.

Intermediate Exchange

The transition from two lines to one line occurs when the lifetimes τ_{HA} and τ_{HB} are approximately equal to the inverse of their frequency separation $(\omega_{HA}-\omega_{HB})^{-1}$ and at this point the lifetimes can be approximated from the expression, $\tau = \sqrt{2}/2\pi(\nu_{HA}-\nu_{HB})$, where ν_{HA} and ν_{HB} give the frequencies in c/s. The full expression for the intensity of absorption comes from the imaginary part of McConnell's general expression for the complex moment

G of equation (9). Gutowsky and Holm[4] give this expression after making several assumptions:

$$(1) \quad P_{HA} = P_{HB} = \tfrac{1}{2}, \qquad \tau_{HA} = \tau_{HB} = 2\tau$$

$$(2) \quad \frac{1}{T_{2HA}} = \frac{1}{T_{2HB}} = 0$$

These assumptions mean that the widths of the individual lines are small compared to their frequency separation. Under these conditions the intensity of absorption becomes,

$$v = \tfrac{1}{4}\gamma H_1 M_0 \frac{\tau(\omega_{HA}-\omega_{HB})^2}{[\tfrac{1}{2}(\omega_{HA}+\omega_{HB}-\omega)^2]+\tau^2(\omega_{HA}-\omega)^2(\omega_{HB}-\omega)^2} \tag{16}$$

In the region where the two individual lines have broadened and are beginning to merge together, the product, $\tau|\omega_{HA}-\omega_{HB}|$, may be estimated by comparing the separation between the positions of the two maxima with the positions in the absence of exchange. This ratio is shown from equation (16) to be

$$\delta\omega_e/\delta\omega = (1-2/\tau^2\delta\omega^2)^{\frac{1}{2}} \tag{17}$$

where $\delta\omega_e$ = the separation during exchange and $\delta\omega$ = the separation in the absence of exchange. It can be seen then that an expression similar to (12) and (15) can be obtained which relates the frequency separation of the lines to the lifetimes, τ_{HA} and τ_{HB}. It should be pointed out, however, that this treatment does not apply when T_{2HA} and T_{2HB} become comparable to the frequency separation $(\delta\omega_e)^{-1}$ and, therefore, the range over which reliable measurements can be made is dependent upon the initial separation of the two lines.

Fast Exchange

In the case where τ_{HA} and τ_{HB} are very small, the situation that exists after the two lines have merged to a single line, the general expression of McConnell's equation (9) simplifies to

$$G = \frac{-\gamma H_1 M_0 T''}{1-i(\omega-\langle\omega\rangle)T''} \tag{18}$$

where

$$\langle\omega\rangle = \omega_{HA}P_{HA}+\omega_{HB}P_{HB} \tag{19}$$

This expression represents a single resonance line centered on a mean frequency with a line width parameter of

$$\frac{1}{T''} = \frac{1}{T_2}+[\sigma\tau T_2/\tau+T_2] = \pi\Delta\nu, \tag{20}$$

where σ is merely the second moment of the separate resonance lines.

$$\sigma = P_{HA}(\omega_{HA}-\langle\omega\rangle)^2+P_{HB}(\omega_{HB}-\langle\omega\rangle)^2 \tag{21}$$

If $\tau \ll T_2$ then equation (20) is further simplified to

$$\frac{1}{T''} = \frac{1}{T_2} + \sigma\tau = \pi\Delta\nu \tag{22}$$

It can be seen, that in this region of rapid exchange, when the two lines have merged to a single line with a line width given by $1/T''$, an expression exists which relates the line width with the rate of exchange or reorientation similar to the expressions developed for slow exchange, equations (12) and (15).

The combination of the three treatments discussed makes it possible for the experimenter to measure three different ranges of reaction rates. If the reaction rate can be increased by standard methods, then this increase can be measured by following the transition from the slow to the intermediate to the rapid exchange condition.

Example of Exchange Reaction

Meiboom, Loewenstein and Grunwald[5] have probably done the largest amount of work in the study of proton exchange reactions. To illustrate the kind of information that can be obtained from these studies let us consider their work on proton exchange in ethanol. They have been able to make quantitative measurements of the hydrogen exchange in ethanol containing different amounts of water.

In a solution of neutral alcohol plus a small amount of water, where the exchange is slow, the spectrum consists of a triplet due to the methyl protons and two overlapping quadruplets due to the methylene protons, and a single line due to the H_2O and finally a triplet due to the hydroxyl proton. The exchange is both base and acid catalyzed. In acid or basic ethanol when the exchange is very fast, the methylene resonance changes into a single quartet and the hydroxyl becomes a single line. The H_2O line broadens and merges with the hydroxyl line.

$\Delta\nu$, the full width of the water line at half maximum, was measured as a function of the acid or base concentration. This width, when measured during slow exchange, is related to the specific rate of exchange of a water proton, R_W, by the equations (12) and (13).

$$R_W = \frac{1}{\tau_W} = \pi\Delta\nu - \frac{1}{T_{2W}} \tag{23}$$

The hydroxyl proton of an ethanol molecule can exchange either with H_2O or with another ethanol molecule. Its total specific rate R_T will be made up of two parts, $R_T = R_A + R_B$ where R_A is the rate of exchange of ethanol with water, and R_B, the rate of exchange between two ethanol molecules. R_A can be obtained from the broadening of the H_2O peak from the equation

$$\frac{R_A}{R_W} = \frac{\tau_W}{\tau_A} = \frac{2(H_2O)}{(EtOH)}$$

R_T, the total rate of exchange of the hydroxyl proton can be obtained from the broadening of the methylene resonance since it is spin coupled to the OH proton. Any perturbation on the OH will be transmitted to the methylene resonance via this coupling.

Graphs of R_T and R_A as a function of acid and base yield straight lines the slopes of which give the various rate constants of interest. The kinetics are explained by the following simple mechanisms:

$$ROH + OH^- \overset{k_1}{\rightleftharpoons} RO^- + H_2O$$
$$ROH + RO^- \overset{k_2}{\rightleftharpoons} RO^- + ROH$$
$$ROH + H_3O^+ \overset{k_3}{\rightleftharpoons} ROH_2^+ + H_2O$$
$$ROH + ROH_2^+ \overset{k_4}{\rightleftharpoons} ROH_2^+ + ROH$$
$$ROH + H_2O \overset{k_5}{\rightleftharpoons} ROH + HOH$$

The rate constants obtained from the graphs were:

$$K_1 = 2.8 \times 10^6 \text{ 1/m sec}$$
$$K_2 = 1.3 \times 10^6 \quad ,,$$
$$K_3 = 3.2 \times 10^6 \quad ,,$$
$$K_4 = 1.8 \times 10^8 \quad ,,$$
$$K_5 = 0.8 \quad ,,$$

EXAMPLE OF BARRIER MEASUREMENT TO HINDERED ROTATION

Piette and Anderson[6] showed that the isomerization of methyl nitrite (CH_3–ONO) and other alkyl nitrites can be observed with NMR by merely lowering the temperature enough to reduce the frequency of rotation about the ON bond. They observed that at room temperature only one line is seen characteristic of the methyl resonance but, as the temperature is lowered, this line broadens and eventually splits into two lines characteristic of two isomers. See Fig. 1.

A trans *B* cis

By applying equation (22) at the higher temperature for rapid reorientation and equation (15) at the lower temperatures during slow reorientation, they were able to measure the barrier to rotation. They were also able to show that this barrier is due almost entirely to the double bond character that exists in the O–N bond.

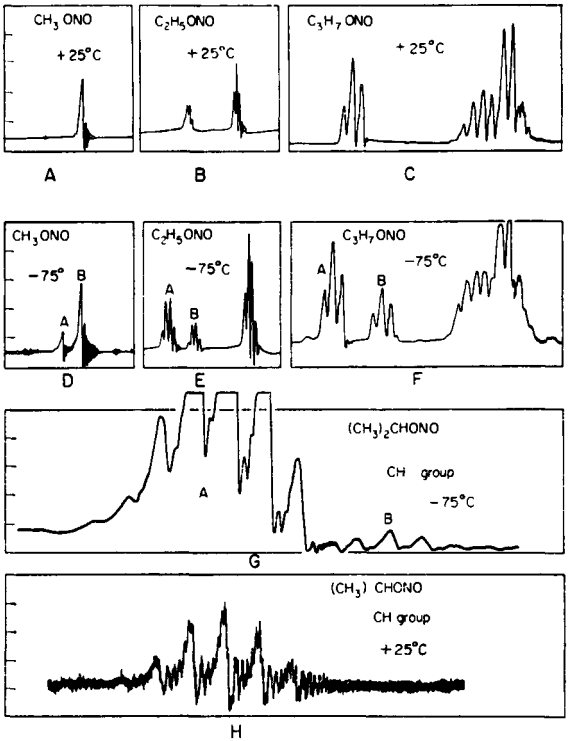

FIG. 1. Proton magnetic resonance of methyl, ethyl, n-propyl and isopropyl nitrite at +25°C (A, B, C, H) and −75°C (D, E, F, G). The cis isomer is assigned to peak A and the trans to peak B for −75°C spectra.

INSTRUMENTAL TECHNIQUES

In each of the expressions derived relating the line width or the frequency separation to the reaction rate, there is a term $1/T_2$ which was defined as the natural line width in the absence of exchange. This parameter must be measured in each kinetic measurement. It is assumed that the natural line width is dependent only upon the magnet inhomogeneity. If this assumption is correct, then T_2 is measured by replacing the sample of kinetic importance with one having a known sharp line and measuring its line width from the decay envelope of the wiggles off the line. In many cases an internal standard is also used. (See Fig. 2.)

In order to make barrier measurements one must follow the reorientation rate as a function of temperature. Thus, it is necessary to be able to vary the temperature over the sample and to control this temperature. This is accomplished with accessories of the type in Fig. 3. The temperature is varied by passing a gas stream around the sample which is held inside a Dewar and spun in order to achieve high resolution conditions.

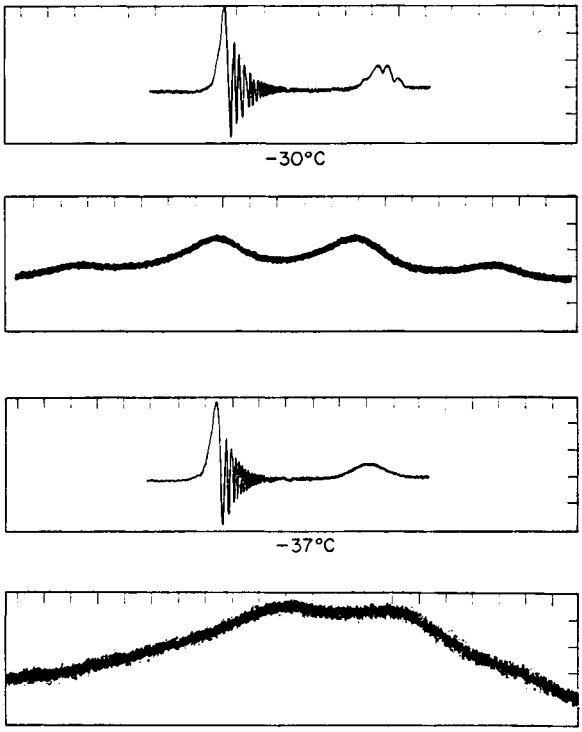

FIG. 2. The phenyl resonance of internal standard toluene at −30°C and −37°C used for T_2 measurements. The broadening of the CH_2 resonance of ethyl nitrite is also shown at the two temperatures.

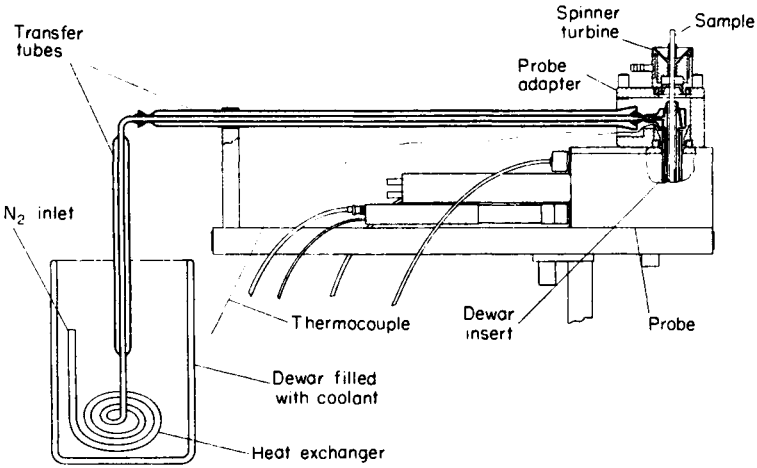

FIG. 3. Variable temperature accessories for high resolution NMR spectrometers.

The line widths are measured by applying a very slow sweep to eliminate the wiggles on the line and then they are calibrated, using the standard side band technique. Figure 4 shows a typical plot that is obtained in a barrier measurement.

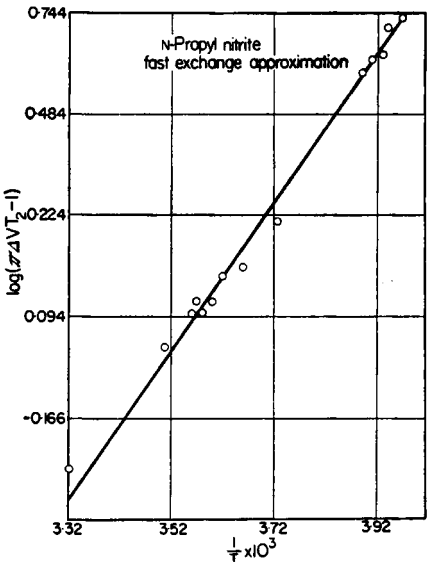

FIG. 4. Typical plot of line width parameter *vs.* temperature used to determine potential energy barrier to rotation.

CONCLUSIONS

It is obvious that the NMR technique for studying rapid reactions has great potential in elucidating information about reactions previously beyond the limitations of standard techniques.

Its ability to study both intra- and intermolecular kinetic phenomena in a chemical system makes the technique potentially one of the most important kinetic tools available to the chemist. The method as yet has not reached its limits of applicability in the field of chemical kinetics.

REFERENCES

1. H. S. GUTOWSKY, A. SAIKA, *J. Chem. Phys.* **21**, 1688 (1953).
2. F. BLOCH, *Phys. Rev.* **70**, 460 (1946).
3. H. M. MCCONNELL, *J. Chem. Phys.* **28**, 430 (1958).
4. H. S. GUTOWSKY and C. H. HOLM, *J. Chem. Phys.* **25**, 1228 (1956).
5. E. A. GRUNWALD, A. LOWENSTEIN and S. MEIBOOM, *J. Chem. Phys.* **27**, 630 (1957).
6. L. H. PIETTE and W. A. ANDERSON, *J. Chem. Phys.* **30**, 899 (1959).

10

ANALYSIS OF HIGH RESOLUTION NMR SPECTRA

WESTON A. ANDERSON
Varian Associates, Palo Alto, California

INTRODUCTION

THE problem of analysis of a high resolution NMR spectrum may be considered as separable into two parts. First, one may analyze a spectrum in terms of the possible molecular configurations, the various chemical shifts, and spin-coupling constants. Secondly, one may try to correlate these constants with other molecular properties of interest. Only the first part of this twofold problem will be considered here.

In all except the simplest cases the inverse problem is much easier to solve, i.e. to calculate the spectrum for a given molecular configuration from a given set of spin-coupling parameters and chemical shifts. However, by matching the observed spectrum with a series of theoretical spectra in which one or more parameters are varied, one may deduce the desired parameters.

If the spin-coupling parameters are small compared to the corresponding chemical shifts, then perturbation theory may be used and the interpretation of spectra is greatly simplified.

METHOD OF ANALYSIS

As a starting point for a theoretical analysis, we must choose a suitable Hamiltonian representing the total energy of the nuclear spin system placed in an external magnetic field, $\mathbf{H}_0$. This Hamiltonian may be written

$$\mathscr{H} = -\hbar\{\sum_i \gamma_i(\mathbf{H}_0+\mathbf{h}_i)\cdot\mathbf{I}_i + \sum_{i<j} J_{ij}\mathbf{I}_i\cdot\mathbf{I}_j\} \tag{1}$$

where $\mathbf{I}_i$ is the vector spin operator of nucleus i, γ_i is its gyromagnetic ratio, $\mathbf{h}_i$ is its chemical shift, and J_{ij} is the spin coupling constant between nucleus i and nucleus j. It is convenient to choose a coordinate frame with the z-axis along the direction of $\mathbf{H}_0$. The chemical shift will also be along this axis and equation (1) then may be written

$$\mathscr{H} = -\hbar\sum_i \{\omega_i I_i^0 + \tfrac{1}{2}\sum_{j\neq i} J_{ij}(I_i^0 I_j^0 + I_i^+ I_j^-)\} \tag{2}$$

where

$$\omega_i = \gamma_i(H_0+h_i), \qquad I_i^0 = I_{zi}, \text{ and } I_i^{\pm} = I_{xi} \pm \sqrt{(-1)}I_{yi}$$

The Schrodinger equation giving the stationary energy levels of this Hamiltonian is simply

$$\mathscr{H}\psi_k = E_k\psi_k \tag{3}$$

The wavefunctions, ψ_k, are the correct functions which are not initially known. One may choose a complete orthogonal set of initial wavefunctions, u_m, and then the correct wavefunctions, ψ_k, will be linear combinations of these functions.[1] Thus

$$\psi_k = \sum_m u_m a_{mk} \tag{4}$$

Normalization of the ψ_k requires

$$\sum_m a^*_{mk} a_{mk} = 1 \tag{5}$$

Substituting (4) and (3) and multiplying both sides of the equation by u_n^* and sum (or integrate) one obtains

$$\sum_m (\mathscr{H}_{nm} - E_k\delta_{nm})a_{mk} = 0 \tag{6}$$

where the matrix element $\mathscr{H}_{nm}$ is given by the sum

$$\mathscr{H}_{nm} = \sum_x u_n^*(x)\mathscr{H}x_m(x) \tag{7}$$

and

$$\delta_{nm} = \sum_x u_n^*(x)u_m(x) = \begin{cases} 1 \text{ for } n = m \\ 0 \text{ for } n \neq m \end{cases} \tag{8}$$

Here x is a discreet spin variable which is somewhat analogous to the distance x of physical space. In physical space, however, x is continuous and one performs an integration over this variable. The form of these matrix elements will become clear when the initial wavefunctions are considered more explicitly.

Equation (6) may be regarded as a set of linear homogeneous equations for the transformation coefficients a_{mk}. The necessary and sufficient condition that these equations have a solution is that the determinant of the coefficients of a_{mk} vanish, i.e.

$$\begin{vmatrix} \mathscr{H}_{11}-E & \mathscr{H}_{12} & \cdots & \mathscr{H}_{1N} \\ \mathscr{H}_{21} & \mathscr{H}_{22}-E & \cdots & \mathscr{H}_{2N} \\ \vdots & \vdots & & \vdots \\ \mathscr{H}_{N1} & \mathscr{H}_{N2} & \cdots & \mathscr{H}_{NN}-E \end{vmatrix} = 0 \tag{9}$$

This algebraic equation is called the secular equation. It is an equation of degree N in the energy and its solution yields the N stationary energy levels (called energy eigenvalues).

Once the energy levels are determined from equation (9), they may be substituted into equation (6) which, with the help of equation (5), will determine the transformation coefficients a_{mk} and thus the correct wavefunctions ψ_k.

It is desirable to choose initial wavefunctions, u_m, which will factor (9) to the greatest extent. Of course, if one could choose the correct wavefunctions, ψ_m, then (9) would be completely factored and would have the form

$$\begin{vmatrix} \mathscr{H}_{11}-E & 0 & \dots & 0 \\ 0 & \mathscr{H}_{22}-E & & \\ \vdots & & & \\ 0 & 0 & & \mathscr{H}_{NN}-E \end{vmatrix} = 0 \tag{10}$$

and the energy eigenvalues would be just $\mathscr{H}_{11}, \mathscr{H}_{22}, \dots \mathscr{H}_{NN}$. Although generally one cannot choose initial wavefunctions which completely factor (9), usually one can find initial wavefunctions which will partially factor (9). Group theoretical arguments are sometimes used to determine suitable initial wavefunctions.[2] Even though this is a powerful method, we shall not have time to go into the details here. Nevertheless we shall be able to use some of the results of group theory.

The simplest initial wavefunctions which one can use are those which diagonalize $(\mathbf{I})^2$ and I_i^0 with the eigenvalues $I_i(I_i+1)$ and m_i respectively. Since the matrix elements of I_i^+ and I_i^- have already been worked out,[3] we can write down all of the matrix elements of the Hamiltonian (2). Using the Dirac notation $(i|H|j) = \mathscr{H}_{ij}$ the diagonal elements are

$$(I_i, \dots m_i, m_j \dots |\mathscr{H}|I_i, \dots m_i, m_j \dots) = -\hbar \sum_i (\omega_i m_i + \sum_{j<i} J_{ij} m_i m_j) \tag{11}$$

and the off-diagonal elements are

$$\begin{aligned} &(I_i \dots m_i, m_j, \dots |\mathscr{H}|I_i \dots m_i-1, m_j+1, \dots) \\ &\quad = -\tfrac{1}{2}\hbar J_{ij}[(I_i-m_i+1)(I_i+m_i)(I_j-m_j)(I_j+m_j+1)]^{\frac{1}{2}} \end{aligned} \tag{12}$$

with all other matrix elements of $\mathscr{H}$ equal to zero. Since according to (12) there exists non-vanishing matrix elements only between states for which one of the quantum numbers m_i differs by ± 1 while another quantum number m_j differs by ∓ 1, it is seen that the secular equation (9) is factored into parts which have the same value of $m = \Sigma_i m_i$.

The perturbing Hamiltonian $\mathscr{H}'$ due to the radio frequency field $2H_1 \cos \omega t$ in the x-direction may be expressed as

$$\mathscr{H}' = -\hbar\gamma H_1 \cos \omega t \sum_i (I_i^+ + I_i^-) \tag{13}$$

Resonance occurs when the frequency ω of the radio-frequency field satisfies the condition $\pm\omega = (E_i - E_j)/\hbar$. Under the conditions of low radio-frequency

power and well resolved lines, it has been shown[4] that the integrated intensity of each resonance line is proportional to the absolute square of the corresponding matrix element of $\Sigma_i I_i^+$, or $\Sigma_i I_i^-$. The calculation of the maximum height poses a far more difficult problem insofar as it involves a knowledge of the line widths. However, to the extent to which one may assume the widths of the different resonance lines in a spectrum to be equal, one is allowed to use the expression for their integrated intensity also as a measure for the maximum line height.

DEFINITIONS AND SIMPLIFICATIONS

Further factoring of the secular equation is possible with certain conditions and approximations. Some definitions will be made in order to express these conditions mathematically.

(1) *Chemical Groups*

All nuclei with the same chemical shift belong to the same chemical group.

(a) *Magnetic equivalence*: The nuclei within a chemical group are said to be magnetically equivalent if each nucleus in the group has the same spin coupling constant to any given nucleus outside of the group. The protons of a methyl group represent a common example of equivalent nuclei.

(b) *Magnetic non-equivalence*: Nuclei with the same chemical shift which fail to satisfy the above definition of magnetic equivalence are said to be magnetically non-equivalent. An example of a molecule of this type is 1,1-difluoroethylene. Here the protons are chemically equivalent, i.e. they have the same chemical shift; however, since each proton has different spin coupling to a given fluorine atom, the protons are magnetically non-equivalent.

If the nuclei of a chemical group are magnetically equivalent then the square of the total angular momentum of that group is a good quantum number,[5] i.e. the secular determinant is factored into parts each with a different total angular momentum for that group. In this case any spin couplings between the nuclei of the group will not affect either the transition frequencies or the line intensities, and thus these couplings may be omitted from the Hamiltonian.

The total spin vector of a magnetically equivalent group $\mathbf{F}_R$ contains the spin operators $\mathbf{I}_r$ in the form

$$\mathbf{F}_R = \sum_r \mathbf{I}_r$$

where the sum is taken over all the nuclei in group R. The magnitude of $\mathbf{F}_R$ can assume all non-negative values $N_R I_r$, $N_R I_r - 1$, $N_R I_r - 2$, ... where N_R is the number of nuclei in group R and I_r is the common magnitude of their

spin. A given value of F_R may occur more than once, i.e. there is a statistical weight associated with each value of F_R. In the case of magnetically equivalent nuclei of spin $\frac{1}{2}$, F_R can assume the values $F_R = \frac{1}{2}N_R - n$ where n is an integer satisfying the condition $0 \leqq n \leqq \frac{1}{2}N_R$. The corresponding statistical weight is given by[6]

$$S_n = \left[\binom{N}{n} - \binom{N}{n-1}\right] \Big/ \binom{N}{n_{\max}} \tag{14}$$

where $\binom{N}{n}$ are the usual binomial coefficients. For example, the protons of a methyl group form a state of total spin $F_R = \frac{3}{2}$ with a statistical weight $\frac{1}{3}$ and also a state of total spin $F_R = \frac{1}{2}$ with a corresponding statistical weight of $\frac{2}{3}$.

A graphical method[7] for the determination of statistical weight factors for a group of n magnetically equivalent nuclei of spin $\frac{1}{2}$ to form states with total spin F_n is sketched below

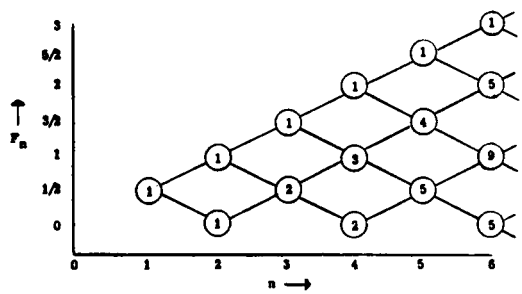

For example, in propane one has 6 protons in one group (A) and 2 in another group (B), so one could form the states with statistical weights as indicated below.

F_A	F_B	Statistical Weight	Remarks
3	1	1	
2	1	5	Part of A_4B_2 solution
1	1	9	Part of A_2B_2 solution
0	1	5	Trivial case—single line
3	0	1	Trivial case—single line
2	0	5	Trivial case—single line
1	0	9	Trivial case—single line
0	0	5	Trivial case—no lines

If all chemical groups contain only magnetically equivalent nuclei then the Hamiltonian may be written with the spin-coupling between magnetically equivalent nuclei omitted:

$$\mathscr{H} = -\hbar \sum_{R} \{\omega_R F_R{}^0 + \tfrac{1}{2} \sum_{S \neq R} J_{RS}(F_R{}^0 F_S{}^0 + F_R{}^+ F_S{}^-)\} \tag{15}$$

This Hamiltonian may then be solved as outlined above using the matrix elements (11) and (12) with I_i replaced by F_R. One must now let each F_R take on all possible values and weight the intensities with the statistical weight for each F_R.

A molecule with chemically equivalent but magnetically non-equivalent nuclei usually has some molecular symmetry. If this is the case, one may symmetrize the total spin wavefunctions and thereby factor the secular equation.[8]

The simplest and possibly the most common type of molecular symmetry is a reflection plane. In this case the proper wavefunctions are either symmetric or antisymmetric upon reflection. Let $u_k(A)$ describe one spin configuration of the nuclei on one side of the plane, $u_k(B)$ will then describe a similar spin configuration of the nuclei on the other side of the plane, and the totally symmetric spin functions will have the form

$$u_k(A)u_k(B), \qquad (u_k(A)u_m(B) + u_m(A)u_k(B))/\sqrt{2}$$

while the antisymmetric spin functions will be

$$(u_k(A)u_m(B) - u_m(A)u_k(B))/\sqrt{2}.$$

Using these wavefunctions, one may then calculate the matrix elements and find the solution as outlined above.

(2) *Basic Group*

A basic group is defined such that all spin-couplings between nuclei belong-ng to different basic groups shall be small compared to their corresponding chemical shifts.[9] This may be expressed mathematically by the inequality

$$\left| \frac{J_{ij}}{\omega_i - \omega_j} \right| \ll 1 \tag{16}$$

where all nuclei i belong to one basic group and nuclei j to another basic group. The simplest example of nuclei in different basic groups is found in a fluorohydrocarbon, which should be divided into at least two basic groups, one containing the protons and the other containing the fluorine atoms. Perturbation theory may be used to advantage when one deals with interactions between nuclei belonging to different basic groups.

PERTURBATION THEORY

Consider the case in which each basic group contains only magnetically equivalent nuclei. The unperturbed Hamiltonian is that of an arbitrary number of uncoupled basic groups.

$$\mathscr{H}^{(0)} = -\hbar \sum_R \omega_R F_R{}^0 \tag{17}$$

with a total energy of

$$E^{(0)}(m_A, m_B, \ldots) = -\hbar \sum_R \omega_R m_R \tag{18}$$

We assume the spin-coupling

$$\mathscr{H}^{(1)} = -\tfrac{1}{2}\hbar \sum_R \sum_{S \neq R} J_{RS}(F_R{}^0 F_S{}^0 + F_R{}^+ F_S{}^-) \tag{19}$$

is a small perturbation. The first order correction to the energy levels is the diagonal matrix elements of the perturbation

$$E^{(1)}(m_A m_B \ldots) = -\tfrac{1}{2}\hbar \sum_R \sum_{S \neq R} J_{RS} m_R m_S \tag{20}$$

The second-order perturbation correction to the energy is

$$E^{(2)}(i) = \sum_{j \neq i} \frac{(i|\mathscr{H}^{(1)}|j)(j|\mathscr{H}^{(1)}|i)}{E^{(0)}(i) - E^{(0)}(j)} \tag{21}$$

where the indices i, j, refer to all of the quantum numbers $F_A, F_B, \ldots, m_A, m_B, \ldots$, of the unperturbed system. The nondiagonal matrix elements $(i|\mathscr{H}^{(1)}|j)$ are identical with those of the total Hamiltonian (15) and are given by (12). Upon substituting the values for the matrix elements, one obtains after simplifying

$$\begin{aligned} E^{(2)}(m_A, m_B \ldots) = -\frac{\hbar}{4} \sum_R \sum_{S \neq R} \frac{(J_{RS})^2}{\omega_R - \omega_S} \\ \times [m_R(F_S{}^2 + F_S - m_S{}^2) - m_S(F_R{}^2 + F_R - m_R{}^2)] \end{aligned} \tag{22}$$

Including second-order terms[10] the frequency of a transition between a state with energy $E(m_A, m_B, \ldots)$ and another with energy $E(m_A - 1, m_B, \ldots)$ is

$$\begin{aligned} \omega = \omega_A + \sum_{R \neq A} J_{AR} m_R + \sum_{R \neq A} \frac{(J_{AR})^2}{2(\omega_A - \omega_R)} \times \\ \times [F_R(F_R + 1) - m_R(m_R + 1) + 2 m_A m_R] \end{aligned} \tag{23}$$

The first-order perturbation wavefunctions ψ_i are given by

$$\psi_i = u_i + \sum_{j \neq i} \frac{u_j (j|\mathscr{H}^{(1)}|i)}{E^{(0)}(i) - E^{(0)}(j)} \tag{24}$$

following the same reasoning outlined above, we assume that the line intensity is proportional to the square of the matrix elements of $F^+ = \Sigma_R F_R{}^+$. Using the first-order wavefunctions above and keeping only terms to first-order when expanding the square, one finds that the line intensity for a transition between a state with energy $E(m_A, m_B, \ldots)$ and one with energy $E(m_A-1, m_B, \ldots)$ is proportional to

$$(F_A-m_A+1)(F_A+m_A)\left\{1-\sum_{R\neq A}\frac{2J_{AR}m_R}{\omega_A-\omega_R}\right\} \tag{25}$$

It is interesting to note that the first-order intensity corrections enhance those lines of a multiplet which lie closest to the group which causes the splitting.

EXACT SOLUTIONS

To illustrate the method of finding a general solution, we shall show all the steps in the calculation of the energy levels and the line intensities for the case of two chemically non-equivalent nuclei of spin $\frac{1}{2}$. ($N_A = 1$, $N_B = 1$) The spin functions shall be labeled by the notation: $u_i = (m_A m_B)$, $u_1 = (\frac{1}{2}\,\frac{1}{2})$, $u_2 = (\frac{1}{2}-\frac{1}{2})$, $u_3 = (-\frac{1}{2}\,\frac{1}{2})$, $u_4 = (-\frac{1}{2}-\frac{1}{2})$. The non-vanishing matrix elements in this case are

$$\begin{aligned}
H_{11} &= -\tfrac{1}{2}\hbar\{\omega_A+\omega_B+\tfrac{1}{2}J\}\\
H_{22} &= -\tfrac{1}{2}\hbar\{\omega_A-\omega_B-\tfrac{1}{2}J\}\\
H_{33} &= +\tfrac{1}{2}\hbar\{\omega_A-\omega_B+\tfrac{1}{2}J\}\\
H_{23} &= H_{32} = -\tfrac{1}{2}J\hbar\\
H_{44} &= +\tfrac{1}{2}\hbar\{\omega_A+\omega_B-\tfrac{1}{2}J\}
\end{aligned}$$

The secular equation (9) factors into two 1×1 matrices and one 2×2 yielding the energy values:

$$\begin{aligned}
E_1 &= -\tfrac{1}{2}\hbar\{\omega_A+\omega_B+\tfrac{1}{2}J\}\\
E_2 &= -\tfrac{1}{2}\hbar\{(\delta^2+J^2)^{\frac{1}{2}}-\tfrac{1}{2}J\}\\
E_3 &= +\tfrac{1}{2}\hbar\{(\delta^2+J^2)^{\frac{1}{2}}+\tfrac{1}{2}J\}\\
E_4 &= +\tfrac{1}{2}\hbar\{\omega_A+\omega_B-\tfrac{1}{2}J\}
\end{aligned}$$

with $\delta = \omega_A-\omega_B$.

The system of linear equations (6) for coefficients a_{jk} is:

$$\begin{aligned}
(H_{11}-E_k)a_{1k} &= 0\\
(H_{22}-E_k)a_{2k}-H_{23}a_{3k} &= 0\\
(H_{33}-E_k)a_{3k}-H_{32}a_{2k} &= 0\\
(H_{44}-E_k)a_{4k} &= 0
\end{aligned}$$

and has the following solution

$$a_{11} \neq 0$$
$$a_{23} = -Qa_{33} \qquad a_{33} \neq 0$$
$$a_{32} = Qa_{22} \qquad a_{22} \neq 0$$
$$a_{44} \neq 0$$

with all other $a_{jk} = 0$ and $Q = J/[\delta + (\delta^2 + J^2)^{\frac{1}{2}}]$

The correct normalized wavefunctions may be written down immediately

$$\psi_1 = u_1$$
$$\psi_2 = (u_2 + Qu_3)/(1 + Q^2)^{\frac{1}{2}}$$
$$\psi_3 = (u_3 - Qu_2)/(1 + Q^2)^{\frac{1}{2}}$$
$$\psi_4 = u_4$$

The relative line intensities L_{ij} are found by taking the square of the matrix elements of $I_A{}^+ + I_B{}^+$ using the correct wavefunctions ψ_i with the result

$$L_{24} = L_{12} = (1 + Q)^2/(1 + Q^2)$$
$$L_{34} = L_{13} = (1 - Q)^2/(1 + Q^2)$$

The results of this calculation are plotted in Fig. 1.

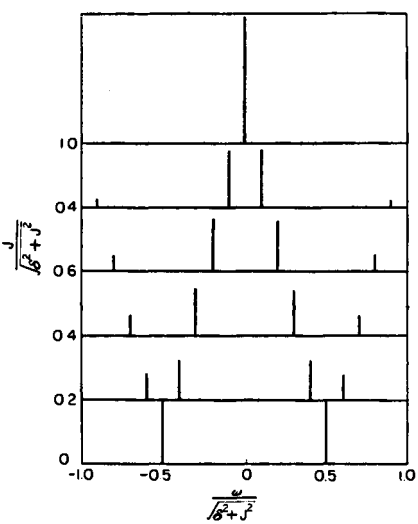

FIG. 1. Theoretical spectra for two non-equivalent nuclei of spin $\frac{1}{2}$.

As the number of nuclei increase, the complexity of the solution increases correspondingly. For just two chemical groups with magnetically equivalent

nuclei of spin $\frac{1}{2}$ in each group, one must solve nth degree equations where there are $n-1$ nuclei in the smaller group.

Here just two parameters, the chemical shift δ and the spin-coupling J, define the solution. By plotting transition frequencies and line intensities vs. the ratio $C = J/\sqrt{(J^2+\delta^2)}$ one can obtain curves which, aside from a scale factor, represent the particular spectrum over the whole range of possible parameters.

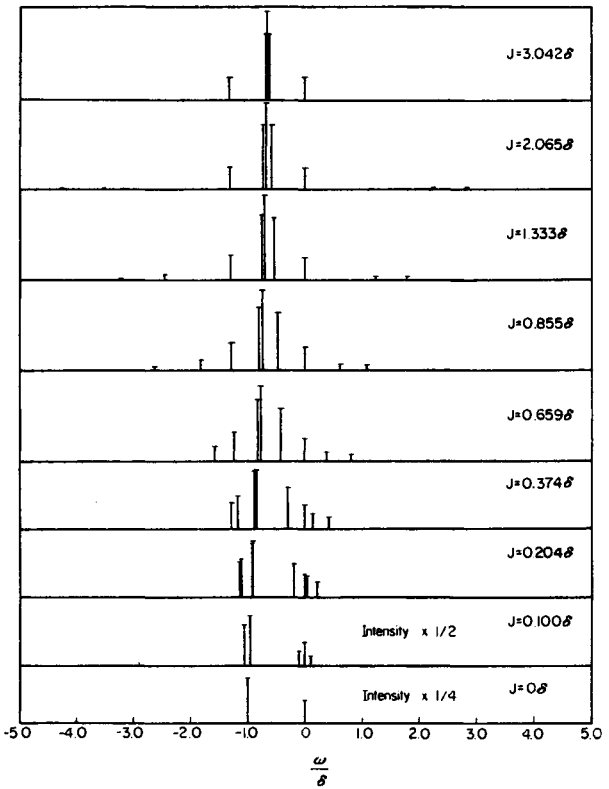

FIG. 2. AB_2 Theoretical spectra.

Such data have been run on the IBM 704 computer at the Radiation Laboratory of the University of California, Livermore, under the direction of Dr. Frank Abell. Results for the AB_2 and A_2B_2 are shown here in Figs. 2 through 5. The notation AB_2 is used to denote that one nucleus in group A interacts with two nuclei in group B, where each nucleus has a total spin of $\frac{1}{2}$. In order to keep all transition frequencies, w, on the graph, the frequencies have been normalized so that the quantity $\omega/\sqrt{(J^2+\delta^2)}$ is plotted vs. $C = J/\sqrt{(J^2+\delta^2)}$. These are dimensionless parameters—thus the units of ω, J, and δ are arbitrary but must be identical.

When more than two chemical groups are involved or when one or more of the groups contain magnetically non-equivalent nuclei, the problem of the presentation of the data becomes difficult because of the large number of parameters involved. For example, a system of three-coupled protons is described by two chemical shifts and three spin-coupling constants. One may eliminate one of the parameters as a scale factor when plotting the results;

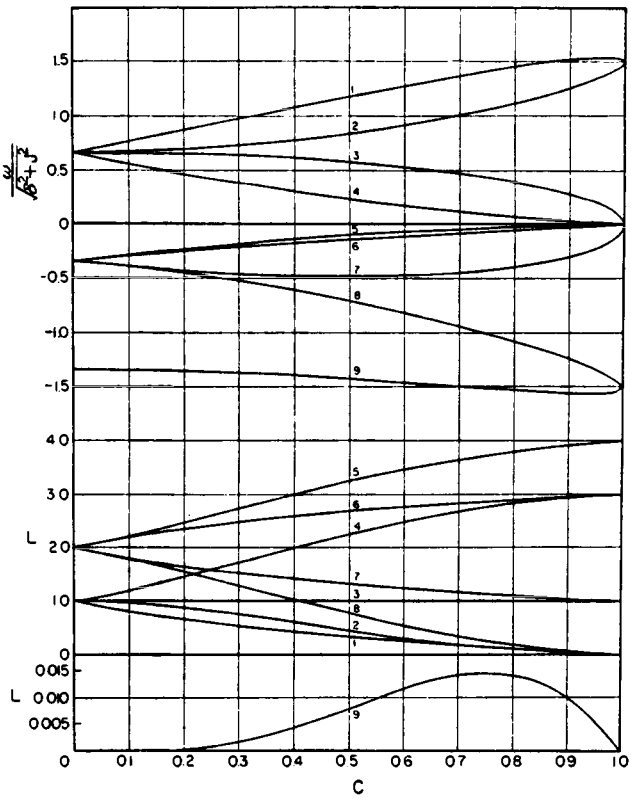

FIG. 3. AB_2 Theoretical spectra.

however, this leaves four independent parameters to be varied in a general solution. The best procedure here is to pick reasonable values and solve the problem only over a very limited range of some of the parameters. From an experimental spectrum often one can obtain a good idea of the approximate value of some of the parameters, leaving fewer to be varied. Here the results of perturbation theory often give good initial parameters for an exact solution. Measurement of the moments[9] of the spectrum can yield values of some of the parameters or give relationships between them leaving fewer to be varied.

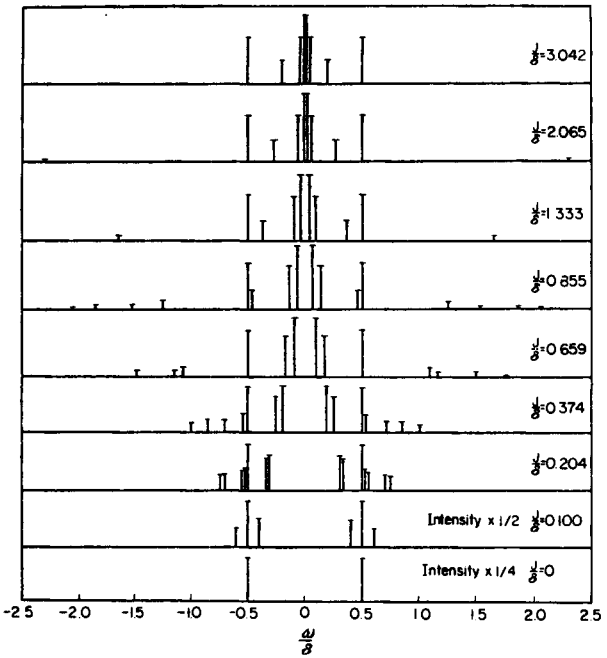

FIG. 4. A_2B_2 Theoretical spectra.

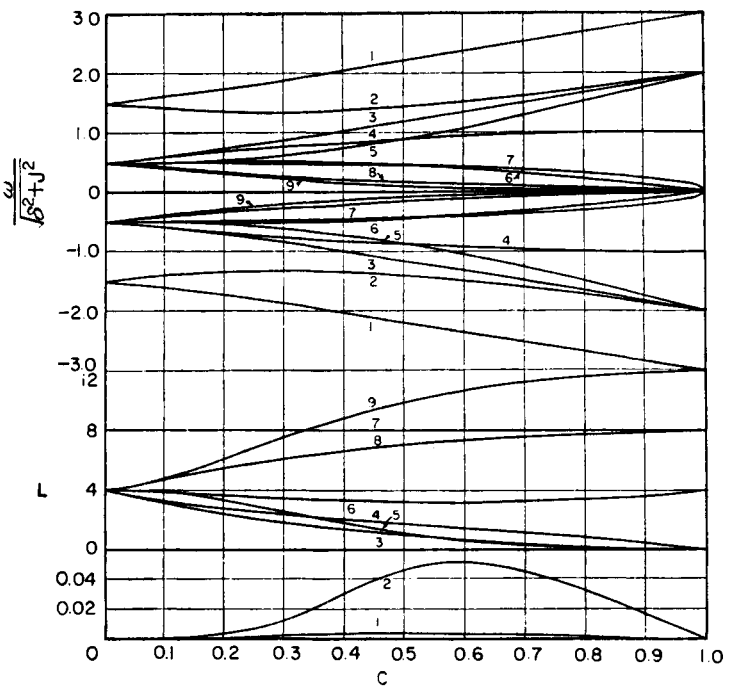

FIG. 5. A_2B_2 Theoretical spectra.

REFERENCES

1. For matrix formulation of Quantum Mechanics see L. I. SCHIFF, *Quantum Mechanics* 1st ed. McGraw-Hill Book Company, Inc., 1949. pp. 127–130.
2. H. M. MCCONNELL, A. D. MCLEAN and C. A. REILLY, *J. Chem. Phys.* **23**, 1152 (1955). BRIGHT WILSON, *J. Chem. Phys.* **27**, 60 (1957).
3. Schiff ibid P142–144.
   E. FEENBERG, G. E. PAKE, *Notes on the Quantum Theory of Angular Momentum*, Addison-Wesley Publishing Company Inc., 1953, pp. 19–25.
   ERING, WALTER and KIMBLE, *Quantum Chemistry*, John Wiley and Sons, Inc., 1954, p. 138.
4. F. BLOCH, *Phys. Rev.* **102**, 104 (1956). (See Eq. 5.10.)
5. E. L. HAHN and D. E. MAXWELL, *Phys. Rev.* **88**, 1070 (1952).
   H. S. GUTOWSKY, D. W. MCCALL and C. P. SLICHTER, *J. Chem. Phys.* **21**, 279 (1953).
6. Wigner, *Gruppentheorie und ihre Anwendung auf die Quanten mechanik der Atomspectren* Chapter 13, J. W. Edwards (1944).
7. E. M. CORSON, *Perturbation Methods in the Quantum Mechanics of* n-*Electron Systems*, Blackie & Son Ltd., London, 1951, p. 189.
8. WIGNER, ibid, Chapters 11 and 12.
9. W. ANDERSON and H. M. MCCONNELL, *J. Chem. Phys.* **26**, 1496 (1957).
10. For third-order correction terms see W. A. ANDERSON, *Phys. Rev.* **102**, 151 (1956).

11

MEASUREMENT OF RADIO-FREQUENCY FIELD H_1

WESTON A. ANDERSON
Varian Associates, Palo Alto, California

MAGNETIC resonance is a standard method of measuring magnetic field in the laboratory. It may also be used to measure the radio-frequency field $2H_1 \cos \omega t$ in the probe.[1] To understand the method it is convenient to consider the spin system in a coordinate frame rotating with the angular frequency of ω_0, the frequency of the strong r.f. field which is to be measured. The component of the r.f. field rotating in the direction opposite to the precessing spins causes negligible effects and may be omitted.[2] When one makes this transformation to the rotating coordinate frame, one finds a static field H_{eff} which is the resultant vector sum $H_0 - \omega/\gamma$ along the Z'-axis and H_1 along the X'-axis of the rotating frame as sketched in Fig. 1.

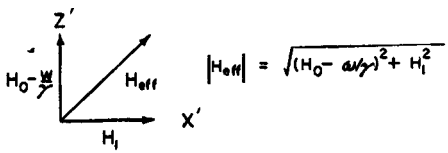

FIG. 1. The effective magnetic fields in a coordinate system rotating at the frequency of the r.f. field.

One may now do a nuclear resonance experiment in the rotating frame. The resonance frequency (Larmor frequency), ω', in this frame is given by

$$\omega' = \gamma H_{eff} = \sqrt{[(\gamma H_0 - \omega)^2 + \gamma^2 H_1^2]}$$

One must make sure that the field used to stimulate this resonance is weak enough so that it will not appreciably perturb the system (far below saturation).

One way to achieve effectively the weak "r.f." field is through modulation of the magnetic field. In this case, a resonance is achieved when the audio modulation frequency ω_m satisfies the resonance condition

$$\omega_m^2 = (\gamma H_0 - \omega)^2 + \gamma^2 H_1^2$$

As long as $\omega_m > \gamma H_1$, this equation will be satisfied at two different values of H_0. To measure H_1 one need only measure the distance d between these signals, keeping the sweep rate fixed, as function of ω_m. The plot of d^2 vs. $\omega_m{}^2$ should yield a straight line with an intercept at $(\gamma H_1)^2$ as sketched in Fig. 2.

These sideband signals are present in the output of the r.f. detector, however, they are small and sitting on the sloping wings of the main resonance peak. If, however, an audio lock-in amplifier is used, one can effectively sup-

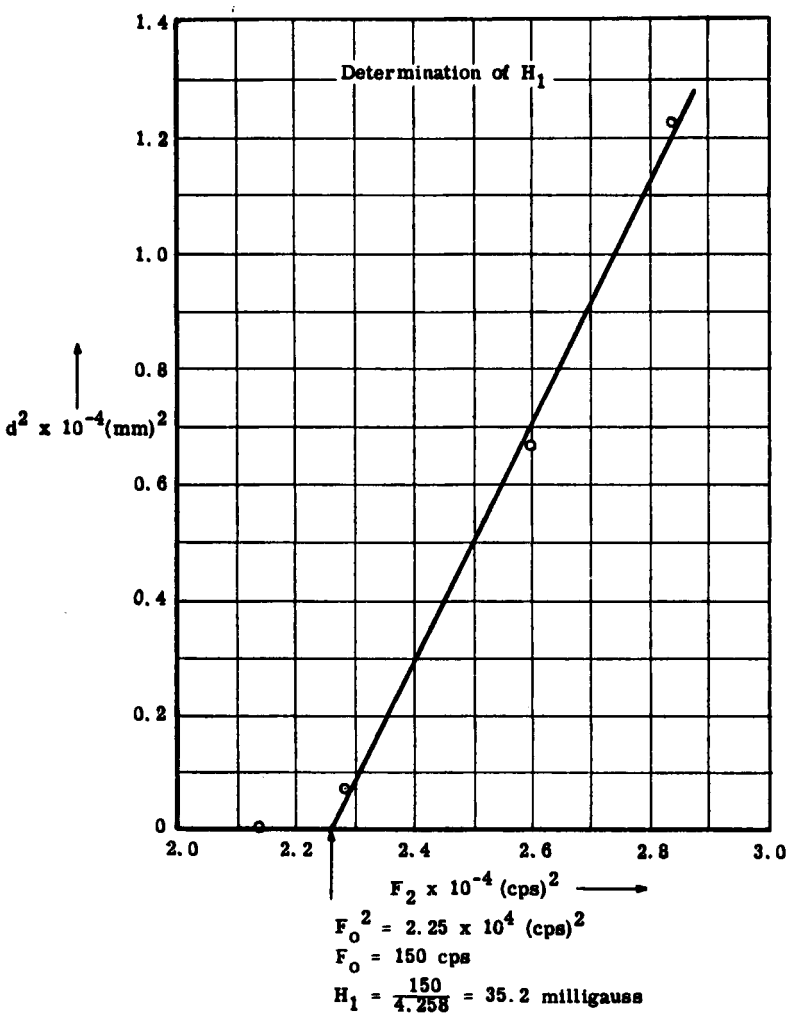

FIG. 2. Plot of square of distance between peaks vs. the square of the audio frequency. The extrapolated value of the best fit to a straight line is used to determine magnitude of the rotating r.f. field H_1.

press the main resonance peak and at the same time enhance the sideband peaks.

The amount of audio field modulation needed has been found so small that the Varian Model V-4250 Sweep Unit cannot be used. It has been found that adequate sweep voltage can be obtained directly from the output of the audio oscillator and in fact usually this voltage must also be attenuated since it may be necessary to run the audio oscillator at nearly full output to drive the audio "lock-in amplifier". A suitable way to attenuate this voltage has been found by placing a small capacitor in series with the sweep coils—about 0.002 μf has been found to be adequate.

When making measurements, it has been found convenient to adjust the r.f. detector to select the usual v-mode and the audio phase detector adjusted to be "in-phase" with the audio field. When these conditions are fulfilled, the sideband signals from the output of the "lock-in" will be in the absorption mode and one of the sideband signals will be inverted; the centerband frequency signal is absent or nearly absent.

The lock-in amplifier may be one similar to the circuit shown in Fig. 3 or the Varian lock-in model V-4270A may be used. If the V-4270A is used, the twin-T filter must be eliminated. This is done by switching S203 to "EXT.

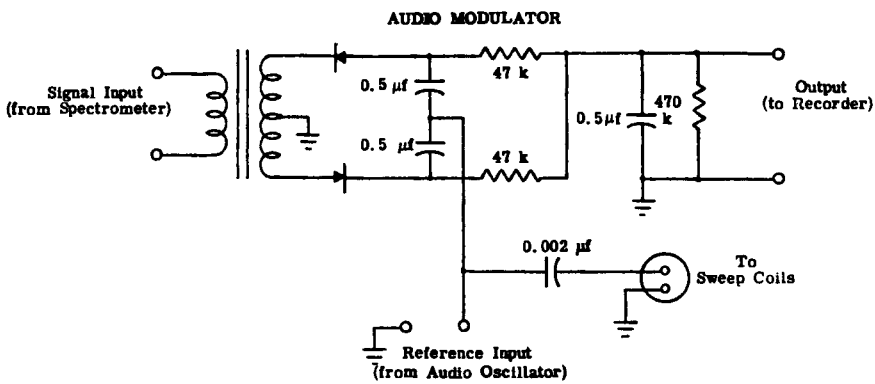

FIG. 3. An audio phase detector circuit.

FILTER" and shorting one of the pins of jack J704 to the chassis. The pin, which is to be shorted, may be determined experimentally. It is the pin which leads to the pin 7 (grid connection) of the 12AX7 tube. The recorder is also plugged into the output of this unit. An external audio oscillator is plugged into the V-4250A Sweep Unit and the sweep frequency is set to "EXT". The sweep coils of the probe are also connected to the external audio oscillator through a 0.002 μF capacitor.

The accuracy of this method of measuring H_1 depends primarily upon the linearity and reproducibility of the sweep rate. Of course, the accuracy also

depends upon the accuracy of the audio oscillator. In practice it has been found that one can measure fields of a few milligauss to an accuracy better than 5 per cent.

One can quickly obtain a rough check on the value of H_1 by adjusting the audio oscillator frequency until the sideband resonances disappear. The accuracy of this method is limited, however, because width of the sideband resonances increases as the ω_m approaches γH_1, becoming infinite when they are equal. A few recordings of the sideband signals at various audio oscillator frequencies are shown in Fig. 4.

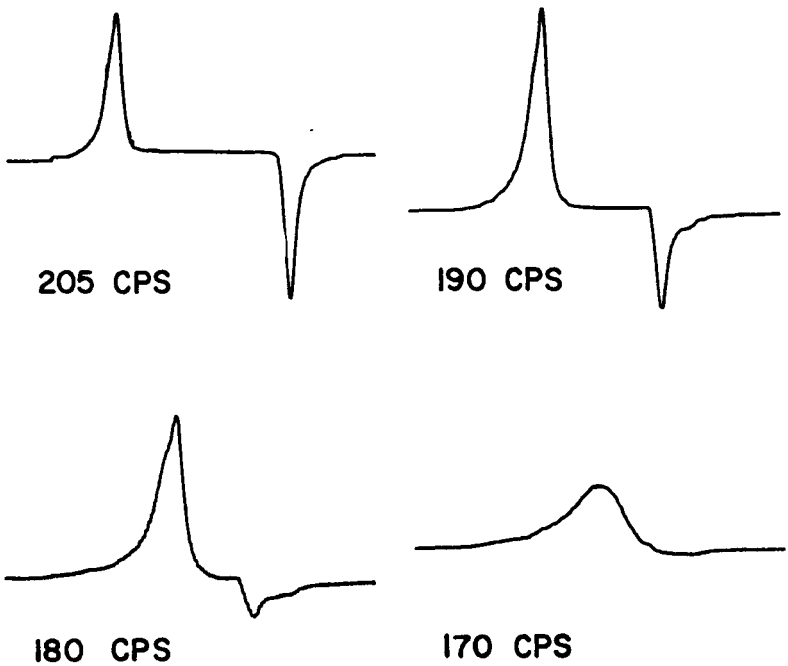

FIG. 4. Typical recordings of the side band signals from a Varian Model V-4270A audio phase detector. The r.f. unit was a Varian Model V-4311 with an attenuator setting of 10 db. A plot of this data yields a value of approximately 40 mg for the r.f. field strength in the probe.

By using a precession attenuator one need only measure H_1 at one attenuator setting. The values of H_1 for all other settings may then be readily computed. Table 1 gives the conversion factors for attenuators calibrated in decibels (db).

TABLE 1

db	Multiply H_1 by	db	Multiply H_1 by
0	1.000		
1	0.891	11	0.282
2	0.794	12	0.251
3	0.708	13	0.224
4	0.631	14	0.200
5	0.562	15	0.178
6	0.501	16	0.158
7	0.447	17	0.141
8	0.398	18	0.126
9	0.355	19	0.112
10	0.316	20	0.100

For each additional 20 dB, multiply H_1 by 0.10.

REFERENCES

1. W. ANDERSON, "Nuclear Magnetic Resonance Spectra of Some Hydrocarbons", *Phys. Rev.* **102**, 151 (1956).
2. F. BLOCH and A. SIEGERT, "Magnetic Resonance for Nonrotating Fields", *Phys. Rev.* **57**, 522 (1940).

12

MEASUREMENT OF RELAXATION TIMES

WESTON A. ANDERSON
Varian Associates, Palo Alto, California

1. INTRODUCTION

THE time constant T_1 is known as the "longitudinal", "thermal", or "spin lattice" relaxation time.[1] It is a measure of the rate at which the magnetization M_z of the nuclear spin system approaches its equilibrium value M_0.

The time constant T_2 is known as "transverse" or "spin–spin" relaxation time.[1] It is the characteristic time in which the individual precessing nuclei get out of phase with each other and thus it corresponds to the decay rate of the transverse components M_x and M_y of the magnetization. An irregularity in the applied magnetic field may also cause M_x and M_y to decay rapidly, however, this cause shall not be included in our definition of T_2, since then T_2 would not be a property of the sample material.

The phenomenological equations of Bloch[1] have been found to be valid for a wide range of sample materials. These equations may be written in the following form:

$$\frac{\mathrm{d}M_x}{\mathrm{d}t}-\gamma(M_yH_z-M_zH_y)+\frac{M_x}{T_2} = 0 \tag{1}$$

$$\frac{\mathrm{d}M_y}{\mathrm{d}t}-\gamma(M_zH_x-M_xH_z)+\frac{M_y}{T_2} = 0 \tag{2}$$

$$\frac{\mathrm{d}M_z}{\mathrm{d}t}-\gamma(M_xH_y-M_yH_x)+\frac{M_z-M_0}{T_1} = 0 \tag{3}$$

The oscillating radio-frequency field $2H_1 \cos \omega t$ along the X-axis is equivalent to two counter rotations fields each of magnitude H_1. Only the component rotating in the same sense as the nuclear precession is effective in producing resonances[2] and the other component shall be neglected. The equation becomes independent of time if a coordinate transformation is made to a coordinate frame which rotates with the effective rotating field. This transformation is

$$M_x = u \cos \omega t + v \sin \omega t \tag{4}$$

$$M_y = -u \sin \omega t + v \cos \omega t \tag{5}$$

where u is the x'-component and v the y'-component of the magnetization in the rotating coordinate system. The new set of equations referred to the rotating axes are

$$\frac{\mathrm{d}u}{\mathrm{d}t}+\frac{u}{T_2}-\Delta\omega v = 0 \tag{6}$$

$$\frac{\mathrm{d}v}{\mathrm{d}t}+\frac{v}{T_2}+\Delta\omega u-\gamma H_1 M_z = 0 \tag{7}$$

$$\frac{\mathrm{d}M_z}{\mathrm{d}t}+\frac{M_z-M_0}{T_1}+\gamma H_1 v = 0 \tag{8}$$

where $\Delta\omega = \gamma H_z-\omega$.

This is a set of linear equations which may be solved for the various experimental conditions. By the proper selection of the reference phase the signal from the r.f. detector of the spectrometer may be made to be proportional to either the quantity u or v.

2. MEASUREMENT OF SHORT RELAXATION TIMES

$$[1/T_2 \gg \gamma \times (\text{field inhomogeneity})]$$

If the time spent in passing through the resonance is long compared to T_1, then the steady state solution to the equations (6) to (8) are valid. This solution is easily found by equating all time derivatives to zero. Solving the resulting algebraic equation yields

$$v = \frac{\gamma H_1 T_2 M_0}{1+(\Delta\omega T_2)^2+(\gamma H_1)^2 T_1 T_2} \tag{9}$$

$$u = \frac{\gamma H_1 T_2^2 \Delta\omega M_0}{1+(\Delta\omega T_2)^2+(\gamma H_1)^2 T_1 T_2} \tag{10}$$

$$M_z = \frac{[1+(\Delta\omega T_2)^2]M_0}{1+(\Delta\omega T_2)^2+(\gamma H_1)^2 T_1 T_2} \tag{11}$$

Here we note that in a sufficiently uniform magnetic field, T_2 may be easily determined by measuring the width of the v-mode line under the condition of

$$(\gamma H_1)^2 T_1 T_2 \ll 1 \tag{12}$$

This condition may be insured by reducing the r.f. field by a factor of ten or more from the value which causes saturation (i.e. causes v to be a maximum). The error in the line width measurement will then be about 1 per cent. One may make sure that the magnetic field is sufficiently uniform by inserting a sample which has a line width much narrower than the width of the line to be measured.

The value of T_1 may be measured by determining the value of H_1 which produces the maximum v-mode signal at resonance.[3] This maximum occurs when $(\gamma H_1)^2 T_1 T_2 = 1$. Substituting for the value of T_2 as measured by the above method and H_1 as measured by the method described in another section, one may compute T_1.

3. MEASUREMENT OF INTERMEDIATE AND LONG RELAXATION TIMES

A number of methods have been used to measure thermal relaxation times. One of the simplest methods is to measure the signal height as a function of time after the sample has been placed in the strong magnetic field. The same result may be achieved saturating the line and observing the recovery time.[3] The measurement is made by periodically sweeping through the resonance with a sufficiently small r.f. field so that the polarization is not appreciably perturbed; i.e., the inequality (12) must be satisfied. The time actually spent on the resonance line should be a small part of the total sweep period so that the effects of the transverse relaxation time T_2 will not play an important role. Under these conditions the height of the v-mode signal will be proportional to the Z-component of magnetization M_z. To obtain the value of T_1 one may plot log $[(v(t = \infty) - v(t)]$ versus t to obtain the best fit to a straight line. The time for the signal to drop to $1/e = 0.368$ of its initial value corresponds to the thermal relaxation time T_1.

A variation of this method of measuring T_1 involves the reversal of the polarization by an adiabatic rapid passage.[4] Adiabatic rapid passage will be obtained if the following two inequalities are fulfilled:

$$\frac{1}{T_2} \ll \frac{1}{H_1}\left|\frac{\mathrm{d}H_0}{\mathrm{d}t}\right| \ll \gamma H_1$$

These conditions may always be obtained by making the sweep rate and H_1 sufficiently large.

If the relaxation time to be measured is a few seconds or longer, the following technique may be used. A repetitive sweep with a period P several times shorter than the relaxation time T_1 is used. The r.f. amplitude is initially adjusted to be as low as is consistent with an adequate signal-to-noise ratio. The gain is adjusted so that the signal just fills half the recorder or scope. The r.f. level is then increased during one sweep through resonance so that the adiabatic conditions apply, and the polarization is inverted. This polarization is then monitored periodically with the low r.f. field. Figure 1 shows a recording of signals from benzene using this technique. The value of the thermal relaxation time T_1 may be determined from a plot of the signals as described above. A quicker method which may be used if one is sure that the decay is exponential is to measure the time interval Δt from the

polarization inversion to the point where signal amplitude goes through zero. The relaxation time T_1 is given by $T_1 = \Delta t/\ln 2$.[5,6]

For thermal relaxation times shorter than about a second one does not have sufficient time to change the attenuator setting twice during the single sweep used to invert the polarization. Here one may choose a sweep period P greater than three times the expected relaxation time and adjust the r.f.

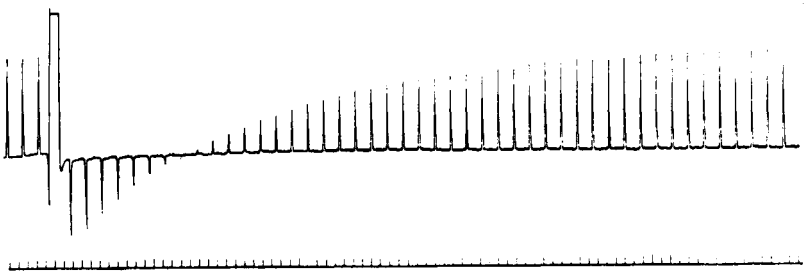

FIG. 1. v-mode signals from benzene. The polarization was inverted by an adiabatic rapid passage using an r.f. field of 4.4 milligauss. The polarization was monitored before and afterward the inversion with an r.f. field of 6.4 micro-gauss. The time markers occur at one sec. intervals.

field for the adiabatic rapid passage condition. The polarization is inverted by the adiabatic passage and then decays back toward M_0. The polarization is sampled at a later time Δt by the returning part of the sine wave or saw-tooth sweep. The time Δt may be adjusted by changing the magnetic field so that the signal vanishes on the return trace. By knowing the period P and this time interval Δt, the value of T_1 is determined by the equation

$$\frac{\Delta t}{P} = \frac{T_1}{P} \ln\left[\frac{2}{1+\exp(-P/T_1)}\right]$$

A plot of T_1/P versus $\Delta t/P$ has been given by Conger and Selwood.[5] Such a plot is reproduced in the Fig. 2.

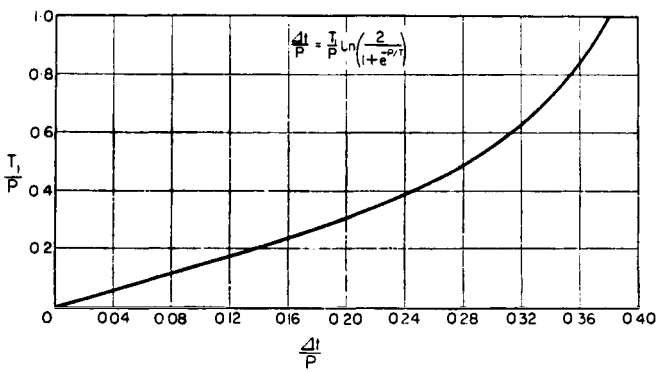

FIG. 2. A graph gives T_1/P vs. $\Delta t/P$.

If a saw-tooth sweep generator is used such as the Varian V-4325 Linear Sweep Unit, it may be necessary to slow down the return trace so that the signal produced during the return is not too small. This may be achieved by the circuit shown in Fig. 3.

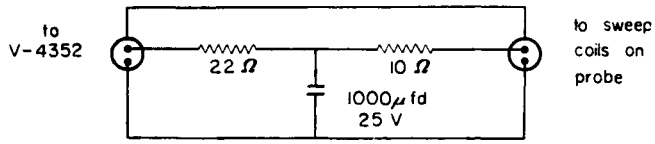

FIG. 3. A simple circuit used to effectively increase the fly-back time of a saw-tooth sweep.

A relatively simple method of measuring T_2 which is applicable even if the natural line width is obscured by magnetic field inhomogeneity has been described recently.[7] In this method one observes the decrease of the transverse polarization in the presence of r.f. field H_1. The decay of this transverse polarization is then a measure of T_2. A convenient method to align the polarization along the r.f. field H_1 is to do an adiabatic rapid passage into the center of the resonance and stop the sweep at this point.[8] In the rotating co-ordinate system the magnetization remains aligned with H_{eff} which at resonance is equal to H_1 and is directed along the X'-axis. In the rotating system the polarization now decays with a thermal time constant corresponding to an applied magnetic field H_1 in a way quite analogous to the growth or decay of the polarization in an external magnetic field of H_1. The time constant for this process thus corresponds to the time constant T_1 measured in a magnetic field of H_1. In most cases this is equivalent to the time constant T_2 as one might expect if all correlation times τ_c are short compared to $1/(\gamma H_1)$. Meiboom[9, 10] has found that neutral water is an interesting exception. Apparently here there is an additional relaxation mechanism which has a correlation time near a millisecond. By the technique described above he has been able to study processes involving these relatively long correlation times.

The prediction that this experiment yields the transverse relaxation time T_2 may be seen from equation (6). At resonance this equation reduces to

$$\frac{\mathrm{d}u}{\mathrm{d}t}+\frac{u}{T_2}=0$$

showing that u-mode signal should decay to zero with a time constant T_2.

A simple circuit to provide the "sweep" for this experiment is sketched in Fig. 4. Here one adjusts for a u-mode detection. With the switch off one adjusts the magnetic field to the resonance value (this is done easier with a weak r.f. field). The switch is then turned on and left there for several relaxation times. The switch is then again turned off and the field will then sweep

back to the resonance value producing a maximum u-mode signal which now decays with the time constant T_2.

The adiabatic rapid passage conditions must be fulfilled upon sweeping to the line center. In addition, the magnitude of the r.f. field H_1 must be large

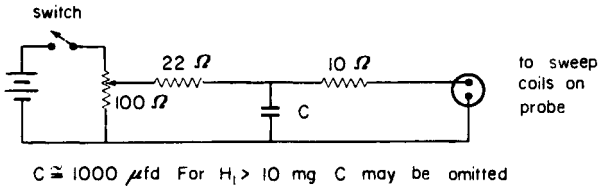

FIG. 4. Circuit used to provide a "sweep" that will stop at the center of resonance.

compared to the inhomogeneities of the applied magnetic field over the sample volume. Figure 5 shows signals from vacuum degassed water obtained by this method. The magnetic field has been adjusted to approximately the

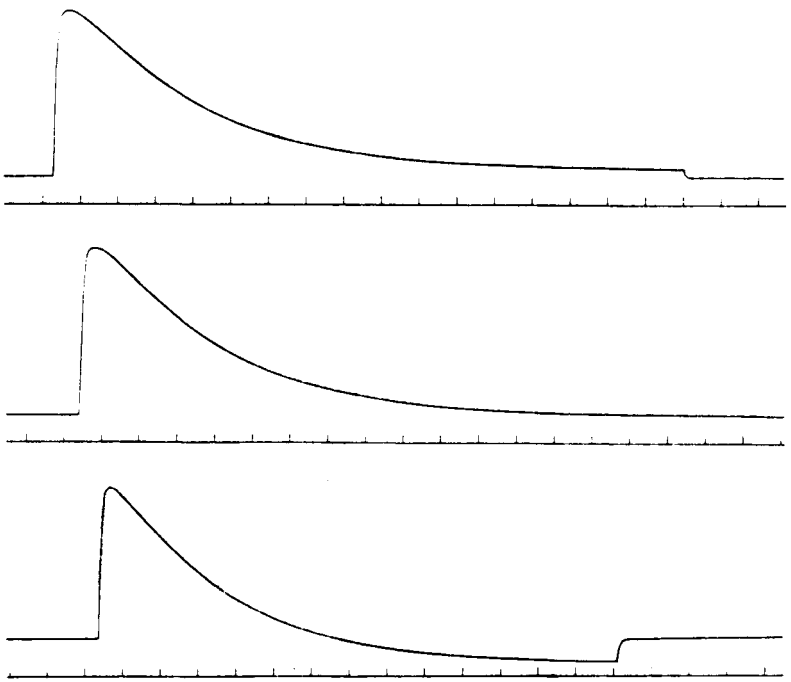

FIG. 5. An example of a recording used to determine the relaxation time T_2 of vacuum degassed water. In the upper trace the magnetic field was slightly below the resonance value; in the center trace it was properly adjusted to the resonance value, and in the lower trace the field was above the resonance value. The time intervals below the recordings are in seconds. The value of the r.f. field H_1 was about 13 milligauss.

resonance value and the bias field switched at the start of each trace. The bias field was then turned off and the curve immediately rises and then decays with the time constant T_2. Later the bias field was again switched on to determine if the field was properly adjusted to resonance. Proper adjustment will be obtained when no shift in baseline occurs as the bias field is switched on.

REFERENCES

1. F. Bloch, "Nuclear Induction", *Phys. Rev.* **70**, 460 (1946).
2. F. Bloch and A. Siegert, "Magnetic Resonance for Non-rotating Fields", *Phys. Rev.* **57**, 522 (1940).
3. Bloembergen, Purcell and Pound, "Relaxation Effects in Nuclear Magnetic Resonance Absorption", *Phys. Rev.* **73**, 679 (1948).
4. D. E. Drain, "A Direct Method of Measuring Spin Lattice Relaxation Times", *Phys. Soc. London* **62A**, 301 (1949).
5. R. L. Conger and P. W. Selwood, "Proton Relaxation in Paramagnetic Solutions", *J. Chem. Phys.* **20**, 383 (1952).
6. W. A. Anderson and J. T. Arnold, "Proton Relaxation Times in H_2O–D_2O Mixtures", *Phys. Rev.* **101**, 511 (1956).
7. Ionel Solomon, "Etude de la Relaxation en Résonance Magnétique par la Méthode de Precession Forcée Transitoire", *Compt rend.* 248, **92** (1959).
   G. Bonera, L. Chiodi, L. Giulotto and G. Lanzi, "l'Measures de T_2 dans les Liquides", *Archives des Sciences* **12**, p. 99 (1959).
   G. Bonera, L. Chiodi, L. Giulotto and G. Lanzi, "A Method for the Measurement of the Nuclear Transversal Relaxation Time, *Nuovo Cimento*, Vol, XIV No. 1, (1 Oct., 1959).
8. N. Bloembergen and P. P. Sorokin, "Nuclear Magnetic Resonance in the Cesium Halides", *Phys. Rev.* **110**, 867 (1958).
9. S. Meiboom, Z. Luz and D. Gill, "Proton Relaxation in Water", *J. Chem. Phys.* **27**, 1411 (1957).
10. S. Meiboom, Bell Telephone Laboratories, Private communication (1959).

13

ELECTRIC SHIMS

WESTON A. ANDERSON
Varian Associates, Palo Alto, California

1. THEORY

THE basic requirement of current shims is the control of magnetic field homogeneity using a suitable arrangement of electric currents.[1, 2] A second condition, almost as important, is that the shims be substantially orthogonal to each other so that the controls will be independent. Obviously it is desirable to have the fewest number of controls that are required to do an adequate job. With these requirements in mind, we shall investigate the types of control which fulfil these requirements. As a convenient starting place, we can expand the magnetic field in the magnet gap by scalar potential Φ which satisfies the Laplace Equation $\nabla^2\Phi = 0$. This expansion is valid in regions containing no electrical currents.

The field is then given by $\mathbf{H} = -\nabla\Phi$.

The center of the sample shall be chosen as the origin of our coordinates. Expanding the potential Φ about this origin leads to the well-known spherical harmonics

$$\Phi = \sum_{m=0}^{n} \sum_{m=0}^{n} r^n P_n^m(\cos\theta)[A_n^m \sin m\phi + B_n^m \cos m\phi]$$

In order to keep the common notation used in the NMR literature describing nuclear resonance experiments we must depart from the common labeling used in spherical coordinates. The strong magnetic field is applied along the Z-axis and the spinning axis is the Y-axis. The axes of the spherical coordinates system are sketched in Fig. 1.

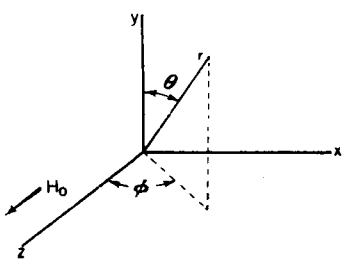

FIG. 1.

The advantage of expanding the potential in spherical harmonics is that it immediately yields the number of independent components in each order of a field derivative. A few examples may clarify this statement. The term with $n = 1$ represents the three components of the field.

$$H_y = -B_1^0, \qquad H_z = -B_1^1, \qquad H_x = -A_1^1$$

The term with $n = 2$ represents the linear field gradients. Although there are nine linear field gradients, only five of these are independent, and these five are given by the terms with $n = 2$. Writing them in both spherical and rectangular coordinates, they take the following forms:

$$\begin{aligned}(\Phi)_{n=2} &= r^2\{B_2^0P_2^0+B_2^1P_2^1\cos\phi+A_2^1P_2^1\sin\phi+\\ &\qquad +B_2^2P_2^2\cos 2\phi+A_2^2P_2^2\sin 2\phi\}\\ &= \tfrac{1}{2}B_2^0(2Y^2-Z^2-X^2)+3B_2^1YZ+3A_2^1YX+3B_2^2(Z^2-X^2)+6A_2^2ZX\end{aligned}$$

By designing shim coils which correspond to the various terms of such an expansion one may obtain a set of electric shims whose controls are substantially independent.[3] However, we shall see some simplifications may be made to cut down the number of required electric shims.

Let the strong magnetic field H_0 be chosen to be in the Z-direction; let the small variations in the field be H' (inhomogeneity). The total field is thus:

$$\mathbf{H} = \mathbf{H}_0+\mathbf{H}'$$

The variation in the resonant frequency of the sample is determined by the variation in H over the sample.

$$|\mathbf{H}| = \sqrt{[(H_0+H_z')^2+H_x'^2+H_y'^2]}$$

In practice H_0 may be the order of 10^4 gauss while H' has been found to be 10^{-1} gauss or less. Thus we may expand with the result

$$|\mathbf{H}| = H_0+H_z'+\frac{H_x'^2+H_y'^2}{2H_0}+\ldots$$

Here we see that the X and Y components of H' contribute at most 10^{-6} gauss to the field variation and therefore they may be neglected. Therefore it is only necessary to consider the field components parallel to the Z-axis.

$$-H_z = \frac{\partial\Phi}{\partial z} = \frac{\partial\Phi}{\partial r}\frac{\partial r}{\partial z}+\frac{\partial\Phi}{\partial\theta}\frac{\partial\theta}{\partial z}+\frac{\partial\Phi}{\partial\phi}\frac{\partial\phi}{\partial z}$$

From the relations

$$\frac{\partial r}{\partial z} = \frac{z}{r} = \sin\theta\cos\phi$$

$$\frac{\partial\theta}{\partial z} = \frac{1}{r}\cos\theta\cos\phi$$

$$\frac{\partial\phi}{\partial z} = -\frac{\sin\phi}{r\sin\theta}$$

and the derivatives of the potential, one may derive an expression for H_z in terms of the spherical coordinates. Spinning the sample average field as seen by the nuclei over the azimuthal angle ϕ[4, 5, 6]

$$\langle H_z \rangle = \frac{1}{2\pi} \int_0^{2\pi} H_z(r, \theta, \phi)\, \mathrm{d}\phi$$

Performing this integration yields the result

$$-\langle H_z \rangle = \tfrac{1}{2} \sum_{n=1}^{\infty} B_n{}^1 r^{n-1} \left[P_n{}^1(\sin\theta + 1/\sin\theta) + \frac{\partial P_n{}^1}{\partial\theta} \cos\theta \right]$$

Thus, spinning effectively cancels all except the $B_n{}^1$ terms. These terms correspond to the maximum variation of $\langle H_z \rangle$ along the y-axis. For example $B_2{}^1$ represents a linear gradient along the y-axis, while $B_3{}^1$ a quadridic variation, and $B_4{}^1$ a cubic variation.

We summarize the results in Table 1.

TABLE 1

Degree of Legendre polynomial	Total No. of field derivatives	No. of orthogonal derivatives	No. of components of H_z	No. of components not spun out	Type of components not spun out
1	3	3	1	1	H_z
2	9	5	3	1	$\frac{\partial H_z}{\partial y}$
3	27	7	5	1	$\frac{\partial^2 H_z}{\partial y^2}$
4	81	9	7	1	$\frac{\partial^3 H_z}{\partial y^3}$
n	$3n$	$2n+1$	$2n-1$	1	$\frac{\partial^{n-1} H_z}{\partial y^{n-1}}$

The analysis in Table 1 shows that only two sets of coils are required to remove linear and quadric gradients remaining after sample spinning. One other factor which needs to be considered is spinning sidebands. It has been

found by adding two more sets of coils corresponding to the linear gradients of H_z along the X and Z axis, these sidebands could be substantially reduced as well as given good non-spinning resolution. Thus, with sample spinning and four sets of coils, one can effectively remove gradients which would otherwise require 13 sets of coils.[3]

2. OPERATING PROCEDURE

For proper operation of the shims, one must insure that the sample is located at the geometric center of the set of electric shims. This is done by observing the position of the NMR signal on the oscilloscope as each linear gradient shim is adjusted. If the position of the signal changes as the X-gradient is changed, the probe should be repositioned along the X-axis. A similar procedure may be used along Y-axis. Centering along the Z-axis appears less critical.

(a) Adjust each shim for best non-spinning resolution. It may be necessary to come back and touch up each shim again after all of them have been initially adjusted. A sample with a single narrow line (distilled water) should be used to determine the homogeneity. The line height may be used as an indication of the resolution.

(*b*) For spinning samples the above procedure should be used before the spinner is turned on. After the spinner is turned on, slight adjustments of the linear gradient shim along the spinning axis and the quadratic shim may be necessary. The shims controlling the linear gradients along the two axes perpendicular to the spinning axis should not be adjusted while spinning the sample.

REFERENCES

1. F. A. Nelson, "Means and Apparatus for Improving the Homogeneity of Magnetic Fields", U. S. Patent No. 2,858,504.
2. James T. Arnold, "Magnetic Resonance of Protons in Ethyl Alcohol", *Phys. Rev.* **102**, 139 (1956).
3. Marcel J. E. Golay, "Field Homogenizing Coils for Nuclear Spin Resonance Instrumentation", *Rev. Sci. Inst.* **29**, 313 (1958).
4. F. Bloch, "Line Narrowing by Macroscopic Motion", *Phys. Rev.* **94**, 496 (1954).
5. W. A. Anderson and J. T. Arnold, "A Line-Narrowing Experiment", *Phys. Rev.* **94**, 497 (1954).
6. G. A. Williams and H. S. Gutowsky, "Sample Spinning and Field Modulation Effects in Nuclear Magnetic Resonance", *Phys. Rev.* **104**, 278 (1956).

14

MAGNETIC FIELD MODULATION FOR HIGH RESOLUTION NMR

WESTON A. ANDERSON
Varian Associates, Palo Alta, California

THE advantage of field modulation techniques for both broad line work and for high resolution is that it provides almost complete freedom from base line drift. This comes about because any change in probe balance due to heating or microphonics changes the d.c. level at the output of the r.f. detector. By passing the output of the detector through an audio amplifier and into an audio phase detector or "lock-in" amplifier, one discriminates against the d.c. level charges and detects only the signal components which have been modulated by the audio sweep field.

Audio field modulation and an audio phase detector, or "lock-in", has been used for some time[1] in broad-line NMR and EPR studies. In these cases the modulation frequency, ω_m, and modulation amplitude, γH_m, are chosen to be small compared to the widths of the observed lines. When this condition is met, the signal output of the audio phase detector is proportional to either the derivative of the absorption or dispersion curve, depending upon which mode is selected.

When the inverse condition is fulfilled, i.e. the modulation frequency is large compared to the line width, separate sideband resonances are obtained. Under conditions of low radio-frequency fields these sideband resonances are useful in calibrating the spacings of high resolution NMR lines.[2] Here the first pair of sidebands is separated from the usual resonance frequency (or field) by just the modulation frequency, the second pair of sidebands by twice the modulation frequency and so on. Analysis shows[3, 4] that *each* sideband resonance signal not only has a component which has a frequency equal to the transmitter frequency, but contains many components, each component with a frequency separated from the transmitter frequency by an integral multiple of the modulation frequency.

This result is illustrated in Fig. 1. Here assume that we modulate the magnetic field so that the instantaneous magnetic field at the sample is $H_0 + H_m \cos \omega_m t$, thus, H_m is the peak amplitude of the field modulation and ω_m is the angular frequency of the field modulation. If we now slowly sweep

the magnetic field, H_0, we find that we not only find a signal at the field value given by $H_0 = \omega/\gamma$ but we also find resonances at $H_0 = (\omega \pm n\omega_m)/\gamma$ where n can take any positive or negative integer value. (If $\gamma H_m \ll \omega_m$ the signals with very large n become vanishingly small.)

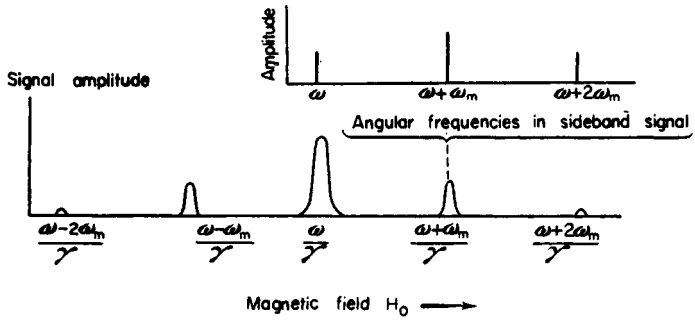

FIG. 1.

Above one of the resonances is sketched the spectrum of frequencies contained in that resonance. In the detector of the receiver, all of the frequencies are mixed with the transmitter frequency converting signals with the transmitter frequency to d.c. and signals at frequency $\omega - n\omega_m$ to $n\omega_m$. Here is where the advantage of this detection scheme becomes apparent. [5, 6] After detection the signals contain audio components as well as d.c. components. Any change of balance in the probe will change the d.c. level and leave the a.c. components unaffected. Thus, by selecting only the a.c. components of the signal, the effects of base-line drift can be minimized.

In order to record the audio signals they must be converted to direct-current signals. This is achieved by the use of the audio "lock-in" which derives a reference signal from the same audio source used to produce the field modulation.

This system appears to be of greatest value when large r.f. field need to be used, either because the lines are somewhat broad (but still not broad compared to the modulation frequency) or that adiabatic rapid passage needs to be used because the signals are weak (for example, in C^{13} resonances). If one wishes to use a modulating frequency of 400 c/s the Varian Model V-4270 may be used without any change. This unit may be used also with modulation frequencies from 400 c/s up to about 800 c/s if the twin-T filter is eliminated. This is done by switching S203 to "EXT. FILTER" and shorting one of the pins of jack J704 to the chassis. The pin which is to be shorted may be determined experimentally. It is the pin which leads to the pin 7 (grid connection) of the 12AX7 tube. The recorder is also plugged into the output of this unit. An external audio oscillator is plugged into the V-4250A Sweep Unit and the sweep frequency is set to "EXT.". The sweep coils of the probe are connected to the sweep unit just as they are when using the unit for broad-line work.

For integration of proton spectra, it is desirable to use an audio modulation frequency between 1000 to 2000 c/s. Here one must use an electrical audio phase detector. (The unit in the Varian V-4270 is a mechanical chopper.) The higher modulation frequencies are better since they remove the spurious sideband signals further from the region of measurement. The upper limit of possible modulation frequencies is determined by eddy current losses in the probe and the amount of audio power available. Not only do the eddy current losses increase with frequency but the index of modulation is inversely proportional to the frequency, which means that for optimum results one must increase the strength of the modulating field linearly with frequency. A circuit for an electrical audio phase detector is given in the section of this book titled "Operation of an NMR Integrating System".

To show the different possible ways the experiment may be performed we shall give some of the results of the analysis.[3] Consider the phenomenological[7] equations with

$$m = M_x + iM_y$$
$$h = H_x + iH_y$$
$$\omega_A = \gamma H_z$$

The equations are then

$$\dot{m} + i\omega_A m - ihM_z + m/T_2 = 0$$
$$\dot{M}_z + \mathrm{Im}(mh^*) + M_z/T_1 = M_0/T_1$$

where Im stands for the imaginary part and * stands for the complex conjugate. If we apply a rotating r.f. field with angular frequency ω the equations become

$$\dot{m}_1 + i(\omega_A - \omega)m_1 + m_1/T_2 = ih_1M_z$$
$$\dot{M}_z + \mathrm{Im}(m_1h_1^*) + M_z/T_1 = M_0/T_1$$

with

$$m = m_1 \exp(-i\omega t)$$
$$h = h_1 \exp(-i\omega t)$$

Let the field modulation take the form

$$\omega_A = \omega_0 + \gamma H_m \cos \omega_m t$$

and define

$$\Delta\omega = \omega_0 - \omega = \gamma H_0 - \omega$$

If the variation of $\Delta\omega$ is sufficiently slow and if $\gamma H_1 \ll \omega_m$ the solution of these equations is

$$m_1 = v + iu = \gamma H_1 M_0 T_2 \sum_{\substack{-\infty \\ k,n}}^{\infty} \frac{J_k(\beta)J_n(\beta)[1 - i(\Delta\omega + k\omega_m)T_2] \exp[i(k-n)\omega_m t]}{1 + (\Delta\omega + k\omega_m)^2 T_2^2 + \gamma^2 H_1^2 T_1 T_2 J_k^2(\beta)}$$

where

$$\beta = \frac{\gamma H_m}{\omega_m} = \frac{\gamma \times \text{modulating field}}{2\pi \times \text{modulating frequency}}, \qquad \Delta\omega = \gamma H_0 - \omega$$

and $J_k(\beta)$ are Bessel functions of the first kind. The usual centerband resonance condition is found by setting $\beta = 0$ with the result

$$m_1 = \gamma H_1 M_0 T_2 \frac{1 - i\Delta\omega T_2}{1 + (\Delta\omega)^2 T_2^2 + \gamma^2 H_1^2 T_1 T_2}$$

The real part of this expression corresponds to the signal one would obtain with 0° r.f. phase shift and in this case it is the usual absorption signal. The imaginary part of this expression corresponds to the signal one would obtain with a 90° r.f. phase shift and in this case the usual dispersion signal is obtained. One can also obtain a centerband resonance which occurs (after detection) at the audio frequency ω_m. The form of this resonance is

$$m_1 = \frac{-2iM_0\gamma H_1 T_2 J_0 J_1 \sin \omega_m t[1 - i(\Delta\omega T_2)]}{1 + (\Delta\omega T_2)^2 + \gamma^2 H_1^2 T_1 T_2 J_0^2}$$

Comparing this equation to the usual d.c. centerband resonance one finds the saturation parameter is $\gamma^2(J_0 H_1)^2 T_1 T_2$ in place of just $\gamma^2 H_1^2 T_1 T_2$. The signal is maximum when $\beta = 1.8$ and is 1.14 times the signal obtainable from the usual centerband resonance. The signal-to-noise ratio is less by the factor $1.14/\sqrt{2}$ since for the same filtering the bandwidth has been doubled. With 0° r.f. phase shift the signal corresponds to the real part of this expression which is the dispersion mode. An absorption signal is obtained here with a 90° r.f. phase shift. In either case the audio phase must be adjusted to 90°.

A sensitive procedure of adjusting the index of modulation for maximum signal response is to observe the first sideband signal. Here, if the audio amplitude and audio phase are correctly adjusted, the first sideband signal should be completely absent. This statement may be verified by observing the form of the first sideband resonance given when $\Delta\omega + \omega_m = 0$ with the result

$$m_1 = \frac{M_0\gamma H_1 T_2 K_1[(J_0 + J_2)\cos \omega_m t + i(J_0 - J_2)\sin \omega_m t][1 - i(\Delta\omega + \omega_m)T_2]}{1 + (\Delta\omega + \omega_m)T_2 + \gamma^2 H_1^2 T_1 T_2 J_1^2}$$

The first term is absent if the audio phase is adjusted to 90° since then signals proportional to $\cos \omega_m t$ will not be detected in the audio phase detector. The second term is absent when $J_0 - J_2 = 0$ which occurs when J_1 is maximum. This is true since $\partial J_1(\beta)/\partial\beta = \frac{1}{2}[J_0(\beta) - J_2(\beta)]$. Thus the modulation amplitude may be adjusted so that this term vanishes.

Of course, a perfectly acceptable method of observing resonance is to observe one of the first sidebands. One may do this, even if the modulation index

is small, by using a larger radio-frequency field H_1. If $\beta \ll 1$, then $J_0(\beta) \simeq 1$, $J_1(\beta) \simeq \frac{1}{2}\beta$ and the sideband resonance condition becomes

$$m_1 = \gamma(\tfrac{1}{2}\beta H_1)M_0T_2\frac{[1-i(\Delta\omega+\omega_m)T_2][\cos\omega_m t+i\sin\omega_m t]}{1+(\Delta\omega+\omega_m)^2T_2^2+\gamma^2(\frac{1}{2}\beta H_1)^2T_1T_2}$$

Comparing this equation to the usual d.c. centerband resonance one finds the saturation parameter is now $\gamma^2(\frac{1}{2}\beta H_1)^2T_1T_2$. Under optimum conditions the signal obtainable is the same size as the usual centerband signal; however, the signal-to-noise ratio is worse by $\sqrt{2}$. Here with 0° r.f. phase shift one may obtain either an absorption or dispersion signal depending upon whether the audio phase shift is 0° or 90° respectively. For that matter one may use either an audio phase control or a r.f. phase control for a complete mode selection. By proper adjustment of the two phase controls one may set each of the two sideband signals to have arbitrary modes.

REFERENCES

1. F. BLOCH, W. W. HANSEN and M. E. PACKARD, "The Nuclear Induction Experiment", *Phys. Rev.* **70**, 474 (1946).
2. J. T. ARNOLD and M. E. PACKARD, *J. Chem. Phys.* **24**, 468 (1951).
3. K. HALBACH, "A New Method of Measurement of Relaxation Times and The Spin of Cr^{53}", *Helv. Phys. Acta* **27**, 259–282 (1954).
   R. KARPLUS, "Frequency Modulation in Microwave Spectroscopy", *Phys. Rev.* **73**, 1027 (1948).
   BERNARD SMALLER, "Magnetic Moment of the Deuteron", *Phys. Rev.* **83**, 817 (1951).
   K. V. VLADIMIRSKII, "Modulation Effects in NMR", *Transl. Sov. Phys. JETP* **6**, 412 (1958).
4. W. ANDERSON, "Nuclear Magnetic Resonance Spectra of Some Hydrocarbons", *Phys. Rev.* **102**, 151 (1956).
5. K. HALBACH, *Helv. Phys. Acta* **29**, 37 (1956).
6. R. V. POUND, "Modulation in Nuclear Paramagnetic Resonance", *Rev. Sci. Instr.* **28**, 966 (1957); and H. PRIMAS, *Helv. Phys. Acta* **31**, 17 (1958).
7. F. BLOCH, *Phys. Rev.* **70**, 460 (1946).

15

OPERATION OF AN NMR INTEGRATING SYSTEM

LeRoy F. Johnson
Varian Associates, Palo Alto, California

1. EQUIPMENT

Basically the instrument discussed here is a Miller integrator using an *RC* time constant of 0.01 sec. The integrating amplifier is a chopper stabilized d.c. amplifier made by the George A. Philbrick Research Associates (Model UPA-2) having a maximum gain of 10^7. The amplifier requires an associated power supply and a control panel with input and output level controls and a capacitator discharge switch.

Since a small amount of random drift in the d.c. output of the r.f. unit can introduce large errors in the integrated spectrum, it is advisable to use some means of eliminating this drift which is caused mostly by minute changes in probe balance. One such method involves using audio-frequency modulation on the probe sweep coils, amplifying the resulting NMR signals at the audio-frequency, and observing them with an audio phase detector. A convenient modulation frequency is about 1200 c/s which produces side-band signals separated from the center band signal by more than the extreme range of chemical shifts encountered in proton NMR studies. It would be difficult to obtain the proper modulation index with greater than 1200 c/s since the frequency response of the sweep coils drops off rapidly above this point.

The basic components used in the modulation-phase detection system are: (1) an audio oscillator capable of delivering 10 volts r.m.s. into a high impedance load (Hewlett Packard Model 200 CD); (2) a power amplifier for supplying approximately 3.2 volts at 1200 c/s into the sweep coils; (3) an audio amplifier with gain of about 15 for amplifying audio signals from the output of the r.f. unit; (4) an audio phase detector for recording *v*-mode signals or for integration, and (5) an audio phase shift network.

The block diagram of the system is shown in Fig. 1. To aid discussion of the operation of the equipment, the various controls on each component are included. The schematic diagram of the system is shown in Fig. 2.

2. SETTING-UP FOR MODULATION AND PHASE DETECTION

Using a water sample, adjust the sawtooth sweep unit to display on the oscilloscope the single sharp v-mode signal with enough sweep amplitude to permit observation of 1200 cycle sidebands. With the audio oscillator delivering about 10 volts to the power amplifier, increase the modulation amplitude control from zero until *small* audio sidebands are seen. Adjust the audio phase shift control to maximize the center band signal. Disconnect the sawtooth sweep unit output. Using the slow sweep unit and a graphic recorder being fed by the phase detector, move to one of the 1200 cycle sidebands.

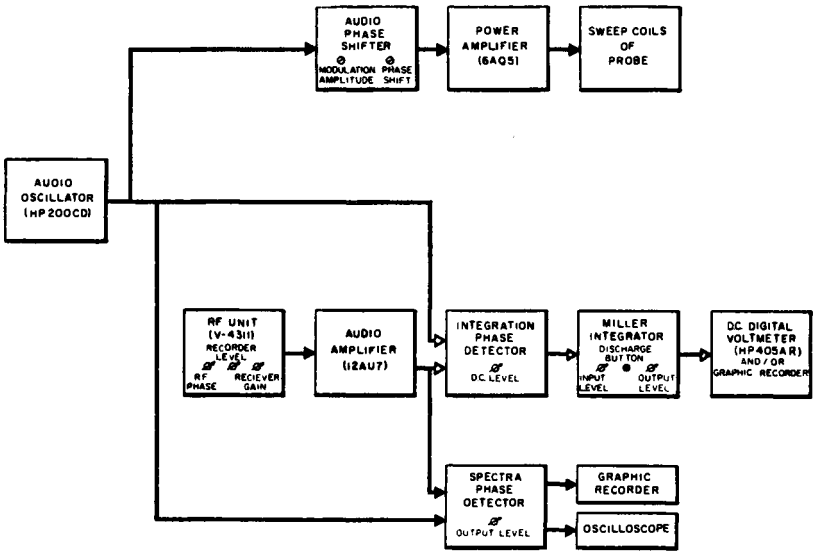

Fig. 1. Block diagram of an NMR integrating system.

Gradually increase the audio modulation amplitude while sweeping back and forth across the first sideband signal. Adjust the audio phase shift control to maintain a v-mode character. The signal will maximize, decrease to zero, and then increase in the opposite direction. The desired setting is reached when the sideband signal is minimized as well as possible. This requires accurate audio phasing and critical adjustment of the modulation amplitude. It is nearly impossible to cancel completely this first sideband signal; however, a reduction to less than two or three per cent of the centerband is not difficult to obtain and will suffice for essentially all purposes. Finally, sweep back to the centerband and operate in the normal manner.

The d.c. output of the audio phase detector is now independent of probe balance fluctuations since the phase detector responds only to 1200 cycle signals.

3. BALANCING THE INTEGRATOR AND ITS PHASE DETECTOR

With the input level control on the integrator panel set at zero and the integrator output level control set at maximum, zero the output of the integrator with the balancing potentiometer which controls the ± 300 volt balance in the d.c. amplifier power supply. The output of the integrator can be measured with a d.c. digital volt meter or with a recorder having a full scale sensitivity of 100 mV. Due to inherent noise in the amplifier it may be impossible to balance the output to zero. However, this is not serious since a few millivolts fluctuation is insignificant when the total integral is over

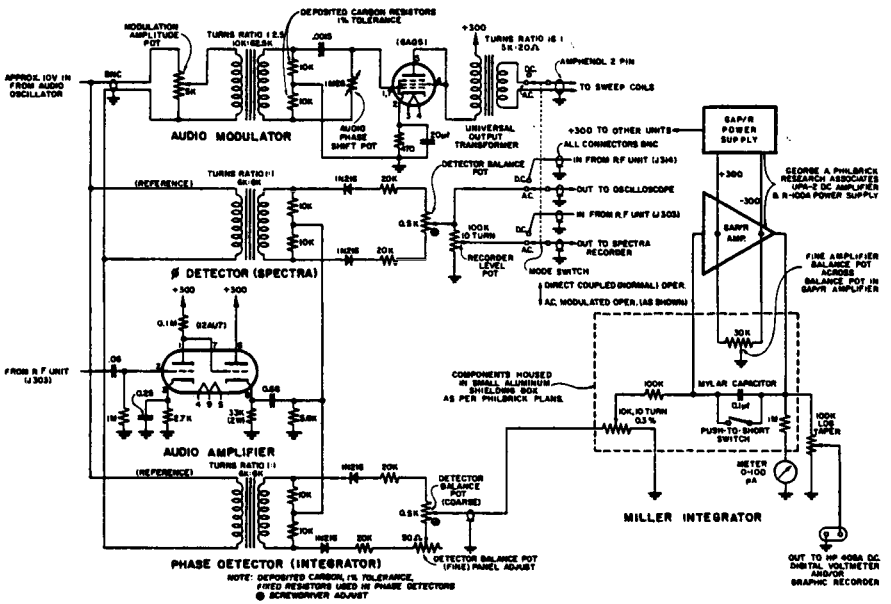

FIG. 2. Typical circuitry for an NMR integrating system.

one volt, which is the case for all but the most dilute samples. With no sample in the probe, advance the integrator input level control to one-tenth maximum and again balance the output of the integrator, this time using the phase detector coarse and fine balance controls. Advance the input level control to maximum and critically adjust the fine balance control of the phase detector.

It will be noted that in Figs. 1 and 2 a second phase detector is shown whose function is to provide a duplicate d.c. signal for simultaneous recording of the v-mode spectrum during the accumulation of the integral. This assures that the unbalanced voltage appearing at the input of the recorder during traverse of the pen is not applied to the integrator input. If it is desired to record only the v-mode spectrum *or* the integral, this second phase detector

can be eliminated. In this case, a single helical potentiometer can serve both as a recorder input attenuator or as the integrator input level control.

4. LEVEL CONTROLS

When integrating signals from a wide variety of samples, it is important to keep from overloading the amplifier stages or overdriving the phase detectors. Because of this, there are five level controls in the integrating channel which allow attenuation of the signals from concentrated solutions or pure liquid samples. These are: (a) the receiver gain selector; (b) the r.f.-unit output voltage divider. (This control is labeled Recorder Level on 60 Mc r.f. units. There is no output attenuator on 40 Mc r.f. units. The 1 megohm resistor in the grid circuit of the 12AU7 audio amplifier can be replaced with a potentiometer to serve this function.); (c) the integrator input level control; (d) the recorder level control; and (e) the integrator output level control. Each of these controls has an independent function which is discussed in the following section.

(a) *Receiver Gain Selector*

The first of the level controls is the receiver gain selector in the r.f. unit. For very dilute solutions this control is set at position 4 for 60 Mc r.f. units, and position 3 for 40 Mc. The highest receiver gain position should not be used when integrating since the resulting noise level could overdrive the audio phase detector. For concentrated solutions and pure liquids, receiver gain positions 2 or 3 will provide sufficient amplification without danger of excessive signal levels appearing at the audio phase detector. For strictly linear operation the detector level meter should not be permitted to exceed 20 microamperes (equivalent to two volts). Since there is an r.f. phase shift associated with a change in the receiver gain selector it will be necessary to adjust the r.f. phase separately for each selector setting.

An alternate way to reduce the signal level from concentrated samples is through reduction of the transmitter power. An increase of 20 db in attenuation will reduce H_1 and therefore reduce the signal level by a factor of 10. This method is not usually as desirable as diminishing the receiver gain since the signal-to-noise ratio is lowered when H_1 is reduced. An advantage of this approach is that the nuclei are less subject to saturation effects at small values of H_1. A slight r.f. phase shift is also associated with a change of attenuation setting so that minor readjustment of the r.f. phase control may be required.

(b) *R.f. Unit Output Voltage Divider*

Just as it is necessary to limit the signal amplitude to the phase detector in the r.f. unit, the same precaution must be observed in the signal level reaching the audio phase detector. Since the reference voltage in the phase detector is about 10 volts, the maximum applied signal should be held to not

more than one or two volts. Due to loss in signal level encountered in the audio phase detector it is necessary to amplify the signal coming from the r.f. unit with a simple triode amplifier–cathode follower stage as shown in the schematic diagram. This stage has a gain of 10 to 15 and *can* produce excessive drive to the audio phase detector when the output of the r.f. unit approaches one or two volts. To limit the signal amplitude reaching the audio phase detector, the r.f. unit output voltage divider is employed. However, the signal at this point should not be attenuated too much, since the signal level at the output of the audio phase detector would then become comparable to the random drift occurring there. If the detector signal is maintained as large as possible, but not permitted to exceed one or two volts, the error due to inherent phase detector drift will be minimized.

(c) *Integrator Input Level*

One volt at the input of the integrator will fully charge the *RC* circuit in a few seconds. Further integration is then impossible. Therefore, the integrator input level control is adjusted to limit the rate of integration so that the total accumulated integral is less than full scale (100V).

(d) *Recorder Level*

If the signals are being graphically recorded, it will generally be necessary to attenuate the output of the audio phase detector due to the high sensitivity of most graphic recorders. A recorder level control is shown on the schematic diagram for this purpose. The recorder can serve as a monitor to determine whether the permissible drive to the audio phase detector is being exceeded. For example, if the recorder has a full scale sensitivity of 100 mV, the recorder level control should be set to 100 mV/volt or one-tenth maximum. In this way, if any signals go off-scale it is evident that the phase detector is also being overdriven.

(e) *Integrator Output Level*

The integrator output level control can be used in two ways depending on the method of measuring the integrated spectrum. When using a single graphic recorder it is desirable to accumulate the integral while recording a normal absorption spectrum. After the complete spectrum has been obtained the recorder is switched to read accumulated integral. The integrator output level provides a convenient adjustment to give full chart response. When the integrating condenser is discharged and the spectrum swept a second time the total integral will then be recorded on the full chart width.

When a three decade digital voltmeter (Hewlett Packard Model 405AR) is used in place of a recorder to obtain better accuracy and more dynamic range in reading out the integrals, the same output level control can be used to adjust the voltmeter to fall near the upper limit of the particular range in use, e.g. 0.900, 9.00 and 90.0 volts. In this way the full accuracy of the voltmeter is utilized.

5. MISCELLANEOUS

Included in this section are comments intended to be an aid in operation and/or construction of the integrating system thus far described.

(a) The frequency response control in the V-4311 r.f. Unit is a five-stage *RC* filter which is used to limit the output of high frequency noise. Position 1 on this control has a time constant which is too large to allow sufficient passage of 1200 c/s signals. To correct this, position 1 should be rewired to bypass the *RC* filter circuits. An alternate method is to operate the r.f. unit as a wide line phase detector and take the output from J-302. However, in this arrangement the recorder level control cannot be used as the r.f. unit output voltage divider.

(b) The appearance of any appreciable 60 c/s component of current in the sweep coils results in sideband satellites which can be very troublesome. It has been found that a d.c. filament supply is a positive solution to this problem which may otherwise be very troublesome to trace if an a.c. filament supply is used.

(c) The d.c. balance stability in the audio phase detector depends upon constant resistances in all parts of this circuit. The two diodes in this stage are sensitive to temperature changes and require thermal lagging and insulation. This may be done by inserting each diode into one of two holes in a single copper block. The entire phase detector should then be covered with insulating material.

(d) In actual use the audio phase control and the modulation amplitude control were found to be quite sensitive. For greater ease of adjustment it would be desirable to determine the correct setting for these controls and then reduce their range and sensitivity with the proper series resistors.

(e) When recording integrated spectra correct r.f. phasing can easily be ascertained from the shape of the integral curve. A sharp signal in the v-mode spectrum produces a correspondingly sharp step in the integrated spectrum. With correct r.f. phasing the integral curve should be flat up to and just after the step. Since the integral curve should be building up in one direction any change towards less integral indicates either improper r.f. phasing or unbalance of the audio phase detector. If the absolute value of the integral curve diminishes just before the NMR peak is recorded a minor adjustment of the r.f. phase control is needed.

(f) When integrating an NMR spectrum which is several p.p.m. in total span, it may be discovered that a single setting of the audio phase detector balance control does not seem to maintain proper balance at both ends of the spectrum. This is due to insufficient minimization of the first sideband signal and is caused by a u-mode signal from the first sideband being recorded with the centerband signals. The solution, of course, is careful elimination of u-mode character in the first sideband and minimization of remaining v-mode.

16

INSTRUMENTATION OF EPR

FORREST A. NELSON
Varian Associates, Palo Alto, California

THE gyromagnetic ratio of the electron is approximately 2.8 megacycles per gauss, so it is quite simple to get magnetic fields high enough for the usual frequency ranges available. Most work in EPR is done at a frequency of approximately 9 to 10 kilomegacycles (a wave length of about 3 cm and in the frequency range called x-band). The field strength of the magnet for $g = 2$ (the free electron) is therefore approximately 3,500 gauss. The large line splittings and shifts often require that the magnet be shifted from a few hundred gauss to well above $g = 2$ resonance. Of course, a frequency sweep of the generator would be possible but the practical problems of generating constant output power over a continuous range and the frequency dependence of microwave plumbing equipment make this approach impractical. All EPR systems therefore include an electromagnet which can be continuously swept over a wide range of field strengths.

This discussion on instrumentation will predominantly cover the specialized equipment used for EPR and emphasis will be placed on the type used by the Varian V-4500 spectrometer. Although regulated voltage supplies and other associated equipment are important, the scope of this presentation will not permit a description of them.

The EPR signals are usually detected by placing the sample material in a microwave cavity located within the magnet air gap. The rest of the instrumentation is designed to measure the difference between the power lost in the tuned cavity with electron resonance and that lost when there is no electron resonance.

The basic components of a simple microwave bridge EPR system are shown in Fig. 1. The signal generator is a klystron tube, one arm of the microwave bridge is terminated by the sample cavity which is located in the magnetic field, H_0. The change in impedance of this cavity at resonance results in an unbalance at the microwave crystal detector. This unbalance represents the EPR signal and after amplification it can be recorded as a spectrum such as Fig. 2a. In normal EPR operation, a sweep generator is used to modulate the field of the magnet with a sine wave. Then a phase

detector operated coherently with this sweep has a recorder output which is proportional to the derivative of the resonance (Fig. 2*b*).

The signal generator is a small klystron with a typical output power of $\frac{1}{4}$ watt. Usually, the relaxation times in electron resonance studies performed at room temperature are sufficiently short that more power than $\frac{1}{4}$ watt could be used. However, low temperature extends relaxation times, thereby requiring less power so that the $\frac{1}{4}$ watt klystron must be attenuated to prevent saturation.

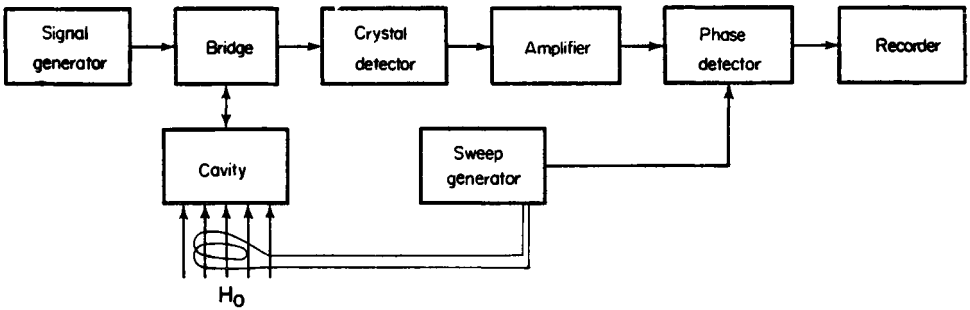

FIG. 1.

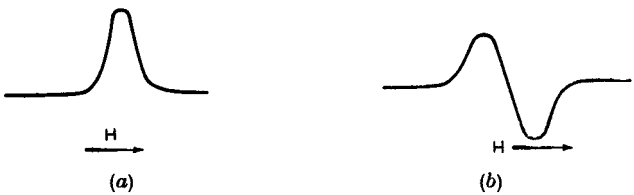

FIG. 2.

Inside the klystron tube, the electrons from a heated cathode are accelerated by an electric field so that they form a beam of almost constant velocity. This beam is directed through the electric field region of a microwave cavity which is tuned approximately to the desired output frequency. Any power which is resonating in this cavity will cause an alternating electric field which will alternately accelerate and decelerate the beam.

After passing through the cavity, the electrons are stopped and sent back through the cavity by a negatively charged electrode called a reflector or repeller. Between the first passage of the beam through the cavity and its return, the accelerated electrons catch up with those slowed down so that upon re-entry the electrons of the beam are in groups. If these groups enter the cavity in the correct phase, they will add energy and thereby perpetuate the oscillation. Increasing the reflector voltage raises the frequency by decreasing the time the electrons spend between their first and second passage through the cavity.

Figure 3 shows a cut-away view of a klystron.

The output frequency of the klystron is controlled by the tuning of the cavity, the voltage of the reflector and the accelerator voltage of the beam. The klystron cavity must be tuned to approximately the correct frequency and the initial velocity of the beam is made constant by a fixed accelerating voltage. The reflector voltage is then varied to control the frequency.

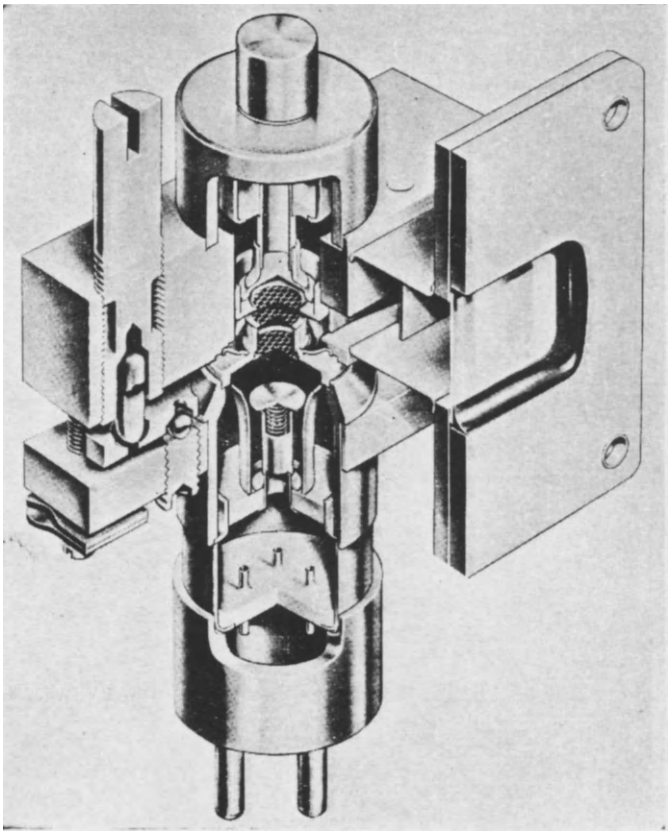

FIG. 3.

Usually the modulation sensitivity is approximately 1 Mc per volt for the reflector and $\frac{1}{3}$ this value for the beam accelerating voltage.

If the reflector voltage is swept over a wide range, the output, as detected by a crystal and observed on an oscilloscope, will approximate that of Fig. 4. The reflector voltage adjusts the elapsed time between the exit of the beam from the cavity and its re-entrance through this cavity, and if the timing is incorrect, the grouped electrons will remove energy from the cavity with

zero output as shown at A, Fig. 4. If they add energy, output is produced as at B of Fig. 4.

The klystron usually is cooled by air or a liquid. This cooling must be constant to prevent vibration or warping of the cavity. Any such deformation can cause a bad frequency and amplitude modulation of the klystron output with a resulting increase of noise on the recorded spectrum. The klystron tube is coupled to a wave guide which transfers the microwave output to the bridge.

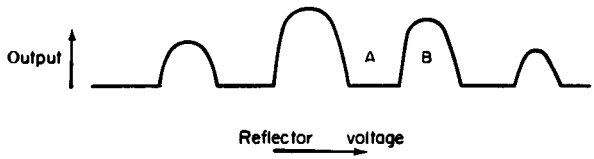

FIG. 4.

A wave guide is used because losses of other transmission lines are high at microwave frequencies. The microwaves propagate down the wave guide in the form of an electromagnetic wave which reflects from the walls and builds up a field pattern where shape and velocity along the guide depend upon ratio of microwave frequency and the dimensions of this guide. As is the case with other transmission lines, power can flow in one or both directions. A wave guide has a characteristic impedance at a given frequency and unless the end of the guide is terminated in this impedance, some of the microwaves will be reflected. This reflection of electromagnetic waves due to mismatch is similar to the partial reflection of light wherever it passes into a material of either higher or lower index of refraction.

Power reflected back into the klystron can affect its output frequency so some isolation is required. In a gyrator type of isolator, a piece of ferrite causes a Faraday rotation of the microwaves in such a way as to give almost no loss forward but a power loss of two or three orders of magnitude in the reverse direction. Another type of isolator also uses resonance in a piece of ferrite. The microwave power from one direction is pushed to a low loss side of the transmission guide, while that from the other direction is rapidly dissipated in the resonance.

The wave guide conducts the klystron power to a hybrid junction (a magic T, which will be described later). Half of the power is dissipated in a load; the rest goes through this magic T to the cavity which contains the paramagnetic sample and is located in the magnet gap.

A microwave cavity of the type used for EPR sensing is a tuned circuit made of a resonant section of wave guide. The losses are very low, so the microwave power reflects back and forth and builds up high electric and

magnetic fields in standing waves. One of the most important parameters of a cavity is its Q.

$$Q = \omega \frac{\text{energy in cavity}}{\text{power loss of cavity}}$$

In order to get maximum power into and out of the cavity, a coupling network is required between the wave guide and the cavity. Optimum coupling, at which the cavity matches the wave guide impedance so that no reflection occurs, reduces the cavity Q to half its unloaded Q.

It can be seen that if constant power is fed into the cavity, the total energy in the cavity will be proportional to Q and the r.f. magnetic field, H_1, is proportional to $\sqrt{(\text{Energy})}$ and therefore to $\sqrt{\text{Q}}$.

The effect of this coupling and cavity Q upon the signal can be seen by the ratio of reflected voltage, E_r, to that incident at the cavity, E_i. This ratio is given by a general transmission line formula:

$$\frac{E_r}{E_i} = \frac{Z_L/Z_0 - 1}{Z_L/Z_0 + 1}$$

where Z_0 is the wave guide characteristic impedance and Z_L is the load impedance (the reflected load of the cavity at the iris). If the load Z_L is equal to the line impedance Z_0, no reflected wave goes back into the wave guide. The change in cavity Q due to EPR resonance results in a proportional change in impedance at the coupling iris so that for small changes from the matched condition the reflected voltage is proportional to the change in Q.

Cavities can be made in many shapes and sizes. The smallest size for a given frequency is a rectangular piece of wave guide one-half wave length long called TE_{101} cavity which has a magnetic field distribution as shown by Fig. 5*a*. The sample is put against one wall where the field is maximum.

The TE_{102} mode rectangular cavity shown by Fig. 5*b* is twice as long with a full wave inside. The Q is higher than that of the TE_{101} and the sample tube

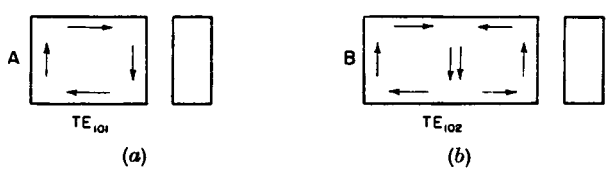

(*a*) (*b*)

FIG. 5. Side view of H_1 field in cavities.

can be inserted in the middle of the cavity with twice the volume of maximum H_1. One advantage of these restangular cavities for magnetic resonance is the fact that the steady magnetic field is across the narrow part of the guide which reduces magnet size.

Cylindrical cavities can also be used for EPR. The smallest such cavity has

a similar mode pattern to that of the rectangular. This is the TE_{111} cylinder as shown in Fig. 6*a*.

Another interesting cavity is the TE_{011} cylindrical type shown by Fig. 6*b*. The field goes longitudinally along the cylinder walls, along the ends and down through the middle of the cylinder. The large minimum diameter of

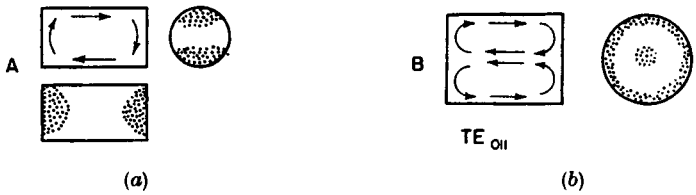

FIG. 6.

the cavity is often a disadvantage for EPR (see Table 1) but this cavity can have the highest Q of those described here and has a useful high field area down the middle. It can be used as a variable frequency cavity because no current passes longitudinally along the walls and, therefore, the end plates can be made adjustable without worrying about contacts. For that reason this type cavity is normally used for wide tuning range wavemeters as well as adjustable EPR cavities.

TABLE 1. INSIDE DIMENSION OF CAVITIES

Cavity type	Dimension in direction of H_0 in wavelengths	Inside dimension in direction of H_0 used for X-band
Rectangular TE_{101}	0.5	~ 1 cm
Rectangular TE_{102}	0.5	~ 1 cm
Cylindrical TE_{111}	0.59	>2.3 cm
Cylindrical TE_{011}	1.22	>4.2 cm

The rectangular TE_{102} is a very useful cavity for EPR. Many wavelengths, λ, can be used, but, even though the Q increases somewhat with size, the H_1 field is distributed so that there is not as close a coupling between the sample and the cavity.

The maximum size of the sample which can be put into a cavity depends on several factors. The region of high H_1 field is limited and the electric field is usually zero at the middle of this zone. In a TE_{102} rectangular cavity the field H_1 drops off as a cosine function from the midpoint of the cavity along the sample tube as shown by Fig. 7A. The electric field, E, is

also zero along the center of this sample tube. The H_1 drop off in Y direction (Fig. 7B) is also a cosine function with zero half-way to the end of the cavity. The electric field shape is a sine function with a zero point where H_1 is maximum.

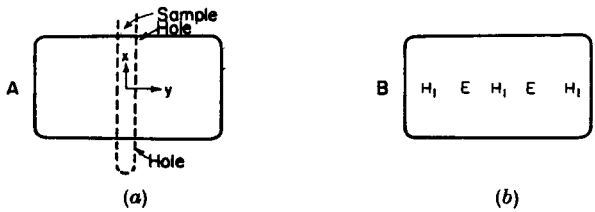

FIG. 7.

The presence of this electric field is important because many dielectrics, such as water or most types of glass, have high loss constants at microwave frequencies. This loss is proportional to the square of the r.f. electric field at the dielectric and results in a degrading of the cavity Q. Quartz has a low loss constant and is a good material to support or contain the sample. Special flat sample holders for aqueous solutions in the TE_{102} cavity are made from thin plates of quartz. The holder is carefully oriented in the cavity so that the solution lies as close as possible to the mid plane where the microwave electric field is zero.

External coupling to and from the cavity can be done in several ways. A loop of wire can be used as Fig. 8A. The flux from one side induces current in the wire and the current induces a magnetic field on the other side of the wall. Another method, Fig. 8B, has a coupling hole or iris. The field couples through this hole so the larger the hole, the greater the coupling. This coupl-

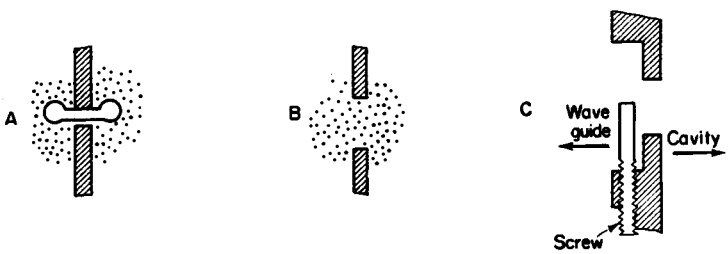

FIG. 8.

ing can also be modified by an inductive or capacitive coupling element near the iris. Figure 8C shows a capacitive coupling screw which increases the coupling. Small holes can be made in cavities without appreciable effect upon either Q or resonant frequency, if they are carefully located. The openings for inserting the sample in a TE_{102} rectangular type cavity (Fig. 5*b*) can have small holes for the sample tube on the edges of the cavity as shown by

Fig. 7, but if these holes become larger than about $\frac{1}{4}\lambda$, leakage of microwave power will be appreciable. Larger holes up to a diameter of about $\frac{1}{2}\lambda$ can be used with long attenuation stacks. The quartz dielectric of Dewars and sample cells lowers the cutoff frequency of the stack but symmetrical location helps to prevent propagation of the most troublesome TE_{11} cylindrical wave guide mode.

Narrow slots can be made in the cavity in such a way that the sample can be illuminated or irradiated with negligible loss of microwave power. If the magnetic field lines cross the slots, the high frequency current travels along the thick metal pieces between with but slight effect on either resonant frequency or cavity Q.

A cavity can be made with two outlets. A simple geometry for such a transmission cavity is secured by making a hole on both ends of a TE_{102} rectangular cavity, Fig. 9. The microwave power can be coupled into the iris, *a*, and the signal taken to the crystal from iris, *b*. The two holes make

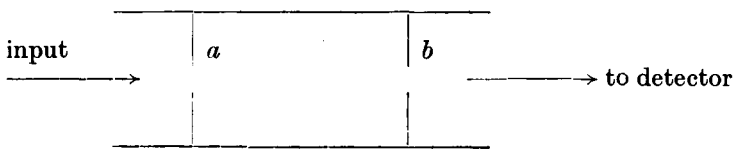

FIG. 9.

a more complicated problem than one. The coupling is no longer to a cavity of unloaded Q, but to a cavity already loaded. Normally the two couplings are made equal and adjusted so that together they match the cavity losses. It is impossible to overcouple such a transmission cavity and approaching unity coupling reduces the Q of the cavity and thereby lowers the signal. The output contains the EPR signal superimposed on the generator coupling through the cavity.

The microwave bridge used with a single port cavity is usually a version of the magic T hybrid junction of Fig. 10. The microwave power from the

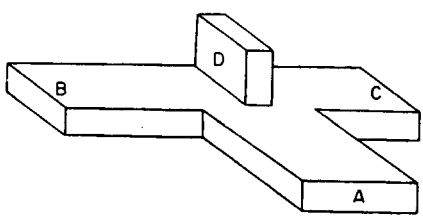

FIG. 10.

klystron enters through arm *A*. At the junction, no power can go into the arm *D* because this guide is too narrow in the *H* plane so the power divides between arms *B* and *C*. If power of equal amplitude and phase approaches the

junction from arms B and C, it will cancel at D which contains the crystal detector, but if the impedances are correct, any separate signal on either B or C will divide into arms A and D. A matched resistor load on arm B will absorb its half of the power from arm A and a tuned cavity properly coupled to arm C will absorb all its power. The crystal in arm D will have no microwave input when the bridge is balanced. As the Q of the cavity is changed by the EPR absorption, the bridge will unbalance and give an output. The reference required for the crystal diode bias can be furnished by reflecting a little microwave energy from arms B or C. A slide screw tuner placed in arm C will reflect some microwave power with phase depending upon position along the waveguide and magnitude depending upon how far the screw is inserted into the waveguide. Such a slide screw is also very useful to cancel out power reflected due to a mismatched cavity; a small loss of signal results but this control is a great convenience.

The magic T has losses due to the signal divisions between arms. Only half of the power from the klystron goes to the cavity and half of the signal power from the cavity gets to the crystal arm. Therefore, the field H_1 in the cavity is reduced by $\sqrt{2}$ and the signal voltage impressed on the crystal is also reduced by $\sqrt{2}$ so the total loss is a factor of 2 unless the klystron has more than sufficient power output, in which case the maximum output signal is reduced by $\sqrt{2}$.

Although the microwave components described herein are the heart of the EPR system, there are more non-microwave electronics in an EPR spectrometer than the microwave parts described. The power supplies for the klystron and the other electronics are exceptionally important and must be very well stabilized in this type of instrument but they will not be described here.

To present the EPR spectrum, the strength of the polarizing magnetic field is varied at both a slow constant rate and also with a rapid sine wave. The slow sweep over a wide range is produced by a variation of the current through the electromagnet. The a.c. sine wave sweep is produced by a pair of coils which are usually fastened to the cavity in such a position that the most uniform part of the field produced by these coils is at the sample location. The magnitude of the required a.c. sweep is determined by the EPR line shape and width and therefore has to be variable from a fraction of a gauss to ten or more gauss.

The frequency of this sweep can be very important. If the a.c. sweep is rapid compared with the relaxation time T_2, the signals will be badly distorted. However, most EPR signals have a relaxation time of less than a microsecond, so sweep rates of 100 kc or higher can be used. The need for such a high frequency is caused by the character of the noise added to the signal by the crystal detector. This noise voltage is inversely proportional to the square root of the frequency and is graphically illustrated in Fig. 11.

An equal bandwidth of noise at 100 kc would have approximately $\frac{1}{50}$ the noise voltage that is produced over the same bandwidth at 40 cycles. The obvious advantages of high frequency sweep are offset by the design difficulties in that it is much easier to sweep at the low frequencies because the cavity walls greatly attenuate the sweep field at high frequencies. These cavity walls act as shorted turns inside the sweep coils. The voltage E_c is induced in these walls by a sine sweep H_s. If units are disregarded:

$$E_c = \frac{d\phi}{dt} = A\frac{dH_s}{dt} = -j\omega AH_s$$

$$I_c = \frac{E_c}{Z_c} = \frac{E_c}{R_c + j\omega L_c} = \frac{-j\omega HA}{R_c + j\omega L_c}$$

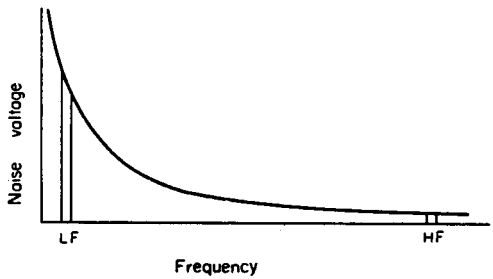

FIG. 11.

where R_c is the resistance of the effective resistance of the walls of area A carrying current I_c, L_c is the effective inductance and j represents a phase rotation of 90° (sine vs. cosine). The value of L_c is more or less fixed but R_c is inversely proportional to the wall thickness and conductance. At 40 cycles ωL_c is negligible compared to R_c although at 100 kc they may be comparable. Therefore, the wall current is approximately:

$$I_c = \frac{-j\omega AH_s}{R_c}$$

The value of this current is small with low frequencies such as 40 cycles per second but at 100 kc this current is 2500 times higher. The phase of this wall current is shifted 90° with respect to the sweep coil current but is of the same phase as the voltage in these walls, so the loss which is $P_c = I_c^2 R_c$ is $(2500)^2$ times as great at 100 kc as it is at 40 cycles with the same thin walls, providing the field inside is the same. As ωL_c approaches R_c, the current phase in the cavity walls shifts in such a way as to produce a field which further reduces the sweep field inside the cavity.

Sweep coils can be made inside the cavity but it is quite difficult to locate the coils so that they will not seriously reduce the Q of the cavity. In addition, they should be designed so as to prevent small vibrations that will

produce changes in cavity resonance. Careful positioning of such coils in the center of the electric field maximum will lower the resonant frequency of the cavity but not affect its Q greatly.

A cavity must not change shape or Q coherently with sweep because such an extremely small change of Q at the sweep frequency will give an output sine wave from the detector which resembles a signal except that it will not necessarily be affected by magnetic field. High sweep currents in the coils and cavity walls, because of their location in the strong field of the magnet, will produce forces on the cavity which are proportional to the magnetic field. These forces can shake the cavity, warp the cavity, or move dust particles inside the cavity so as to give false output. It is a difficult design problem to make a cavity with the sweep stability required for high sensitivity EPR.

The homogeneity of the sweep field inside the cavity is important because all the samples should have the same optimum sweep amplitude. Actually even though the sample may go from side to side in the Te_{102} rectangular cavity, the effective size of the sample is less than the cavity width because the EPR coupling of the sample is proportional to H_1^2. The cosine shape of H_1 along the sample produces a signal proportional to $\cos^2$ shape with maximum at the center of the cavity and zero at the edges, so over 80 per cent of signal is produced in the middle half of the sample tube. Therefore, a constant amplitude sweep over this central half of the sample tube will produce almost maximum signal-to-noise.

The output from the microwave crystal detector has a d.c. voltage from the reference vector and during EPR resonance, because of the a.c. sweep, there is also an a.c. signal output at sweep frequency. The phase and magnitude of the a.c. output is determined by the slope of the resonance line of the spectrum being measured. The a.c. signal from the crystal may have to be amplified as much as 10^5 or 10^6 and then it is put into a phase detector which gives the output for a recorder. This recorder signal will be the derivative of the spectrum because the amplified a.c. signal is proportional to the slope of the resonance lines.

Phase detection, which is used in several places in an EPR spectrometer, is desirable for reasons other than selection of phase. The bias of the detector for weak signals, as was discussed previously, is a form of phase detection. An ideal detector would give an output voltage directly proportional to the input voltage but a crystal at low signal level gives an output proportional to the square of the input voltage and then gradually gets more linear with increased level. Therefore, a weak microwave signal will give a very weak output and a nonlinear output-to-input ratio as shown by signals *a* and *b* of Fig. 12*a*. If a constant microwave reference voltage R_t of greater amplitude than the weak signals is added to the diode detector as is shown by Fig. 12*b*, the signals riding on the reference d.c. of the output will not only be greater but their relative sizes will be proportional to their input

ratios. Also, this microwave reference makes the detector a simple phase detector (referred to later).

Most EPR equipment gives a pure absorption resonance because of the nature of the bridge used, but with some systems both the absorption and dispersion signals are present and must be separated. A large coherent reference signal has the ability to reduce or eliminate any signals or portions of a

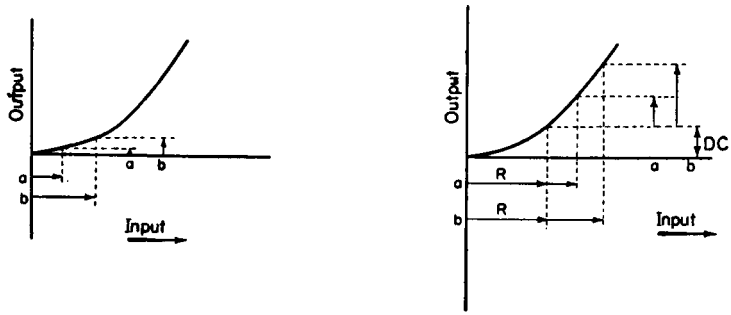

(a) (b)

FIG. 12.

signal which is 90° phase shifted from this reference. Figure 13 shows how this is accomplished. The detector itself is sensitive to magnitude only but, when signal S is added to a reference R, the resultant magnitude depends upon the phase angle. Figure 13*a* shows a signal added in the same phase which results in an increased amplitude for detection. A 180° shift of the signal will subtract vectors but a signal shifted so that it adds orthogonally (Figure 13*b*) will make almost no change in magnitude provided the reference is several times larger than the signal.

FIG. 13.

Another advantage of a large reference carrier is that it can improve signal-to-noise of the system. A signal at frequency ω may be fed into the detector with a wide band of noise. If the signal is very weak, the detector will produce an output which contains energy at beat frequencies of the noise spectrum. These will have low frequency components which cannot be eliminated by narrowing the band width of the amplifier after detection. A strong signal or a strong reference of frequency ω at the input to the detector will produce

signal-to-noise beats but no noise-to-noise beats. Therefore, noise which is not located close to the carrier frequency can be reduced by limiting the band width after detection. The large d.c. output caused by the reference is not too important in the case of the microwave crystal detector because the output goes to an a.c. amplifier which removes the d.c. portion of this output, but in other applications where a d.c. voltage cannot be tolerated, it must be bucked out by another voltage or a balanced phase detector must be used.

Figure 14 shows a balanced audio-frequency detector of the type often used to drive the recorder. The reference output from diodes D_1 and D_2 are subtracted and results in zero output with no signal, but a signal input of the

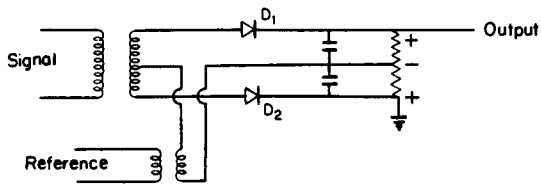

FIG. 14.

same phase will increase the input to one diode and decrease that to the other so that the output difference is no longer zero. Balanced phase sensitive detectors are most common at audio frequencies but they can be designed for frequencies as high as microwaves. Often, at low frequencies, a mechanical chopper makes the best phase detector.

The frequency of the klystron for EPR is set by the klystron tuning and by the beam and reflector voltage, as previously discussed, but the microwave tuned circuits such as the cavity are so sharp that frequency stability is always a problem. A tuned circuit at frequency ω_0 has a bandwidth relation to Q given by:

$$\omega_B = \frac{\omega_0}{Q}$$

The band width ω_B is the frequency separation between half power points. A cavity with a Q of 10,000 and a frequency of 10 kilomegacycles will have half power points $\frac{1}{2}$ Mc on each side of resonance. Two things happen if the frequency of the generator does not correspond to that of the cavity: the sensitivity of the instrument is lowered and, worse than that, noise may increase enormously. The latter condition is caused by the fact that microwave generators usually have an output which is frequency modulated by noise. Thus, the frequency sensitive impedance of the cavity when it is slightly off resonance will result in the production of an amplitude modulated noise due to the microwaves reflected back into the detector.

The microwave frequency can be stabilized by two methods. The generator frequency can be controlled by the cavity or it can be separately stabilized.

The klystron tube can be stabilized by a "stalo" which is an extremely high Q cavity coupled to the tube so that it reduces the frequency shift. Another approach is to put part of the klystron output into a system which contains a high Q cavity and has an active feedback to the klystron reflector voltage to keep this tube frequency the same as the resonant frequency of the cavity. This system works because the microwave energy reflected from the high Q reference cavity will be phase shifted if this cavity is not resonant at the generator frequency. A phase detection system gives a d.c. error voltage output which compensatingly adjusts the klystron frequency.

A different frequency control is an automatic control to keep the frequency of the generator the same as the resonant frequency of an EPR reflection cavity. Not only will generator frequency variation be corrected, but if the cavity changes, the frequency will follow along. In this system the klystron is frequency modulated a small amount at a rate of 10 kilocycles or more and then the microwave reflection off the cavity will vary at a rate coherent with this frequency modulation. The output of the EPR microwave crystal will have an amplitude modulation whose amplitude and phase are determined by how far from the cavity resonance and on which side of resonance the klystron is operating. A phase detector operating at the modulation frequency produces a d.c. output voltage which controls the klystron so that its average frequency is the same as the cavity resonant frequency.

The magnet system is basically the electromagnet and the power supply for the magnet. An electromagnet is necessary because the field must be varied over such a wide range. The homogeneity of the magnetic field usually does not have to be as high as that required for NMR because the resonant lines are seldom less than 100 milligauss in width and the useful length of samples is less than 2 cm for X band. This means that a gradient of about 1 part in 50,000 for the two centimeters can be tolerated for most work.

The gap of the magnet used for X-band EPR usually is about 2 inches or greater, depending upon cavity shape and cryogenic equipment used. The magnetic field in the gap of a magnet with cylindrical shaped pole caps can be made quite uniform until the gap-to-diameter ratio gets greater than about 1 to 6. At larger gaps, the field drops off rapidly from the center of the gap. Special ring shim pole caps, which have their edges raised the correct amount above the pole cap faces, improve the field uniformity near the central gap region and permit use of gap-to-diameter ratios of almost 1 to 2. These ring shim caps do not operate well above 6 or 7 kilogauss but they are used extensively for X band EPR which requires the best magnet homogeneity at about 3.4 kilogauss.

The field strength of the magnet of a given geometry is roughly proportional to the product of current and the number of turns. The turns are determined by the design of the magnet, so, if the iron has high or constant permeability, the field strength would then be a direct ratio to the current,

but in practice saturation of the iron produces a curve such as in Fig. 15. At the low fields usually used for EPR, the magnet will be operating in the most linear range.

The magnet power supply should have current regulation. The resistance of the magnet changes with temperature and a constant voltage would result

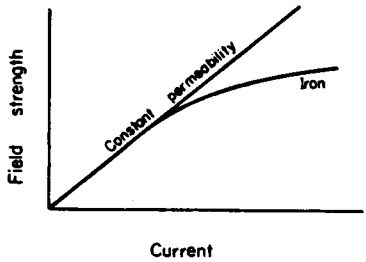

FIG. 15.

in a variation of the magnet current and, therefore, the flux. The usual current regulator connects the output from an unregulated, rectified a.c. supply through the magnet, some gate tubes and an information resistor as shown by Fig. 16.

The voltage from the d.c. supply forces a current through the system. The magnitude of this current is determined by the d.c. supply voltage and the combined resistances of the d.c. supply, magnet, information resistor and gate tubes. The voltage across the information resistor (product of current

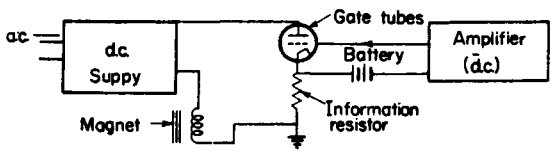

FIG. 16.

and resistance) is connected to a bucking reference voltage and any difference between these voltages appears on the input of an amplifier which in turn changes the resistance of the gate tubes. This resistance change modifies the current by the amount required to equalize the voltages of the information resistor and the reference. The current through the magnet is therefore determined only by the information resistor value and the reference battery voltage.

The wide range of the current sweep required for EPR can be produced by a gradual change of the reference voltage. This is a very useful sweep method because almost no current goes through the reference circuit and the magnet current is directly proportional to the reference voltage.

There are many uses for an EPR spectrometer which require special equipment. Solid state study of crystals often requires a directional change of the steady magnetic field in the sample. This is usually done by one of two methods: rotation of the sample in the cavity or rotation of the magnet around the cavity containing its fixed sample. The former method can change the cavity tuning because of the rotation of an irregular dielectric in the cavity, but with moderate care in sample shape, good results are obtained. Rotation of the magnet requires that the cavity be oriented so that its microwave field is always perpendicular to the magnetic field. Also, the sweep field has to remain in the direction of the magnetic field. This is easily accomplished at low sweep frequencies by mounting the sweep coil on the rotating magnet, but at high frequencies this is usually not practical. Rotation of the magnet with coils fixed to the cavity will permit a 90° swing ($\pm$ 45 degrees) with a sweep decrease at the extremes of $1/\sqrt{2}$ of maximum. This decrease is caused by the fact that the small sweep is added to a very large constant vector, and, therefore, only that portion of the sweep vector in the direction of this large field will change the field magnitude.

Many of the variations of EPR instruments have not been discussed. Apparatus for low temperature work often requires special materials and techniques but in general the same principle of operation is used and the extra accessories or modification are added to the basic instrument.

17

CHEMICAL APPLICATIONS OF EPR

LAWRENCE H. PIETTE
Varian Associates, Palo Alto, California

THE reason EPR spectroscopy has been able to make a significant contribution in the general field of chemistry stems from its ability to unequivocally detect the presence of free radicals in chemical systems. This ability to detect and, in many cases, to identify free radicals is inherent in the basic phenomenon of electron magnetic resonance since EPR spectrometers can respond only to systems containing unpaired electrons such as free radicals.

Once EPR has established that free radicals are present in chemical systems, it then remains for the chemist to apply this powerful tool to fundamental studies on the nature and chemical properties of these unstable intermediates. It is these two applications of EPR in the various phases of chemistry on which I will elaborate.

The role of free radicals in chemistry, as studied by EPR, can be discussed in terms of the following fields of interest:

(1) Free radical intermediates in organic reactions.
(2) Reaction kinetics.
(3) Surface chemistry.
(4) Irradiation damage.
(5) Free radical induced polymerizations.
(6) Low temperature trappings of free radicals.

1. FREE RADICAL INTERMEDIATES IN ORGANIC REACTIONS

For years organic chemists have suggested that free radicals exist as intermediates in many typical organic reactions. Some, such as Michaelis,[1] went so far as to propose, as early as 1938, that all oxidation-reduction reactions of organic molecules, in biological systems at least, proceed in two successive univalent steps, the intermediate state being a free radical.

In many cases the only verification of the existence of free radical intermediates was dependent upon the "lead-mirror reaction", magnetic susceptibility measurements and potentiometric oxidation-reduction titrations. The magnetic and "lead-mirror" methods are too insensitive and slow for general

applications, and the potentiometric method, which is capable of higher sensitivity than the other techniques, can only be applied to systems that produce reasonably stable potentials in an electromotive cell. None of these techniques is capable of identifying the radical intermediates. The development of highly sensitive paramagnetic resonance spectrometers has made it possible to verify the existence and to identify free radical intermediates in a number of organic reactions. Their ability to detect as low as 2×10^{11} free radicals and to respond in times less then 100 microseconds has rendered all other techniques obsolete.

One of the earliest verifications and identifications of free radical intermediates by EPR was made on the oxidation and reduction products of hydroquinones and quinones. For years chemists suggested that the condensation of the biologically important diacetyl went through a free radical intermediate and was a precursor to ring formation in biological systems. They suggested the mechanism

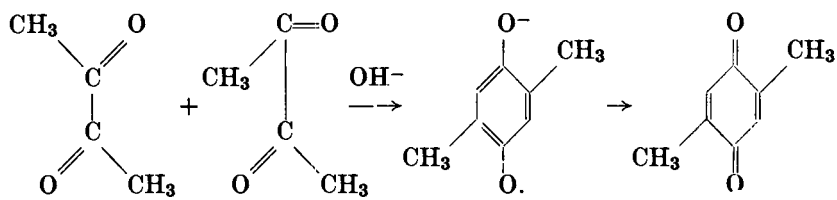

The semiquinone intermediate is a free radical and should give an EPR spectrum consisting of a large septet as a result of the unpaired electron being split by the six methyl hydrogens and each of these lines being split again three times by the weak coupling to the two ring hydrogens. This

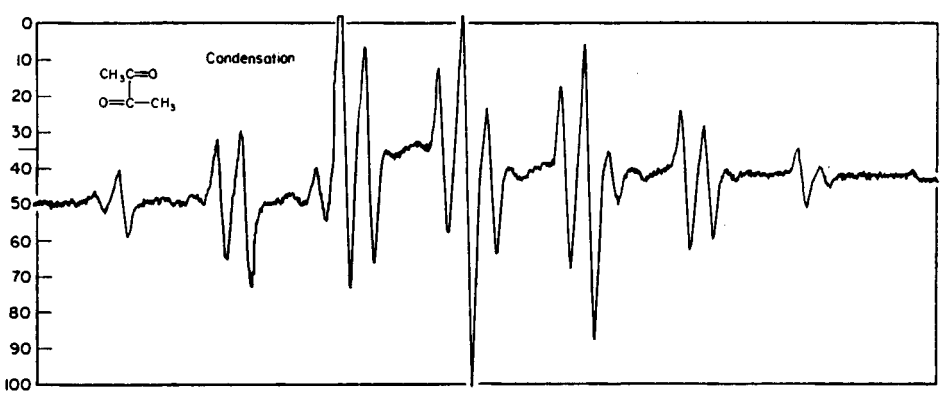

FIG. 1. The Semiquinone formed in the basic condensation of diacetyl. The spectrum consists of twenty-one lines.

is exactly the spectrum obtained when diacetyl is condensed in the presence of base. (See Fig. 1.) The semiquinone intermediate was verified by reducing the 2, 5 dimethyl–benzoquinone in the presence of acid. This reduction yielded the same intermediate and the same spectrum which was observed in the condensation reaction. Other work on these semiquinones has led to positive identification of many of the side products formed in the simple oxidation-reduction reaction.

Detection and identification of free radicals are not the only results obtainable from the EPR spectrum. A measure of the unpaired electron density at various sites in the molecule is obtained directly from the spectrum. This information results from a measure of the hyperfine coupling (splitting between lines) produced by the interaction of the unpaired electron with its neighboring magnetic nuclei.

Qualitatively speaking, the longer the length of time that the unpaired electron spends in the vicinity of a magnetic nucleus, the greater will be the hyperfine interaction between the two. Thus it can easily be seen how a measurement of the hyperfine coupling constant would yield information as to the relative unpaired electron density around the different magnetic nuclei in the molecule.

In attempting to derive a theory for the relation between unpaired electron densities at the various nuclei and the hyperfine interaction, especially in aromatic molecules, one is faced with an apparent paradox. In the first place, we know the interaction must be some kind of dipolar interaction involving the nucleus and the electron, but in the case of liquids this dipolar interaction averages to zero because of the rapid tumblings of the molecules. Only the contact hyperfine or Fermi interaction can survive this tumbling. If, however, the odd electron is confined to a π molecular orbital, then there is zero odd electron density at the in-plane aromatic hydrogens since the π orbital has a node at these hydrogens and therefore the contact hyperfine interaction is also zero. It remains, however, that since a coupling is observed experimentally, there must be some residual contact interaction between the electron and the nucleus. This residual interaction, according to McConnell[2] and others,[3] results from a configurational interaction or mixing of the pure π-orbital character of the unpaired electron molecular orbital and the σ-orbital character of an excited state. This mixing of excited states with σ-character yields a finite density of the unpaired electron wave-function at the edge protons and produces the hyperfine splitting experimentally observed. They have shown that the hyperfine splitting due to one proton can be reduced to the simple expression $A = Q \cdot \rho$ where Q is a constant for aromatic molecules equal to 10–100 gauss.

The obvious extension of these results would be to relate the unpaired electron density at the various carbon atom sites in the ring with the Hammett sigma functions for aromatic substitution.

2. REACTION KINETICS

In the past, two techniques utilizing EPR have been used to study the kinetics of free radical reactions. The first technique involves relating some changes in the spectral features of the resonance absorption with the rate of the reaction. The second method merely utilizes the EPR spectrometer as an analytical tool for studying the time rate of change of the concentration of free radical intermediates formed in the reaction.

The first method was applied by Weissman[4] and his group to the study of very rapid electron exchange reactions. The electron exchange generally takes place between a free radical and a diamagnetic molecule. The second order rate constants for these reactions are generally about 10^7 to 10^8 l/msec. Most of the studies have been made on aromatic negative ions.

If one takes naphthalene and reacts it with sodium or potassium in the presence of a suitable solvent, the negative ion of naphthalene is formed. This negative ion is a free radical that gives an EPR spectrum consisting of twenty-five lines. The twenty-five line hyperfine pattern is due to the coupling of two sets of different protons to the unpaired electron. The four protons on one ring split the electron into five lines and then the four protons on the other ring split each of these lines five more times, giving a total of twenty-five lines. As one adds a very small concentration of diamagnetic naphthalene, the individual lines begin to broaden and shrink in amplitude. As more naphthalene is added, these lines merge together into one broad line and eventually sharpen to a single line. This change in the spectral features of the resonance lines is due at first to a very slow electron exchange between the negative ion and the naphthalene molecule and then a gradual increase in the frequency of exchange. This change in the resonance line widths is directly related to the rate constant for the electron exchange. If one plots the change in line width as a function of the concentration of the pure naphthalene added, the rate constant is obtained from the slope of the line.

A third technique exists for studying very rapid free radical reactions which resulted as a consequence of some recent instrumental modifications of standard EPR equipment. This is a method which utilizes the EPR cavity as both the reaction vessel and the detecting head for the free radicals formed during the course of a reaction. The method utilizes a simple flow system for studying fast reactions. In this system the two reactants flow simultaneously into a mixing chamber, are mixed, and then pass directly into the cavity (see Fig. 2). Depending upon the reaction rate and the flow rate, either stopped or continuous flow systems similar to those developed by Britton Chance[5] and others can be used. Liquid flow systems of this type have the advantage that they can be applied to the study of free radical formations with half-lives of only 5 milliseconds or longer.

We have used both stopped flow and continuous flow systems to study the rate of formation of the semiquinones. These formation reactions are far too

fast to study by ordinary methods. If one flows hydroquinone and basic alcohol saturated with oxygen into the mixing chamber and then into the cavity, a steady state concentration of these semiquinones is formed depending upon the flow rate. The measurement of this steady state concentration at various flow rates yields the rate constant for formation. If, however, one

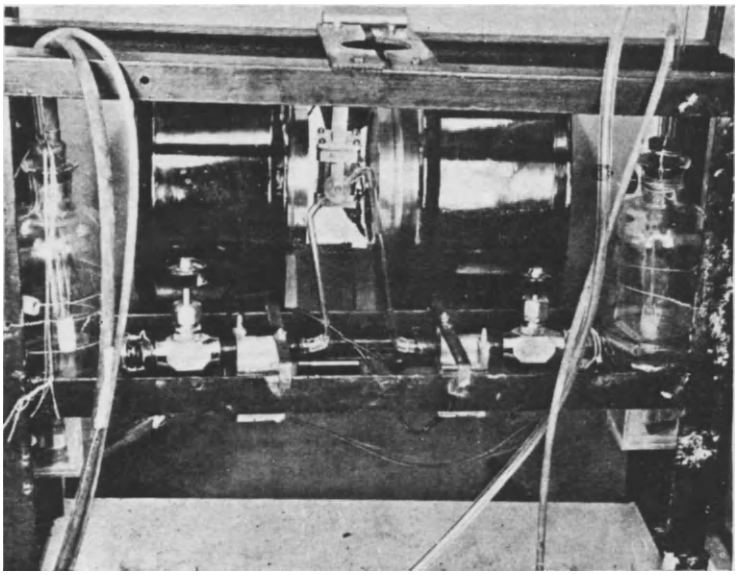

FIG. 2. This is a photograph of a research prototype flow system using gas drive. Note mixing chamber at the entrance of the EPR cavity. This is a twelve jet mixer designed by Dr. R. Berger of Utah State University.

flows and mixes faster than the two reactants can react to form the semiquinone and if the flow is stopped in the cavity, the formation can be displayed directly on the oscilloscope or the recorder by adjusting the spectrometer for maximum resonance signal. Figure 3 shows a plot of signal intensity vs. time directly after the flow has stopped. The sharp drop of intensity to zero in the time during the flow indicates that the flow is faster than the reaction. The exponential rise then occurs after the flow has stopped. An analysis of this curve yields the rate constant or the half-life directly. By varying the various parameters in the reaction, it is possible to obtain the true mechanism for the formation.

The obvious extension of these flow techniques with EPR is in the field of biochemistry. It seems quite possible now that the rapid enzyme substrate reactions that have been studied spectrophotometrically by Chance[5] and Roughton[6] can be studied also by EPR. Such a study should establish whether or not the intermediate in the enzyme reaction is truly a free radical.

Flow methods as described here theoretically can be applied to gaseous systems also. It is conceivable that, by working with very low pressures and thus high flow rates, one could study reactions such as hydrogen atoms or ozone with olefins, or the halogenation of hydrocarbons and a host of other gaseous reactions believed to give free radical intermediates. The one severe limitation in working with gaseous systems is that the lifetime of the intermediate will be considerably shorter and may very well be outside the range of the resolving time of standard equipment.

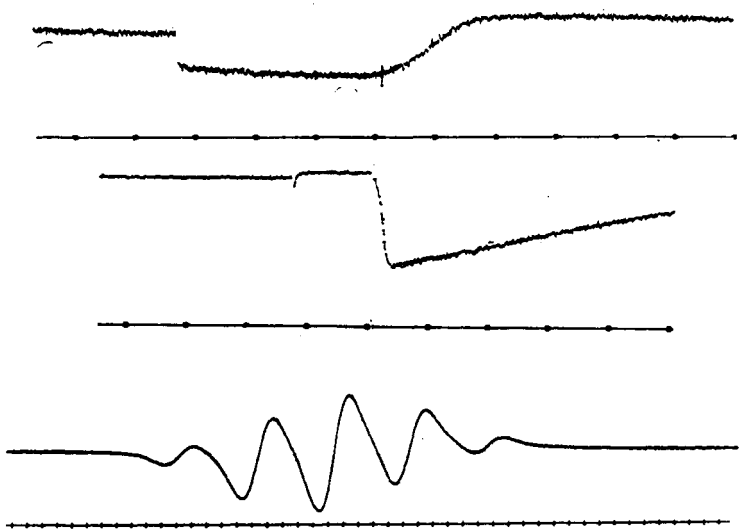

FIG. 3. (1) and (2) are plots of signal intensity vs. time. Markers indicate one second intervals. During flow, signal level is zero, when flow is stopped, signal level rises according to rate of formation and then decays slowly. (3) Spectrum of intermediate in hydroquinone oxidation.

3. STUDY OF SURFACE CHEMISTRY

It would seem that because of the sensitivity of EPR to slight changes in the nature of an unpaired electron, that this technique should be applicable to studies of surfaces on which unpaired electrons are trapped. This has been borne out fairly well in some studies that have been made on carbon black, graphite and charred carbohydrates.

If one takes a sample of carbon black and looks at the EPR spectrum under normal atmospheric conditions, he will observe a single line with a width of about 15 gauss. (See Fig. 4.) When this same sample is evacuated, it is observed that the line width changes to about 7 gauss. (See Fig. 5.) If oxygen is now introduced into this evacuated sample, the line immediately broadens to a value at least twice that observed at atmospheric conditions. In each of these cases, the total intensity of the line does not change; only

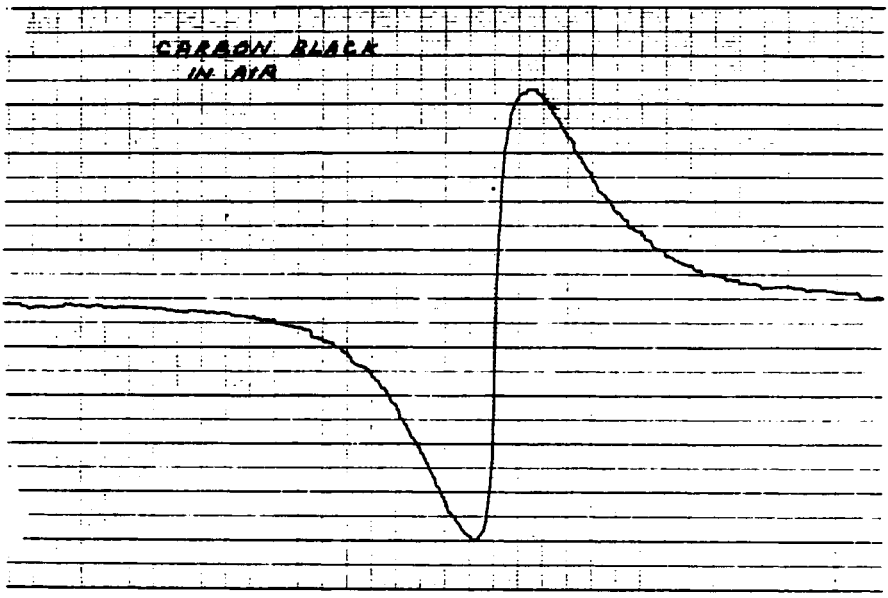

FIG. 4. EPR spectrum of carbon black at atmospheric conditions.

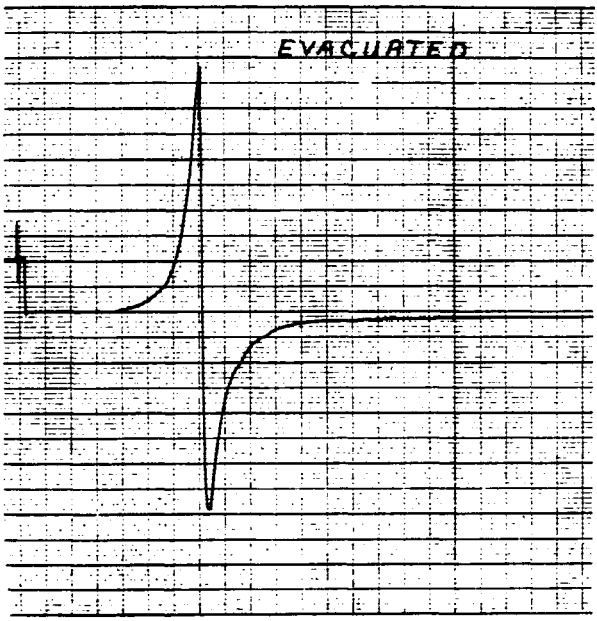

FIG. 5. EPR spectrum of carbon black evacuated.

the line width changes. (See Fig. 6.) If the sample is evacuated once more and nitrogen admitted and then oxygen introduced on top of this, the line remains the same as it was when evacuated. The results seem to indicate that once nitrogen is on the surface the oxygen has no effect on the sample.

It appears from these results that the oxygen when admitted interacts with the unpaired electron at the surface. This interaction is probably a dipolar interaction and acts merely to broaden the line but not to reduce the

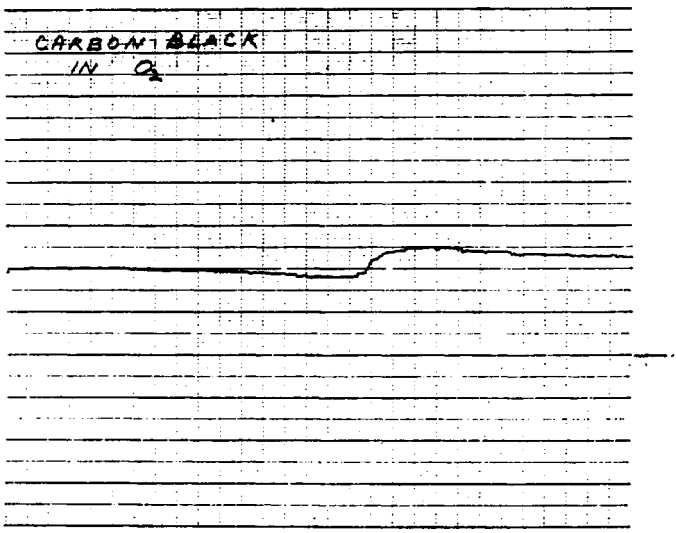

FIG. 6. EPR spectrum of carbon black in atmosphere of oxygen.

total free radical concentration. Collins[7] observed that, when these carbon blacks are heated to a very high temperature (< 1400°C), the free radical disappears, but as the temperature is raised even further, another free radical appears. He concludes that the free radical initially was due to unpaired π electrons trapped in large aromatic type compounds condensed on the surface of the carbon. The second radical to appear is assigned to sigma electrons resulting from broken carbon—carbon bonds at lattice defects.

4. IRRADIATION DAMAGE

The greatest amount of work which has been done with EPR has probably been in the field of irradiation damage. Since the EPR technique is capable of detecting free radicals and in many cases identifying them, it is an extremely important tool in the field of irradiation damage. If one irradiates a solid organic material such as a protein, polypeptide or a polymer, with high energy ionizing radiation, a free radical is produced in almost every case (see Figs. 7 and 8.) The stability of these radicals depends upon the lattice

in which they are formed. In many cases they are stable for years. An analysis of the free radical spectrum frequently enables one to determine where the radical is stabilized in the molecule. These spectra can be extremely complex. This complexity generally arises from the fact that the radicals are stabilized in polycrystalline material. The hyperfine interaction which serves as the fingerprint by which free radicals are identified is not a pure isotropic type

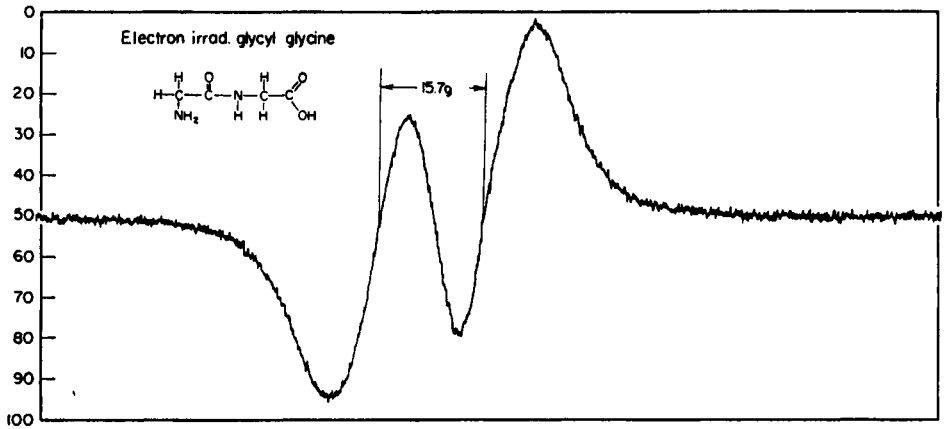

FIG. 7. EPR spectrum of electron irradiated glycyl glycine.

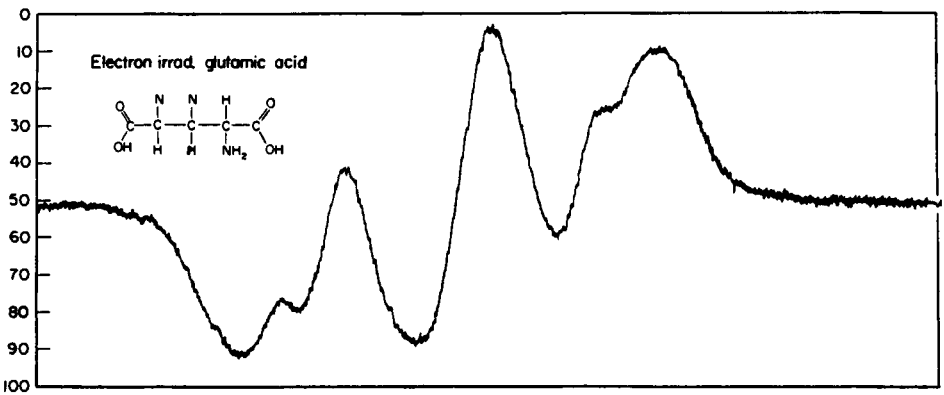

FIG. 8. EPR spectrum of electron irradiated glutamic acid.

of interaction. The hyperfine Hamiltonian contains both an isotropic term and an anisotropic term. The anisotropic term is a dipole–dipole type of interaction and in liquids can be averaged out by rapid tumbling of the molecules. In polycrystalline solids the anisotropic interaction is reduced by averaging over all possible orientations of the molecule. Very often in polycrystalline materials there is incomplete averaging and the simple multiplets of the

isotropic Fermi interaction can be smeared. This complication can be eliminated if the irradiation damage studies are carried out on single crystals. In this way all of the orientation parameters are known and a complete interpretation of the spectrum is possible.

In polymer studies it is generally not possible to work with single crystals and therefore isotope substitution and temperature studies have been very useful in elucidating the types of free radical sites in the polymer. Orientation studies have been successful, however, on stretched thin films.

Temperature kinetic studies have met with the most success in determining the types and numbers of radicals stabilized in polymers. Voevodsky[5] recently reported on a temperature study of free radicals produced in polyethylene by electron irradiation. He found that at 77°K only one type of radical was produced during irradiation which corresponded to an alkyl radical

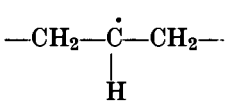

with a radical yield $G_1 = 2.9$ (where G = number of free radicals produced per 100 eV). When the irradiations are carried out at room temperature, two radicals are produced, one similar to the 77°K radical and one with an entirely different spectrum and a lower yield $G_2 = 0.16$. This second radical is identified as an allyl radical

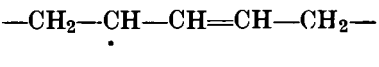

which results from a free valence migration of the alkyl radical type (1) to a radiation induced defect and subsequent formation and stabilization of the allyl radical type (2).

Voevodsky[8] maintains that the alkyl radical (1) is the primary radical formed and is stable only at low temperatures. At high temperatures it can recombine or be captured in a lattice defect to produce the allyl radical (2). He concludes, therefore, that the radiation yield of the allyl radical (2) should reach that for the alkyl radical (1) as the number of radiation induced defects in the lattice is increased. His predictions were verified by irradiating at 77°K and then heating to 120°C in order to remove all radicals and to produce a large number of defects and then re-irradiating at room temperature. Upon re-irradiation the yield for the allyl radicals (2) increased to $G = 3.0$.

Similar studies have been made by Gordy[9] and others on the mechanism of oxygen uptake by the radical formed in irradiated teflon. Controlled O_2 addition and temperature variation have enabled them to measure the bond angle of the ROO· radical formed, and also the heat of rupture of the C—O bond in this RO_2· radical.

Generally speaking, a wealth of information is readily obtained from the EPR spectra of these trapped radicals in polymers above and beyond the simple identification of the radicals and determination of radiation yields. Important information on the principles governing chemical transformations in the solid phase can also be deduced from careful interpretation of these spectra under various experimental conditions.

5. POLYMERIZATION REACTIONS

Recently Hotta and Anderson[10] of the University of Maryland showed how EPR can be used in the study of peroxide initiated polymerizations. Polymerizations were induced directly in the cavity by ultraviolet radiation of the monomer plus a small amount of benzoyl peroxide initiator. By altering the technique of irradiation they were able to study the radicals present during three stages of polymerization: (1) initial or monomeric radicals, (2) propagating radicals, (3) occluded polymeric radicals.

The initial radicals were obtained by ultraviolet irradiations of nonomer plus initiator at 77°K where polymerization cannot take place. The propagating radicals were formed by irradiating at room temperature for short periods and then quenching the polymerization at 77°K. The polymeric radicals were observed as stabilized radicals in the gels after prolonged irradiation at room temperature. The course of polymerization was followed by making frequent viscosity measurements.

They studied the polymerization of styrene, 2-methyl styrene and methyl methacrylate and found that, in each case, the benzoxyl radical abstracts a proton from the monomer to initiate polymerization except in the case of styrene where abstraction is energetically unfavorable and addition of the benzoxyl radical occurs. These conclusions are made from the interpretation of the hyperfine patterns obtained for the various radicals.

The same EPR spectrum was obtained for the irradiated monomer of methyl methacrylate as for the propagating and polymerized radical. They also obtained this radical in thermally induced polymerizations. The radical is formed by proton abstraction and gives a five line EPR spectrum believed to be associated with the

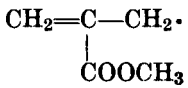

radical. However, when the radical was formed by thermal-induced polymerization and then irradiated at room temperature with strong ultraviolet they found a weaker quartet between the five line pattern. Ingram[11] and Abraham[12] observed this same spectrum for irradiated poly methylmethacrylate at room temperature and interpreted it in terms of a different geometric configuration. Hotta and Anderson argue that this is not the case and

that the spectrum they observed is a result of photo-dissociation of the polymer molecules and is actually due to two radicals, one of which is assigned to the monomer radical and the other to a chain ending polymer radical.

The interpretation of Hotta and Anderson agrees quite well with some temperature kinetic studies made on irradiated poly methylmethacrylate at our laboratories.[13] We found that if the temperature is slowly raised from room temperature to +100°C that a different rate of disappearance is noted for the quintet versus the quartet in the spectrum. (See Figs. 9 and 10.)

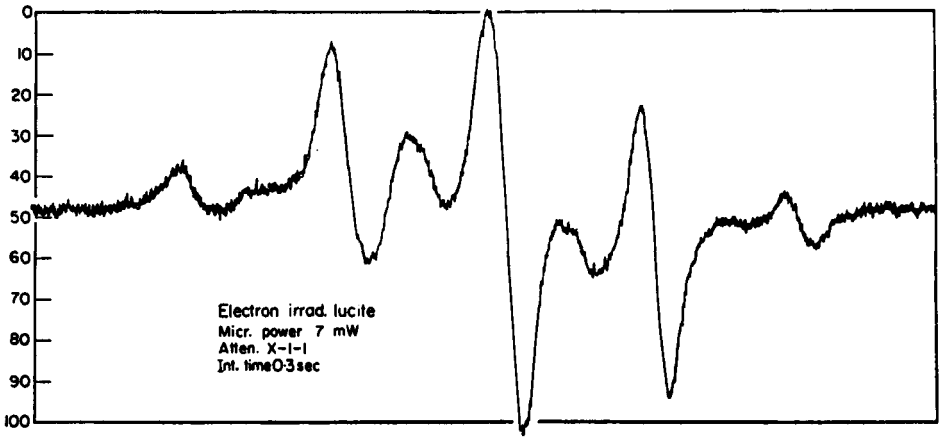

FIG. 9. EPR spectrum of electron irradiated poly methylmethacrylate at room temperature.

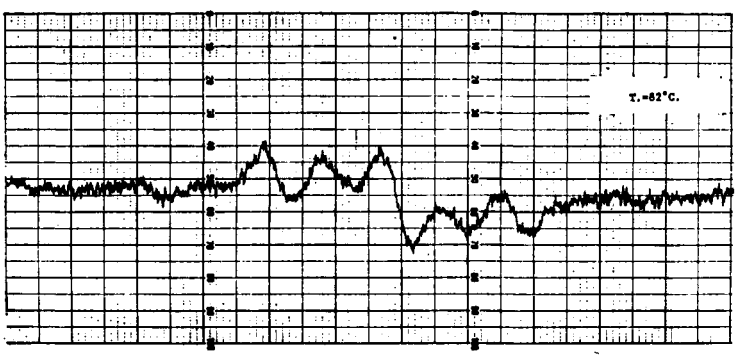

FIG. 10. Electron irradiated poly methylmethacrylate at +82°C.

Figure 11 is a plot of the intensity of the two different radicals as a function of temperature. The dotted line is the intensity change expected from a decrease in Boltzman factor. We found that the quintet disappeared much faster than did the quartet which would be expected if the quintet is due to

trapped monomer radicals and therefore the result confirms Anderson and Hotta's interpretation.

6. LOW TEMPERATURE TRAPPING

The trapping of free radicals at very low temperatures was first initiated by Broida and his group at the National Bureau of Standards. Their initial work involved trapping nitrogen atoms and observing their electronic spectra This same trapping technique is being used in conjunction with EPR studies.

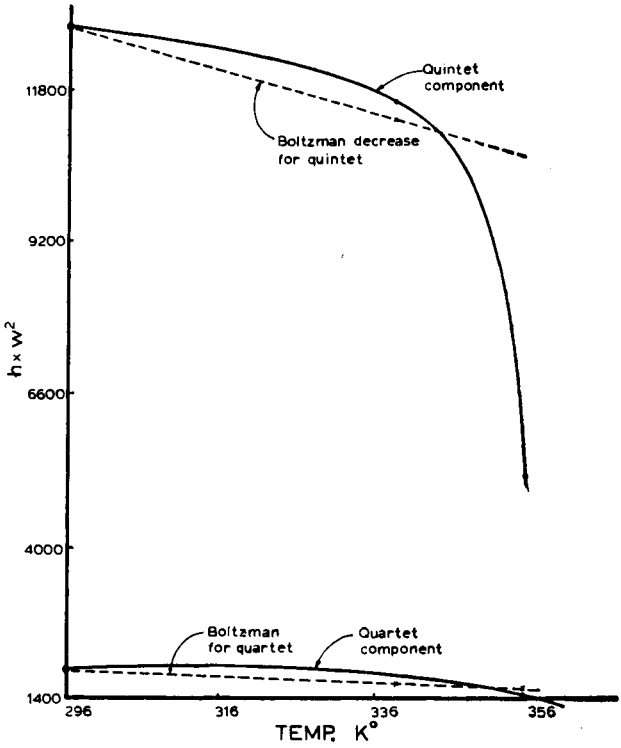

FIG. 11. Plot of intensity vs. temperature of the two radicals stabilized in poly methylmethacrylate.

The trapping technique is extremely useful for quenching reactions and stabilizing highly reactive intermediates. Once stabilized, the EPR spectra of the radicals can be obtained and many of the intermediates identified.

Jen[14] and Foner succeeded in stabilizing H atoms, N atoms, NH_2 radicals and many others by forming the intermediates in a microwave discharge and condensing them on a cold finger in various matrices at 4.2°K. They have also been able to use this technique for studying the matrix itself. By observing the deviations in the hyperfine coupling constant and the g values of H atoms

stabilized in various matrices they were able to show that there are multiple trapping sites available to the H atoms in the matrix. These deviations arise from perturbations of H atom energy levels by the matrix fields.

Cochran[15] recently showed how this trapping technique coupled with EPR measurements is extremely valuable for studying the elusive free radicals generated in simple-photo-dissociations. He succeeded in observing the EPR spectra of such unstable radicals as the methyl and ethyl radical by photolyzing the appropriate alkyl iodide at 4.2°K.

In many cases it is not necessary to go down as low as 4.2°K to stabilize these reactive radicals. Livingston[16] showed that H atoms are stabilized in concentrated sulfuric and perchloric acids at 77°K, but we found that it is necessary to go to 4.2°K to stabilize them in ordinary ice. (See Fig. 12.) We

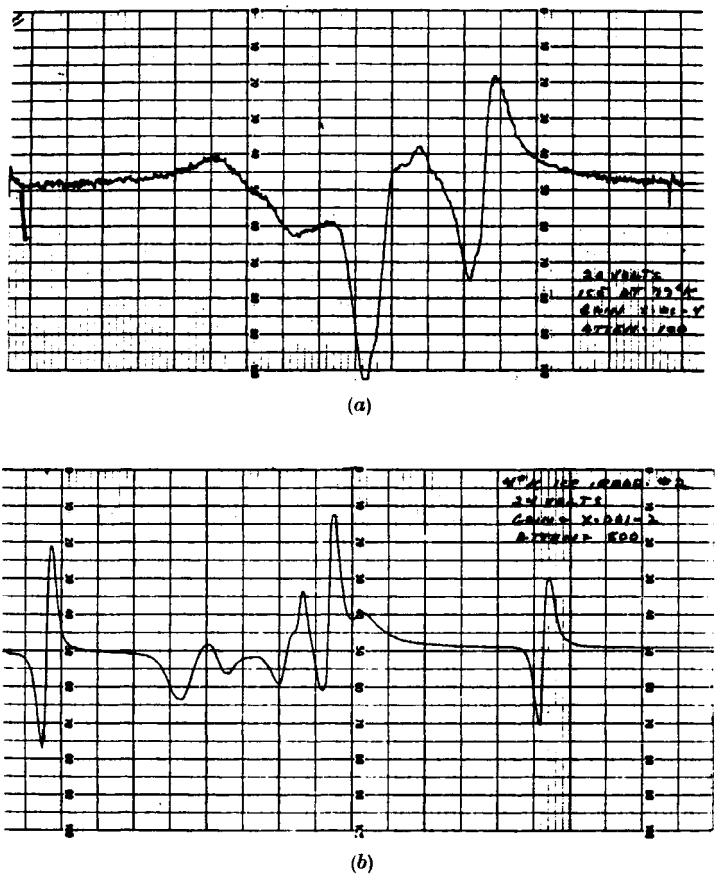

(a)

(b)

FIG. 12. Figure (a) is electron irradiated ice at 77°K showing only the $g = 2$ region of the spectrum. Figure (b) is electron irradiated ice at 4.2°K. Center portion is $g = 2$ region. Outside lines are associated with the H atom.

have been successful in stabilizing methyl and ethyl radicals at the higher temperatures also when formed by the ultraviolet irradiation of methanol acetone and ethanol. (See Figs. 13 and 14.)

Low temperature studies with EPR can also yield valuable information about the rates of diffusion of radicals through various media and the degree

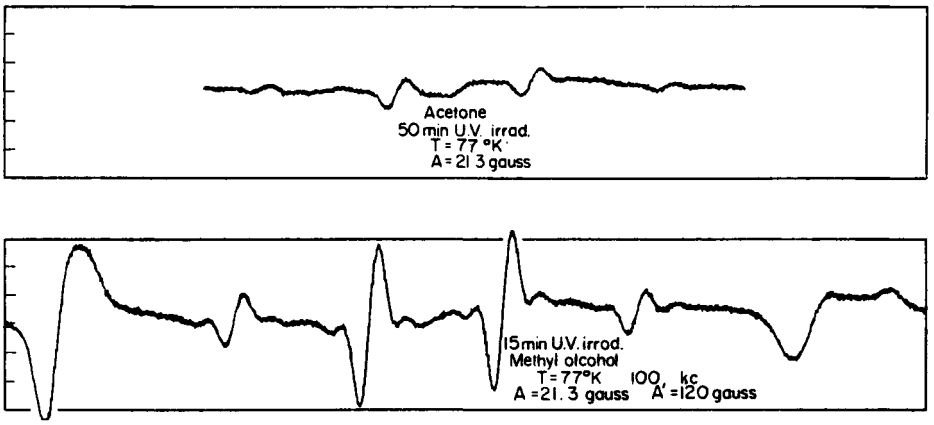

FIG. 13. Ultraviolet irradiated acetone and methyl alcohol. The four line pattern is characteristic of the methyl radical.

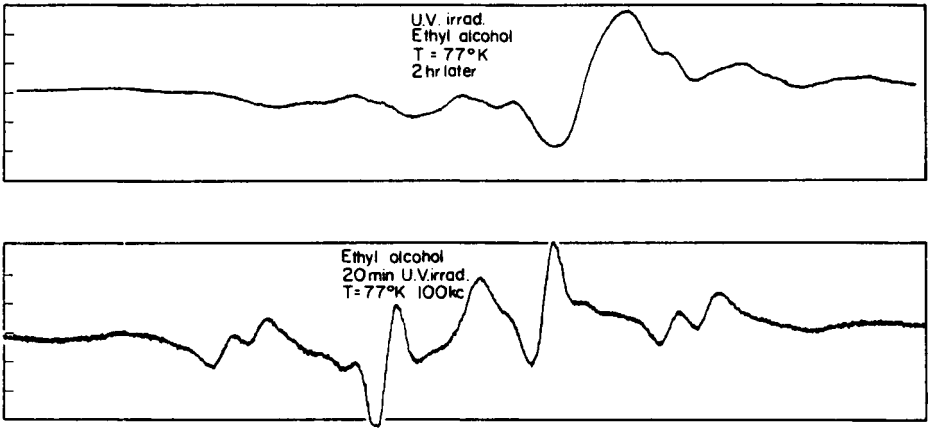

FIG. 14. Ultraviolet irradiated ethyl alcohol at 77°K. First spectrum is made immediately after irradiation. Second spectrum 2 hours later.

of freedom to internal rotation of various groups within the molecule. Fujimoto and Ingram[17] have studied the rate of diffusion of · OH radicals through a medium of solid isopropyl alcohol at 110°K. They were able to follow this diffusion rate by measuring the rate of formation of the isopropyl

radical produced by proton abstraction of the α carbon hydrogen by the ·OH radical. They noticed that the seven line pattern observed for the

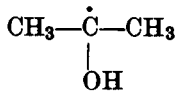

radical changed to a six line pattern when the material was cooled to 77°K. This change is attributed to hindered rotation about the C—C bond. Thus, by quantitatively studying this change in the spectrum as a function of temperature it should be possible to obtain the energy barrier to rotation. (See Figs. 15 and 16.)

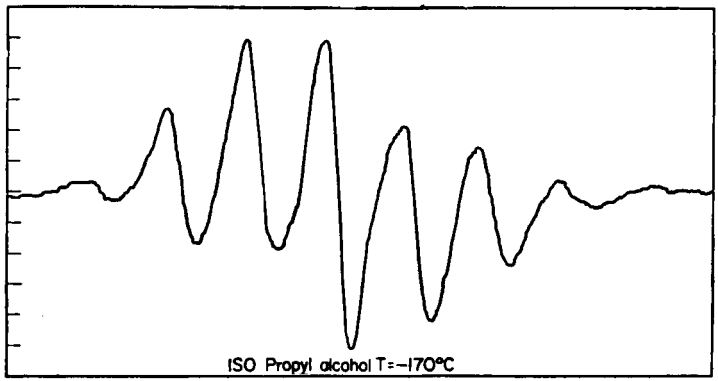

FIG. 15. Ultraviolet irradiated isopropyl alcohol at −170°C. Free rotation about the C–C bond yields the seven line pattern at −170°C.

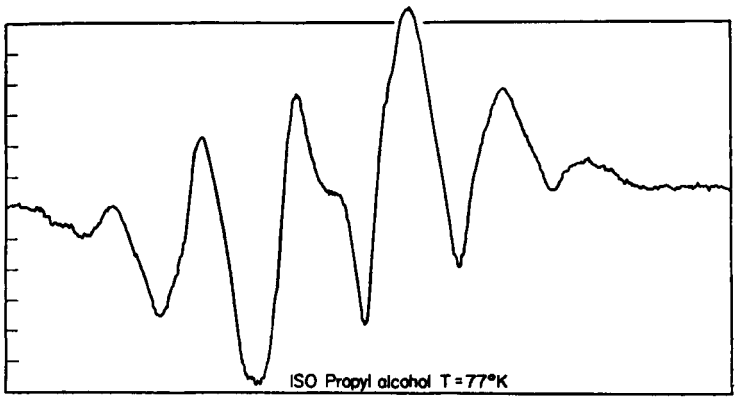

FIG. 16. Isopropyl radical stabilized at 77°K. At 77°K restricted rotation sets in and the spectrum reduces to what appears to be six lines.

It would seem reasonable that these quenching techniques could be applied to gaseous reactions such as simple detonations. One could perhaps design a shock tube in which the products formed in a detonation are quenched by rapid condensation on a cold finger at 4.2°K and then obtain the EPR spectra of the frozen intermediates.

It is quite obvious from the limited number of applications that have been mentioned here that the full potential of EPR as a tool for fundamental chemical research has certainly not been reached at this early date. The tool for the chemist is a new one and the information from it is not completely understood and therefore should be exploited to its utmost until all possible applications have been established. Only in this way can it be truly evaluated with respect to the other tools available to the chemist.

REFERENCES

1. L. M. Michaelis and M. P. Schubert, *Chem. Revs.* **22**, 437 (1938).
2. H. M. McConnell, *J. Chem. Phys.* **24**, 784 (1956).
3. D. J. E. Ingram, *Free Radicals as Studies by E.S.R.* Butterworths, London, England, 1958 Chapter 4.
4. S. I. Weissman, *J. Chem. Phys.* **25**, 890 (1956); Ward and Weissman, *J. Am. Chem. Soc.* **76**, 3612, (1954).
5. Britton Chance, "Rates and Mechanisms of Reactions", Vol. VIII, *Techniques of Organic Chemistry*, Interscience Publishers, N.Y., N.Y., 1953, Chapter X.
6. F. J. W. Roughton ibid, Chapter IX.
7. R. L. Collins, M. D. Bell and G. Kraus, *J. Appl. Phys.* **30**, 56 (1959).
8. V. V. Voedvodsky, *The Fourth International Symposium on Free Radical Stabilization.* National Bureau of Standards, 1959.
9. W. Gordy, W. B. Ard and H. Shields, *Proc. Nat. Acad. Sci.* **41**, 996 (1955).
10. K. Hotta and R. S. Anderson, *Fourth International Symposium on Free Radical Stabilization.* National Bureau of Standards, 1959.
11. D. J. E. Ingram, M. C. R. Symons and M. G. Townsend, *Trans. Am. Soc.* **54**, 409 (1958).
12. R. J. Abraham, H. W. Melville, D. W. Ovenall and D. H. Whiffen, *Trans. Far. Soc.* **54**, 1133 (1958).
13. Varian EPR at Work, No. 12.
14. C. K. Jen, S. N. Foner; E. L. Cochran and V. A. Bowers, *Fourth International Symposium on Free Radical Stabilization.* National Bureau of Standards, 1959.
15. E. L. Cochran, ibid.
16. R. Livingston, H. Zeldes and E. H. Taylor, 1955 *Disc. Far. Soc.* No. 19, p. 166.
17. M. Fujimoto and D. J. E. Ingram, *Trans. Far. Soc.* **54**, 1304 (1958).

18

THEORY OF EPR SPECTRA

ROBERT C. REMPEL
Varian Associates, Palo Alto, California

WE can begin by mentioning situations in which paramagnetism occurs. In the first place in most chemical bonding the valence electrons form closed shells. In these valence shells orbital and spin momenta cancel and the substance is diamagnetic. Exceptions occur when:

(a) Normal bonds are broken to leave unpaired electrons. Examples of this are free radicals produced by radiation damage, intermediate states in chemical reactions that occur via one electron transfer and charring of sugar and pitches.

(b) Atoms are present for which shells inside the valence shell are not filled, so that unpaired electrons are always present. These are the transition elements. The first transition group is the iron group in which the electrons start filling the $3d$ shell after the $4s$ valence electrons have filled. Other transition groups are the $4d$ palladium group, the $4f$ rare earth group, the $5d$ platinum group, and the $5f$–$6d$ actinide group.

We shall discuss in a rather simple way the basis of the paramagnetic spectrum from free radicals.

Resonance can also be observed from such things as F and V centers in alkali halide crystals, donors and acceptors in semiconductors, and cyclotron resonance in metals. It might also be mentioned that in O_2, NO, and NO_2 molecules the bonding electrons do not pair off and one can observe resonance.

In discussing electron resonance the first interaction to be considered is the Zeeman interaction. This has the form

$$\mathscr{H} = g\beta \mathbf{H} \cdot \mathbf{S}$$

where

$\beta = eh/4\pi mc$ is the Bohr magneton,
$\mathbf{H}$ is the applied magnetic field, and
$\mathbf{S}$ is the electron spin.

For the free electron g has the value 2.0023. In most free radicals g lies very close to this value, somewhere in the range 2.002 to 2.004.

The spin of the electron can be characterized by its projection, m, along the magnetic field. The energy level diagram of a free electron is shown in Fig. 1.

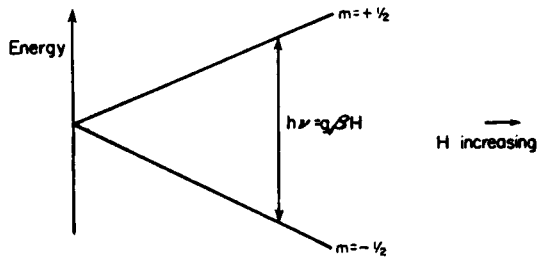

FIG. 1.

Transition can be induced between these levels by applying an oscillating magnetic field of frequency ν at right angles to the d.c. field. The relation between field and frequency for resonance of the free electron is

$$\begin{aligned}\nu &= (g\beta/h)H \\ &= H\cdot(2.8\times10^6)\ \text{c/s}\end{aligned}$$

For a field of 3300 gauss this gives a microwave frequency of about 9500 Mc.

From a chemist's point of view the next most important interaction is the hyperfine interaction. Its importance lies in the fact that it may be used to identify free radicals. The contact hyperfine interaction has the form

$$A\mathbf{I}\cdot\mathbf{S}$$

where I is the nuclear spin. The complete Hamiltonian is now

$$\mathscr{H} = g\beta\mathbf{H}\cdot\mathbf{S}+A\mathbf{I}\cdot\mathbf{S}$$

If we take H to be in the z-direction, to first order in the hyperfine interaction,

$$\begin{aligned}\mathscr{H} &= g\beta HS_z+AI_zS_z \\ &= g\beta Hm+AMm\end{aligned}$$

M, the magnetic quantum number of the nucleus has the values $-I$, $-I+1$, ..., I. m, the electronic quantum number, has the values $-S$, $-S+1$, ..., S. By writing this equation as

$$\mathscr{H} = g\beta(H+AM/g\beta)m$$

it can be seen that the hyperfine interaction is equivalent to a magnetic field $AM/g\beta$ produced on the electronic spin by the nucleus. The energy level diagram for $I = S = \frac{1}{2}$ is shown in Fig. 2.

During a resonance transition the electronic spin will change by $m = \pm 1$ while the nuclear spin is unaffected. The resonant fields of the two transitions are

$$H_1 = \frac{h\nu}{g\beta} - \frac{A}{2g\beta},$$

$$H_2 = \frac{h\nu}{g\beta} + \frac{A}{2g\beta},$$

with a field difference

$$\Delta H = \frac{A}{g\beta}$$

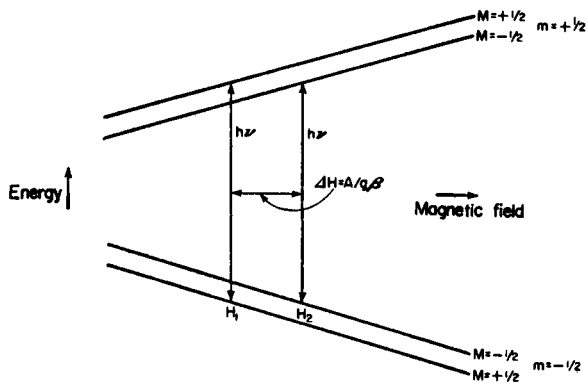

FIG. 2.

The hyperfine coupling constant A is a measure of the S character of the electronic wave function at the site of the nucleus. The hyperfine interaction, first derived by Fermi from the relativistic Dirac equation, is

$$\frac{8\pi}{3} g_I \beta_N \beta |\psi(0)|^2 \mathbf{I} \cdot \mathbf{S}$$

where β is the Bohr magneton, β_N is the nuclear magneton (1/1836th of the Bohr magneton), g_I is the nuclear g-factor, and $\psi(0)$ is the electronic wave function at the site of the nucleus. $|\psi(0)|^2$ has the dimensions of cm^{-3}. Multiplying by 10^{24} so that the electron density $|\psi(0)|^2$ is in units of $(\text{Å})^{-3}$ and dividing by $g\beta$ to put the result in equivalent gauss

$$\frac{8\pi\beta_N\beta}{3g\beta} = 21.2 \text{ gauss} - (\text{Å})^3$$

Some typical nuclear g-values are:

Nucleus	g_I
H^1	5.58
N^{14}	0.40
V^{51}	1.46
Mn^{55}	1.38

For atomic hydrogen the hyperfine constant is 508 gauss. One then finds

$$|\psi(0)|^2 = \frac{508}{21.2 \times 5.58}$$
$$= 4.3(\text{Å})^{-3}$$

In an organic free radical the hyperfine couplings from the various nuclei can be used to give information about the fraction of time the electron spends at the nuclear sites.

Figure 3 illustrates the free radical DPPH.

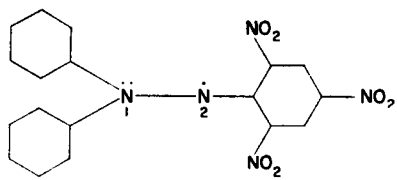

FIG. 3.

The spin Hamiltonian for this molecule is

$$\mathscr{H} = g\beta \mathbf{H} \cdot \mathbf{S} + (A_1 \mathbf{I}_1 + A_2 \mathbf{I}_2) \cdot \mathbf{S}$$

where A_1 and A_2 are the hyperfine constants for the interaction with nitrogen nuclei, 1 and 2, respectively. Hyperfine coupling with other nuclei are negligibly small. For DPPH in solution one observes the 5-line pattern of Fig. 4,

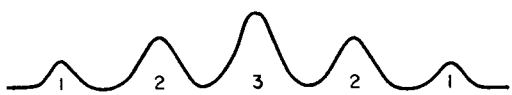

FIG. 4.

with a 1:2:3:2:1 intensity ratio and a separation of about 15 gauss between adjacent lines. The spin of N^{14} is 1. From the hyperfine interaction with each nitrogen a 3-line pattern will result. If the unpaired electron spent uneven amounts of time on the two nitrogens, nine lines would result—each hyperfine line from one N^{14} would be split into three lines from the interaction with the other N^{14}. The five-line pattern shows that the unpaired spin spends almost equal time on each nitrogen. With equal coupling the five-line pattern

is formed as illustrated in Fig. 5. Substituting in our formula, at each nucleus,

$$|\psi(0)|^2 = \frac{15}{21.2 \times 0.40}$$
$$= 1.77(\text{Å})^{-3}$$

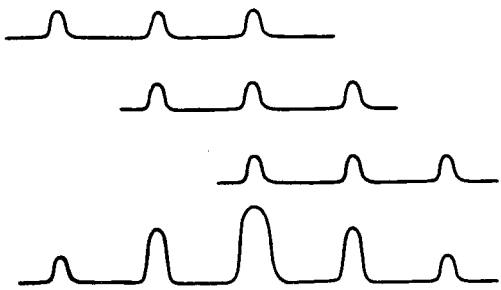

FIG. 5.

It should be pointed out that the existence of a five-line pattern implies only that the hyperfine couplings are equal to within the line width of the resonance.

As discussed previously, to observe hyperfine coupling to a nucleus it is necessary that the electron wave function be non-zero at this point. On a molecular orbital picture σ electrons have the property of a finite electron density at the nucleus for which they are centered while π electrons vanish at this point.

It would be expected that hyperfine splittings would not be observed in aromatic free radicals since the unpaired electron is in a π orbital. This π orbital gives not only zero unpaired electron density at the ring carbons, but also zero unpaired electron density at the edge protons as these lie in the plane of the ring. The observed hyperfine splitting in these radicals can be explained by configurational mixing.

Configurational mixing stems from the coulomb interaction between the ground π state and the excited molecular state. In the excited molecular state the π electron is paired against a bonding σ orbital and the unpaired spin is in an excited σ state. The observed hyperfine splitting arises from the admixture of this excited σ state.

An additional mechanism is required to account for the hyperfine splittings from methyl protons attached to an aromatic ring. Configurational mixing of the type previously discussed will give an exceptionally small, if any, unpaired electron density at the methyl protons. One configuration mixing would be required to obtain unpaired electron density at the methyl carbon; another would be required to put unpaired spin density on the protons.

Splitting from these methyl protons is due to hyperconjugation. The electron orbital on the ring proton will overlap the 1*s* electrons of the hydrogens. The coulomb interaction between these two states will then admix some of the 1*s* wave function to the wave function of the unpaired electrons. This is a direct mixing without the use of excited molecular states. Accordingly a small overlap can produce an appreciable effect. Hyperfine splittings predicted by hyperconjugation agree quite well with experiment.

As an example of a free radical in which configurational mixing and hyperconjugation must be considered, we take 2, 5, dimethyl benzo-semi quinone. This radical has the structure of Fig. 6.

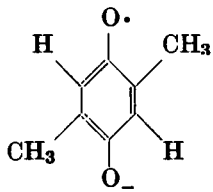

FIG. 6.

Configurational mixing places a finite unpaired electron density at the edge protons. The unpaired electron density at the methyl protons comes from hyperconjugation. Since the edge protons are equivalent, they have the same hyperfine constants and the hyperfine pattern from them will be a 1:2:1 triplet, as shown in Fig. 7. If the protons of the two methyl groups have

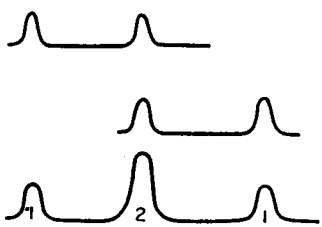

FIG. 7.

equivalent couplings, the hyperfine pattern from them will be of a seven-line pattern with a 1:6:15:20:15:6:1 intensity ratio. The final pattern will be a twenty-one line pattern with each of the three ring proton lines split into seven lines by the methyl interaction.

We have so far considered only the isotropic hyperfine interaction $\mathbf{I} \cdot \mathbf{S}$. This interaction clearly contains no angular factors and is unaffected by the orientation of the molecule with respect to the magnetic field. The other

electron–nuclear interaction to be discussed is the dipole–dipole interaction between the two spins. This interaction is

$$\mathscr{H} = \left[\frac{\boldsymbol{\mu}_e \cdot \boldsymbol{\mu}_N}{r^3} - \frac{3(\boldsymbol{\mu}_e \cdot \boldsymbol{\gamma})(\boldsymbol{\mu}_N \cdot \boldsymbol{\gamma})}{r^5}\right]$$

$\boldsymbol{\mu}_e = -g\beta\mathbf{S}$ is the electron dipole moment,

$\boldsymbol{\mu}_N = g\beta_N\mathbf{I}$ is the nuclear dipole moment, and $\boldsymbol{\gamma}$ is the vector from the electron to the nucleus.

To first order this may be written as

$$\mathscr{H} = g\beta g_N\beta_N \frac{(3\cos^2\theta - 1)}{r^3} I_z S_z$$

where θ is the angle between r and the magnetic field, **H**. To be used in the spin-Hamiltonian this interaction is averaged over the spatial wave function of the unpaired electron. Dividing by $g\beta$ to convert to magnetic field and using $\beta_N = 5.05$ gauss$-$(Å)^3, the equivalent magnetic field at the electron is

$$H_{\mathrm{dd}} = 5.05\, g_N \left\langle \frac{3\cos^2\theta - 1}{r^3} \right\rangle I_z$$

where $\langle(3\cos^2\theta - 1)/r^3\rangle$ is averaged over the wave function and r is in (Å). This is often called the anisotropic hyperfine interaction.

For a proton

$$H_{\mathrm{dd}} \sim 28\langle 1/r^3\rangle \text{ gauss}$$

It can be seen that for r of the order of 1 Å this anisotropic hyperfine is the same order of magnitude as typical isotropic hyperfine splittings in organic free radicals.

In a rigid polycrystalline or amorphous lattice all orientations will occur with equal probability. As shown by Andrew, under these conditions the coupling with a proton will give a double peaked line with a separation between peaks of 28 $\langle 1/r^3\rangle$ gauss. Other sources of broadening usually mask these peaks, especially when the system contains more than one proton, and the net effect is a considerable broadening of the individual hyperfine lines. This broadening and loss of detail from anisotropic hyperfine interactions should be kept in mind when attempting to identify free radicals produced by radiation damage in solid lattices which are not single crystals.

In a liquid the nuclear relaxation time is much longer than the tumbling period of the molecule. I_z is a constant and

$$H_{\mathrm{dd}} = 5.05\, g_N I_z \left\langle \frac{3\cos^2\theta(t) - 1}{3} \right\rangle$$

$\theta(t)$ is a random function which, on the average, varies by one radian in a correlation time τ_c. The corresponding correlation, or tumbling, frequency is

$\nu_c = 1/(2\pi\theta_c)$. $3\cos^2\tau - 1$ averaged over all solid angles is zero. When the tumbling frequency ν_c becomes comparable to the static anisotropic hyperfine spread of $g\mu\beta_N\langle 1/\gamma^3\rangle$, expressed in frequency units, the anisotropic splitting will start to collapse. For tumbling frequencies much larger than the static anisotropic spread, the line will be markedly narrowed. The motional narrowing discussed here is virtually the same as that experienced in NMR, the only difference being that the field splitting must be related to frequency through the Bohr magneton instead of the nuclear magneton.

Another effect very much akin to motional narrowing is exchange narrowing. With hydrazyl (DPPH) in solution it is found that, as the concentration is raised, the lines broaden and run together. In crystalline hydrazyl only a single narrow line appears. The overlap of unpaired electron wave functions from adjacent DPPH molecules leads to electron exchange between the two molecules. As the DPPH concentration is raised to the point where the average exchange frequency is comparable to the hyperfine splitting, the structure starts to collapse. In the solid the exchange frequency is very high, probably of the order of 10^{10} c/s, and a very narrow single line is observed. In exchange narrowing the electron resides on a large number of DPPH molecules in a time corresponding to the reciprocal of the hyperfine angular frequency. The electron sees all possible nuclear orientations in this time and, since the average of the hyperfine interaction over all these orientations is zero, all structure is removed.

The last point to be discussed is the calculation of paramagnetic intensity or (number of spins) from this first harmonic presentation given at the phase detector.

The waveform from the microwave detector due to the sinosoidal magnetic field sweep is graphically depicted in Fig. 8 coming out to the right. The signal from the phase detector is given by the first harmonic content of this waveform.

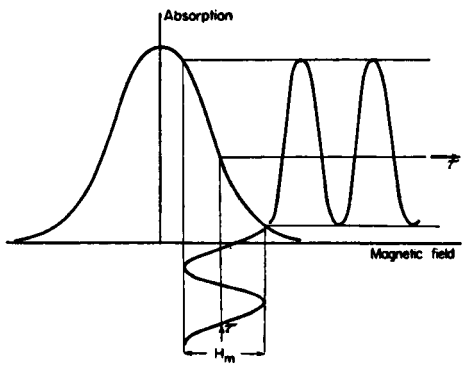

FIG. 8.

The paramagnetic intensity is determined by the area under the absorption curve. For very small signal amplitudes the spectrometer output is proportional to the derivative of the absorption curve. Resonance intensity may then be obtained by a double integration of the output curve. For maximum sensitivity, however, one would like to use a sweep amplitude comparable to, or slightly greater than, the line width. In this case the output is clearly not proportional to the derivative of the absorption curve and a double integration of the output curve will not give the correct intensity.

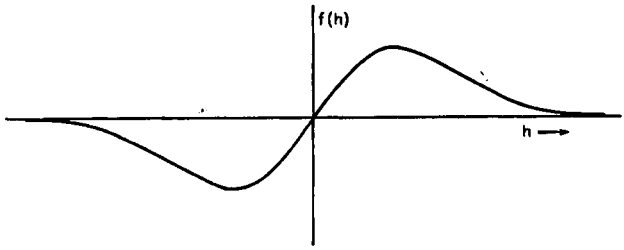

FIG. 9.

Andrew has shown that, without any approximation, the first moment of the output curve is proportional to the product of intensity and sweep field. Let $f(h)$ be the output curve, where h is the magnetic field measured from the center of the resonance. (See Fig. 9.) The first moment is

$$M_1 = \int_{-\infty}^{+\infty} hf(h)\,\mathrm{d}h$$

and the intensity is given by

$$\text{Intensity} = \frac{KM_1}{H_m}$$

where H_m is the amplitude of the field modulation and K is some constant.

19

BIOLOGICAL APPLICATIONS OF EPR

R. H. SANDS

Department of Physics, The University of Michigan, Ann Arbor, Michigan

IN recent months the applications of EPR to biochemical problems have shown a marked increase of successes. These and other biological applications are reviewed and critically discussed.

For an understanding of Electron Paramagnetic Resonance (EPR) Spectrometry the author recommends several books and two excellent review articles together with the Technical Information Bulletins of Varian Associates[1-5].

Unfortunately not all atoms and molecules of interest are susceptible to study by this new technique. They must exhibit a resultant electronic magnetic moment. Of these, there are four classes of compounds that are of particular biological interest: (a) odd molecules and free radicals, (b) biradicals, (c) triplet electronic states, and (d) transition element ions. The first three classes might well be expected to occur biologically in (a) univalent redox reactions, (b) enzymatic oxidations (dehydrogenations) (c) radiation damage and (d) photosynthesis.

For the past quarter of a century, the idea has been current that free radicals may participate in biological processes. As far back as 1931, Haber and Willstatter[6] proposed that a great majority of enzymatic dehydrogenations involved free radical intermediates. In reviewing the history of this one-electron transfer hypothesis in biological oxidations, it is of interest to note that most of the reactants in the metabolic redox systems are even molecules; that is, all electrons occur in pairs. It certainly is within reason to expect then that all electron transfers among these molecules would occur in pairs; however, there exist several instances where the chain of electron transport has as one of its links a substance, such as cytochrome, which can transfer but one electron under oxidation or reduction. These substances are the metallo-organics. Clearly then, there must exist certain molecules which proceed in their two electron transfer by one-electron steps.

It is at this juncture in biochemistry that Michaelis made his now famous proposal "that all oxidations of organic molecules, although they are bivalent, proceed in two successive univalent steps, the intermediate state being a free radical"[7]. Perhaps for the sake of rigor one should understand the term "odd

molecule" here, rather than "free radical", but in either event the implication is clear.

The validity of this proposal is subject to experiment, and it is to Michaelis's credit that he supported it experimentally as well as he did. Spectrophotometric kinetic studies have indicated intermediaries between the fully reduced and the fully oxidized states of various biologically active substances which acted like free radicals. Unfortunately, however, until the advent of electron paramagnetic resonance, the only recourse for direct proof was to static susceptibility measurements which at their best could detect no less than 10^{-6} moles. (Recently Brill[8] at the University of Pennsylvania has perfected a static balance capable of detecting 10^{-7} molar solutions of paramagnetic molecules.) Whereas some occasional studies, such as those of Pauling, Coryell *et al.*[9] on the magnetic susceptibility of hemoglobin, have been of great value, little has been accomplished in checking Michaelis's assumption due to this low sensitivity. EPR has aided by increased sensitivity in many cases, and has made a much greater contribution by distinguishing among paramagnetic ions, odd molecules and free radicals.

Much work has been performed with EPR on the non-enzymatic oxidation reductions of the simpler biologically occurring quinone and quinoid compounds,[10] and it may be concluded that these compounds pass through two successive one-electron transfer processes on their way to the final state. Furthermore the lifetime of the paramagnetic semiquinone radical is dependent upon the isomeric form in agreement with observed differences in the oxidation potentials, and also upon the pH of the solution (the free radical produced by dehydrogenation of the hydroxyl group is stabilized in alkaline solution, while that from dehydrogenation of the amino group is stabilized in acid solution). A partial list of the compounds yielding observable free radical concentrations is tabulated in Table 1.

TABLE 1. A PARTIAL LIST OF SYSTEMS IN WHICH FREE RADICALS HAVE BEEN OBSERVED UNDER REDOX EQUILIBRIUM

p-benzoquinone	homogentrisic acid	phenanthrene quinone
o-benzoquinone	polyporic acid	phenophthalein
catechol	tocopherol	ascorbic acid
pyrogallol	1,5 naphthalenediol	nicotinic acid
gallic acid	1,4 naphthoquinone	p-phenylene diamine
quaiacol	1,2 naphthoquinone	p-aminophenol
arsinol	juglone	benzidine
resorcinol	menedione	diacetyl (see V. A. *EPR at Work*, n. 13)
4-ethyl resorcinol	vitamin K_1	benzil
4-propyl resorcinol	vitamin E	ninhydrin
4-butyl resorcinol	phthiocol	riboflavin
4-amyl resorcinol	anthraquinone	FMN
4-hexyl resorcinol	anthraquinone β-sulfonic acid	
2-nitro resorcinol	alizarin	indigo
gentrisic acid	carminic acid	adrenaline

At this point, the question of polymerization arises. If the lifetime of the free radical intermediate is sufficiently short, the probability of a given polymeric reaction is quite small. This can be seen by studying the parabenzoquinone redox reaction shown in Fig. 1. At pH 7 no polymeric side product is

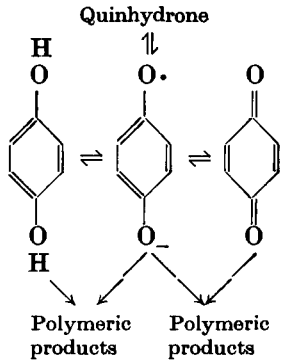

FIG. 1. Quinone–hydroquinone redox reaction.

detectable, but at pH 8 a color change belies these side reactions and at pH 9 a dark brown precipitate appears which is very similar to the melanin pigments. This is the subject of Varian Associates' *EPR at Work*, Numbers 2, 3 and 4 of a Series.

The control of such free radical reactions by a biological system may thus be performed by both pH and antioxidants. The role of antioxidants is a subject in itself, and their activity in biological systems is of even more interest because of the problem of radiation damage. The antithesis of this effect is produced by radiosensitizers which are good oxidants; e.g. O_2, quinones, etc. Furthermore, those organics that form active free radicals upon reduction are particularly good as sensitizers, suggesting the role of free radicals in radiation damage. The experiments to verify this latter role are few; however, considerable effort is currently being devoted toward this end, and the results will be of great interest. The following early experiment was one which demonstrated free radical production as a secondary process in radiation damage: 10^{-5} M riboflavin was reduced by ethyl alcohol radicals formed by reaction with OH and H radicals produced by 650 kV X-rays on the water–3 per cent alcohol–riboflavin mixture. Experiments such as those reported by Gordy *et al.*[11] if carried to a proper conclusion may offer support here also. In regard to antioxidants, one notes that they often operate by forming dimers, thus reducing the free radical concentration by two with each dimer; e.g. cysteine (a sulfahydril) going to

cystine (a disulphide). An excellent monitor of antioxidant level may be obtained by titrating against a standard free radical solution and using EPR as a detector. Blois *et al.*[12] have had wonderful success using optical absorptions of such solutions as quantitative measures of reduced free radical and hence antioxidant concentrations. It is interesting to note that such measures may prove to be unique radiation dosage monitors. More research needs to be done on the clinical applications of EPR than is being done at the present time.

The sensitivity of EPR makes possible the observation of free radical intermediates *in vivo*. This has far-reaching implications; however, experiment is slow, largely due to the need for technological developments along the way. Toward this end the first experiments were those of Commoner *et al.*[13] with lyophilized samples. Signals were obtained for a great variety of samples including yeast, blood, rabbit organs, germinated digitalis seeds and barley leaves. As is often the case with preliminary work, many of the signals were false in the sense that they were due to paramagnetic ions or physical damage due to freeze drying and not to metabolically active free radicals.[14] Nevertheless, the simple fact that signals were observed was sufficient to stimulate further effort, and some beautiful results have been forthcoming. Before discussing these, it is perhaps well to give an example of the possible damage that can result from freeze drying. The spectrum recorded from whole human blood is reproduced in the Varian Associates', *EPR at Work*, No. 8 of a Series; this reveals the partial conversion of hemoglobin to methemoglobin and the physical damage to both molecules by the lyophilization. In addition one records a free radical signal apparently associated with the snapping open of the porphyrin ring structures of the hemoglobins.

One of the most intriguing biochemical processes is that of photosynthesis —the conversion of photo-energy to chemical energy. Since this process clearly involved oxidation-reduction steps, it is possible that EPR may help answer some of the questions. The question of greatest concern is whether the initial molecule is an excited one or a free radical or an ionized species and whether the process is a single or multiple quantum one. Calvin and Sogo[15] and Commoner *et al.*[16] made preliminary EPR studies on the chlorophyll system. Light sensitive signals were observed. In attempts to identify the source of the EPR signal, Sogo, Pon and Calvin[17] and Tollin and Calvin[18] have reported some excellent work. They have shown by kinetic studies under various conditions of sample preparation and temperature, that the initial species responsible for the magnetic resonance is not likely to be either a triplet state of chlorophyll or a free radical intermediate in the following chain of enzyme reactions. Their conclusion is that it is most likely a trapped electron residing on the chlorophyll molecule which renders this molecule a semiconductor of sorts. This would be consistent with previous assertions

by Bradley and Calvin[19] and independently by Katz that a semiconductor state is probable.*

Some progress has been made in examining enzymatic oxidation-reduction reactions by EPR. Again free radicals have been observed—originally by Beinert[20], Commoner *et al.*[16], Ehrenberg and Ludwig[21], and Malmstrom *et al.*[22] The early work of Beinert has shown that the signals observed for a particular two flavin enzyme, fatty acyl (CoA) dehydrogenase, are not associated with the primary enzyme-substrate reaction but rather occur on reoxidation of the enzyme-substrate complex by molecular oxygen. This situation might or might not prevail with the other double flavin enzymes and much careful work is required here to clarify matters. Beinert also has been able to show by comparison with optical kinetics that radicals observed on a particular single flavin enzyme, cytochrome reductase, are probably intermediates in the enzyme substrate reaction itself. No direct proof of this has been attempted for other systems to date.†

One of the most important questions in enzyme chemistry is that of the role of paramagnetic ions in enzymatic reactions. Preliminary results have been reported by several authors with more complete descriptions to follow. This appears to be one place where EPR is providing much needed answers that cannot be obtained by any other means. Bray *et al.*[23] have reported monitoring molybdenum in xanthine oxidase reactions although they do not mention the oxidation state observed. Malmstrom *et al.*[24] report detecting Mn^{++} in enolase reactions and Malmstrom *et al.*[25] have studied Cu^{++} in laccase. Nakamura and Brill[26] have had similar results on laccase with the Rankine balance.[8] Beinert and Sands[27] have studied Cu^{++} in cytochrome oxidase. Figure 2 displays the kinetic results for both the optical and EPR studies. These authors also have investigated the role of Fe^{+++} in cytochrome

*Further work by Tollin *et al.*[30] and Sogo *et al.*[31] has been reported, as well as some recent work by Allen, Piette and Murchio[32], on other photosynthetic pigments. This work covered such systems as *chlorella pyrenoidosa*, non-photosynthetic *chlorella*, the blue-green alga *anabaena cylindrica* and the non-sulfur purple bacterium *rhodopseudomonas palustris*. The work by Allen *et al.* is particularly significant in that it was done under favorable physiological conditions and demonstrated that the action spectra for the free radical production corresponded to that for photosynthesis within experimental error.

Some recent research on free radicals in photodynamic systems has been reported by Smith, Santamaria and Smaller[33]. The model system used was 1.2×10^{-3} M hematoporphyrin (sensitizer) and human blood serum (substrate) diluted 1:3 in phosphate buffer at pH 7.3. The samples were irradiated with light from a high-pressure mercury arc at −20°C and at −196°C. EPR signals were produced and photodynamic action proceeded only in the presence of oxygen and hematoporphyrin. Both processes were inhibited when ascorbic acid or cysteine was introduced. From these and other results it was proposed that an initial triplet state of hematoporphyrin was formed by light absorption and this state combined with oxygen to form an oxyradical which could then react with the substrate to produce sensitizer and oxidized substrate.

†Since the preparation of this manuscript additional research has been reported by Kubo *et al.*[34], Nakamura[35], and Yamazaki *et al.*[36].

reductase.[28] They have demonstrated that no free radical signal appears on reduction with DPNH until after all of the iron (28 per cent) has been reduced. Since DPN was shown to drive the reaction in reverse to produce the radical but not the iron, it was their tentative conclusion that the electron flow sequence went substrate → flavin → iron. Whether the iron is an intermediary in the interaction with other electron acceptors is still open to question and EPR may be able to provide the answer.*

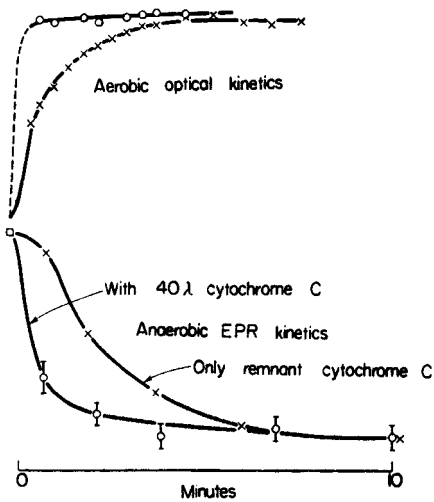

FIG. 2. Optical and EPR kinetics for cytochrome oxidase–ascorbic acid system.

The whole problem of carcinogenesis is still open for study. In an attempt to correlate the action of such a variety of carcinogenic agents as sodium hydroxide, ultraviolet and ionizing radiations and thousands of organic compounds, a free radical intermediate always suggests itself. Smog studies and recent work by Lyons *et al.*[29] point up the high active radical content of soot and tobacco smoke and their possible connections with lung cancer although no direct proof seems to exist to date.

*Similar studies[37] on succinic and DPNH dehydrogenase reveal EPR signals stemming from what is presumably a paramagnetic ion in the enzyme, which has not been identified. The signal remains unexplained to date and may be quite significant in understanding the mechanism of the reaction. In addition Fe^{+++} and free radical signals were observed and followed in both enzyme–substrate systems, although the Fe^{+++} did not seem to participate in the succinate reaction.

Mitochondria and submitochondrial particles have been studied by Commoner and Hollocher[38], [39], and by Beinert and Sands[40]. The latter investigators have shown that the same signals observed for succinic and DPNH dehydrogenase (reported above) are to be observed in the mitochondria. Both of the above researches add credence to the belief that these EPR signals are fundamental to the enzyme–substrate reactions under physiological conditions.

In summary one may say that free radicals have been implicated in
(a) biological oxidation-reduction reactions,
(b) radiation damage and photosynthesis, and perhaps
(c) carcinogenesis.

Electron paramagnetic resonance has brought sufficient sensitivity and discrimination to observe free radical intermediates directly in many of these reactions; however, present results are of a preliminary nature and the validity of certain published conclusions is subject to more careful study. Much work remains, and EPR will serve as a unique and powerful tool in such investigations.

REFERENCES

1. E. R. Andrew, *Nuclear Magnetic Resonance*, Cambridge University Press.
2. J. E. Wertz, *Chem. Rev.* **55**, 829 (1955).
3. G. E. Pake, *Advances in Solid State Physics*, Vol. II, Chapter I, ed. F. Seitz, Academic Press, 1956.
4. Technical Information Bulletin, Vol. 1 and 2, Varian Associates, Palo Alto, California.
5. D. J. E. Ingram, *Spectroscopy at Radio and Microwave Frequencies*, Butterworths (1955); and D. J. E. Ingram, *Free Radicals as Studied by Electron Spin Resonance*, Academic Press, 1958.
6. F. Haber and R. Willstatter, *Ber. Deut. Chem. Gesell.* **64B**, 2844 (1931).
7. L. Michaelis, in *Currents in Biochemical Research*, ed. S. E. Green, Interscience, New York, 1946.
8. A. S. Brill, H. derHartog, and V. Legallais, *Rev. Sci. Inst.* **29**, 383 (1959).
9. L. Pauling and C. D. Coryell, *Proc. Nat. Acad. Sci.* **22**, 159–210 (1936).
10. M. S. Blois, Jr., and R. H. Sands, "Free Radicals and Biological Systems", *Proceedings First Annual Conference of the Biophysical Society*, Columbus, Ohio (1957).
    M. A. Adams, M. S. Blois, Jr., and R. H. Sands, *J. Chem. Phys.* **28**, 1744 (1958).
    M. S. Blois, Jr. and J. E. Maling, *Biochem. and Biophys. Res. Comm.*, in press.
11. W. Gordy, W. B. Ard and H. Shields, *Proc. Nat. Acad. Sci.* **41**, 983–996 (1955).
12. M. S. Blois, Jr., *Nature* **181**, 1199 (1958).
13. B. Commoner, J. Townsend and G. E. Pake, *Nature* **174**, 689 (1954).
14. R. H. Sands, H. E. Weaver and P. A. Franken, "Paramagnetic Ions in Blood Sera", *Proceedings First Annual Conference of the Biophysical Society*, Columbus, Ohio (1958).
15. M. Calvin and P. B. Sogo, *Science* **125**, 499 (1957).
16. B. Commoner *et al.*, *Proc. Nat. Acad. Sci.* **42**, 710 (1956).
    B. Commoner *et al.*, *Science* **126**, 57 (1957); B. Commoner *et al.*, *Proc. Nat. Acad. Sci.* **44**, 1099 (1958); B. Commoner and B. B. Lippincott, *Proc. Nat. Acad. Sci.* **44**, 1110 (1958).
17. P. B. Sogo, N. G. Pon and M. Calvin, *Proc. Nat. Acad. Sci.* **43**, 387 (1957).
18. G. Tollin and M. Calvin, *Proc. Nat. Acad. Sci.* **43**, 895 (1957).
19. D. F. Bradley and M. Calvin, *Proc. Nat. Acad. Sci.* **41**, 8, 563 (1955).
20. H. Beinert, *J. Biol. Chem.* **225**, 465–478 (1957).
21. A. Ehrenberg and G. D. Ludwig, *Science* **127**, 1177 (1958).
22. B. Malmstrom *et al.*, *Nature*, in press.
23. R. C. Bray *et al.*, *Biochem. J.* **71**, 24 (1959); **73**, 193 (1959).
24. B. Malmstrom *et al.*, *Biochem. et Biophys. Acta* **30**, 1 (1958).
25. B. Malmstrom *et al.*, *Nature* **183**, 321 (1959).
26. T. Nakamura and A. S. Brill, *Fed. Proc.* **18**, 292 (1959).
27. R. H. Sands and H. Beinert, *Biochem. and Biophys. Res. Comm.* **1**, 175 (1959).

28. H. BEINERT and R. H. SANDS, *Biochem. and Biophys. Res. Comm.* **1**, 171 (1959).
29. M. J. LYONS *et al.*, *Nature* **181**, 1003 (1958).
30. G. TOLLIN, P. B. SOGO and M. CALVIN, *Ann. N.Y. Acad. Sci.* **74**, 310 (1958).
31. P. SOGO, M. JOST and M. CALVIN, *Rad. Research suppl.* **1**, 511 (1959).
32. M. B. ALLEN, L. H. PIETTE and J. C. MURCHIO, to be published.
33. D. E. SMITH, L. SANTAMARIA and B. SMALLER, *Proc. Symposium on Free Radicals in Biological Systems*, Academic Press, 1960.
34. H. KUBO, H. WATARI and T. SHIGA, *Bull. Soc. Chim. Biol.* **41**, 981 (1959).
35. T. NAKAMURA, *Biochem. and Biophys. Res. Comm.* **2**, 111 (1960).
36. I. YAMAZAKI, H. S. MASON, and L. H. PIETTE, *Biochem. and Biophys. Res. Comm.* **1**, 336 (1959).
37. HELMUT BEINERT and R. H. SANDS, *Biochem. and Biophys. Res. Comm.*, **3**, 41, (1960).
38. B. COMMONER and T. C. HOLLOCHER, Jr., *Proc. Nat. Acad. Sci.* **46**, 405 (1960).
39. T. C. HOLLOCHER, Jr., and B. COMMONER, *Proc. Nat. Acad. Sci.* **46**, 416 (1960).
40. R. H. SANDS and HELMUT BEINERT, *Biochem. and Biophys. Rec. Comm.*, **3**, 47, (1960).

20

PHOTOCHEMICAL STUDIES WITH EPR

LAWRENCE H. PIETTE
Varian Associates, Palo Alto, California

FREE radicals have long been known to play an important role in photochemical processes. A number of methods have been used to elucidate information as to their exact role. The techniques used range anywhere from elaborate "trapping" and "flashing" methods to simple product analyses.

The "trapping" technique yields information on free radical formations in the solid state and involves dissolving the photosensitive compound of interest in a suitable solvent which is photo-insensitive. The two are irradiated at a temperature low enough to stabilize any free radicals but high enough to produce sufficient mobility so as not to inhibit their initial formation. Once stabilized, an optical absorption is made of the free radical intermediates.

Flash photolysis is probably the most powerful of all the techniques since it yields more detailed information and, unlike the trapping technique, is not limited by any sort of solubility problem. The only real limitation on flash photolysis is that it can only be applied to gaseous systems. This method involves making two rapid flash discharges on the gaseous system of interest. The first flash of very high intensity serves to decompose the gases and is of very short duration, 10^{-4} seconds; the second flash of much lower intensity serves to record the optical absorption of the intermediates formed by the first flash. By changing the time intervals of the second flash, rate data is obtained on the intermediate life times.

Probably the most widely used method for studying photochemical reactions is the "product analysis" method. This method can be used on any system and merely involves analyzing all the products formed in a photochemical reaction. Once the products are known, one works backwards to infer what free radical intermediates would have been formed in order to give the products obtained.

With the development of EPR spectroscopy another method for studying photochemical reactions that is potentially the most powerful tool available for such studies is added to the above mentioned procedures. EPR is an especially advantageous approach since it will only respond to systems containing unpaired electrons, such as free radicals, and therefore the identification

of their existence as intermediates in photochemical reactions is inherent in its basic operation. The technique is more versatile than the others in that it can be applied to gaseous, liquid, or solid systems over a large range of temperatures.

The sensitivity, response and temperature variation features of the technique make it most adaptable for studying photochemical reactions in the steady or dynamic state. Using a highly sensitive EPR spectrometer, it is now possible to conduct direct ultraviolet irradiations *in situ* and simultaneously measure the steady state concentration of the free radical intermediates formed. The identification of these free radical intermediates can very often be inferred from their characterisitic hyperfine patterns. Establishing sufficient steady state concentrations which can be observed is achieved by suitable adjustment of the rate of formation and/or the rate of decay of these intermediates. The decay rate is the simplest parameter to adjust and is accomplished by a simple temperature variation, provided the decay reaction has a finite activation energy.

Once a steady state is established, the reaction kinetics become extremely simplified. Rate constants and activation energies for the decay reaction are obtained directly from the steady state approximation of the rate expression.

If we assume that the formation of the intermediate in the photochemical process and its subsequent decay follows a simple first order reaction, the following rate expressions can be written:

$$h\nu + A \rightarrow A^* \tag{1}$$

$$A^* \xrightarrow{k} \text{products} \tag{2}$$

$$\frac{\mathrm{d}A^*}{\mathrm{d}t} = -k(A^*) + u \tag{3}$$

where u is the rate of formation of A^* and is dependent upon our photolysing source. At the steady state $\mathrm{d}A^*/\mathrm{d}t = 0$ and the steady state approximation becomes

$$k(A^*)_s = u \tag{4}$$

We can measure $(A^*)_s$ and u experimentally, and then solve for k.

Substituting k in the Arrhenius expression we obtain

$$\frac{u}{(A^*)_s} = v_0 \exp(-E_a/RT) \tag{5}$$

$$-\ln\frac{u}{v_0} + \ln(A^*)_s = E_a/RT \tag{6}$$

Thus, a plot of $\ln(A^*)_s$, the steady state concentration of the intermediate, against $1/T$, yields a straight line, the slope of which is E_a/R. Thus, it can be seen that steady state photochemical systems studied by EPR can yield a wealth of information.

We have applied this method quite successfully to some basic studies on the photodissociation of primary, secondary and tertiary butyl hydroperoxides.[8] The steady state free radical intermediates in each case were identified and their rates of decay measured at various temperatures.

The direct irradiations and temperature variation were accomplished by using an EPR spectrometer equipped with a 100 kc field modulation system. The 100 kc field modulation improved the sensitivity of the spectrometer by a factor of 16 over that of the 400 c/s instrument we had previously used. This enhancement of sensitivity is essential in observing the n-butyl hydroperoxide steady state intermediate. The cavity contains radiation slots which permit the entry of ultraviolet with negligible effects on the cavity microwave properties. (See Fig. 1.) The cavity contains special sample ports which

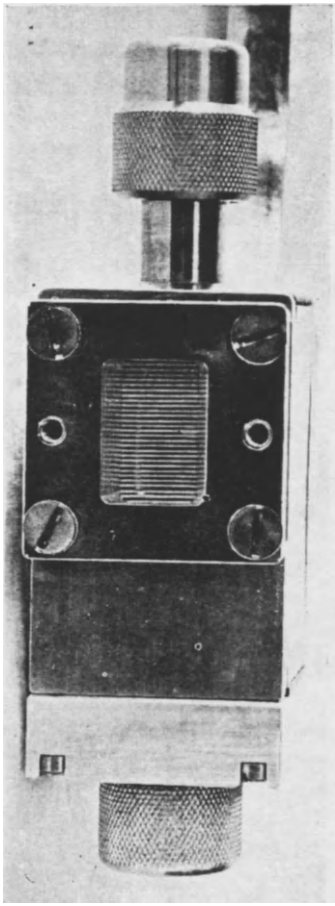

FIG. 1. 100 kc field modulation microwave cavity with slots for direct photo irradiation.

permit the insertion of an 11 mm o.d. open ended quartz Dewar insert. Temperature variation and control is achieved by using a simple heat exchanger system. Dry nitrogen is passed through a copper coil, immersed in liquid nitrogen, and conducted through a Vycor transfer tube, with contained heater, to the quartz Dewar insert. The cooling gas passes around the quartz sample tube and is exhausted through the top of the cavity Dewar. (See Fig. 2.) Temperature control is achieved by varying the flow rate of the cool-

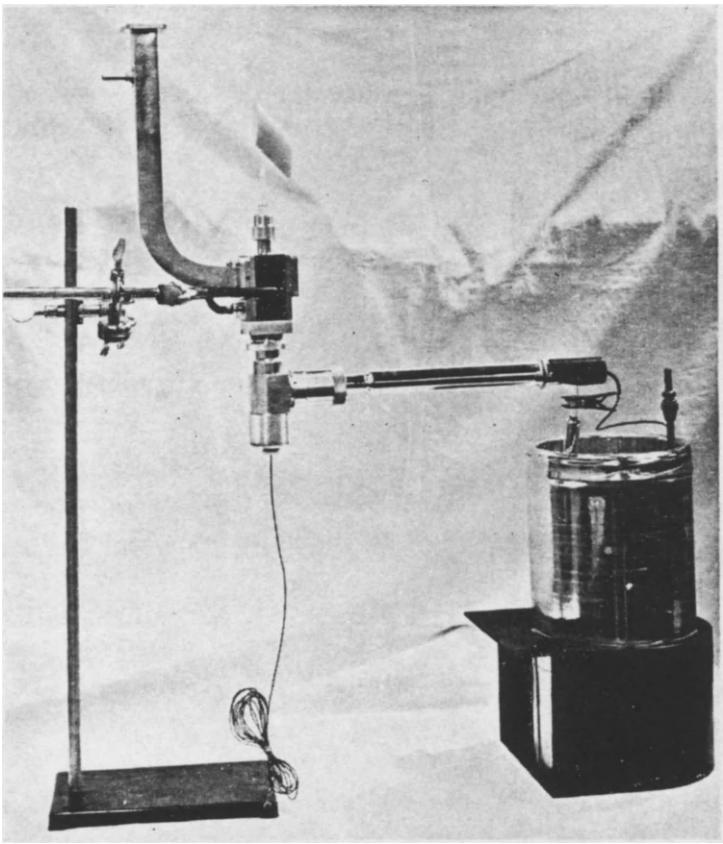

FIG. 2. Temperature flow apparatus for varying and controlling the temperature over the sample. System is shown out of the magnet.

ing gas and controlling the heater current. A simple G.E. medium pressure mercury lamp, H85C3, is used as the ultraviolet source. The ultraviolet radiation is focused on the cavity slots by means of an aluminized parabolic mirror. The entire system is contained in an aluminum box with an attached aluminum leaf shutter so that the light can be rapidly extinguished. Rapid decay rates are displayed on a Sanborn Model No. 151 recorder.

Electron resonance spectra of the steady state free radicals produced in the photolysis of n-butyl, sec-butyl and t-butyl hydroperoxide are illustrated in Fig. 3. These spectra are interpreted from the hyperfine pattern observed and from a consideration of the possible free radicals that can be formed in the dissociation.

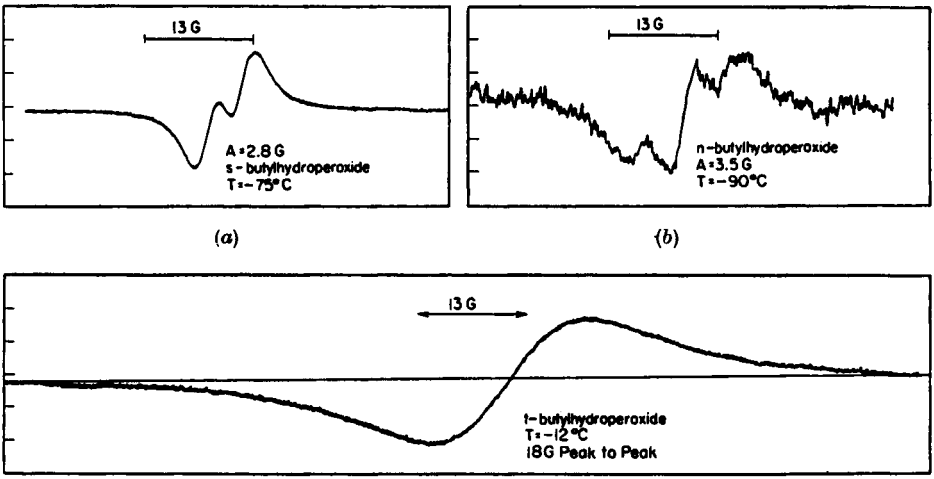

FIG. 3. *a*. Steady state n-butoxy free radical produced by ultraviolet irradiation at $T = 183°K$. A = hyperfine coupling.

b. Steady state sec-butoxy free radical at $T = 203°K$. A = hyperfine coupling.

c. Steady state t-butoxy free radical at $T = 270°K$. A = hyperfine observed. In each case the center of resonance did not deviate from $g = 2.003$ for DPPH.

From simple bond energy considerations alone, the photo-induced dissociation would be expected to take place at the O—O bond, yielding the alkoxy and the hydroxy radical. The possible formation of alkyl R· and $\cdot HO_2$ radicals by rupture at the C—O bond cannot be ignored completely. Ingram *et al.*,[1] produced such alkyl radicals at 77°K in peroxide–alcohol solutions as a result of ultraviolet irradiation. In addition, the possible production of peroxy ROO· and hydrogen radicals cannot be ignored, even though the bond energy of the O—H bond is greater.

If alkyl radicals are formed in the steady state, the n-butyl radical $CH_3CH_2CH_2CH_2\cdot$ so formed would be expected to give a hyperfine pattern of possibly three lines, each of which is further split into three more lines, for a total nine line pattern, or alternatively, if the α and β methylene protons are equivalent (α and β to the oxygen in the hydroperoxide), five equally spaced lines would be obtained. The sec-butyl alkyl-radicals $CH_3\dot{C}HCH_2CH_2$

could possibly yield seven equally spaced lines as a result of the coupling with the five equivalent β carbon protons and the proton on the α carbon. Finally, the t-butyl radicals

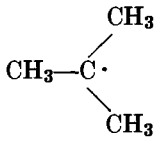

could conceivably give a ten line pattern as a result of coupling with all nine equivalent β protons. In each case, the expected hyperfine couplings in these alkyl-radicals would be 20 to 30 gauss, as have been observed for alkyl radicals stabilized by other techniques.[2–4] If alkoxy radicals RO· are formed in each case, however, it would be expected that the unpaired electron density at the α and β carbons would be attenuated by the oxygen and would therefore have a reduced value at the α carbon proton and a negligible value at the β carbon. The attenuation at the α carbon could conceivably be an order of magnitude and, as a consequence, a simple triplet would be anticipated in the n-butoxy, a doublet for the sec-butoxy, and a single line for the t-butoxy radical, with coupling constants of 2 to 3 gauss. If peroxy radicals ROO· were formed in each case, the unpaired electron density of the α carbons might be further attenuated by the second oxygen another order of magnitude and no hyperfine interaction with any of the protons on the α or β carbons would be resolved.

A triplet has been observed with a hyperfine coupling of 3.5 gauss for the n-butyl case, a doublet of 2.8 gauss for the sec-butyl and a single line for the t-butyl and therefore these steady state free radicals are identified as the alkoxy radicals. A resonance for the hydroxy radical which would have been produced simultaneously with the alkoxy radical was not observed. It would be expected that the lifetime of the hydroxy radical is far too short at the temperatures at which these experiments were conducted, and hence would not be observed.

In order to decrease the decay rate of the n-butoxy radicals sufficiently to create an observable steady state concentration, it was necessary to operate at temperatures in the vicinity of 175°K. The sec-butoxy radicals require temperatures below 230°K and the t-butoxy radicals require temperatures below 273°K. These steady state temperatures reflect the decreased order of reactivity of these radicals, i.e. n-botoxy > sec-butoxy > t-butoxy.

Rate studies of the decay process can be made on the three free radicals observed by merely measuring the time rate of decay of these signals when the ultraviolet lamp is extinguished. Figure 4 represents typical decay curves. The decay curves were found to fit a second order dependence very nicely, and this was checked by varying the initial steady state concentration two or three fold. Rate constants of approximately 10^5 l/m sec were obtained for

the recombination of two alkoxy radicals. The decay rates were also obtained from the steady state approximation, equation (4).

The steady state concentration can be measured by comparing the first moment of the resonance lines of the sample with the first moment measured for a known concentration of aqueous vanadyl ion. U, the rate of formation of the free radicals as determined by the lamp intensity, was obtained by lowering the temperature to a value at which the decay rate was negligible and by

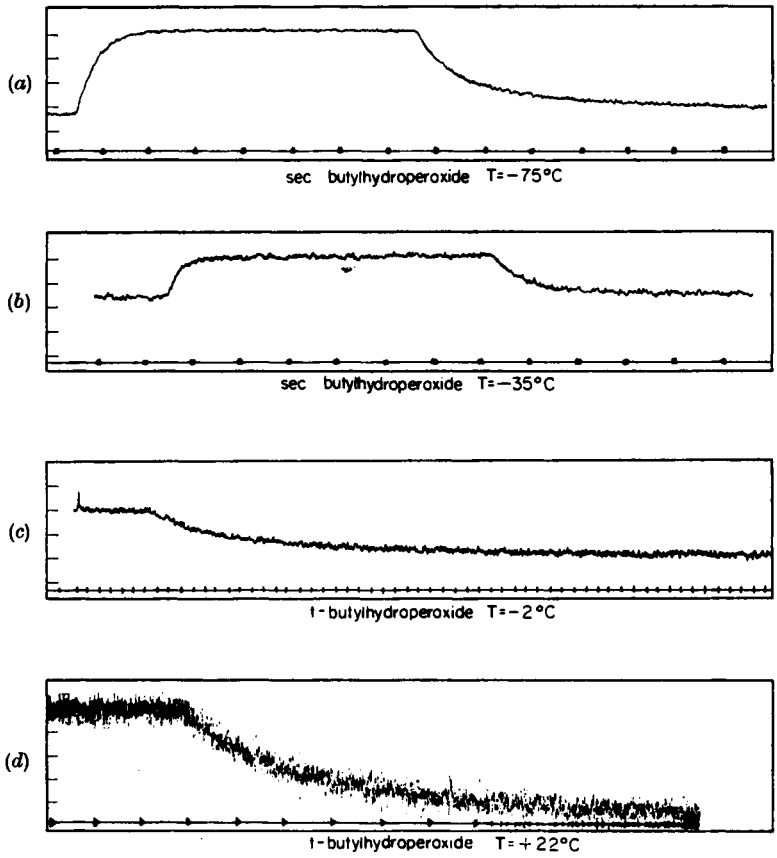

FIG. 4. *a*. Decay curve for the sec-butoxy radical at $T = -75°C$. Far left shows the rise time as the light is turned on then the steady state is attained the light is then extinguished and subsequent decay curve on the right is obtained. X-axis is graduated in 1 sec intervals.

b. Decay curve for sec-butoxy radical at $T = -40°C$.

c. Decay curve for t-butoxy radical at $T = -20°C$. X-time scale has been changed.

d. Decay curve for t-butoxy radical at $T = 22°C$.

measuring the time necessary to produce a certain concentration of free radicals.

Activation energies were obtained by measuring the rate constants at various temperatures. Figure 5 is a typical Arrhenius plot, the slope of which yields the activation energy for the decay process. Table 1 gives these activation energies for the secondary and tertiary radical decay.

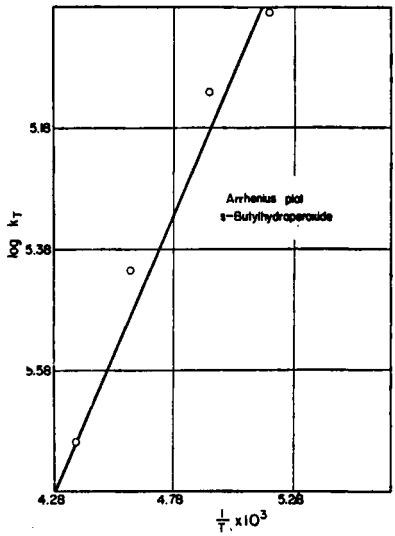

FIG. 5. Arrhenius plot for sec-butoxy free radical. The slope of the line is equal to E_a/RT.

TABLE 1

Compound	$k_t \times 10^{-5}$ m sec/l	$t_{1/2}$ sec	E_a kcal/m	$\nu^* \times 10^{-8}$ m sec/l
n-butyl hydroperoxide		0.1 sec (−90°C)		
sec-butyl hydroperoxide	4.9 (−40°C)	0.25 sec	4 ± 1	6.4 (−40°C)
t-butyl hydroperoxide	0.16 (−9°C)	3 sec	4 ± 1	1.2 (−9°C)

* ν = Arrhenius frequency factor.

The full potential of this new technique for studying photochemical dissociations can only be realized when one compares the wealth of information present with the ease and rapidity at which it is obtained. The instrumentation is such that one is not limited to merely steady state photochemical

studies. Considerable work has been done on the temperature kinetics of free radical recombinations from frozen media, such as glasses. This would be analogous to absorption studies with the trapping technique discussed previously.

We have done some interesting photochemical studies on simple alcohols that illustrate this EPR trapping technique. As mentioned above, optical absorption studies on radicals require trapping them in glassy solvents. We have found that one can get sufficient concentrations for EPR measurements by trapping directly in the material of interest, which in this case is the appropriate alcohol.

Upon irradiating ethyl alcohol at 77°K one obtains the complex spectrum given in Fig. 6*a*. At first glance the spectrum appears to be either a simple

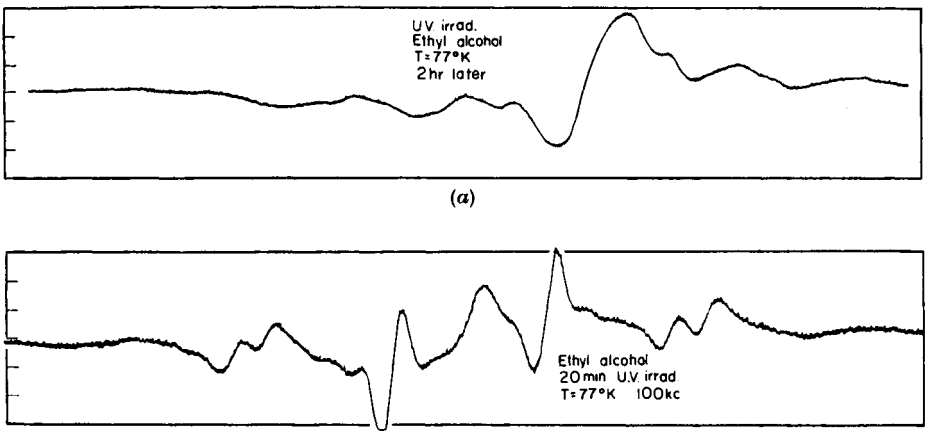

FIG. 6. *a*. EPR spectrum of ethyl alcohol irradiated with ultraviolet at 77°K. *b*. Same spectrum two hours later.

quartet, each line of which is split into two, or perhaps a quartet with a six line pattern superimposed upon it. Voedvodsky[5] has obtained this same spectrum immediately after irradiating in the presence of H_2O_2, but claims that during irradiation only a quartet is obtained. He claims the two spectra differ only by a strong line in the center and attributes the spectrum to the radicals formed by the reactions

$$H_2O_2 + h\nu \rightarrow 2OH\cdot$$

$$OH\cdot + CH_3CH_2OH \rightarrow HOH + CH_3CH_2O\cdot$$

$$CH_3CH_2O\cdot + h\nu \rightleftarrows CH_3\cdot + H{-}\overset{\overset{\displaystyle H}{|}}{C}{=}O$$

The third reaction predominates during photolysis, but when the light is off, the $C_2H_5O\cdot$ is thermally more stable. We cannot verify his results with direct irradiation and only obtain what he assigns to the mixture of the two radicals.

When methyl alcohol is irradiated, one obtains the spectrum of Fig. 7. A portion of the spectrum is easily interpreted as a quartet due to a methyl radical. The splittings agree exactly with those obtained by others[6] for

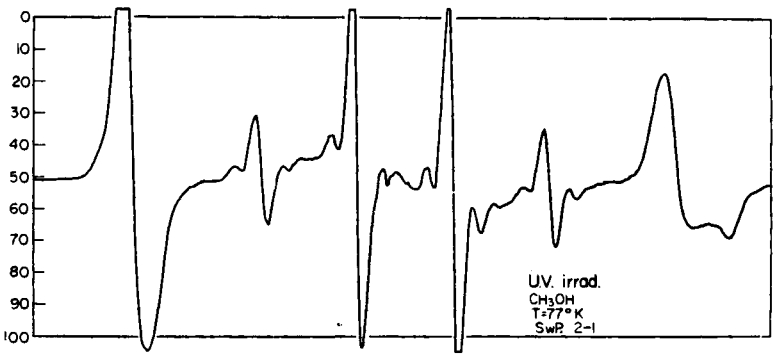

FIG. 7. EPR spectrum of ultraviolet irradiated methyl alcohol. Center quartet is due to $\cdot CH_3$.

methyl radicals in irradiated CH_3I. But the spectrum also contains two lines which are symmetric about $g = 2.0$ with a splitting in excess of 120 gauss. One might be inclined to assign this to the $\cdot OH$ but this assignment is incompatible with results obtained for irradiated CH_3OD. When CH_3OD is irradiated the same spectrum is obtained as for CH_3OH. (See Fig. 8.) Thus the $\cdot OH$ must be ruled out. When, however, CD_3OH is irradiated, one obtains the spectrum of Fig. 9 which consists of a seven line pattern expected for the

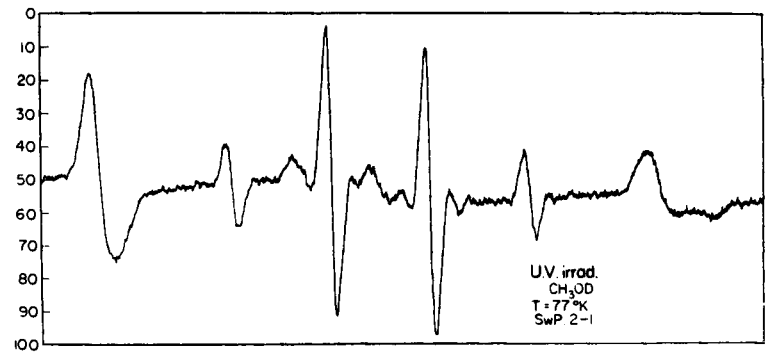

FIG. 8. EPR spectrum of ultraviolet irradiated CH_3OD.

$\cdot CD_3$ radical, plus another unresolved multiplet. The 120 gauss doublet, however, is no longer observed.

In order to give a splitting of 120 gauss, it is necessary that there be a very large unpaired electron density at a single proton. The H-atom for example, gives a splitting of 500 gauss. At present no positive identification of this doublet can be made, but it is hoped that temperature studies on the decay rates of the two radicals plus some ENDOR[7] experiments will shed more light on the interpretation.

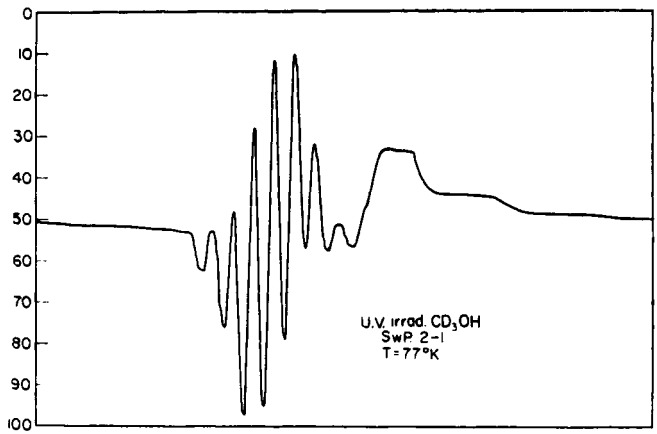

FIG. 9. EPR spectrum of ultraviolet irradiated CD_3OH. Center seven lines is due to $\cdot CD_3$.

As can be seen from these last two illustrations, there is much to be desired in the interpretation of EPR spectra of free radicals in photo irradiations. It is hoped, however, that EPR, coupled with the existing photochemical tools previously mentioned, will yield a more complete understanding of photochemistry in general.

REFERENCES

1. I. F. GIBSON, D. J. E. INGRAM, M. C. R. SYMONS and M. TOWNSEND, *Trans. Faraday Soc.* **53**, 914 (1959).
2. W. GORDY and H. SHIELDS, *Proc. Natl. Acad. Sci., U.S.* **41**, 983 (1955).
3. B. SMALLER and N. S. MATHESON, *J. Chem. Phys.* **38**, 1169 (1958).
4. R. S. ALGER, T. A. ANDERSON and L. A. WEBB, *J. Chem. Phys.*, **30**, 695 (1959).
5. V. V. VOEDVODSKY, *4th International Symposium on Free Radical Stabilization.* National Bureau of Standards, 1959.
6. E. L. COCHRAN ibid.
7. D. J. E. INGRAM, *Free Radicals as Studied by E.S.R.* Academic Press, 9958, p. 95–97.
8. L. H. PIETTE and W. C. LANDGRAF, *J. Chem. Phys.* **32**, 1107 (1960).

21

PARAMAGNETIC RESONANCE RESPONSE OF COLOR CENTERS

JAMES S. HYDE
Varian Associates, Palo Alto, California

THE term "color center" is usually reserved for those defects that give rise to visible coloration in crystals which, if they were perfect, would be colorless when observed in white light.

The coloration arises, of course, from two electronic states or energy levels separated by an energy difference corresponding to the energy of a photon, $h\nu$, where the frequency, ν, falls in the visible portion of the spectrum. Light will be removed in a characteristic bandwidth from incident white light, as electrons are excited from the ground state to the higher energy state, and the result is that the crystal appears colored. The most commonly studied materials have been the alkali halides. These normally clear crystals undergo quite a spectacular series of color changes when treated in various ways, and as a result, attracted the attention of investigators many years ago.[1]

We would like to use a more general definition of this term "color center", in which the restriction to the visible portion of the electromagnetic spectrum is removed. We will use it always to refer to a defect in an otherwise perfect, nonconducting crystal. It may be associated with a fault in the regular array, as an interstitial or a missing atom, or it may involve an impurity atom. Ionic, valence and semiconducting crystals can possess "color centers". We exclude metals and molecular crystals where defects are of basically different types.

We are concerned here with electron paramagnetic resonance. Many color centers will contain unpaired electron spins and, as such, will be paramagnetic. The reason for introducing the general definition of color centers is that magnetic resonance experiments in solids fall into several classifications, each with common characteristics. We wish to use this term for one of these groups. The classifications into which we would divide electron paramagnetic resonances are those involving (1) conduction electrons, (2) free radicals, (3) transition or rare earth elements and (4) color centers. We explicitly exclude resonances of transition or rare earth impurities from this fourth

classification, even though the term "color center" might otherwise seem appropriate.

Color centers will characteristically be very dilute—perhaps of the order of one part in a million concentration and often much less. One can visually detect F-center concentrations in the alkali halides in the range between 10^{16} and 10^{17} centers per cm^3: i.e. KBr changes from pale to dark blue in this range of densities. The sensitivities of the best spectrometers in use today are of the order of 10^{11} electron spins at room temperature for a one gauss line width. Since line widths may be very much greater (200 gauss for F-centers in Li F), since audio modulation of the magnetic field is usually much less than the overall line width, since complications arising from long spin-lattice relaxation (T_1) and consequent saturation at low r.f. power levels often occur, and since a 50:1 signal-to-noise ratio is desirable, sensitivity is usually a very serious problem indeed.

Often electron traps will be produced during growth of the crystal, and any process that ejects electrons into the conduction band of the crystal will lead to filling of the traps, provided that the trap is sufficiently deep that the trapped electron is thermally stable. Shallow traps in semiconductors can only be studied at liquid helium temperature.

In ionic crystals, such as the alkali halides, there is evidence that fairly low energy irradiation—of the order of a few electron volts—is sufficient to create electron traps and subsequently to fill them. Additive coloring in which a stoichiometric excess of one of the constituents of a diatomic crystal is introduced—leading to vacant sites of the opposite constituent—is often used to create traps in the alkali halides.[2]

On the other hand, different methods are necessary with a strongly bound valence crystal such as diamond.[3] Gamma or X-ray irradiation does not damage this material, but neutron or other heavy particle irradiations will produce interstitial ions and lattice vacancies which are paramagnetic.

The paramagnetic species may often be an atom or ion which is in a location such that not all of the possible chemical bonds are formed and the total spin remains unpaired. An example would be a substitutional donor atom in silicon. Four of the electrons form chemical bonds with the neighbors, but the fifth remains unpaired and is paramagnetic. The F-center in alkali halides, which consists of a single electron replacing a missing halogen ion and interacting rather strongly with the nuclear spins of the six nearest neighbors, is another example of a paramagnetic color center. In both of these examples the electrons are attracted to the center by coulomb potentials. On the other hand, some paramagnetic color centers are described more accurately by the "hole" concept. That is, the electron traps themselves contain species with unpaired spins; if electrons are injected into the conduction band and subsequently trapped, these centers are no longer paramagnetic.

The hole is characteristically more strongly localized—interacting with only a few nuclei and often possessing a well resolved hyperfine spectrum.

One common characteristic of color center resonances is that the line width nearly always is caused by inhomogeneous broadening;[4] that is, the line width arises from unresolved hyperfine interactions. In fact, this characteristic so determines the resonance behavior and is so general that we might well have replaced the term "color center" with "inhomogeneous systems". This type of broadening is in sharp contrast to the situation encountered in the studies of transition or rare earth elements where often there is a paramagnetic center in each unit cell and the observed line width arises from dipole–dipole interaction of the spins. For very dilute systems with a random distribution of spins in the various unit cells, Kittel and Abrahams[5] have derived an expression for the dipole–dipole line width: $\Delta H = 5.3\, g\mu_B N$, where N is the number of paramagnetic centers per cm^3. For the concentrations of color centers usually encountered, this line width is much less than experimentally observed. If $g = 2$ and $N = 10^{17}$, $\Delta H = 10^{-2}$ gauss. Even when the hyperfine interaction with the shell of nearest neighbors can be resolved, the residual width of each line generally arises from hyperfine interaction with more distant neighbors.

One can visualize the interaction of the spin with the nuclei as consisting of an isotropic and an anisotropic part. The isotropic fraction is a measure of the electron wave function at the nuclei in question. The anisotropic part comes from interaction of the separated nuclear and electronic magnetic moments—where then the angle between the moments is important. Each nucleus may be one or another of the possible isotopes with random distribution throughout the lattice and each will be oriented with nearly equal probability in one of several quantized angles with respect to the electron spin. Since the electron–nuclei interaction drops off as the distance from the center increases and each electron sees a different combination of nuclear magnetic moments, it is clear that, as a rule, the electrons will be in a continuous distribution of states. Only in the total absence of nuclear spin or in the case of large paramagnetic concentration will observed widths arise from electron–electron-spin interaction.

It might be well to ask what has become of the concept of spin–spin interaction and the resulting transverse relaxation time T_2. It will be recalled that for a homogeneous line the resonance width is a measure of T_2. This interaction conceptually can be thought of as composed of the following two comparable parts: (1) The nearby spins will be randomly distributed in the permissible quantized directions and the result is that their M_z components will give rise to a distribution of local magnetic fields at the various spin sites. (2) Again, all spins precess at nearly the same frequency and interaction of the M_x and M_y components permits exchange of spins, shortening of lifetimes and consequent spread in energy.[6]

Now in the inhomogeneous system the first effect—that is, the modification of the local magnetic field by neighboring electron spins—is very similar to modification by neighboring nuclear spins. The shortening of lifetimes is complicated indeed, since now the spins are precessing at a distribution of frequencies and interact to various degrees. Portis[7] has derived an expression for the limiting of lifetimes by spin–spin interactions in dilute inhomogeneous systems. However, the natural line width (or "spin packet width", or "width of spins which interact with one another") is often determined not by T_2 but by T_1. That is, the lifetime of a spin state, or loss of phase coherence in the Bloch[8] formulation is determined by T_2 or T_1, whichever is shorter, and each will lead to a broadening of the line. The result is that often one replaces T_2 by T_1 in theoretical treatments.

The puzzle of relaxation times in these systems applies also to T_1. Often the spin-lattice relaxation times are very long indeed and show a concentration and temperature dependence for which no adequate theoretical explanation has been made.

Inhomogeneous systems are often recognized by their saturation behavior, which differs markedly from the behavior of homogeneous systems[4]. That is, one finds that the susceptibility χ'' becomes proportional to $1/H_1$ as H_1 increases, where H_1 is the r.f. field, rather than $1/H_1^2$, as predicted by the Bloch equations. Portis gave a theoretical analysis[7] some years ago and the present author has recently given a new treatment[9].

There is another behavior characteristic of inhomogeneous systems that is of more general importance than one might at first suspect. This is the rapid passage response, which has been treated theoretically by Portis[10] and investigated experimentally in some detail by the author[11]. If a spectrometer is employed which has a microwave bridge with frequency stabilization to an exterior reference cavity, and which is set to observe the dispersion mode, an unusual response is observed in F-centers of LiF and NaF at room temperature and high r.f. power (χ'' is well-saturated). Field modulation is used, and one finds that the resonance signal is ninety degrees out of phase with respect to the modulation, and instead of tracing out a curve which is the derivative of the dispersion, the recorder plots an undifferentiated absorption curve.

The explanation is as follows: Bloch[8] in his Nobel Prize paper discussed the response of a single line of very long T_1 when the d.c. field was kept away from the line long enough for the spins to come to equilibrium and then swept rapidly through the line. The observed signal had an amplitude proportional to the field at which equilibrium was reached, the shape of an absorption rather than dispersion line, and a sense depending on whether the equilibrium field was above or below the resonance field. We visualize the inhomogeneous system as composed of very many overlapping weakly interacting narrow lines and the modulation field H_m sweeping rapidly back

and forth sinusoidally through a group of the packets. ($H_m \ll$ the overall line width.) If T_1 is of the order of $1/\omega_m$, where ω_m is the modulation frequency, then while the modulation field is slowly changing—near the top or bottom of its swing—the spin packets can reach equilibrium. The field then sweeps rapidly through the packets that lie between the two ends of the modulation sweep. The maximum resonance signal occurs when the modulation field is between the extrema, and therefore lags by ninety degrees. The intensity of the signal is proportional to the number of spins at the center of the sweep and one thus traces out the envelope of the absorption. We will not go into further details here, but it should be mentioned that if $\omega_m \gg 1/T_1$, both theoretical and experimental results show that the phase lag will be 180°—with the line shape still given by the distribution of spins in the local magnetic fields.

Of what use is this? One of the main advantages is in disentangling overlapping resonances. T_1 is the crucial crystal parameter determining whether rapid passage will occur. If the T_1s of overlapping lines differ, a modulation frequency or a temperature can be found such that one of the resonances satisfies rapid passage conditions and is ninety degrees out of phase with respect to the other. Proper adjustment of the phase-sensitive detector then permits observation of one or the other. Rapid passage can also be used to obtain information on relaxation times. Often one is in the rapid passage region for other reasons, as in the investigation of donors in silicon where very low temperatures and therefore long T_1s are used. Then, only the dispersion is detected—the absorption is strongly saturated. The donor experiments in silicon have been carried out under rapid passage conditions.

A powerful technique has been developed by Feher[12] to resolve the hyperfine structure of inhomogeneously broadened lines—the "Electron Nuclear Double Resonance" (ENDOR) method. In ordinary magnetic resonance the quantum mechanical selection rules bar changes of the surrounding nuclear spin during an electron transition. Thus the orientations of the surrounding nuclei remain unchanged and the nuclei precess at a variety of frequencies depending on the value of the local magnetic field at the nucleus which arises from the spinning electron. In the ENDOR technique the EPR line is partially saturated by a strong microwave field and then an auxiliary r.f. field is applied in such a manner as to induce nuclear magnetic resonance transitions. The scheme is to observe the saturated EPR line and sweep the radio frequency. Whenever this frequency is the same as the nuclear precession frequency, nuclear spins are flipped, the local magnetic field of the resonating electrons is changed and they go off resonance, while at the same time other off-resonance electrons suddenly find themselves satisfying the resonance condition as their nearby nuclei are suitably changed. The result is a change in the EPR saturation parameter and an increase in the EPR signal. This will occur, as mentioned, whenever the radio frequency is the same as the

precession frequency of a particular group of nuclei—and in this manner hyperfine interactions with perhaps half a dozen concentric shells of nuclei can be studied.

Thus we have a picture of the type of problems and the fascination which color center systems present. The complex of interlocking electron, nuclear and lattice interactions is only beginning to be understood. It seems certain that the field of color center resonance will become of increasing importance as the number of high sensitivity spectrometers in use increases and as crystals improve in quality. Only a small fraction of the crystals which Seitz[13] lists as typically ionic, covalent or semiconducting have been investigated at this date.

We have now reviewed and discussed in a general way color center EPR phenomena. In this latter portion of the discussion we will review rather briefly several typical experiments.

Although the resonance from color centers in alkali halides was detected by several early investigators, the first definitive experiment was carried out by Kip, Kittel, Levy and Portis[14]. They recognized that dipole–dipole interaction could not explain the observed width of F-centers in KCl—which they found to be 54 gauss for 10^{17} centers per cm^3. They suggested that the width arose from hyperfine interaction and proposed the following model: Potassium has a nuclear spin of $\frac{3}{2}$—that is, there are four permitted angular orientations. There are six nearest neighbors and there are thus $4^6 = 4096$ combinations of spins. Many involve the same energy of interaction, however, and there are in fact just $2 \cdot (6I) + 1$ energy levels. The 4096 states divide into these 19 lines as follows:

9	8	7	6	5	4	3	2	1	0
1	6	21	56	120	216	336	456	546	580.

"0" refers to the central line and the other numbers to the lines on either side.

In this manner they could calculate the expected envelope of the resonance and they found agreement with the experimental line shape.

The crucial experiment was then performed. K^{39} is 93 per cent abundant and K^{41}, 7 per cent abundant—each with spins of $\frac{3}{2}$ but different nuclear magnetic moments. These investigators obtained a crystal of $K^{41}Cl$ and found that the width of the observed resonance decreased in proportion to the magnetic moment. There was however a 15 per cent discrepancy and Kip *et al.* were able from this description to calculate the extent of the interaction with the second nearest neighbors (Cl^- ions). From these data expressions were derived for the concentration of the F-center wave function at first and second nearest neighbors. The consistency of the experiments was regarded as conclusive verification of the usual (de Boer) model for the F-center.

It is interesting now to consider Feher's double resonance experiment on

F-centers in KCl.[15] We have an explicit check of the work by the Berkeley group. Feher carried out the double resonance experiment, as described earlier, at 1.2°K. He found changes in the EPR saturation parameter corresponding to the nuclear resonance of K^{39}, Cl^{37}, K^{41}, and Cl^{35} with remarkable detail. The anisotropic, isotropic and quadrupolar portions of the interactions were found. The comparison of the two experiments is very satisfying.

Feher	*Kip* et al.
h (K) 7.72 oe.	h (K) 7.56 oe.
h (Cl) 2.50 oe.	h (Cl) 2.57 oe.

Another area that has been investigated extensively and which serves as a typical example of resonance in inhomogeneous systems is that of donor centers in silicon. P, As and Sb are introduced substitutionally into the Si lattice. Four of the electrons form chemical bonds with neighbors, while at sufficiently low temperatures the fifth is trapped at the donor in a coulomb potential and remains unpaired. The first reported resonances were carried out with a conventional EPR spectrometer,[16] and showed a resolved hyperfine structure with the number of lines expected from the nuclear spins of the various donors. Each line was, however, several gauss wide and the saturation behavior showed that they were inhomogeneously broadened—presumably because of interaction with Si^{29} nuclei (which are only 4.7 per cent abundant).

The first double resonance experiment was reported by Feher[12] on $P(I = \frac{1}{2})$. The EPR spectrometer was set on one of the hyperfine lines and the line partially saturated. Two double resonance lines associated with the donor nucleus were observed; the first corresponded to interactions of the nuclear spin with the electron spin in the upper energy state, the other with the interaction with the electron spin while it is in the lower energy state. It is clear that there will be slight difference in the frequency at which these two classes of nuclei resonate since in the one case the magnetic field at the nucleus arises from the *sum* of the applied d.c. field and the field from the spinning electron and in the other case, from the difference. The splitting corresponds to $2g\mu_B H$ and provides a direct measurement of g without the necessity of knowing the electron wave function at the nucleus. In addition, a number of other resonances were observed at lower frequencies. These arise from Si^{29} interaction. The donor electron extends over a hundred or more atoms and therefore will see several of these nuclear moments. Recently Feher[17] has analyzed the data to obtain detailed information on the donor wave function.

As a final example, we consider the work of Kanzig and co-workers on V-centers produced in the alkali halides by X-ray irradiation. They have

found complicated resonances with many lines and marked anistropy from perhaps a dozen centers. Several of these have been analyzed—we consider here the one first published.[18, 19, 20] This spectrum can be shown to arise from a halogen (X_2^-) molecule oriented along the (110) axis and not associated with any other defect. One can therefore describe the center as a self-trapped hole. The separation of the two atoms of the molecule-ion is less than the usual separation in the lattice, and the bond is covalent. That such a color center can be formed in an ionic crystal is one of the very important and unexpected results of color center magnetic resonance spectroscopy.

Consider the KCl spectrum. Natural Cl contains two isotopes; each of spin $\frac{3}{2}$. There are then three combinations of the nuclei of the Cl_2^-, Cl^{35}—Cl^{35}, Cl^{37}—Cl^{37} and Cl^{35}—Cl^{37}. Each nuclear spin can be oriented in four ways. There are therefore 4^2 states. If the nuclei are the same, these states will be distributed into $2(\frac{3}{2}\times 2)+1$ equally spaced energy levels of intensity ratios 1, 2, 3, 4, 3, 2, 1. For Cl^{35}—Cl^{37}, however, there will be sixteen lines of equal intensity. The observed spectrum fits this scheme, which accounts for perhaps half the lines. The remainder are explained by consideration of the anisotropy of the hyperfine splitting.

An interesting supporting experiment has been performed by Delbecq, Smaller and Yuster[21]. They identified an optical absorption band associated with the above center. This was a band hidden under the V_1 band and slightly displaced; it had not previously been detected. They then bleached the crystal with intense light polarized along the $(0\ \bar{1}\ 1)$ axis. The effect of this bleaching was to decrease the $(0\ \bar{1}\ 1)$ density and markedly *increase* the $(0\ 1\ 1)$ density; that is, the molecule ions apparently reorient along the other axis. Finally this group carried out bleaching experiments with polarized light which were correlated with accompanying changes in magnetic resonance absorption.

It should be mentioned that even the narrow resonances found in these experiments are inhomogeneously broadened by interaction with the spins of nearby nuclei. Castner[22] has found examples of V-center resonances, however, where the width is only a few times greater than that expected from dipole–dipole interaction, and has investigated their saturation behavior.

Let us summarize briefly. It is not our intention to provide a comprehensive review of color center work. We do wish, however, to emphasize our own point of view concerning this subject. That is, that the field is not a peculiar and narrowly limited application of resonance techniques, but rather one of the major divisions. Again, we would not think of inhomogeneous broadening as an unfortunate and unusual occurrence, but as a general and expected phenomenon. We would not avoid rapid passage conditions as hopelessly complicating the situation, but would exploit them to probe more deeply into paramagnetic materials. The examples discussed above illustrate the work which has been done and encourage us to go further.

REFERENCES

1. N. F. MOTT and R. W. GURNEY, *Electronic Processes in Ionic Crystals*, London, Oxford University Press, 1940.
2. F. SEITZ, "Color Centers in Alkali Halide Crystals, II", *Rev. Mod. Phys.* **26**, 7 (1954).
3. J. H. E. GRIFFITHS, J. OWEN and I. M. WARD, "Magnetic Resonance in Irradiated Diamond and Quartz", Report of the Conference on Defects in Crystalline Solids held at Bristol in 1954 published by the Physical Society, London, 1955, p. 81.
4. A. M. PORTIS, "Electronic Structure of F-centers: Saturation of the Electron Spin Resonance", *Phys. Rev.* **91**, 1071 (1953).
5. C. KITTEL and ELIHU ABRAHAMS, "Dipolar Broadening of Magnetic Resonance Lines in Magnetically Diluted Crystals", *Phys. Rev.* **90**, 238, (1953).
6. J. H. VAN VLECK, "The Dipolar Broadening of Magnetic Resonance Lines in Crystals", *Phys. Rev.* **74**, 1168 (1948).
7. A. M. PORTIS, "Spectral Diffusion in Magnetic Resonance", *Phys. Rev.* **104**, 584 (1956).
8. F. BLOCH, "Nuclear Induction", *Phys. Rev.* **70**, 460 (1946).
9. J. S. HYDE, "Saturation of the Magnetic Resonance in Dilute Inhomogeneously Broadened Systems", *Phys. Rev.* **119**, 142, (1960).
10. A. M. PORTIS, "Magnetic Resonance in Systems with Spectral Distributions", Tech. Note No. 1, Sarah Mellon Scaife Radiation Laboratory, University of Pittsburgh, Pittsburgh, Pa. (1955).
11. J. S. HYDE, "Magnetic Resonance and Rapid Passage in Irradiated LiF", *Phys. Rev.* **119**, 1483, (1960).
12. G. FEHER, "Observation of Nuclear Magnetic Resonances via the Electron Spin Resonance Line"", *Phys. Rev.* **103**, 834 (1956).
13. F. SEITZ, *The Modern Theory of Solids*, McGraw–Hill, New York, 1940.
14. A. F. KIP, C. KITTEL, R. A. LEVY and A. M. PORTIS. "Electronic Structure of *F*-centers: Hyperfine Interactions in Electron Spin Resonance", *Phys. Rev.* **91**, 1066 (1953).
15. G. FEHER, "Electronic Structure of *F*-centers in KCl by the Electron Spin Double Resonance Technique", *Phys. Rev.* **105**, 1122 (1957).
16. R. C. FLETCHER, W. A. YAGER, G. L. PEARSON, A. N. HOLDEN, N. T. READ and F. R. MERRITT, "Spin Resonance of Donors in Silicon", *Phys. Rev.* **94**, 1392 (1954).
17. G. FEHER, "Electron Spin Resonance Experiments on Donors in Silicon, Part I: Electronic Structure of Donors by the Endor Technique", *Phys. Rev.* **114**, 1219 (1959).
18. W. KANZIG, "Electron Spin Resonance of V_1-centers", *Phys. Rev.* **99**, 1890 (1955).
19. T. G. CASTNER and W. KANZIG, "The Electronic Structure of *V*-centers", *J. Phys. Chem. Solids* **3**, 178 (1957).
20. T. O. WOODRUFF and W. KANZIG, "Paramagnetic Resonance Absorption of *V*-center in LiF", *J. Phys. Chem. Solids*, **5**, 268 (1958).
21. C. J. DELBECQ, B. SMALLER and P. H. YUSTER, "Optical Absorption of Cl_2–Molecule Ions in Irradiated Potassium Chloride", *Phys. Rev.* **111**, 1235 (1958).
22. T. G. CASTNER, Jr., "Saturation of the Paramagnetic Resonance of a *V*-center", *Phys. Rev.* **115**, 1506 (1959).

22

PARAMAGNETIC IONS IN CRYSTALS

R. C. REMPEL
Varian Associates, Palo Alto, California

1. INTRODUCTION

PARAMAGNETIC resonance occurs when unpaired electrons are present. In any closed shell orbital and spin momenta cancel, leaving only diamagnetism. In chemical bonding, the valence electrons form closed shells and no paramagnetism occurs. Exceptions occur when: (a) normal bonds are broken or modified to leave unpaired electrons. Examples of this are free radicals, F-centers, and V-centers, (b) atoms are present for which shells inside the valence electrons are not filled so that unpaired electrons are always present. These are the transition elements. The first transition group is the iron group in which the electrons start filling the $3d$ shell after the $4s$ valence electrons have filled. Other transition groups are the $4d$ palladium group, the $4f$ rare earth group, the $5d$ platinum group, and the $5f$–$6d$ uranium group.

2. THE GENERAL HAMILTONIAN

We shall now consider the effect of first placing a free ion in the crystalline electric field and then applying an external magnetic field. We shall particularly emphasize the theory as it relates to ions of the $3d$ iron group. For hydrated salts of this group the crystalline field is stronger than the spin–orbit interaction but weaker than the Russell–Saunders energy which couples the individual orbital and spin momenta to form a resultant **L** and **S**. The coupling between **L** and **S** is broken so that, while M_L and M_s are still good quantum numbers, total angular momentum is not. The crystalline field splits different M_L levels by several thousand wave numbers and generally only a single orbital level is left lying lowest. The orbital motion is then quenched and does not contribute to magnetic properties. Spin–orbit interaction will, however, mix in higher orbital states and this will give zero field splittings and departures of the g-value from 2.

The Hamiltonian of the ion can be written as

$$\mathscr{H} = \mathscr{H}_F + V + \mathscr{H}_{LS} + \mathscr{H}_M + \mathscr{H}_N.$$

$$\mathscr{H}_F = \sum_k \left(\frac{P_k^2}{2m} - \frac{Ze^2}{r_k}\right) + \sum_{j<k} \frac{e^2}{r_{jk}}$$

is the coulomb interaction of the electrons with the nucleus and with each other. V is the electrostatic energy from the crystalline electric field.

$$\mathscr{H}_{LS} = \lambda \mathbf{L}\cdot\mathbf{S}$$

is the spin–orbit interaction

$$\mathscr{H}_M = \beta \mathbf{H}\cdot(\mathbf{L}+2\mathbf{S}), \qquad \beta = \frac{e\hbar}{2mc};$$

is the interaction of the electrons with the magnetic field. $\mathscr{H}_N$, the interaction with the nucleus, contains the hyperfine interaction, a term from the magnetic field at the nucleus due to orbital and spin moments of the electrons, and the quadrupole interaction. For simplicity, and because of its importance, we shall explicitly include only the hyperfine interaction

$$\mathscr{H}_N = A\mathbf{I}\cdot\mathbf{S}$$

3. THE CRYSTAL FIELD

To illustrate crystal field splitting, we shall consider the effect of a cubic octahedron on the levels of a single d electron. Figure 1 shows, in a two dimensional manner, the value functions for the five m_l states of a d electron. In the free ion these wave functions are degenerate. The wave functions can

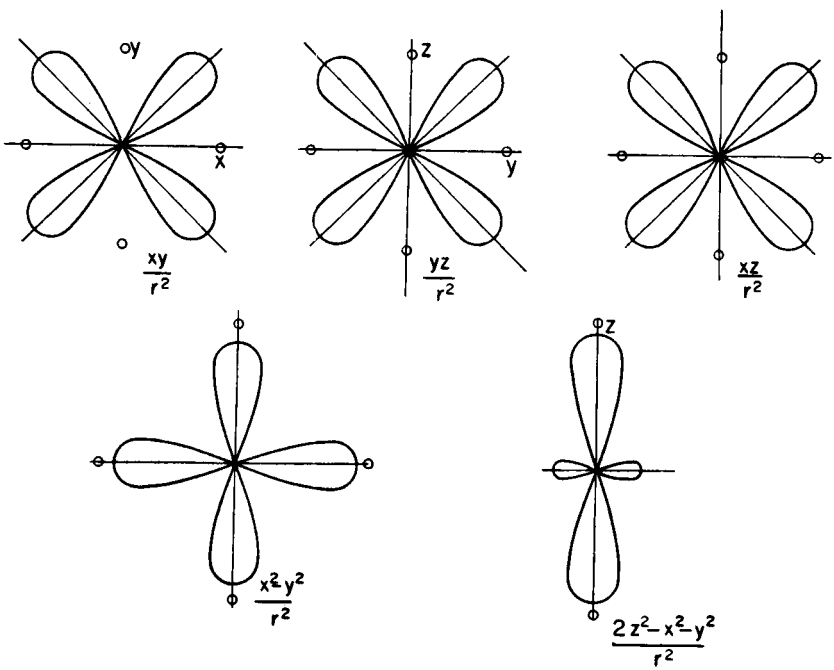

FIG 1.

be written as a function of r times angular factors of the form xy/r^2, yz/r^2, xz/r^2, $(x^2-y^2)/r^2$, and $(2z^2-x^2-y^2)/r^2$, respectively. The dots on the axis represent negative diamagnetic atoms.

The first three of these orbitals are called the d_ϵ orbitals and the last two are called the d_γ orbitals. As the electrons furthest from negative ions will have the lower electrostatic energy, the d_ϵ orbitals will lie lower than the d_γ orbitals.

A detailed treatment of crystal field splitting has been given by Bethe. In general, it is found that the lower the symmetry of the crystal field, the less degeneracy is left in any level. Figure 2, taken from the book by

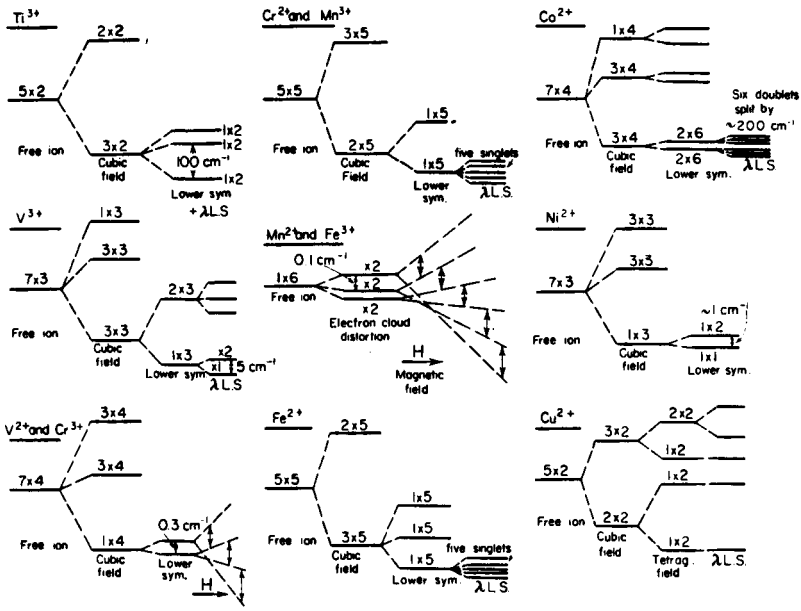

FIG. 2.

Ingram,[1] shows the effect of the crystalline field on all the $3d$ group ions. The theory proceeds according to whether the cubic field leaves an orbital singlet lowest. This is true for V^{2+}, Cr^{3+}, and Ni^{2+}. Cr^{2+}, Mn^{3+}, and Cu^{2+} can also be considered in this same category, even though the cubic field leaves an orbital doublet lowest. The reason is that the spin–orbit interaction has no matrix elements between these two states. If the cubic field leaves a degenerate lowest orbital level, as in Ti^{3+} V^{3+}, Fe^{2+}, and Co^{2+}, lower symmetry fields and the spin–orbit interaction will split the level by the same order of magnitude. For reasons to be mentioned later, resonance, if observed at all, will be observed only at very low temperatues. Table 1 lists the $3d$ ions and their ground states.

TABLE 1

Ion	Number of electrons in $3d$ shell	Ground state
Ti^{3+}	1	^2D
V^{3+}	2	^3F
Cr^{3+} and V^{2+}	3	^4F
Mn^{3+} and Cr^{2+}	4	^5D
Fe^{3+} and Mn^{2+}	5	^6S
Fe^{2+}	6	^5D
Co^{2+}	7	^4F
Ni^{2+}	8	^3F
Cu^{2+}	9	^2D

4. DERIVATION OF THE SPIN-HAMILTONIAN

The Hamiltonian representing the change in energy from this lowest orbital level is

$$\mathscr{H}' = \beta\mathbf{H}\cdot(\mathbf{L}+2\mathbf{S})+\lambda\mathbf{L}\cdot\mathbf{S}+A\mathbf{I}\cdot\mathbf{S}.$$

A perturbation calculation is now made, mixing in higher states, to obtain zero field splittings and departues of g-values from 2. The ground state is taken as $|0)$ and the higher orbital states as $|n)$. First order perturbation theory gives

$$(0|\beta\mathbf{H}\cdot(\mathbf{L}+2\mathbf{S})+\lambda\mathbf{L}\cdot\mathbf{S}+A\mathbf{I}\cdot\mathbf{S}|0).$$

There is a general theorem which says that the expectation value of orbital angular momentum is zero for a singlet orbital state. Terms in $\mathbf{L}$ then vanish and we are left with

$$2\beta\mathbf{H}\cdot\mathbf{S}+A\mathbf{I}\cdot\mathbf{S}.$$

The second order correction to the energy levels is

$$-\sum_{n\neq 0}\frac{|(0|\beta\mathbf{H}\cdot(\mathbf{L}+2\mathbf{S})+\lambda\mathbf{L}\cdot\mathbf{S}+A\mathbf{I}\cdot\mathbf{S}|n)|^2}{E(n)-E(0)}.$$

Terms not involving L vanish by orthogonality and we are left with

$$-\sum_{n\neq 0}\frac{[(\beta\mathbf{H}+\lambda\mathbf{S})\cdot(0|\mathbf{L}|n)][(\beta\mathbf{H}+\lambda\mathbf{S})\cdot(n|\mathbf{L}|0)]}{E(n)-E(0)}$$

$$=\sum_{ij}\Lambda_{ij}[\beta^2H_iH_j+2\beta\lambda H_iS_j+\lambda^2S_iS_j],$$

$$=\sum_{ij}\Lambda_{ij}[\beta^2H_i\cdot(2\delta_{ij}+2\mathbf{L}_{ij})\cdot S_j+\lambda^2S_i\mathbf{L}_{ij}S_j+AI_iS_j\delta_{ij}]$$

where

$$\Lambda_{ij} = \sum_{n\neq 0} \frac{(0|L_i|n)(n|L_j|0)}{E(n)-E(0)}.$$

Dropping the first term above as a constant and adding first and second order terms, we arrive at the spin–Hamiltonian

$$\mathscr{H}_s = \sum_{ij} [\beta H_i \cdot (2\delta_{ij} + 2\lambda\Lambda_{ij}) \cdot S_j + \lambda^2 S_i \Lambda_{ij} S_j + \mathrm{A} I_i S_j \delta_{ij}]$$

or

$$\mathscr{H}_s = \beta \mathbf{H} \cdot g \cdot \mathbf{S} + \mathbf{S} \cdot D \cdot \mathbf{S} + A \mathbf{I} \cdot \mathbf{S},$$

where g and D are tensors. Inclusion of the direct magnetic interaction between the nucleus and the orbital and spin momenta of the electrons leads to an anisotropic hyperfine coupling, i.e. one of the form $\mathbf{I} \cdot A \cdot \mathbf{S}$ with A a tensor. While several terms contribute to this effect, the reader may readily verify that one of them, $\mathbf{L} \cdot \mathbf{I}$, leads to terms of this sort.

5. DISCUSSION

The magnetic interaction shows that the spin is not completely free. The magnetic moment vector now has the components $\beta g_x S_x$, $\beta g_y S_y$, and $\beta g_z S_z$ relative to the x, y, z symmetry axes of the crystal. Neglecting nuclear interactions, the term $\mathbf{S} \cdot \mathbf{D} \cdot \mathbf{S}$ is responsible for the zero field splittings of the energy levels. For tetragonal or trigonal symmetry the spin–Hamiltonian can be written as

$$\mathscr{H}_s = \beta[g_{11} H_z S_z + g_\perp (H_x S_x + H_y S_y)] + D S_z^2 + A I_z S_z + B(I_x S_x + I_y S_y),$$

with z the symmetry axis. Lower symmetry requires the inclusion of a term $E(S_x^2 - S_y^2)$ and the replacement of $g_\perp$ and B by g_x, g_y, B, and C.

The great importance of the spin–Hamiltonian lies in the fact that the complete resonance behavior, at any frequency, can be described through relatively few parameters. It may truly be said that the goal of the experimentalist is to determine the parameters of the spin–Hamiltonian for whatever ion is being considered.

6. DEGENERATE LOWEST ORBITAL LEVEL

In discussing this case, two general theorems need be mentioned. The first is Kramer's theorem which states that every system with an odd number of electrons will have even degeneracy when placed in an external electric field. The second is the Jahn–Teller effect which states that a system having a degenerate ground state will spontaneously distort to remove as much degeneracy as possible—by doing this the energy is lowered.

In general the lower symmetry fields and the spin–orbit coupling split the levels by about 100 cm^{-1}. If there is an even number of electrons, the states will all be singlets and the resonance will be observed only for frequencies

greater than the zero field splittings. If there is an odd number of electrons, the ground state will be a doublet. As the next doublet will be some 100 cm^{-1} higher, this ground level can be considered an isolated doublet and described by an effective spin $S' = \frac{1}{2}$. For either of these cases, because of very close lying higher orbital states, the spin-lattice relaxation time will be very short and resonance can be observed only at liquid hydrogen–liquid helium temperatures.

7. S-STATE IONS

We now come to the special case of ions which have no orbital angular momentum to be quenched. This happens when the shell is half full, with the orbital angular momenta of the electrons cancelling and the spins aligned. In the $3d$ group these are the $3d^5\ {}^6S_{5/2}$ ions Fe^{3+} and Mn^{2+}. Using a combination of spin–orbit and crystal field interactions to mix excited states of the form $3d^5\ {}^4P$ to the basic $3d^5\ {}^6S$ state, Van Vleck and Penney have found that it is necessary to go to third order in the perturbation to get a tetragonal field splitting and that it is necessary to go to fifth order to get a cubic field splitting. Abragam and Pryce[2] have proposed another mechanism involving the dipole–dipole interaction between electron spins. It is not at all certain as to which of these mechanisms prevails.

However, for purposes of establishing a spin–Hamiltonian it is not necessary to understand the origin of the terms. Recall that for $S = \frac{1}{2}$, by using the commutation relations and $S_x^2 = S_y^2 = S_z^2 = \frac{1}{4}$, any expression in S_x, S_y, and S_z can be reduced to a constant or one linear in S_x, S_y, or S_z. For $S = 1$ any expression can be reduced to $(S_x \pm iS_y)$, S_z, S_z^2, $(S_x \pm iS_y)^2$, and $(S_x \pm iS_y)S_z$. This process can be continued up to $S = 5/2$. General arguments indicate the spin–Hamiltonian should contain only even powers of the spin operators. Terms containing sixth and higher powers of the spin operators can be reduced to ones containing fourth and lower powers. The most general cubic field spin–Hamiltonian is

$$\mathscr{H}_s = \beta g \mathbf{H}\cdot\mathbf{S} + a(S_x^4 + S_y^4 + S_z^4) + A\mathbf{I}\cdot\mathbf{S}\ .$$

For tetragonal symmetry the general spin–Hamiltonian is

$$\mathscr{H}_s = \beta[g_{11}H_zS_z + g_\perp(H_xS_x + H_yS_y)] + 2(S_x^4 + S_y^4 + S_z^4) + \\ + bS_z^4 + DS_z^2 + AI_zS_z + B(I_xS_x + I_yS_y).$$

8. RELAXATION PROCESSES

For paramagnetic ions the dominant relaxation process is not that due to the effects of thermal motion on the dipole–dipole interactions between neighboring spins. It is, instead, due to the effect of this motion of the crystalline electric field. As has been seen, the parameters of the spin–Hamiltonian have their origin in the crystalline electric field and the spin–orbit coupling.

If these fields are time varying because of thermal vibrations of the lattice, the parameters of the spin–Hamiltonian will correspondingly be time varying. The spectral density of the parameters at the various transition frequencies will then cause relaxation. For a spin–Hamiltonian of the form

$$\mathscr{H}_s = \beta \mathbf{H} \cdot g(t) \cdot \mathbf{S} + D(t) S_z^2 + E(t)[S_x^2 - S_y^2]$$

relaxation will occur through the time variation of g and D. As these two parameters have a common origin, they will be correlated and relaxation from the two will not be independent. It is interesting to note that the term $\beta \mathbf{H} \cdot g(t) \cdot \mathbf{S}$ is a field dependent process.

The crystalline field enters the parameters of the spin–Hamiltonian most strongly through the energy denominator, $E(n) - E(0)$, in the expression for Λ_{ij}. For close spacing of higher orbital levels from the lowest, this term will be quite small and the parameters will be very sensitive to changes in the crystalline field. For this reason ions with close lying orbital levels can generally be observed only at very low temperatures.

REFERENCES

The following references give comprehensive treatments of paramagnetic resonance in crystals.

1. D. J. E. Ingram, *Spectroscopy at Radio and Microwave Frequencies*, London, Butterworths, 1955.
2. Abragam and Pryce, *Proc. Roy. Soc.* A, **205**, 135 (1951).
3. B. Bleaney and K. W. H. Stevens, *Rep. Progr. Phys.*, **16**, 108 (1953).
4. K. D. Bowers and J. Owen, *Rep. Progr. Phys.*, **18**, 304 (1955).

For more detailed references to the literature the reader is referred to (2), (3) and (4).

23

DYNAMIC NUCLEAR POLARIZATION IN LIQUIDS*

WESTON A. ANDERSON
Varian Associates, Palo Alto, California

AT the 1953 Spring Meeting of the American Physical Society, Albert Overhauser proposed[1] that the nuclear spins of a metal could be polarized by saturation of the spin resonance of the conduction electrons in a metal. This theoretical prediction was soon verified by Carver and Slichter[2] who observed the nuclear resonance signal of lithium metal in a magnetic field of 30.5 gauss. Without saturating the electron resonance, the nuclear signal was so weak that it was lost in the noise while a signal of about twenty times noise was observed with the saturating field on. They estimated an enhancement of about 100-fold was obtained.

To explain this enhancement, Overhauser made use of Fermi statistics which would normally apply only to electrons in metals. It was soon recognized that enhancements of nuclear polarization might be observed in other paramagnetic substances as well.[3, 4, 5, 6]

A necessary condition for a polarization enhancement is that a coupling exists between the nuclei and the unpaired electrons. This coupling may either be dynamic or static, yielding somewhat different results in the two cases. In the first case, the coupling provides a relaxation mechanism supplying or absorbing the energy required for a relaxation transition. Radio-frequency transitions are made between the levels involving a spin change of a single electron. In the second case, the static coupling allows radio-frequency transitions involving simultaneous nuclear and electron spin changes. The important relaxation mechanisms here are just the usual ones which relax the electron spins. We shall now consider some of the various mechanisms in detail.

Consider first a dynamic hyperfine ($I \cdot S$) coupling. Figure 1*a* represents the separate energy levels of the electron and nucleus in the applied magnetic field. The symbols + and − are used to indicate the orientation of the

* This material was reported at the 1959 Summer Meeting of the American Physical Society, Honolulu, Hawaii; *Bull. Am. Phys. Soc.* **4**, 361 (1959).

electron and nucleus relative to the applied field. The magnetogyric ratio of the electron is negative while that of the nucleus has been assumed to be positive. The nuclear spin is assumed to be $\frac{1}{2}$. Here the r.f. field causes a net number of electron transitions from $-$ to $+$ while the relaxation processes try to restore the system to thermal equilibrium by producing a net number of electron transitions from $+$ to $-$; however, in doing so these processes

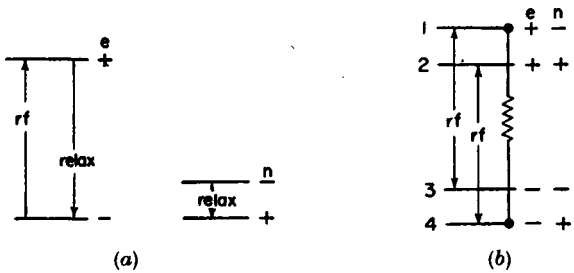

FIG. 1.

simultaneously produce nuclear spin transitions from $-$ to $+$. The enhancement in the nuclear polarization may be determined by a nuclear resonance experiment. In the absence of an r.f. field, thermal equilibrium is maintained by these relaxation processes and the usual processes involving single electron spin charges. To obtain an appreciable nuclear polarization enhancement, one must make the rate of transition produced by the r.f. field large compared to the natural rates determined by relaxation processes; i.e. the r.f. field must be sufficiently large to produce saturation of the electron resonance signal.

The energy levels of the combined system are sketched in Fig. 1*b*. Here, if the r.f. field is sufficiently strong, equal populations will be maintained between levels (1) and (3) and levels (2) and (4), while a normal Boltzman population is maintained between levels (1) and (4) by the dynamic $I \cdot S$ coupling. These relaxation processes are indicated on the diagram by the resistor symbol —∧∧∧—.

An equation relating the nuclear polarization L, (as determined by nuclear resonance) with the saturating r.f. field H_1 is given by[7, 5]

$$L = L_0\left[1 + K\frac{\gamma_e}{\gamma_n}\frac{T_{1e}T_{2e}\gamma_e^2H_1^2}{1+(\Delta\omega_e T_{2e})^2+\gamma_e^2H_1^2T_{1e}T_{2e}}\right] \tag{1}$$

Here the quantity K depends upon the type of coupling and other nuclear relaxation processes. For the dynamic $I \cdot S$ coupling $K = T_{1n}T_{1n}'$ where T_{1n} is the nuclear thermal relaxation time while T_{1n}' is just the contribution due to the $I \cdot S$ coupling with the electrons. The quantity L_0 is the nuclear polarization at thermal equilibrium.

If we define an enhancement factor by $A = (L-L_0)/L_0$, equation (1) may be written

$$A^{-1} = A_{\max}^{-1}\,[1+\alpha P^{-1}]$$

where $A_{\max}$ corresponds to the maximum theoretical enhancement which one would obtain in the limit of infinite r.f. power, P is the saturating power, and α is a constant given by

$$\alpha = \frac{1+(\Delta\omega_e T_{2e})^2}{\beta\gamma_e^2 T_{1e} T_{2e}}$$

where $\beta = H_1^2/P$.

An example of a coupling of the dynamic $I \cdot S$ type in liquids is furnished by the now well-known alkali metal ammonia solutions. Carver and Slichter[8] studied Na–Ammonia solutions at low field and found the proton enhancement increased with Na concentration, reaching a value near 500 at 0.9 molar solution of sodium. The results of Carver and Slichter were obtained in magnetic fields of approximately 12 gauss. Figure 2 shows some data I have

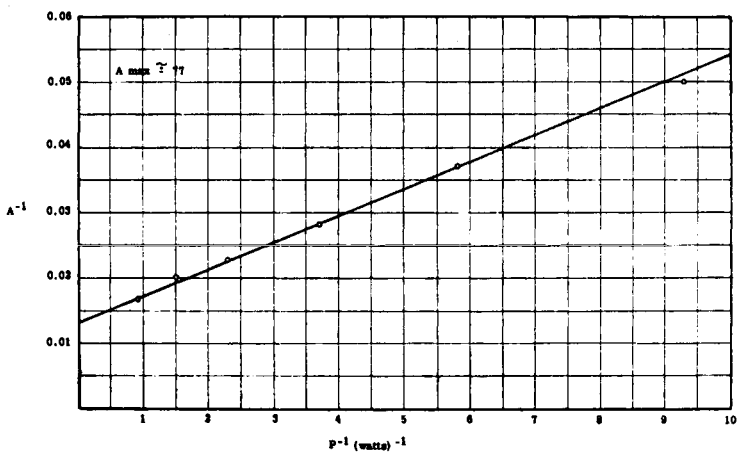

FIG. 2. Inverse enhancement a^{-1} vs. inverse microwave power P^{-1} for sodium–ammonia solution.

taken at approximately 3.6 kgauss. Here the inverse enhancement has been plotted, vs. inverse microwave power. The curve has been plotted in this form since a straight line should result. The extrapolation of this straight line gives the enhancement one would obtain with infinite microwave power. In this, extrapolated enhancement is only about 77 compared to the theoretical value of about 660. Although the sodium concentration was unknown, it has been estimated from electron line width data and from color to be approximately a one molar solution. Some of the reasons for the differences of polarization obtained at high field and low field are discussed below.

Next consider another dynamic polarization mechanism using a dipole–dipole coupling between the electrons and nuclei. Here all of the levels are connected by resistors in the equivalent circuit diagram, representing the fact that the dipole–dipole matrix elements connect all of the energy levels. However, for the purpose of illustration only the largest matrix element is indicated in Fig. 3. It is the one which involves both nuclear and electron

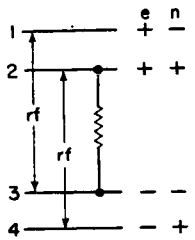

FIG. 3.

flip with a transfer of two units of angular momentum. Here again the r.f. field equalizes the populations of the levels (1) and (3) and levels (2) and (4), while a Boltzman distribution is maintained between the levels (2) and (3) connected by the relaxation matrix element. In this simplified picture one would expect to obtain a negative enhancement of approximately 660 for protons. However, when one includes all of the matrix elements, this value is reduced by a factor of two, i.e. in equation (1), $K = -\frac{1}{2}$.

A liquid demonstrating a dipole–dipole coupling is napthalene negative ion in a solvent of dimethoxyethane. Here the unpaired electron on the ion interacts with the protons on the solvent molecules with a time dependent dipole coupling. Bennett and Torrey[9] have studied this system in a field of approximately 18 gauss. They observed negative polarizations up to approximately 65. If one extrapolates their data, one finds a maximum enhancement of approximately 280, not far from the expected 330.

I have obtained a sample of this ion in the same solvent from Dr. Thomas Tuttle of Stanford. A plot of inverse enhancement vs. inverse microwave power is shown in Fig. 4. Here the maximum observed enhancement was approximately 120 with an extrapolated value of 150. About three weeks later the extrapolated value decreased to 125 while the nuclear relaxation time increased from *70* msec to *180* msec. These data are shown in Fig. 5. Here the inverse enhancement vs. inverse power was plotted at two different microwave frequencies, showing that in this case one obtains the same extrapolated enhancement using different microwave frequencies. This is again justified by theory, provided the electron resonance is single. If one plots the enhancement vs. microwave frequency for the two cases given above, one finds a line which can be closely fitted with a Lorentzian curve which within experimental error fits the microwave absorption curve. This is not true of some of the cases involving static coupling which are discussed below.

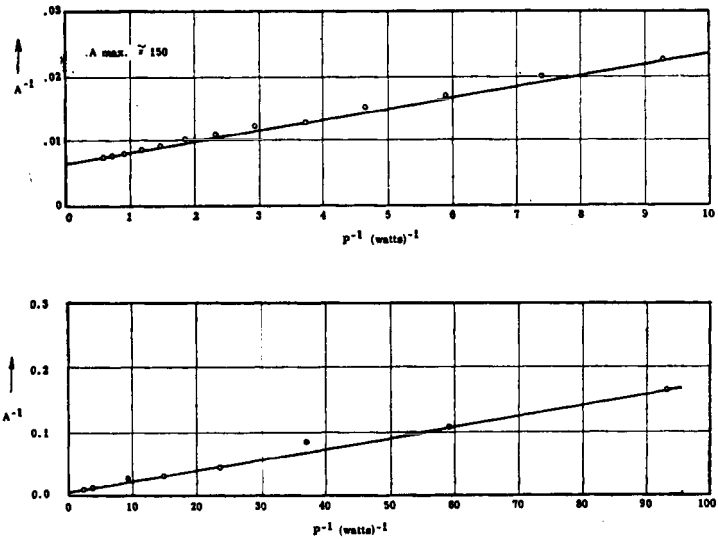

FIG. 4. Inverse negative enhancement A^{-1} vs. inverse microwave power P^{-1} for naphthalene negative ion in dimethoxyethane.

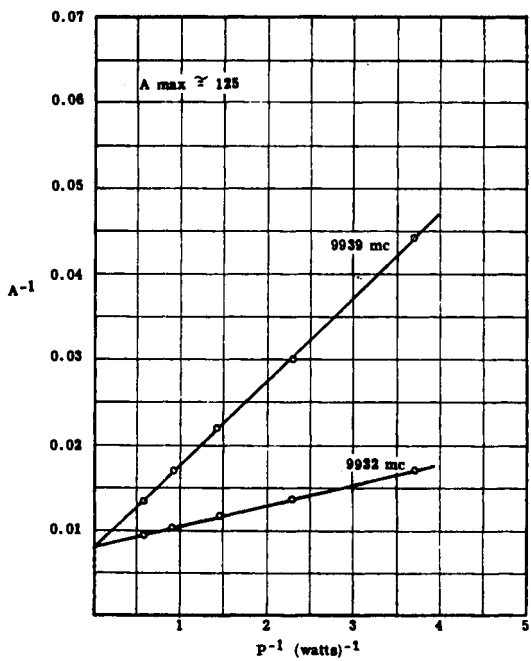

FIG. 5. Inverse negative enhancement A^{-1} vs. inverse microwave power P^{-1} for naphthalene negative ion in dimethoxyethane.

Another sample which also shows a dynamic dipole–dipole coupling is a solution of peroxylamine disulfonate. This has been studied by Abragam[10] and his co-workers at both low field and high field (3300 gauss). In this case the electron line is split into three lines by the nitrogen allowing a maximum negative theoretical enhancement of approximately 110. This closely agrees with the values obtained by Abragam's group and the extrapolated value we have obtained which is shown in Fig. 6.

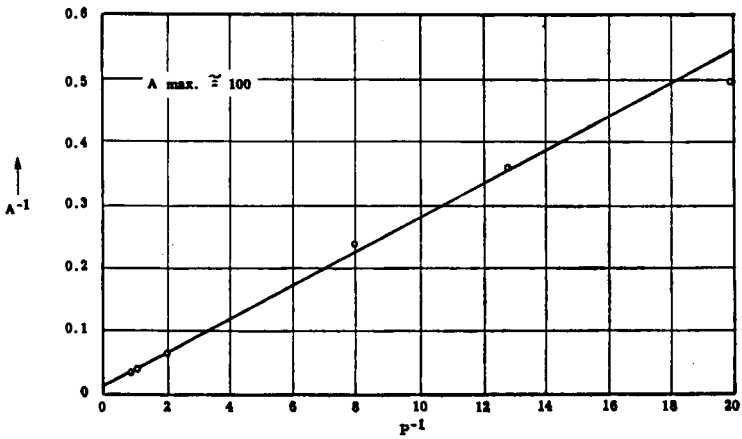

FIG. 6. Inverse negative enhancement A^{-1} vs. inverse microwave power P^{-1} for 0.023 molar solution of K_2 on $(SO_4)_2$.

A static $I \cdot S$ interaction may also be used to produce nuclear polarization.[11] This interaction mixes the states indicated by $(+-)$ and $(-+)$, allowing r.f. transitions between the levels (1) and (4). Here one must apply the r.f. field H_1 parallel to the constant field H_0. The usual electron relaxation mechanisms provide the relaxation transitions which tend to keep a Boltzman population ratio between levels (1) and (3) and levels (2) and (4) as sketched in Fig. 7. Thus, by irradiating at a frequency $\omega_e + \omega_n$ one obtains a large negative nuclear polarization.

If instead one has a static dipole–dipole interaction, one may also irradiate at a frequency $\omega_e - \omega_n$ and obtain a positive polarization as one may see from a study of the diagram in Fig. 8. Here the static dipole interaction causes

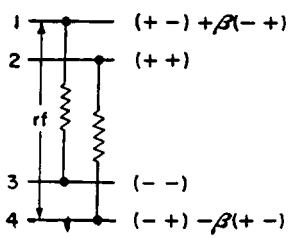

FIG. 7.

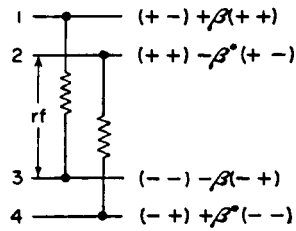

FIG. 8.

mixing of all of the energy levels, however the dominant mixing is between the closely spaced levels as sketched in Fig. 8. Thus one expects to obtain a positive enhancement for $\omega < \omega_e$ and a negative enhancement for $\omega > \omega_e$. Figure 9 shows an example of this type of behavior. This is a natural crude oil obtained from Dr. Edwin Poindexter. The oil is quite fluid—the consistency of light machine oil—yet it behaves quite like a solid as far as the enhanced nuclear polarization is concerned. Poindexter[12] has reported the

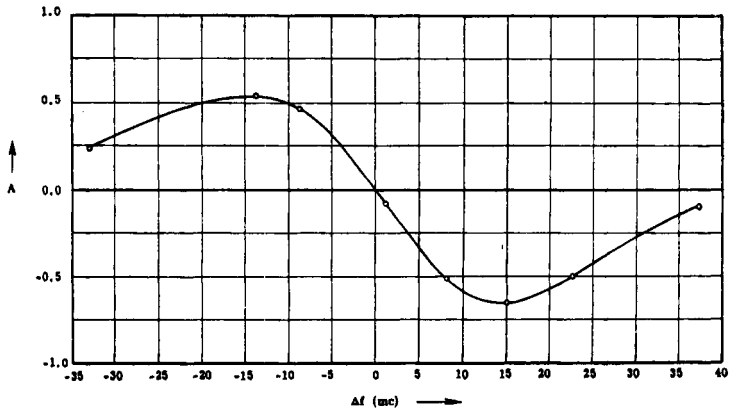

Fig. 9. Enhancement, A, vs. microwave frequency deviation, Δf, of Brookhaven crude oil.

results of a very similar oil at a field of approximately 18 gauss. He has found a negative enhancement of approximately 15 and maximum negative enhancement of approximately 300 after a rather long extrapolation.

Another example of a static or semi-static dipole–dipole interaction is a liquid or gas absorbed on the surface of a substance which contains unpaired electrons. Systems of this type have been studied by Uebersfeld and his coworkers.[13] They have seen both positive and negative polarizations in liquids of benzene and toluene and gases of ammonia and hydrogen sulfide absorbed on sugar char. Figure 10 shows the results of a similar system, that of toluene on a commercial carbon black—Spheron 6 (Godfrey Cabot Co.). The resonance lines of the phenyl protons are plotted here. This is an intermediate case showing effects of both static and dynamic dipole coupling. Even with the liquid absorbed on the carbon the proton lines are only a few milligauss wide. Heating the sample increases the positive enhancement and decreases the negative enhancement, indicating the correlation time is longer than $1/\omega_e$.

In the examples given above only electron–nuclear systems have been considered. One can also obtain small polarization enhancements in spin systems which have nuclear–nuclear coupling.[14, 15, 16, 17]

One of the points I wish to stress is the extreme sensitivity of the extrapolated enhancement to the correlation time[18] in these systems. In the

region of very short correlation times, i.e., $\tau_c \ll 1/\omega_e$, one obtains nearly a full enhancement. As the correlation time becomes longer or the magnetic field is increased, thereby increasing ω_e, one obtains reduced enhancements. This comes about because of the lack of energy density in the correlation spectrum near the electron Larmor frequency, ω_e. This might be put into semiquantitative form by making K of equation (1) proportional to $(1+\omega_e^2\tau_c^2)^{-1}$ in the region of $\tau_c < 1/\omega_n$.

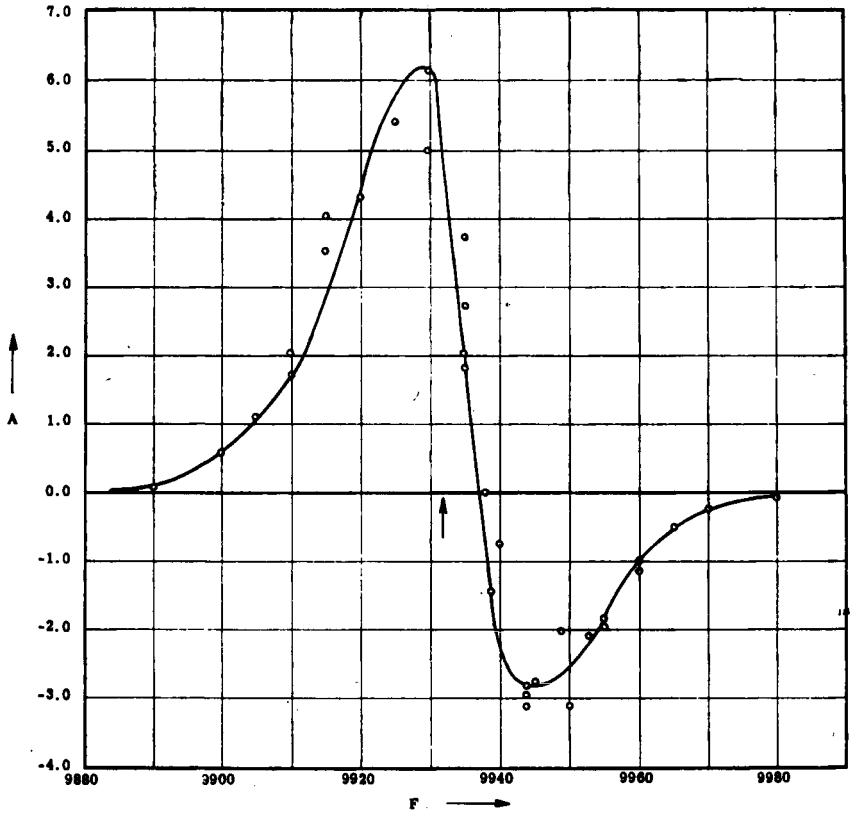

FIG. 10. Enhancement, A, vs. microwave frequency, F, for toluene on Spheron 6.

In the case of extremely long correlation times we finally obtain essentially no nuclear polarization while irradiating at the electron Larmor frequency ω_e. However, here we have the possibility of obtaining nuclear polarization by irradiating at the frequencies $\omega_e \pm \omega_n$. As the correlation time τ_c shortens, these two resonances become broader, their width becoming proportional to $1/\tau_c$. In the limit of $\tau_c \ll 1/\omega_n$ the two lines greatly overlap and since they produce opposite nuclear polarizations, the net signal becomes negligibly small.

The peroxylamine disulfonate furnishes a good example of a dipole–dipole interaction with extremely short correlation time (less than $10^{-10}/2\pi$ sec) allowing one to obtain nearly the maximum theoretical dynamic polarization at 10^{10} c/sec. The napthalene negative ion shows about half the full theoretical enhancement at 10^{10} c/sec and essentially the full enhancement at 5×10^7 c/sec showing that the correlation time is near $10^{-10}/2\pi$ sec. The crude oil, however, shows a very small dynamic polarization at 10^{10} c/sec (note the small asymmetry in Figure 9 due to the residual effect) and a larger effect at 5×10^7 c/sec. The oil also shows a "static" type interaction which one might expect is the correlation time near $\omega_p^{-1} = 10^{-7}/3\pi$ or larger.

The dynamic $I \cdot S$ interaction of the Na–Ammonia solution appears to have a correlation time in the neighborhood of $10^{-10}/2\pi$ sec. The toluene–carbon black system shows a residual dynamic $I \cdot S$ interaction superimposed upon a "static" dipole–dipole interaction.

Figure 11 is a photograph of the equipment. The klystron supply and the AFC are to the right, the 15 Mc radio-frequency unit and sweep circuits are

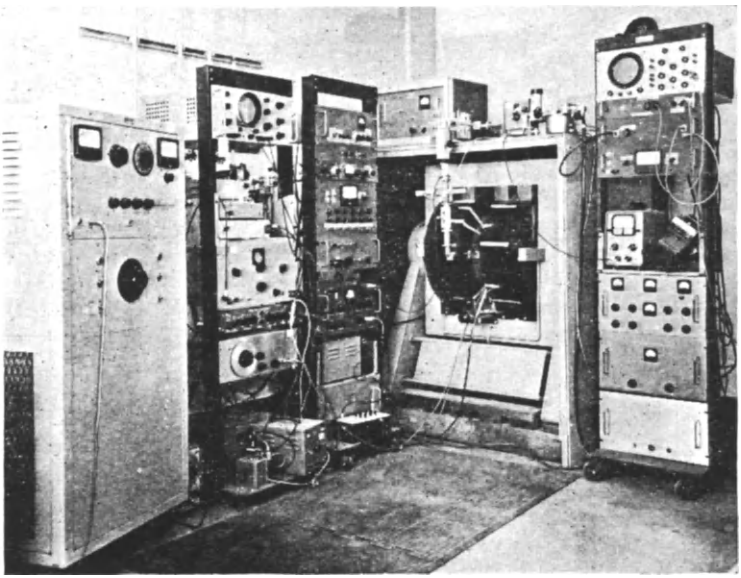

FIG. 11.

to the left. The microwave power source was a Varian V-58 klystron. The radio-frequency system uses a single coil bridge T circuit.[19]

Figure 12 shows some proton signals obtained from a sodium ammonia solution. This is the same sample from which the line areas of Fig. 2 were obtained. Notice the broadening of the line with increasing microwave power with some indication of the line splitting at the higher power levels. The line

on top left is the unenhanced line, while the successive lines were made under the condition of increasing microwave power. Each line was swept through twice to check reproducibility of the data. Observation of the electron resonance line showed that it was not symmetrical, having characteristics similar to those of conduction electron resonances found in metals in cases where the skin depth is comparable to or smaller than the particle size.[20, 21] On the other hand, the whole sample is penetrated by the 15 Mc r.f. field. We postulate that the central part of the sample is shielded from the microwave field

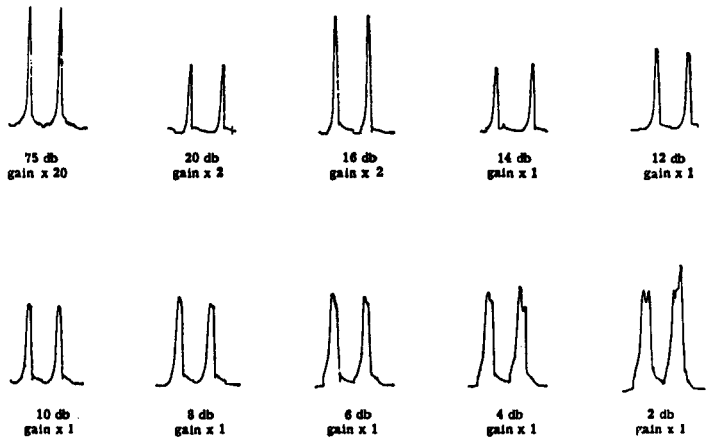

FIG. 12. Proton resonance of sodium–ammonia solutions vs. attenuation of microwave power.

and thus it experiences a normal Knight shift while saturation of the electron resonance line in the outer portion of the sample partially equalizes the electron spin populations and thus partially removes the source of this shift.[22] To the present time I have made no accurate measurements of this shift—the direction of the shift is toward higher applied magnetic fields—just opposite to the direction usually found in metals. This is in agreement with the observation of McConnell and Holm[23] but is not in agreement with theory.[24]

REFERENCES

1. ALBERT OVERHAUSER, "Polarization of Nuclei in Metals", *Phys. Rev.* **91**, 476 (1953); and *Phys. Rev.* **92**, 411 (1953).
2. T. R. CARVER and C. P. SLICHTER, "Polarization of Nuclear Spins in Metals", *Phys. Rev.* **92**, 212 (1953).
3. F. BLOCH, "Recent Developments in Nuclear Induction", *Phys. Rev.* **93**, 944 (1954). (See also *Phys. Today*, April 1954, p. 30.)
4. A. W. OVERHAUSER, "Polarization of Nuclei in Metals by Magnetic Resonance", *Phys. Rev.* **94**, 768 (1954).
5. J. KORRINGA, "Orientation of Nuclei by Saturation of Paramagnetic Resonance", and "Electron Resonance in *F*-Centers", *Phys. Rev.* **94**, 1388 (1954).

6. A. ABRAGAM, "Overhauser Effect in Non-metals", *Phys. Rev.* **98**, 1729 (1955).
7. F. BLOCH, "Dynamical Theory of Nuclear Induction II", *Phys. Rev.* **102**, 104 (1956).
8. T. R. CARVER and C. P. SLICHTER, "Experimental Verification of the Overhauser Nuclear Polarization Effect", *Phys. Rev.* **102**, 975 (1956).
9. L. H. BENNETT and H. C. TORREY, "High Negative Nuclear Polarizations in a Liquid", *Phys. Rev.* **108**, 499 (1957).
10. A. ABRAGAM, J. COMBRISSON and I. SOLOMON, "Nuclear Polarization by the Overhauser Effect in Solutions of Paramagnetic Ions", *C.R. Acad. Sci.* **246**, 157 (1957).
11. C. D. JEFFRIES, "Polarization of Nuclei by Resonance Saturation in Paramagnetic Crystals", *Phys. Rev.* **106**, 164 (1957).
12. EDWARD POINDEXTER, "An Overhauser Effect in Natural Crude Oil", *Nature* **182**, 1087 (1958).
13. J. L. MOTCHANE, E. ERB and J. UEBERSFELD, "An Apparatus for the Study of Magnetic Double Resonance Application to Carbon", *C.R. Acad. Sci.* **246**, 1833 (1958); and "Nuclear Polarization Effect in Liquids and Gases Absorbed upon Carbons", *C.R. Acad. Sci.* **246**, 2121 (1958).
14. I. SOLOMAN, "Relaxation Processes in a System of Two Spins", *Phys. Rev.* **99**, 559 (1955); and "Nuclear Magnetic Interactions in the *HF* Molecule", *J. Chem. Phys.* **25**, 261 (1956).
15. J. WERTZ, P. L. SAIN and R. L. BATDERF, "Multiple Thermal Relaxation Times and Nuclear Spin Energy Transfer in Liquids", *Phys. Rev.* **102**, 920 (1956).
16. A. ABRAGAM and W. PROCTOR, "A New Method of Dynamic Polarization of Nuclei in Solids", *C.R. Acad. Sci.* **246**, 2253 (1958).
17. N. BLOEMBERGEN and P. P. SOROKIN, "Nuclear Magnetic Resonance in the Cesium Halides", *Phys. Rev.* **110**, 865 (1958).
18. N. BLOEMBERGEN, E. M. PURCELL and R. V. POUND, "Relaxation Effects in Nuclear Magnetic Resonance Absorption", *Phys. Rev.* **73**, 679 (1948).
19. H. L. ANDERSON, "Precise Measurement of the Gyromagnetic Ratio of H_e^3", *Phys. Rev.* **76**, 1462 (1949).
20. G. FEHER and A. F. KIP, "Electron Spin Resonance in Metals I Experimental", *Phys. Rev.* **98**, 337 (1955).
21. FREEMAN J. DYSON, "Electron Spin Resonance in Metals II Theory of Electron Diffusion and the Skin Effect", *Phys. Rev.* **98**, 349 (1955).
22. W. D. KNIGHT, "Electron Paramagnetism and Nuclear Magnetic Resonance in Metals", *Solid State Physics*, New York, Academic Press, Inc., (1956), vol. 2, p. 93.
23. H. M. MCCONNELL and C. H. HOLM, "Electronic Structure of Sodium–Ammonia Solutions by Nuclear Magnetic Resonance", *J. Chem. Phys.* **26**, 1517 (1957).
24. W. E. BLUMBERG and T. P. DAS, "Knight Shift in Sodium Ammonia Solutions", *J. Chem. Phys.* **30**, 251 (1959).

24

COLOR CENTER "WORKSHOP" EXPERIMENT

JAMES S. HYDE
Varian Associates, Palo Alto, California

LiF which has been irradiated by Co^{60} gamma rays is to be investigated with EPR equipment. The sample, about $2 \times 4 \times 10$ mm, is glued to the end of a glass tube. A speck of DPPH is contained in the bottom of the tube.

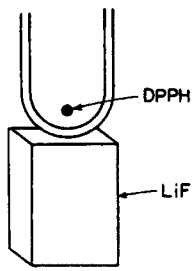

The DPPH sample exhibits a strong homogeneously broadened resonance of a few gauss width and quite short spin lattice relaxation time.

Under irradiation, F-centers are created in LiF. This center consists of a vacant negative ion site occupied by a single trapped electron, and hence it is paramagnetic. The electron interacts strongly with the nuclei of the surrounding shell of Li^7 ions (spin $\frac{3}{2}$) and less strongly with more distant neighbors. The result is a broad smeared-out resonance which may be visualized as composed of very many extremely narrow overlapping non-interacting lines. As discussed in the "color center" lecture, this "inhomogeneous" system is very easily saturated ($T_1 = 2 \times 10^{-4}$ sec). Under saturation conditions the absorption signal χ'' is very small, but a large dispersion signal χ' of unusual behavior is found. The line shape of this resonance resembles a gaussian curve (not the expected derivative of the dispersion) and is the distribution of spins in the various local magnetic fields. The phase of the resonance signal is no longer the same as the modulation field, but lags by 90° if $\omega_m T_1 < 1$ and by 180° at the line center if $\omega_m T_1 > 1$. This is a manifestation of rapid passage behavior, as discussed in more detail in the lecture.

Thus we have the simultaneous resonances from LiF and DPPH both occurring at $g = 2$. The experiments described below are to be performed at room temperature using the Varian low-power bridge. This bridge permits observation of the dispersion or absorption, since stabilization of the klystron is to a reference cavity and not the sample cavity. This is accomplished by proper adjustment of the phase of the microwave signal reflected from the sample cavity with respect to the phase of the crystal bias or leakage reflected from the slide screw tuner. The variable isolator provides adjustable attenuation of the power reaching the sample cavity, without attenuating the power reflected from this cavity back into the bridge.

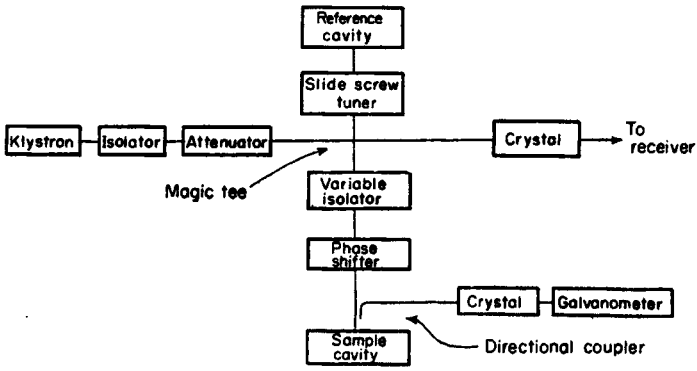

We will use the bridge with about 17 db isolation of the sample cavity. There are two critical adjustments which must be made in use of this bridge. The first is that the resonant frequency of the sample and reference cavities must be the same. A method which we have used is to display the klystron mode sweep on the oscilloscope with the reference cavity detuned.

The small pip arises from the isolated sample cavity, and this should be centered on the top of the mode. The reference cavity is now tuned to the same frequency and the klystron locked in. Fine adjustment is made by observing the signal reflected from the sample cavity with a directional coupler, crystal and galvanometer. Very slight tuning of the reference cavity will bring the two cavities into alignment giving a minimum signal reflected from the sample cavity.

The other adjustment is that of the phase shifter to detect pure absorption or dispersion. While there are several methods, the presence of the DPPH permits a straight forward display on the scope. The experiment begins at this point. The field is swept broadly at 20 cycles and superimposed is a narrow 100 kc sweep. Phase sensitive detection is employed at 100 kc, and the result is that the derivative of the dispersion, absorption, or a mixture of the two appears on the scope. We will adjust the phase so that we detect pure dispersion.

The low frequency sweep is now turned off, and a curve run at 100 kc. The phase sensitive detector is set to detect in-phase resonances. We obtain a curve like this:

We now set the 100 kc phase sensitive detector at the 90° out-of-phase position, leaving gains unchanged. Depending on the accuracy of the setting, both the DPPH and LiF resonances are nearly phased out, showing that both resonances have the same phase.

We now switch to audio-frequency modulation (40 cycles). At this frequency we expect the LiF signal to be 90° out of phase, since $\omega_m T_1 < 1$. We begin by running a curve with the audio-frequency phase sensitive detector at the 90° out of phase position.

The receiver integrating time constant is longer than at 100 kc, but the curve is nevertheless noisier. The DPPH signal can be seen, if one looks closely, on the scope display, even though the modulation frequency is 40 cycles rather than 100 kc. But this strong resonance does not appear on the recorder.

If now, without changing gains, we switch to the in-phase position, we find, as expected, the following curve:

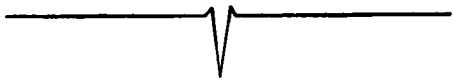

Generally speaking, one has many experimental variables, at one's disposal: temperature, microwave power level, dispersion or absorption, field modulation frequency and amplitude, and the setting of the phase sensitive detector. The main point of this experiment is to illustrate one experimental technique by which two overlapping resonances can be disentangled.

In addition, the experiment accomplishes the following objectives:

(1) Illustration is made of the use of a bridge by which either χ'' or χ' can be observed.

(2) It is shown that physical systems can be found where resonance response depends on the modulation frequency.

(3) Since the phase of the LiF resonance depends on whether $\omega_m T_1 <$ or > 1, we have bracketed T_1 between $1/40 \times 2\pi$ and $1/10^5 \times 2\pi$.

(4) With this bridge under these operating conditions the limiting noise is the crystal and not demodulation of klystron f.m. noise, as evidenced by improvement in signal to noise between 100 kc and 40 c.

(5) The experiment illustrates the idea that in EPR solid state work an unusual premium is placed on understanding of the equipment and the various operational techniques.

SUBJECT INDEX

Abragam's group 273
Absorption, curve for ethyl benzene 136
, formula 24, 129
Acetone, ultraviolet-irradiated spectrum 221
3α-acetoxy pregnane-20-one, hydrogen analysis 136
AFC system, block diagram 67
, modulation, output voltages from cavity 68
Alcohols, distinguishing primary from secondary 112
Alkyl nitrites, isomerization 147, 148
Anisole-d_3, deuterium location in 127
Arrhenius, equation 144, 242
, plot for sec-butoxy free radical 248
Attenuator, conversion factors 168
Audio frequency detector 203
Audio frequency modulation, NMR spectrometer 134–138
Audio phase detector, circuit 166
recordings 167

Barrier measurement, hindered rotation example 147, 148
, instrumental techniques 148–150
Basic group, definition 156
Benzene, v-mode signals from 172
Biochemistry, EPR used in 54, 211
Biological applications of EPR 233–239
Bloch, equations 142–145, 169, 255
, nuclear induction experiment 6
Bohr magneton 224, 226
Boltzmann, condition 5
, constant 46
, distribution 30, 133
, factor 35, 47
, statistics 7
, values for methyl methacrylate 219
Brookhaven crude oil, microwave frequency deviation 274
n-butoxy, ultraviolet irradiation 245, 246
, decay curves 247
Butyl hydroperoxides 248
, photodissociation 243
, spectra 245, 247
t-Butyl radicals 246, 248

Carbon black, spectra 213, 214
, spheron 6 274, 275
Carcinogenesis study 238
Chemical applications of EPR 207–223
Chemical exchange 34
Chemical groups, definitions 154
Chemical shift 13, 14, 15, 27–31, 39
, dilute CCl_4 solution 28
, heavy nuclei 27
, of water, benzene and toluene 14, 15
, proton 27
, solvent effects 29
, steroids 118
Chloroform and acetone system, equilibrium constant 37
Chloroform, hydrogen analysis 136
Coenzyme φ group, structure studies 119
Color centers, paramagnetic resonance response 252–260
, "Workshop" experiment 279–282
Complex formation 35–37
Contact hyperfine interaction 53
Crossed-coil NMR detector 6, 7, 8, 83
, Varian model 84
Crystal field 262, 263
Crystals, paramagnetic ions in 261–267
Cytochrome oxidase–ascorbic acid, optical and EPR kinetics 238
Cu^{++}, in laccase and cytochrome 237
, spectrum 52
Cycling the magnet method 94–96
Cyclopropane, NMR spectrum of a trisubstituted 32

Deuteration, measuring degree of 126
Deuterium, location in anisole-d_3 127
Dewar insert 244
Dimethoxyethane, microwave power for naphthalene negative ion 272
Dimethylaminopropylamine, structure 40–42
2,5 dimethyl benzo-semi quinone, radical structure 229
Dimethylformamide, NMR spectrum 35, 36
1, 4-dioxane, proton spectrum of 111
p-dioxane, hydrogen analysis 136
Dispersion and absorption, formulae 24, 129
Diterpene derivatives, NMR spectra 109
DPPH, free radical 227, 231
, sample irradiation by gamma rays 279–282
Dynamic nuclear polarization in liquids 268–278

Electric shims 176–179
, operating procedure 179
Electromagnetic spectrum 20
Electron S-state 53
ENDOR experiments and method 251, 256
Enzyme chemistry 237
Enzyme-substrate reaction, free radical signal 54
EPR, biochemistry 54
, biological applications 233–239
, chemical applications 207–223
, description of phenomenon, 45, 46
, filtering of signals 18, 19
, instrumentation 191–206
, kinetics for cytochrome oxidase–ascorbic acid 238
, meaning of 1
, NMR differences from 17
, photochemical studies 241–251
, polymer chemistry 54
, sample cavities 18
, signal, on oscilloscope 73, 77
, plots of intensity vs. time 212
, recorder trace 76
, scanning rates 80
, with field modulation 74, 78, 79
, spectra 19, 51–55, 213, 214, 215, 218, 220, 221, 222, 249, 250, 251
, theory of 224–232
, spectrometer, A.F.C. System 68, 71
, and spectroscopy 17
, block diagram 67
, iris adjustment 71
, operating fundamentals 65–80
, sample cavity and iris 70, 72
, slide screw tuner 72
, uses for 206
, X-band 50
, spectroscopy 17, 44–45, 241, 242
Ethyl alcohol, 249
, EPR ultraviolet irradiated spectrum 221, 249
Ethyl benzene, absorption curve and integral of a dilute solution 136
, hydrogen analysis 136
Ethyl nitrite, CH_2 resonance 149
, proton magnetic resonance of 148
Exact solutions, spectra analysis 158–162
Exchange reaction, examples 146, 147
, fast 145, 146, 210
, intermediate 144, 145
, physical model of 141
, rate constants 147
, slow 143, 144
Fe^{+++} in cytochrome 237
Feher's double resonance experiment 257 258
Fermi, hyperfine interaction 209, 216, 226–228
, statistics 268
Field trimmer, NMR Signal resolution 61
Flash photolysis technique 241
Fly-back time, circuit to increase 173
Formaldehyde, structure 40–42

Gas drive, research prototype flow system using 211, 212
Glycyl glycine, spectrum of irradiated 215
Glutamic acid, spectrum of irradiated 215
Gyromagnetic properties of sub-atomic particles 1
Gyromagnetic ratio 3

Hammett sigma functions 209
Harvard University, first NMR experiments 2
Heavy water, signals from H_2O impurity 123, 124
Hewlett Packard model, 220 CD 185
, 405 AR 189
High Resolution NMR, as an analytical tool 122–139
, birth of 14
, infrared comparison 100, 101
, instrumentation 81–99
, magnetic field modulation 180–184
, operating fundamentals 56–64
, spectra 15, 16
, spectra analysis 151–163
, structure determining tool 100–121
Homodyning 9
Hydrazyle (DPPH) 231
Hydrogen analyses, NMR integrated intensities, from 136
Hydrogen bonding 37, 38
Hydrolysis, rate studied by NMR 41
Hydroquinones, oxidation and reduction products 208
, spectrum 212
17α-Hydroxy-progesterone, hydrogen analysis 136

Ice, electron irradiated spectra 220
Infrared red, compared with high resolution NMR 100, 101
Instrumental techniques, NMR for the physical chemist 148–150
Instrumentation, EPR 191–206
Instrumentation of high resolution NMR 81–99

Integrating system, operation of NMR 185–190
Integrator balancing 187
Ions, paramagnetic, in crystals 261–267
, *s*-state 266
Irradiation, damage 214–217
, lithium fluoride by gamma rays 279–282
Isopropyl alcohol, ultraviolet irradiated spectrum 222
Isopropyl nitrite, proton magnetic resonance 148

Jahn–Teller effect 265
Johnson noise 39

Kinetic phenomenon on resonance lines 141–147
Klystron, cavities and their properties 195–198, 201
, cut-away view 193
, tuning 203
, uses in instrumentation 194–197
, Varian V-58 276
Klystron modes on oscilloscope 69
, with cavity absorption 70
Knight shift 277
Kramer's theorem 265
Kronig–Kramer's relations 49

Larmor, equation 4, 7, 13
, frequency 34, 164, 275
Larmor precession, 7, 46
, frequency 22
, theorem 3, 5
Lead-mirror reaction methods 207
Leakage, controlled phase 9
, NMR detector 8, 9
Level controls in NMR integrating system 188, 189
Liquids, dynamic nuclear polarization 268–278
Lithium fluoride, irradiation by gamma rays 279–282
Lock-in amplifier 166
Lorentzian line 78, 271
Low temperature trapping 219–233
Lucite, electron irradiated, EPR spectrum 55
Lunacrine, NMR spectrum 107
Lunine, NMR spectrum 107, 108

Magnet, flux stabilizer diagrams 98, 99
, power diagram 97
Magnetic, equivalence, 154
, non-equivalence 154
Magnetic field, effect on electrons 101, 102
Magnetic field homogeneity 23
, modulation for high resolution NMR 180–184
Magnetic moment, description 45
, N^{14} and N^{15} 13
Magnetic resonance, nitrites 148
, radio-frequency field measurement 164
, textbooks 2
Marginal oscillator NMR detector 82
Maryland University 217
Maser solid state programme 52
McConnell method 142, 143
Methane, effective constants in substituted 103
Methyl acetylene, calculated and observed spectrum 113
Methyl alcohol, ultraviolet irradiated spectra 221, 250
Methyl groups, use of NMR spectroscopy 117
Methyl methacrylate, polymerization studies and spectra 217, 218
, radicals, intensity vs. temperature plot 219
2-Methyl styrene, polymerization studies 217
Michaelis's assumption 233, 234
Michigan University 44, 233
Microwave, detector waveform 231, 232
, magnetic fields 49
, naphthalene 272
, potassium 273
, power, Brookhaven crude oil 274
, Sodium-ammonia solution 270, 277
, stabilization of frequency 203, 204
, toluene 275
Modulation, setting up for 186–188

Naphthalene, negative ion, microwave power for 272
, reaction with sodium or potassium 210
1, 4-Naphthosemiquinone, EPR spectrum 53
National Bureau of Standards 13, 219
Nobel prize in physics 2, 255
NMR, as an analytical tool 122–139
, audio-frequency modulation 134–138
, crossed-coil detector 6, 7, 8
, EPR, differences from 17
, first experiments 2
, high resolution, instrumentation 81–99
, magnetic field modulation 180–184
, operating fundamentals 56–64

NMR, structure determining tool 100–121
, integrating devices and intensities 135, 136
, integrating system, operation of 185–190
, typical circuitry 187
, intensity ratios 131–133, 136
, meaning of 1
, operating fundamentals 56–64
, physical chemist, for 140–150
, quantitative analysis 129–133
, reaction kinetics 140–150
, signal amplification 86–89
, signal modes 9, 10
, signal shapes 59–64
, spin rate effect 92
, spectrometers, variable temperature accessories 149
spectrometry, high resolution 21–43, 31, 38–40, 56–64, 129–133
, apparatus 25, 26, 81–99
, spectrum, proton 23
, steroid 40
, structural applications 32, 33
, tri-substituted cyclopropane 32
, spectra, multiplet patterns 105–107, 109
NMR spectrometer, performance 14
, working of, diagram 6
NMR transitions, energies and intensities of 110
NMR-EPR Spectrometers, background and fundamentals of 1–20
NMR-EPR spectroscopy, background and fundamentals of 1–20
Nuclear polarization in liquids, dynamic 268–278

Orbital level, degenerate lowest 265
Organic reactions, free radical intermediates 207–209
Overhauser effect 52

Paddles, NMR spectrometer 59, 85, 86
Palo Alto, California 1, 21, 56, 140
Paramagnetic ions in crystals 261–267
Paramagnetic resonance response of color centers 252–260
Pennsylvania University 234
Pentaborane, structure of mono-bromo 33
Peroxylamine disulfonate, dipole–dipole interaction 276
Perturbation theory 157, 158
Phase coherence 22
Phase detection, in EPR instrumentation 201, 202
, setting up for 186–188
Phase detector, balancing of 187
, input and output signals 75
, principles for 90–92
Phenyl resonance of internal standard toluene 149
Philbrick (George A.) Research Associates model UPA-2 185
Phosphine, phosphorus nuclei in 15, 16
Phosphorus, P^{31} signals, from phosphoric acids 128, 129
, P^{31} spectrum from polymerization of phosphate groups 128
Photochemical studies with EPR 241–251
Photosantonic acid, structure of 43
Physical chemist, NMR for 140–150
Physical model of exchange reaction 141
Photosynthesis 236
Planck quantum 4
Polymerization reactions 217–219
Potassium, microwave power for molar solution 273
Potential barriers 35
Probe, in NMR spectrometer 10–12, 25, 26
, tuning and balancing 58
, Varian model crossed coil 84
Product analysis method 241
n-Propyl nitrite, proton magnetic resonance 148
Proton magnetic resonance of nitrites 148
Protons, dihedral angles for adjacent 115
Protons, high resolution NMR spectrometry 21
, NMR spectra 23, 111
Pyridine, high resolution NMR spectrum 16

Quantitative analysis, high resolution NMR spectrometry 129–133
Quinone, hydroquinone redox reaction 235
, natural, structural determination of 120
, oxidation and reduction products 208

Radiation laboratory, University of California 160
Radical, DPPH 227, 231
, intermediates in organic reactions, free 207–209
, reactions 216
, rapid free 210
, research prototype flow system 211
Radio frequency, Field H_1, measurement 164–168

Radio frequency, power level effect on integrated intensity ratios in toluene 132
Reaction kinetics, EPR chemical applications 210–212
, NMR application 140–150
Reactions in polymerization 217–219
Redox reaction, list of systems with free radicals 234
, quinone-hydroquinone 235
Relaxation processes in crystals 266
Relaxation, thermal 22, 48
Relaxation time 3, 133
, longitudinal 169
, measurement of 169–175
, spin-spin 169
, toluene, effect on integrated intensity ratios 132
, transverse 169
, vacuum degassed water, determination 174
Resonance lines, theoretical explanation of kinetic phenomenon 141–147
Riboflavin reduced by ethyl alcohol radicals 235
Rotation, hindered, barrier measurement example 147
, potential energy barrier plot 150

Sanborn Model No. 151 recorder 244
Santonin, irradiation products, structure of 42
Saturation phenomenon 25
Schrodinger equation 152
Sec-butoxy radical Arrhenius plot 248
, decay curve 247
Semiquinone, diacetyl, formed in basic condensation of 208
, 2, 5, dimethyl benzo-, radical structure 229
, rate of formation 210
, spectrum 208
Sensitivity, high resolution NMR spectrometry 38–40
Shielding constants 102, 103
Shims, electric 176–179
, operating procedure 179
Signals, u- and v-mode 131
Slow passage with extremely narrow NMR signals 23
Sodium-ammonia solution, correlation time 276
, microwave power for 270
, proton resonance 277
Spectra analysis, high resolution NMR 151–163
, spin $\frac{1}{2}$ 159
, theoretical, AB_2 160, 161
Spectra analysis, A_2B_2 162
Spectrometer, array 11
, EPR, operation fundamentals 65–80
, uses for 206
, NMR-EPR 1–20
, NMR, variable temperature accessories 149
, nuclear isotope 10
, sensitivity, criteria of 11
, Varian 65
Spectrometry, NMR high resolution 21–43, 31, 38–40
Spectroscopy, EPR 44–55
, NMR-EPR 1–20
, wide line NMR 11, 13
Spheron 6, carbon black 274, 275
Spin $\frac{1}{2}$, elements with 21
Spin-coupling, between nuclei 30, 31
, constants for protons 114
Spin-Hamiltonian equation, derivation 264, 265
Spin–spin, coupling interaction 103, 104
, splitting 15, 16
Stanford University, first NMR experiments 2
Steroid, NMR spectrum of a dilute solution 40
, NMR spectra 116–118
, i-, NMR spectra 115
Structural applications, coenzyme φ group 119, 120
, NMR, high resolution 100–121, 122–139
, NMR spectra 32, 33, 40–43
, quinone, natural 120
, use of integral of absorption curve 119
Styrene, polymerization studies 217
Surface chemistry, study of 212–214
Sweep, fly-back time, circuit to increase 173
, resonance center stop, circuit to provide 174
Synchroverter, improper switching 76

Tautomeric mixture, analysis of 138
Terpenes, analysis of a mixture 125
Thermal relaxation 22, 48
Toluene, hydrogen analysis 136
, phenyl resonance of internal standard 149
, relaxation time effect on integrated intensity ratios 132
, r.f. power level effect on intensity ratios 132
, Spheron 6, microwave frequency 275
Trapping technique 241, 249

Utah University 211

Varian Associates 241
, EPR at work, bulletins 233, 235, 236
Varian low-power bridge 280
Varian Model, Sweep Unit, V4250A 166, 181
, V-4325 linear 173
, V-4270 and A 166, 167, 181, 182
, V-4311 r.f. unit 167, 190
V-center resonances 258, 259

Water, hydrogen analysis 136
, signals in high purity D_2O 123, 124
Wide line NMR spectroscopy 11, 13
"Workshop" experiment, Color Center 279–282

Xanthoperol, structure 108

Zeeman effect 2, 224